PERMAFROST DYNAMICS IN 20TH AND 21ST CENTURIES ALONG THE EAST-SIBERIAN AND ALASKAN TRANSECTS

A

THESIS

Presented to the Faculty

of the University of Alaska Fairbanks

in Partial Fulfillment of the Requirements

for the Degree of

DOCTOR OF PHILOSOPHY

By

Tatiana Sergeevna Sazonova

Fairbanks, Alaska

May 2003

Reproduced with permission of the copyright owner. Further reproduction prohibited without permission.

UMI Number: 3092294

Copyright 2003 by
Sazonova, Tatiana Sergeevna

All rights reserved.

UMI®

UMI Microform 3092294
Copyright 2003 by ProQuest Information and Learning Company.
All rights reserved. This microform edition is protected against
unauthorized copying under Title 17, United States Code.

ProQuest Information and Learning Company
300 North Zeeb Road
P.O. Box 1346
Ann Arbor, MI 48106-1346

Reproduced with permission of the copyright owner. Further reproduction prohibited without permission.

PERMAFROST DYNAMICS IN 20TH AND 21ST CENTURIES ALONG THE EAST-SIBERIAN AND ALASKAN TRANSECTS

By

Tatiana Sergeevna Sazonova

RECOMMENDED:

Matthew Sturm

D. Berg

David Verbyla 3 APRIL 2003

Keith Echelmeyer

V. Romanovsky

Advisory Committee Chair

Paul Layer

Chair, Department of Geology and Geophysics

APPROVED:

O. Woodall

Dean, College of Science, Engineering and Mathematics

Dean of the Graduate School

4-23-03

Date

Reproduced with permission of the copyright owner. Further reproduction prohibited without permission.

Abstract

High latitude ecosystems where the mean annual ground surface temperature is around or below 0°C are highly sensitive to global warming. This is largely because these regions contain vast areas of permafrost which will begin to degrade when the mean annual ground temperatures will be above 0°C. The Alaskan and East Siberian transects, centered on the 155° WL and 135° EL, were chosen evaluate permafrost – atmosphere interactions. The analysis of measured air and ground temperatures from these two transects show that from late 1950^{s} an increase and its magnitude is from 2.5 up to 5°C/100 years, and is comparable to trends predicted by majority of global warming scenarios.

A simple and accurate model for evaluating the permafrost dynamics was developed in Geophysical Institute Permafrost Lab (GIPL). The GIPL model is the union of the modified Kudryavtsev's approach, which is the set of analytical formulas for active layer thickness (ALT) and mean annual ground temperatures (MAGT) calculations, with the Geographic Information System (GIS). The evaluation of the GIPL performance showed that the relative error for MAGT does not exceed 33% and 32% for the ALT.

The GIPL model was used for the hindcast of the permafrost dynamics in the 20th century, using climatic parameters provided by Dr. David McGuire. The results showed that in 20th century there was a number of relatively cold and warm periods during which changes in MAGT were 1 to 3°C and up to 1 m for the ALT.

The forecast for the period of 2000-2100 was performed using climatic parameters from six Global Climate Models provided by Arctic Climate Impact

Reproduced with permission of the copyright owner. Further reproduction prohibited without permission.

Assessment program. The results showed that by the end of 21st century mean annual ground temperatures will be 2 to 6°C warmer and the ALT from 0.2 to 1 m deeper. In some areas within both transects the degradation of permafrost from the surface will start by 2100.

Reproduced with permission of the copyright owner. Further reproduction prohibited without permission.

Table of Contents

Abstract..... iii

Table of Contents..... v

List of Figures..... x

List of Tables..... xv

Acknowledgements..... xvi

CHAPTER 1. INTRODUCTION..... 1

CHAPTER 2. PAST AND RECENT CHANGES IN PERMAFROST TEMPERATURES IN EASTERN SIBERIA AND ALASKA..... 5

ABSTRACT..... 5

INTRODUCTION..... 5

DATA DESCRIPTION..... 8

ANALYSIS OF MEASURED TEMEPERATURES..... 10

East-Siberian transect..... 10

NUMERICAL CALCULATIONS OF THE PAST TEMPERATURE DYNAMICS..... 13

The East-Siberian and Alaskan transects..... 14

DISCUSSION..... 17

CONCLUSIONS..... 21

CHAPTER 3. A MODEL FOR REGIONAL-SCALE ESTIMATION OF TEMPORAL AND SPATIAL VARIABILITY OF THE ACTIVE LAYER

Reproduced with permission of the copyright owner. Further reproduction prohibited without permission.

THICKNESS AND MEAN ANNUAL GROUND TEMPERATURES 39

ABSTRACT 39

INTRODUCTION 40

DESCRIPTION OF THE GIPL MODEL 44

Modified Kudryavtsev's Approach 45

Evaluation of the snow cover influence 47

The thermal effects of surface vegetation cover 49

Calculating the thermal offset and MAGT at the bottom of the active layer 50

Calculating active layer thickness 52

Evaluating the performance of the modified Kudryavtsev approach ... 53

Comparison of mKA approach to a numerical model 53

Comparison with measured MAGT 55

Geographic Information System (GIS) approach for evaluating the spatial dynamics of the MALT and MAGTs 56

The Overall Performance of the GIPL Model 58

CONCLUSIONS 62

ACKNOWLEDGEMENTS 63

CHAPTER 4. PERMAFROST DYNAMICS IN 20th AND 21st CENTURIES ALONG THE EAST-SIBERIAN TRANSECT 82

ABSTRACT 82

Reproduced with permission of the copyright owner. Further reproduction prohibited without permission.

INTRODUCTION..... 83

ENVIRONMENTAL AND PERMAFROST CONDITIONS ALONG EAST-SIBERIAN TRANSECT..... 85

Geographic location..... 85

Climate..... 86

Permafrost and ground ice..... 87

Soils and their thermophysical properties..... 90

THE DESCRIPTION OF THE MODEL AND THE INPUT PARAMETERS USED FOR THE HINDCAST AND THE PROJECTION OF THE PERMAFROST DYNAMICS..... 92

Boundary conditions and input parameters for period 1901 – 2000 94

Climatic parameters..... 94

Validation of HADCM2 GCM..... 97

Vegetation and soils thermal properties..... 98

Permafrost dynamics within the East-Siberian transect during 1900-2000. 99

Boundary conditions and parameters for the forecast for the period 2000-2099..... 101

PROJECTIONS OF PERMAFROST DYNAMICS FOR THE PERIOD OF 2000-2099..... 105

CONCLUSIONS..... 108

ACKNOWLEDGEMENTS..... 110

Reproduced with permission of the copyright owner. Further reproduction prohibited without permission.

CHAPTER 5. PERMAFROST DYNAMICS IN 20th AND 21st CENTURIES ALONG THE ALASKAN TRANSECT 131

ABSTRACT..... 131

INTRODUCTION..... 132

ENVIRONMENTAL AND PERMAFROST CONDITIONS ALONG THE ALASKAN TRANSECT..... 133

Climate..... 134

Vegetation..... 136

Soils 137

Permafrost conditions..... 138

THE DYNAMICS OF THE ALT AND THE MAGTs FOR THE 20th and 21st CENTURIES ALONG THE ALASKAN TRANSECT..... 140

Boundary conditions and input parameters for period 1901-2000..... 141

Climatic parameters..... 141

The permafrost dynamics in 20th century..... 144

Boundary conditions used for the forecast of the permafrost dynamics.. 146

The forecast of the permafrost dynamics along the Alaskan transect for the period of 2000-2099 151

CONCLUSIONS..... 153

CHAPTER 6. GENERAL CONCLUSIONS..... 178

Reproduced with permission of the copyright owner. Further reproduction prohibited without permission.

THE COMPARISON OF THE EAST-SIBERIAN AND ALASKAN TRANSECTS IN TERMS OF SPATIAL AND TEMPORAL DYNAMICS OF PERMAFROST..... 178

The spatial dynamics of MAGTs..... 178

The spatial features of the ALT dynamics and changes in areas with permafrost degradation..... 180

THE ICE COMPLEX IN THE EAST-SIBERIAN AND ALASKAN TRANSECTS..... 184

ENVIRONMENTAL IMPACTS CAUSED BY CHANGES IN PERMAFROST..... 186

Permafrost –Atmosphere interaction..... 186

Impacts on ecosystems..... 187

Impacts on the infrastructure..... 187

PRIMARY CONCLUSIONS OF THIS RESEARCH..... 188

References cited..... 200

Reproduced with permission of the copyright owner. Further reproduction prohibited without permission.

List of Figures

Figure 2.1: The East Siberian and the Alaskan transects.....23

Figure 2.2: Continuous and discontinuous permafrost zones in Alaska and locations of the permafrost observatories.....24

Figure 2.3: Interpolated trends in mean annual air and ground (1.6 m depth) temperatures for the period of 1956 – 1990 along the East-Siberian transect.....25

Figure 2.4: Mean winter snow thickness, mean annual air and ground (1.6 m) temperatures in Amga, one of the stations where ground temperatures were cooling.....26

Figure 2.5: Mean winter snow thickness, mean annual air and ground (1.6 m) temperatures in Zhigansk, one of the locations where rates of ground warming exceeds the rate of warming air temperatures.....27

Figure 2.6: Mean annual air and ground (1.6 m) temperatures in Tongulakh, a site where permafrost degradation will occur if any more warming occurs.....28

Figure 2.7.: Seasonal trends of air temperatures for the period of 1956 – 1990 along the East-Siberian transect.....29

Figure 2.8: Calculated mean annual temperatures in active layer and near the permafrost surface in Yakutsk (A) and Fairbanks (B).....30

Figure 2.9: Temperature profiles in Yakutsk.....31

Figure 2.10: The comparison of calculated mean annual ground temperatures in Yakutsk with measured temperatures in Churapcha, about 100m from Yakutsk.....32

Figure 2.11: Calculated mean annual temperatures in active layer and near the permafrost surface in Tiksi and Barrow.....33

Figure 2.12: Measured mean annual air and permafrost (1.6 meters depth) temperatures (dashed line) and their 10-years running average values (solid line) at the Churapcha meteorological station, East Siberia.....34

Figure 2.13: The correlation between mean annual permafrost and air temperatures in Churapcha.....35

Reproduced with permission of the copyright owner. Further reproduction prohibited without permission.

Figure 2.14: The correlation between averaged permafrost and air temperatures in Churapcha.....36

Figure 3.1: East-Siberian and Alaskan transects.....64

Figure 3.2: Active layer thickness calculated using numerical model and Kudryavtsev's method for Barrow.....65

Figure 3.3: MALT calculated using numerical model and Kudryavtsev's method for Tiksi.....66

Figure 3.4: MAGTs calculated using numerical model and Kudryavtsev's method for Barrow.....67

Figure 3.5: MAGTs calculated using numerical model and Kudryavtsev's method for Tiksi.....68

Figure 3.6: Measured and Calculated MAGTs for Amga.....69

Figure 3.7: Measured and Calculated MAGTs for Namtsy.....70

Figure 3.8: Measured and Calculated MAGTs for Isit.....71

Figure 3.9: ALT for the Alaskan transect (Had CM2 GCM).....72

Figure 3.10: Block-Diagram of GIS Approach.....73

Figure 3.11: Calculated and measured MAGTs for East-Siberian transect.....74

Figure 3.12: Ranges of variation of MAGTs with certain levels of confidence.....75

Figure 4.1: The geographic location of the East-Siberian transect showing the major rivers and the physiographic provinces.....111

Figure 4.2: Active layer thickness and mean annual ground temperatures within the East-Siberian transect. Derived form the Map of Landscapes and Permafrost Conditions in Yakutia (scale 1: 2500 000), Academy of Science of USSR, Siberian Branch, Institute of Permafrost, P.I.Melnikov ed. Digitized by the Permafrost Lab, GI, UAF.....112

Figure 4.3: Schematic Map of Ice Complex distribution within the East-Siberian Transect (Courtesy of M.N. Grigoriev).....113

Figure 4.4: Soil types within the East-Siberian transect Derived using (Elovskaya et al, 1978) and (Krasnyi, 1978).....114

Reproduced with permission of the copyright owner. Further reproduction prohibited without permission.

Figure 4.5: Comparison between measured and modeled using HAD CM2 GCM mean annual air temperatures, seasonal range of air temperatures and snow cover thickness (averaged for the period of 1966-1989).....115

Figure 4.6: Output climatic parameters from HadCM2 GCM for the year 2000.....116

Figure 4.7: Snow cover types distribution derived from a snow density classification (after Feldman et al., 1998).....117

Figure 4.8: The active layer thickness dynamics within the East-Siberian transect in 20th century calculated using climatic parameters from HadCM2 GCM.....118

Figure 4.9: Output climatic parameters from CCC GCM for the year 2000.....119

Figure 4.10: Output climatic parameters from CSM GCM for the year 2000.....120

Figure 4.11: Output climatic parameters from GFDL GCM for the year 2000.....121

Figure 4.12: Output climatic parameters from HadCM3 GCM for the year 2000.....122

Figure 4.13: Output climatic parameters from ECHAM GCM for the year 2000.....123

Figure 4.14: The active layer thickness distribution for the year 2000 according to six GCMs used in the forecast.....124

Figure 4.15: The active layer thickness distribution for the year 2025 according to six GCMs used in our forecast.....125

Figure 4.16: The active layer thickness distribution for the year 2050 according to six GCMs used in our forecast.....126

Figure 4.17: The active layer thickness distribution for the year 2075 according to six GCMs used in our forecast.....127

Figure 4.18: The active layer thickness distribution for the year 2099 according to six GCMs used in our forecast.....128

Figure 5.1: The Alaskan transect, major geographical regions, and topography (modified from ESRI topographic map).....155

Figure 5.2: Permafrost distribution (Circum-Arctic Map of Permafrost and Ground Ice Conditions, 1997). The soils within the Alaskan transect (derived from the State Surficial Geology Map of Alaska, www.nps.gov/akso/gis). The major types of vegetation (from the Top - Soil Cover vegetation map using Global Characteristics Database, edcdaac.usgs.gov/glcc/globdoc2_0.html).....156

Reproduced with permission of the copyright owner. Further reproduction prohibited without permission.

Figure 5.3: The map of the loess deposits locations. (modified from State Surficial Geology Map of Alaska, www.nps.gov/akso/gis). Gray color indicates areas with loess.....157

Figure 5.4: Mean annual air temperatures in Barrow, according HADCM2 GCM.....158

Figure 5.5: Winter average snow thickness; mean annual air temperature and seasonal range of air temperatures according to HADCM2 GCM for the year 2000.....159

Figure 5.6: Grid points of Nimbus 7 dataset, and meteorological stations used for the correction of satellite data.....160

Figure 5.7: Mean annual ground temperatures and the ALT dynamics in 20th century.....161

Figure 5.8: Winter average snow thickness; mean annual air temperature and seasonal range of air temperatures according to CCC GCM for the year 2000.....162

Figure 5.9: Mean annual air temperatures in Barrow, according CCC GCM.....163

Figure 5.10: Winter average snow thickness; mean annual air temperature and seasonal range of air temperatures according to CSM GCM for the year 2000.....164

Figure 5.11: Mean annual air temperatures in Barrow, according CSM GCM.....165

Figure 5.12: Winter average snow thickness; mean annual air temperature and seasonal range of air temperatures according to GFDL GCM for the year 2000.....166

Figure 5.13: Mean annual air temperatures in Barrow, according GFDL GCM.....167

Figure 5.14: Winter average snow thickness; mean annual air temperature and seasonal range of air temperatures according to HADCM3 GCM for the year 2000.....168

Figure 5.15: Mean annual air temperatures in Barrow, according HADCM3 GCM.....169

Figure 5.16: Winter average snow thickness; mean annual air temperature and seasonal range of air temperatures according to ECHAM GCM for the year 2000.....170
Figure 5.17: Mean annual air temperatures in Barrow, according ECHAM GCM.....171

Figure 5.18: The ALT distribution for the year 2000, according to six GCMs.....172

Figure 5.19: The ALT distribution for the year 2025, according to six GCMs.....173

Reproduced with permission of the copyright owner. Further reproduction prohibited without permission.

Figure 5.20: The ALT distribution for the year 2050, according to six GCMs.....174

Figure 5.21: The ALT distribution for the year 2099, according to six GCMs.....175

Figure 6.1:The relative increase in MAGTs for the East-Siberian transect according to six GCMs.....191

Figure 6.2: The relative increase in MAGTs for the Alaskan transect according to six GCMs.....192

Figure 6.3: The relative increase in ALTs for the East-Siberian transect according to six GCMs.....193

Figure 6.4: The relative increase in ALTs for the Alaskan transect according to six GCMs.....194

Figure 6.5: Percentage of the total area of the East-Siberian transect where permafrost degradation has started.....195

Figure 6.6: Percentage of the total area of the Alaskan transect on which permafrost degradation has started.....196

Figure 6.7: The Ice Complex in Duvanyi Yar, Eastern Siberia. (Photo taken by S. Davidov).....197

Figure 6.8: The destruction of the four stores building in Cherskyi, Eastern Siberia, as a result of thermokarst processes beneath the building. (Photo was taken by V.Romanovsky).....198

Figure 6.9: The damage of the pipeline in Western Siberia caused by heat flow from the pipeline and permafrost thawing. (Photo taken by S.Yu. Parmuzin).....199

Reproduced with permission of the copyright owner. Further reproduction prohibited without permission.

List of Tables

Table 2.1: Trends in mean annual air and ground (1.6 m) temperatures within the East-Siberian transect.....37

Table 2.2: Trends in mean annual air temperatures within the Alaskan transect.....38

Table 3.1: Input variables and parameters.....76

Table 3.2: Output variables.....77

Table 3.3: Statistical analysis of Kudryavtsev's model correspondence with numerical model.....78

Table 3.4: Thermophysical properties for the sites within East-Siberian transect.....79

Table 3.5: Comparison of calculated and measured active layer thickness for Alaskan transect.....80

Table 3.6: Comparison of calculated and measured MAGTs for the East-Siberian transect.....81

Table 4.1: Thermal properties of soils within East-Siberian transect (adopted from Feldman et al., 1988).....129

Table 4.2: ACIA – designated GCMs.....130

Table 5.1: Comparison of measured (www.wrcc.dri.edu/summary/climsmak.html) and simulated (HADCM2) mean annual air temperatures for the year 2000.....176

Table 5.2: Comparative analysis of five GCMs using HADCM2 as a reference for the year 2000.....177

Reproduced with permission of the copyright owner. Further reproduction prohibited without permission.

Acknowledgements

First and foremost I would like to thank my advisor Professor Vladimir Romanovsky for the guidance, support, encouragement, and giving me the opportunity to conduct the exciting research. Dr. Romanovsky provided me with his expertise on thermal regime modeling and permafrost processes.

Professor David Verbyla, Department of Forest Sciences SALRM, helped me tremendously by providing his expertise, introducing me to basic concepts of Geographic Information Systems.

I was very fortunate to work with my colleagues Dr. Gennadyi Tipenko and Dr. Dmitri Sergueev. Dr. Tipenko helped me with mathematical modeling. Dr. Sergueev provided help and guidance with gathering data and the information for the Alaskan and East-Siberian transects.

I would like to thank Dr. John Walsh and Dr. McGuire for introducing me to Global Climate Models and teaching me the fine art of dealing with large datasets.

Professor Keith Eckelmeyer guided and supported me throughout my stay at UAF and provided me with editorial help when I was writing the thesis.

Professor James Beget and Dr. Matthew Sturm provided me with their expertise and guidance.

This research was sponsored by National Science Foundation, Office of Polar Research and State of Alaska.

I would like to thank my family – my mother Liudmila Peskovskaya, my brother Vladimir Peskovskyi, and especially my husband Justin Mabie for their constant support.

Reproduced with permission of the copyright owner. Further reproduction prohibited without permission.

I would like to dedicate this manuscript to memory of my grandparents – Lubov Sazonova, Sergei Sazonov, Leonid Smolyak, and my father Yuryi Smolyak.

Reproduced with permission of the copyright owner. Further reproduction prohibited without permission.

CHAPTER 1. INTRODUCTION

The world's environmental conditions are constantly changing at different rates and on various scales. Some of those changes can be rapid, having a considerable impact on high-latitude terrestrial ecosystems. The evaluation of such impacts requires a comprehensive understanding of ecosystems response to forcing, that result from global climate change (IGBP, 1990).

Permafrost is a major determinant of northern high latitude vegetative and hydrological characteristics. A warming in the Arctic is expected to result in higher soil temperatures, a longer growing season, a deeper active layer, warmer permafrost temperatures and a northward movement of the permafrost boundary (Maxwell, 1992). The rate of carbon loss in Arctic ecosystems can be accelerated by the thawing of permafrost, providing a positive feedback mechanism for carbon dioxide and methane in the atmosphere (Oechel et al., 1993).

Because of problems with collecting data over large high-latitude regions a transect approach is considered to be the most effective method for modeling permafrost dynamics. The transect method analyzes permafrost dynamics along several latitudinal transects where different types of environmental conditions exist and a significant amount of data is available. The results of this analysis can be used to interpolate permafrost dynamics over other temporal and spatial domains where enough data is not available for a comprehensive analysis.

The objectives of my thesis research include: 1) the development of a spatially distributed model with sufficient accuracy and spatial resolution to evaluate permafrost

Reproduced with permission of the copyright owner. Further reproduction prohibited without permission.

dynamics on a regional scale, 2) compiling Geographic Information System (GIS) for two transects, 3) evaluation of permafrost dynamics along the transects in over the past century through application of the Geophysical Institute Permafrost Lab (GIPL) model and climatic forcing for the 20th century, 4) forecast of permafrost dynamics for 21st century using the GIPL model and six scenarios of climate warming. The outputs of the Global Climate Models (GCM) were used as climatic forcing for the GIPL model. These six GCMs were developed in Canadian Climate Center (CCC), National Center for Atmospheric Research (CSM), Geophysical Fluid Dynamics Laboratory (GFDL), Max Planc Institute for Meteorology (ECHAM) and Hadley Climate Center (HADCM2 and HADCM3).

The International Geosphere – Biosphere Program has established five high latitudinal transects to study the impact of climate change on ecosystems (IGBP, 1996). Two of them, the designated Far East-Siberian and Alaskan transects (Figure2.1), were chosen for the scope of this research. These two transects differ significantly in the available information on climate, vegetation, and soil properties. Despite these differences, previous investigations and point-by- point comparisons of different sites has shown that variations in ground temperatures within the transects are consistent (Shender, et al., 1999; Romanovsky et al., 2001).

The second chapter of this thesis presents the analysis of measured climatological and permafrost data along the two transects. The numerical simulation of permafrost dynamics for data sites within the transects has been performed to confirm a point-by-point correlation.

Reproduced with permission of the copyright owner. Further reproduction prohibited without permission.

Chapter three gives a general description of the model that was developed in Geophysical Institute Permafrost Lab (GIPL). This model incorporates a modified Kudryavtsev's approach into GIS. A detailed description of the modified Kudryavtsev's approach, including the discussion of its shortcomings and advantages is provided. The overall performance of the GIPL model is evaluated using statistical and probability analysis.

The fourth chapter addresses the East-Siberian transect and includes general information on climate, vegetation, soils, and permafrost. Hindcast and forecast of permafrost dynamics along the East-Siberian transect were done using the GIPL model. The hindcast was done using climatic parameters derived from the combination of HADCM2 GCM with observational grids (McGuire et al., 2001). A comparison of modeled climatic parameters with field measurements has been performed. For the forecast, climatic parameters from six GCMs were provided by Arctic Climate Impact Assessment program (ACIA). The results of the calculations include spatially distributed active layer thickness and mean annual ground temperatures and presented in digital map format for the period 2000 - 2100 with a temporal resolution of one year.

Chapter five describes environmental conditions and permafrost dynamics along the Alaskan transect. The same GCMs outputs are used as an external forcing mechanism for the model. The results provide active layer thickness and mean annual ground temperature dynamics within Alaskan transect from 1900 to 2100.

The sixth chapter concludes the research by making a comparison of permafrost dynamics along the two transects. This comparison was based on the results from

Reproduced with permission of the copyright owner. Further reproduction prohibited without permission.

Chapters 4 and 5. Possible environmental impacts of the permafrost dynamics based on the comparison are also discussed. General conclusions are provided at the end of the chapter.

Chapters 2 through 5 are stand alone manuscripts and have been or will be submitted for publication. The first paper was written with my coauthors who are Dr.Vladimir Romanovsky, Dr. Gennadyi Tipenko, and Dr. Dmitri Sergueev. The second is coauthored with Dr. Vladimir Romanovsky. Dr. Romanovsky developed the modified Kudryavtsev's approach, which became a central part of the GIPL model. I wrote a code for active layer thickness and mean annual ground temperatures calculations and created an algorithm to incorporate this approach into the GIS. Dr. Vladimir Romanovsky is also a coauthor on my third and fourth papers along with Dr. John Walsh, who provided a valuable insight on the Global Circulation Models and supplied climatic outputs from these models. All coauthors provided help and guidance, assisted with modeling and analysis, and editing the papers. As a first author I contributed the major part of research and writing.

Reproduced with permission of the copyright owner. Further reproduction prohibited without permission.

CHAPTER 2. PAST AND RECENT CHANGES IN PERMAFROST TEMPERATURES IN EASTERN SIBERIA AND ALASKA*

ABSTRACT

Air and ground temperatures measured in Eastern Siberia and Alaska has been compiled and analyzed. The analysis of mean annual air temperatures measured at 52 points within the East-Siberian transect during the period of 1956 – 1990 demonstrate a significant positive trend ranging from 0.065 to 0.59 °C per 10 years. Positive trend was also observed in mean annual ground temperatures for the same period. Mean annual air temperatures have also increased since the 1956. Numerical modeling of ground temperatures has been performed for Fairbanks, Yakutsk, Tiksi and Barrow for the last 100 years. The results showed that variations of ground temperatures took place at the same time periods in Yakutsk and Fairbanks, and in Tiksi and Barrow.

INTRODUCTION

Increasing atmospheric concentrations of greenhouse gases may significantly alter Earth's climate. The predicted climatic warming may be most pronounced in the Arctic and should be detectable there first (Nelson et al., 1993). General circulation models project global mean equilibrium temperature increases of between 1.8°C and 5.2°C in case of doubling of preindustrial CO_2 concentrations (Maxwell, 1992). Newer estimates,

---

* Prepared for the submission under the same title with authors Tatiana S. Sazonova, Vladimir E. Romanovsky, Gennady S. Tipenko and Dmitri O. Sergueev in *Arctic, Antarctic, and Alpine Research*.

Reproduced with permission of the copyright owner. Further reproduction prohibited without permission.

which incorporated possible effects of future changes of anthropogenic aerosols concentrations, lowered projections of temperature change to the level of between 1°C and 3.5°C by 2100 (Kattenberg, 1996). The temperature rise in arctic regions may be two to three times greater than the global average. However, in order to project the climatic consequences of terrestrial processes into the future at Arctic Basin scales, much more information has to be collected from the circumpolar-wide area including the vast Russian arctic and sub-arctic regions.

The long-term climatic trend will occur against a background of short-term (inter-annual, decadal and inter-decadal time scales) variability in the air temperature and precipitation. To distinguish such a trend, it is necessary to obtain more information about short-term climatic variability. The temperature regime of permafrost is a sensitive indicator of the interannual and decade- to century-variability in climate and long-term changes in the surface energy balance where very small changes can produce amplified changes in permafrost temperatures. Permafrost plays the role of a natural low pass filter for climatic signals, increasing the signal (decadal to century climatic change) to noise (interannual and sporadic temperature fluctuations) ratio.

A recent increase (last 30 – 40 years) in air temperatures has been reported for many regions in the Arctic and sub-Arctic (Chapman and Walsh, 1993; Jones, 1994; Nicholls et al., 1996; Serreze et al., 2000). Many scientists interpreted it as an evidence of the predicted global warming (Santer et al., 1996). This increase, which was the most

Reproduced with permission of the copyright owner. Further reproduction prohibited without permission.

pronounced in Alaska and East Siberia, produced subsequent increase in the permafrost temperatures recorded at many monitoring stations within the Arctic.

As a part of a NSF (National Science Foundation)/OPP (Office of Polar Program)/ARCSS (Arctic System Science) sponsored ATLAS (Arctic Transitions in the Land-Atmosphere System) project, we collected data on regional air and near-surface permafrost temperatures in the continuous permafrost zone of East Siberia spanning last 30 to 40 years. These data allow for detailed analysis of temporal and spatial variability of these parameters. This paper presents the results of such analysis of both measured and calculated data for the East Siberian transect and comparison with similar information from the Alaskan transect.

The Tiksi-Yakutsk East Siberian transect, designated as the Far East Siberian transect in the International Geopshere- Biosphere Program (IGBP) Northern Eurasia Study project (IGBP-NES) (IGBP, 1996), is centered on the 135° meridian, and is a collaborative effort of IGBP-NES with the GAME project of the WCRP (Figure 2.1). This transect is bounded by the Arctic Ocean in the north, 60°N latitude in the south, and by the 122° and 138° meridians (an area approximately the size of Alaska). The entire transect is located within the Sakha (Yakutia) Republic, Russian Federation (Figure 2.1). The Alaskan transect spans both continuous and discontinuous permafrost zones of Alaska and is located along the Dalton, Elliot, Alaska and Richardson Highways (Figures 2.1 and 2.2).

Reproduced with permission of the copyright owner. Further reproduction prohibited without permission.

DATA DESCRIPTION

Recently, new data for the 52 meteorological stations within the continuous permafrost zone in east Siberia were obtained. The data include monthly averaged air temperature, snow cover depth and ground temperature at several depths (0.05 m down to 3.2 m). The ground temperature data are available only for 31 stations. The period of measurements range between 110 and 50 years for the air temperatures and about 40 to 20 years for the ground temperatures.

Only 29 of these stations are situated within the East-Siberian transect (Figure 2.3). Most of the stations, within or outside of transect, have operated for more than 40 years (Table 2.1). Average mean annual temperatures vary within the transect area from lower than -16°C in the Verkhoyansk region (data available since 1880) to -8°C near the southern limits of the transect. The data include daily (for a limited number of stations), monthly, and annual values of air temperatures and precipitation, 10-day mean depths of snow cover, snow density, and water equivalent, and the number of days with snow cover for each month. At these stations, measurements of the bare ground surface temperatures during the summer and snow surface temperatures during the winter were also collected. In addition to this, 21 stations within transect have several shallow boreholes (0.1 to 3.2 meters deep) where yearly to daily temperature measurements were performed. High inertia mercury thermometers were used for the ground temperature measurements. Such thermometers provide accuracy about $\pm$ 0.1 °C. Generally, the accuracy and quality of measurements varied depending on the year of collection, but the measurement technique

Reproduced with permission of the copyright owner. Further reproduction prohibited without permission.

and equipment have remained the same for the last 25 years. All available data on air and ground temperatures and on snow cover characteristics from these 29 meteorological stations were incorporated into the GIS (Geographic Information System) "East Siberian Transect", which is under development at the University of Alaska Fairbanks (Romanovsky et al., 2001). These data are on file at the NSF/ARCSS Data Center.

Temperature data from the Alaskan transect presented in this paper were collected at the permafrost observatories along the trans-Alaskan pipeline (Figure 2.2). These observatories were established during the late 70s and early 80s by the University of Alaska (Osterkamp, 1985). Each of these sites includes a relatively deep borehole (typically 40 to 80 meters) where permafrost temperatures have been measured every year since early or mid 80s. At three sites in the continuous permafrost zone and at four sites in the discontinuous zone, temperatures have been recorded daily since 1986 at eleven levels (air, ground surface, three in the active layer, three straddling the permafrost table and three in the permafrost to a maximum depth of 1 m) using an automatic temperature logger attached to thermistor sensors in a plastic rod installed in the ground (Romanovsky and Osterkamp, 1995). In the mid-late 90s several new observatories were established and several existing observatories were upgraded. This upgrade included hourly to daily measurements of the liquid ground water content using TDR equipment at three to four depths in the active layer and near-surface permafrost. More information on equipment and data collection techniques is available from other publications (Osterkamp and Harrison, 1981; Osterkamp, 1985; Osterkamp and Romanovsky, 1999).

Reproduced with permission of the copyright owner. Further reproduction prohibited without permission.

ANALYSIS OF MEASURED TEMPERATURES

The East-Siberian Transect

All available air and ground temperature series were used to calculate mean annual temperatures for all years for each station. Although the temperature in boreholes was measured at several depths, for our analysis we chose to focus on a depth of 1.6 m, which turned out to provide the longest and the most representative records.

To assess the long period trend in air and ground temperatures for the period 1956 – 1990, the linear regression was used. Calculated trends in air and ground temperatures for all stations were compiled and converted into an ArcView format. Then the interpolation has been done to obtain a regional picture of variations in temperature changes within the East-Siberian transect. We used software ArcView for creating a map of temperature changes and temperature trends distributions. For the interpolation, Inverse Distance Weighted interpolator within the Surface Analyst application was used. This method gives values to each cell in the output grid theme by weighting the value of each point by the distance that point is from the cell being analyzed and then averaging the values. All points (stations) were taken into account during interpolation.

As a result, two maps of trends in air and ground temperatures for the period 1956-1990 were created (Figure 2.3). These maps are a valuable source of information about regional variations in air and ground temperatures within the East-Siberian transect for the last 30 years. All stations, except for one, demonstrate a statistically significant

Reproduced with permission of the copyright owner. Further reproduction prohibited without permission.

positive trend in air temperature within a range from 0.065 to 0.59 °C per 10 year (Table 2.1). The only negative trend at the Saniyakhtat station is not statistically significant. The data shown in Figure 2.3 are in good agreement with published surface air temperature trend estimations for the entire Northern Hemisphere (Chapman and Walsh, 1993; Serreze et al., 2000). At the same time, because of their better spatial resolution, these data show that, for this region, the more significant trends tend to occur in the lower latitudes (between 55° and 65° North), rather than in the Arctic and High Arctic. Ground temperature trends generally follow the trends in air temperatures (Table 2.1 and Figure 2.3) with more pronounced warming in the lower latitudes. Unlike the air temperatures, the ground temperatures were warming more rapidly in the western part of the transect in comparison with its eastern part. Also, four sites show small but statistically significant negative trends in ground temperatures (Table 2.1). The trend values vary between –0.19 °C and 0.78 °C per 10 years. The average trend for the entire region is 0.26 °C per 10 years, which is very similar to the average trend in the air temperatures (0.29 °C per 10 years).

The differences in the direction of trends in air and near-surface permafrost temperatures, though not typical, show the possibility of complex reaction of the permafrost temperature regime to the air temperature changes at some particular sites. Thus, there are four sites within transect where the air temperatures experienced a positive trend while the ground temperatures were cooling (sites Dzharzhan, Krest-Khal'dzhai, Okhotskiy Perevoz and Amga, Table 2.1, Figure 2.4). On the other hand, at

Reproduced with permission of the copyright owner. Further reproduction prohibited without permission.

some sites the ground temperature trends significantly exceeded the rate of the air temperature warming (Zhigansk, Ytyk-Kel' and Uchur, Table 2.1, Figure 2.5). The major sources of these discrepancies are the local climatic (precipitation, wind) and ground surface (ground vegetation and snow cover dynamics) conditions. Changes in these conditions may significantly alter the local response of permafrost to the air temperature variations (Smith and Riseborough, 1996).

Significant and persistent increases in the ground temperatures during several decades late in the 20th century brought permafrost to the edge of degradation in several regions of the East Siberian transect (Fedorov, 1996). Figure 2.6 shows an example of this process for the site Tongulakh (61.55 N°, 124.33 W°). Permafrost is still stable at this site, but any further warming in the air temperatures and/or increase in snow cover will start the long-term process of permafrost degradation.

The analysis of mean seasonal air temperatures for the period 1956 – 1990 has been performed (Figure 2.7). Spring (averaged over March, April, and May) and winter (averaged over December, January, and February) trends are positive almost everywhere within the transect. Trends in mean spring air temperatures vary from 2.5° to 10 °C/100 years within the entire transect, with the largest trends in south-eastern part. Spring trends can be explained in part by early disappearance of snow cover and influence of the bare ground. At present time there is not enough information available on snow and vegetation to find the reason for these large spring trends.

Reproduced with permission of the copyright owner. Further reproduction prohibited without permission.

Winter trends are positive in the eastern and central parts and negative in northern and western parts of the transect. The magnitude of winter trends does not exceed 5°C/100 years and is around 2.5°C/100 years almost everywhere (Figure 2.7).

Summer and autumn trends are negative for most of the transect. Summer trends are positive in the south-western part of the transect and in small regions in the eastern part. The magnitude of positive trends is up to 6.5°C/100 years. Except the small areas with positive trends, on the rest of territory summer trends are negative and are around -1°C/100 years. Autumn trends are positive only in the northern part of the transect and do not exceed 2.5°C/100 years.

The analysis of seasonal trends of air temperatures shows that the positive trends of mean annual air temperatures were caused mostly by spring warming trends with the small input of winter trends. Winter temperatures warmed up but summer temperatures were getting colder for the period of 1956 – 1990, therefore climate was getting more moderate.

Alaska is another region that showed a significant positive trend in the air temperature during 1960-1995 (Chapman and Walsh, 1993; Serreze et al., 2000). Because air temperatures throughout Alaska are often highly correlated (Hamilton, 1965; Hansen and Lebedev, 1987; Zhang and Osterkamp, 1993), the air temperature trends during this period are more spatially uniform there (Table 2.2).

NUMERICAL CALCULATIONS OF THE PAST TEMPERATURE DYNAMICS

Reproduced with permission of the copyright owner. Further reproduction prohibited without permission.

Most of the measured data covered only the period of significant positive trends in both air and ground temperatures. However, it is well known that this period was preceded by 20 to 30 years of cooling in high latitudes of the Northern Hemisphere (Eischeid et al., 1995; Serreze et al., 2000). To place the measured of the last 20 to 40 years active layer and near-surface permafrost temperature into a longer-term prospective, numerical modeling of the permafrost temperature regime for the last 70 years at several sites within the East Siberian and Alaskan transects with intensive measurement datasets was employed.

The East-Siberian and Alaskan Transects

Numerical models used in these studies are described in (Romanovsky et al., 1997). Site-specific calibration of the models was accomplished using annually measured temperature profiles at the Yakutsk Permafrost Institute experimental site and daily mean temperatures measured at the ground surface and at several depths in the first three meters of soil. Daily air temperatures and decadal snow cover thicknesses from the Yakutsk meteorological station were used to complete the model calibration and to extend the calculations back in time. The lower boundary of the calculation domain was set at 125 meters with a constant geothermal heat flux there. Drilling records were used to determine the lithology and the initial thermal properties of the soils in the thawed and frozen states. The thermal properties (including unfrozen water content curves) were refined using a trial and error method (Osterkamp and Romanovsky, 1997; Romanovsky and Osterkamp, 2000). Results of calculations of the mean annual temperatures in the

Reproduced with permission of the copyright owner. Further reproduction prohibited without permission.

active layer and near-surface permafrost at the Yakutsk Permafrost Institute experimental site are shown in Figure 2.8A.

These results show that during 1930-1996, there were several intervals with warmer soil temperatures in 1930s, late 1940s, late 1960s, late 1970s-early 1980s, and especially in late 1980s-early 1990s. Generally, the temperatures were decreasing from 1930s to early 1960s, and since then they were increasing (2°C average increase between 1960 and 1996). These long-term fluctuations in permafrost temperature (with period of 60 to 70 years) can be easily recognized from the set of calculated mean annual permafrost temperature profiles shown in Figure 2.9. These profiles reflect long-term cooling, which started in late 1920s and progressed through 1960s. The decrease in permafrost temperatures was about 2.5-3 °C at the permafrost table and about 1 °C at the 15 meters depth. During the period 1960-1996, the permafrost temperatures rebounded practically to the initial temperature profile of 1929. For these calculations we didn't have a measured initial temperature profile. First, we assumed that the permafrost temperatures in 1929 were somewhat colder than at present. However, after 67 years of the model's run, we finished up with much colder than measured temperature profile in 1996. Only after the postulation that the initial (1929) temperature profile was very similar to the present-day one, we were able to obtain at the end of calculations the temperature profile (filled circles in Figure 2.9), which was reasonably close to the measured in 1996 profile (filled squares in the same Figure).

Reproduced with permission of the copyright owner. Further reproduction prohibited without permission.

Measured ground temperature data from our GIS "East Siberian Transect" provide an opportunity to test the results of our numerical reconstructions of the active layer and upper permafrost temperature dynamics for the Yakutsk site. The comparison of these calculations with measured ground temperatures at the Churapcha site (100 km east of Yakutsk) shows good agreement (Figure 2.10). The correlation coefficient between measured and calculated temperatures at 1.6 meters depth for the period 1958-1994 was 0.88.

Similar simulations of the past temperature regimes were made for several sites along the Alaskan transect (Romanovsky and Osterkamp, 1996, 1997; Osterkamp and Romanovsky, 1999). One of the reconstructions was made for 1929-1998 for a Fairbanks site (Figure 2.8B). The calculations show that the ground temperatures during the 1940s were warmer than the 1930s, 1950s and 1960s, but that the mean annual temperatures in the active layer and near-surface permafrost were not as warm as in the 1990s. During the 1980s and most of the 1990s, the mean annual ground surface temperatures at this site were above 0°C. Permafrost remains stable and survives only because of the insulating effect of the organic mat at the ground surface and the related thermal offset in the active layer. The Yakutsk and Fairbanks temperature time series show significant and somewhat surprising similarities (Figure 2.8). However, there is some lag in the soil temperature variations at the Fairbanks site compared to Yakutsk.

To compare the active layer and permafrost temperature dynamics in sub-Arctic (Yakutsk and Fairbanks) with the Arctic sites, a suite of similar calculations was

Reproduced with permission of the copyright owner. Further reproduction prohibited without permission.

performed for the Siberian site Tiksi (71.59 N, 128.92 E) and the Alaskan site at Barrow (71.18 N, 156.47 W) sites. At Barrow the mean annual ground and permafrost surface temperatures have a range of more than 5°C from about -7°C to -13°C (Figure 2.11). The ground temperatures were warmer for the late 1920s and 1940s than for the 1980s and 1990s (Romanovsky and Osterkamp, in press). However, in 1998, the ground temperatures at Barrow were the highest for the entire period of calculations (1923-1998). The mean annual air and ground temperature variations at the Tiksi site in Siberian Arctic show generally similar patterns. The warmest time was during the mid and late 1930s when the mean annual temperatures in the near-surface permafrost (1 to 3 meters depth) were between –8°C and –9°C. For the rest of the time these temperatures were generally below –10°C and only in early 1990s they warmed up to –9.5° and –9°C (Figure 2.11).

DISCUSSION

Data from the East Siberian transect, both air and ground temperatures, show a significant warming trends during the 1956-1990 period, which is in a good agreement with the atmospheric Global Climate Models projection. However, the spatial patterns of this warming noticeably differs from these model predictions. Instead of increasing with latitude as predicted by the models, the data show that the largest warming trends in both air and permafrost temperatures were observed in the East Siberian sub-Arctic (55° N to 65°N). The rate of temperature increase here is almost twice that of compared to the higher latitudes (Figures 2.3, Table 2.1). As can be seen from comparison between

Reproduced with permission of the copyright owner. Further reproduction prohibited without permission.

Figures 2.8 and 2.11, the latest increase in temperatures in lower latitudes started in the beginning of 1960s, whereas in the higher latitudes the turning point from the mid-century cooling to the latest warming came in the mid 1970s. The same spatial and temporal patterns of the latest warming are typical for Alaska (Figures 2.8 and 2.11, Table 2.2). In the West Siberia, the trends in the latest warming are very similar for the all latitudes (Pavlov, 2000). According to Przybylak (2000), this is rather typical situation for the entire circumpolar North.

Generally, the increase in ground temperatures within the East Siberian transect is in concert with the air temperatures warming. However, there are several sites where these two variables are in conflict. At four sites the ground temperatures were decreasing in 1956-1990, while the air temperatures had a positive trend for the same period (Table 2.1). More detailed analysis of the air and permafrost temperatures and snow cover dynamics at the Amga site shows that the permafrost temperatures correlate more strongly with the snow cover thicknesses than with the air temperatures (correlation coefficients are 0.45 and 0.005 respectively). Snow cover thickness decreased by 10% on average during 1965-1990 (from 0.24 m to 0.22 m). Because of relatively shallow snow at this site (it's annually maximum thickness varied between 0.17 m and 0.29 m during this period), the sensitivity of the ground temperatures to the variations in the snow thickness is very high.

At some sites, the ground temperatures were increasing much faster than the air temperatures (Zhigansk, Ytyk-Kel' and Uchur, Table 2.1). Again, probably the most

Reproduced with permission of the copyright owner. Further reproduction prohibited without permission.

reasonable explanation is the positive trend in the snow cover thickness. For example, at the Zhigansk site, the major increase in permafrost temperature occurred during 1965-1980. The winter maximum snow cover thickness for the same period increased from 0.3 m to 0.6 m (Figure 2.5). There also could be other reasons for the rapid permafrost temperature change at these sites. They can relate to changes in the surface conditions (such as vegetation and moisture regime) or even to the surface disturbances at the meteorological stations. Unfortunately, we do not have enough information to evaluate these other possibilities.

East Siberian air and soil temperature data were used to test a common but lately often scrutinized postulation that the permafrost temperatures are a reasonably good indicator of climate change. Comparisons between mean annual air and permafrost temperatures at the Churapcha station (Figures 2.12 and 2.13) show that on interannual time scale, these two parameters vary differently, with a correlation coefficient between these two variables is 0.49 for the 1957-1992 time period. This coefficient will be even smaller for any shorter time interval. At the same time, the 10-year running means (Figure 2.12) show much better correlation (correlation coefficient is 0.87). The longer averaging intervals increase this correlation even more (Figure 2.14). Hence, these data suggest that the permafrost temperatures replicate the longer time scale (decadal and longer) changes in climate (air temperatures) much better than the interannual variations. The prime cause of this is a significant interannual variability (but usually not a long-term trend) in the snow cover depths and durations and the time lag associated with ground temperatures.

Reproduced with permission of the copyright owner. Further reproduction prohibited without permission.

Better correlation between air and permafrost temperatures can be achieved by averaging measured time series not only in time but also in space. Correlation coefficients based on mean annual temperatures from the sites within the East Siberian transect vary between 0.005 (Amga site) and 0.58 (Tongulakh). Simple averaging of correlation coefficients over all stations is 0.24. However, when we averaged all measurements of the mean annual air temperatures obtained at each station within the transect for each year and then did the same averaging for the permafrost temperatures, the correlation coefficient between these spatially averaged air and permafrost temperatures was 0.51 for the period 1956-1990. Hence, the spatial averaging over the entire region has a similar effect as the temporal averaging procedure for any single site. As was mentioned earlier, the average trend for the entire region was 0.26 °C per 10 years for permafrost temperatures and 0.29 °C per 10 years for air temperatures.

Disturbances related to forest fires significantly increase the probability of permafrost degradation in the near future. Our temperature measurements and calculations show that for most of the time after 1975, the mean annual ground surface temperatures at the Fairbanks sites were, and probably will be, above 0°C. Permafrost remains stable and survives only because of the insulating effect of the organic mat at the ground surface and the related thermal offset in the active layer. Severe forest fires usually destroy this organic layer, exposing the underlying mineral soils to the surface. Drying of the active layer will further reduce the thermal offset. This can reset the mean annual temperatures at the bottom of the active layer to level above 0°C. In this case,

Reproduced with permission of the copyright owner. Further reproduction prohibited without permission.

permafrost will start to thaw and if permafrost is ice-rich, the thermokarst processes will take off, significantly affecting ecosystems and creating numerous problems for infrastructure (Osterkamp et al, 1997; Osterkamp et al, 2000).

CONCLUSIONS

The analysis of mean annual air temperatures measure at 52 points within the East-Siberian transect during the period of 1956 – 1990 demonstrate a significant positive trend ranging from 0.065 to 0.59 °C per 10 years. A positive trend was also observed in mean annual ground temperatures for the same period. The most significant trends in mean annual air and ground temperatures were in the southern part of the transect, between 55° and 65° NL. Generally positive trends in mean annual ground temperatures are smaller in comparison with trends in mean annual air temperatures, except several sites where the discordance between air and ground temperatures can be explained by mean winter snow dynamics.

In addition to trends in mean annual air temperatures, seasonal trends were calculated. The spring trends of air temperatures were positive and the largest in magnitude, and were major contributor to mean annual trends. Winter trends are smaller than spring trends. Summer and autumn trends are negative with small magnitude up to -1°C/100 years. Additional research is required to determine the nature of large spring trends and negative summer and autumn trends.

Reproduced with permission of the copyright owner. Further reproduction prohibited without permission.

Statistical analysis of mean annual ground and air temperatures shows that these temperatures are correlated. Further analysis proved that the correlation between mean annual air and ground temperatures is improving when these two temperatures are averaged in time or in space.

The numerical modeling of ground temperatures at 4 sites (2 in Alaska and 2 in East-Siberia) for the 21st century shows that decadal fluctuations with the periods ranging from 10 to 20 years took place in both regions. The magnitudes of these fluctuations did not exceed 1 to 2°C. The fluctuations of mean annual ground temperatures were synchronized in Fairbanks and Yakutsk, and in Barrow and Tiksi. The magnitude and timing are slightly different for each of the sites.

Reproduced with permission of the copyright owner. Further reproduction prohibited without permission.

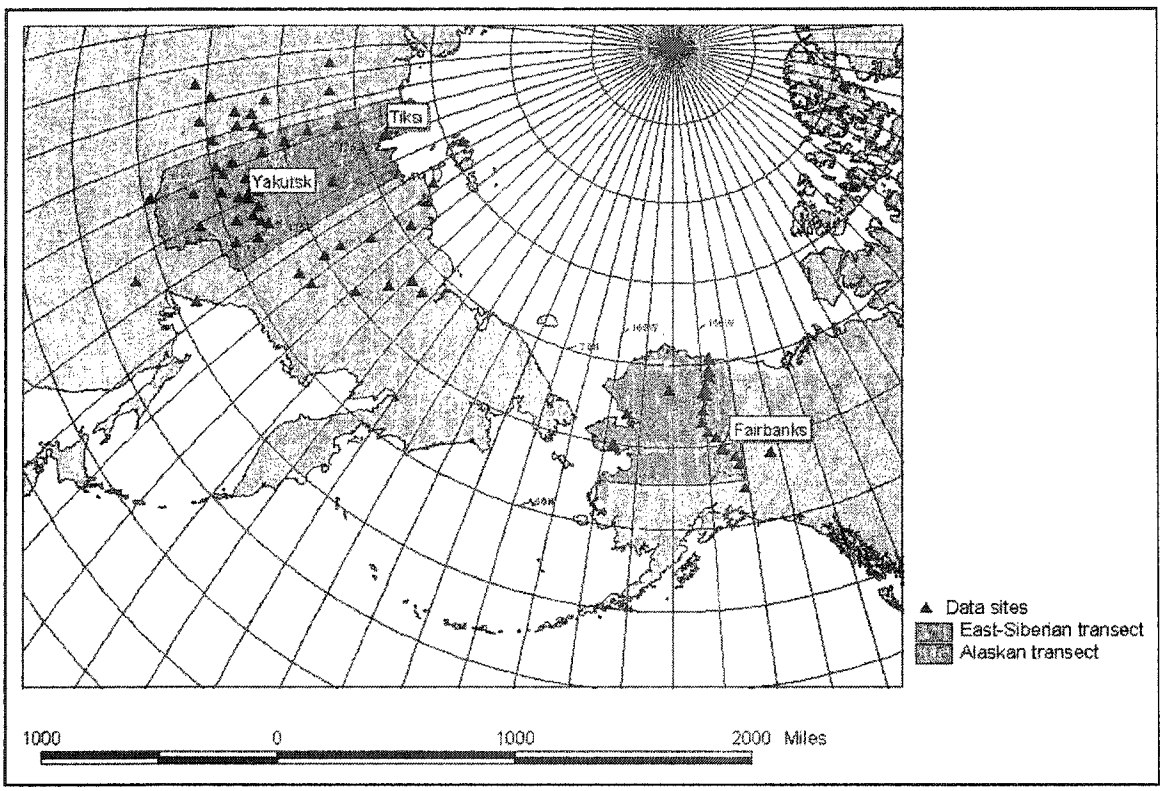

Figure 2.1: The East Siberian and the Alaskan transects

Reproduced with permission of the copyright owner. Further reproduction prohibited without permission.

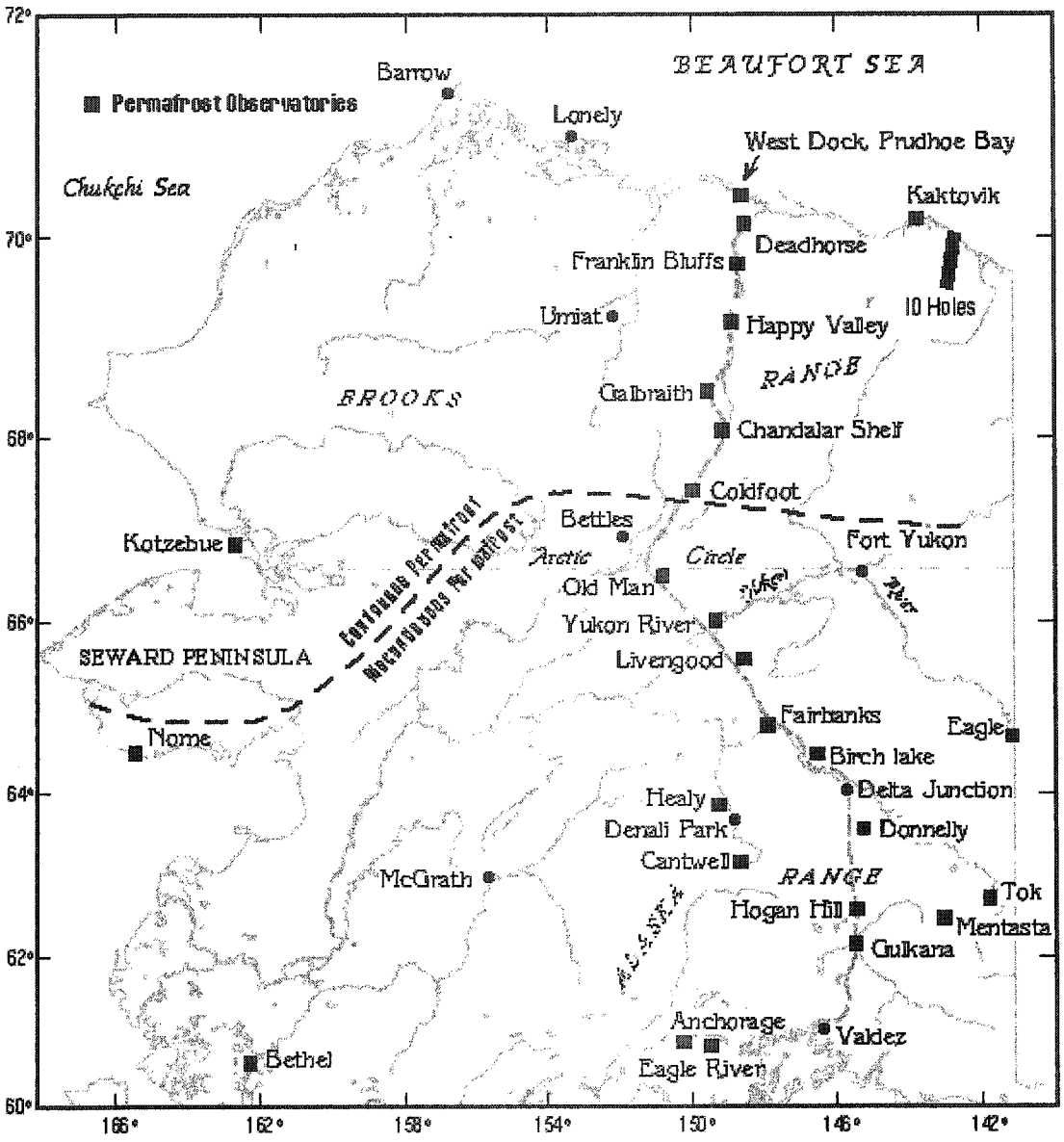

Figure 2.2: Continuous and discontinuous permafrost zones in Alaska and locations of the permafrost observatories.

Reproduced with permission of the copyright owner. Further reproduction prohibited without permission.

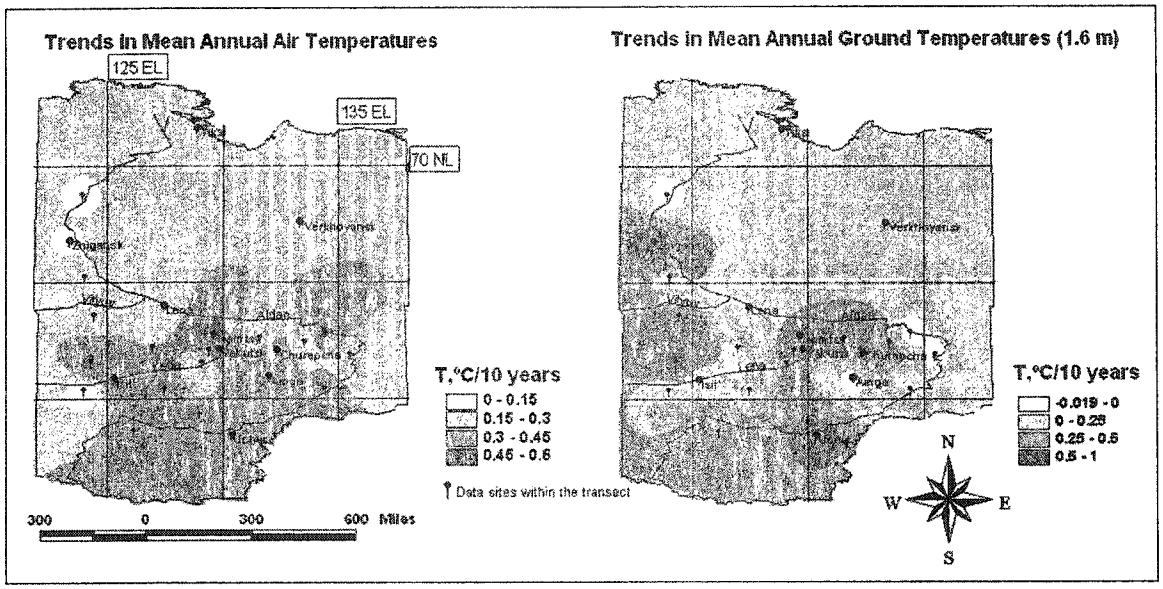

Figure 2.3: Interpolated trends in mean annual air and ground (1.6 m depth) temperatures for the period of 1956 – 1990 along the East-Siberian transect

Reproduced with permission of the copyright owner. Further reproduction prohibited without permission.

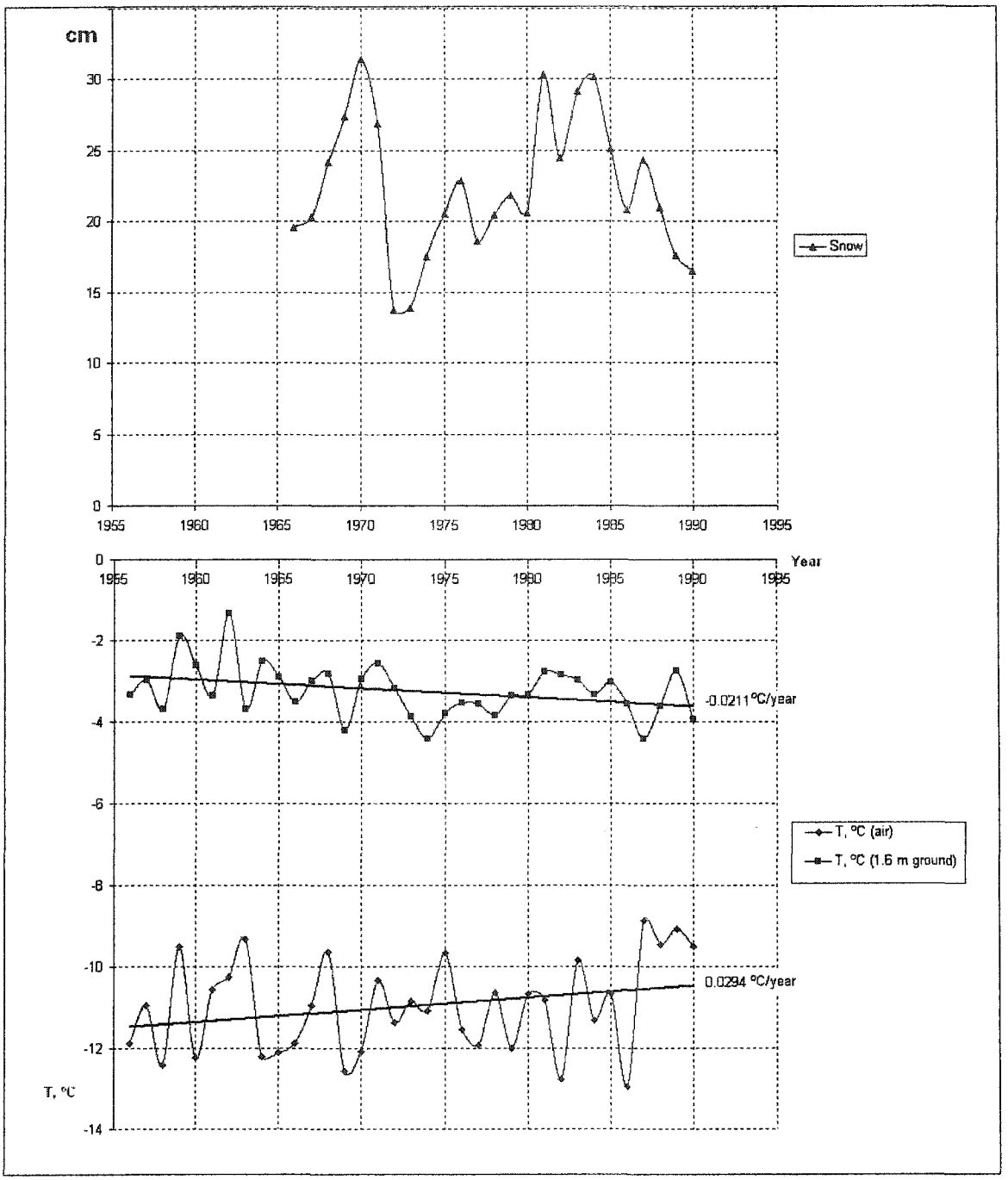

Figure 2.4: Mean winter snow thickness, mean annual air and ground (1.6 m) temperatures in Amga, one of the stations where ground temperatures were cooling.

Reproduced with permission of the copyright owner. Further reproduction prohibited without permission.

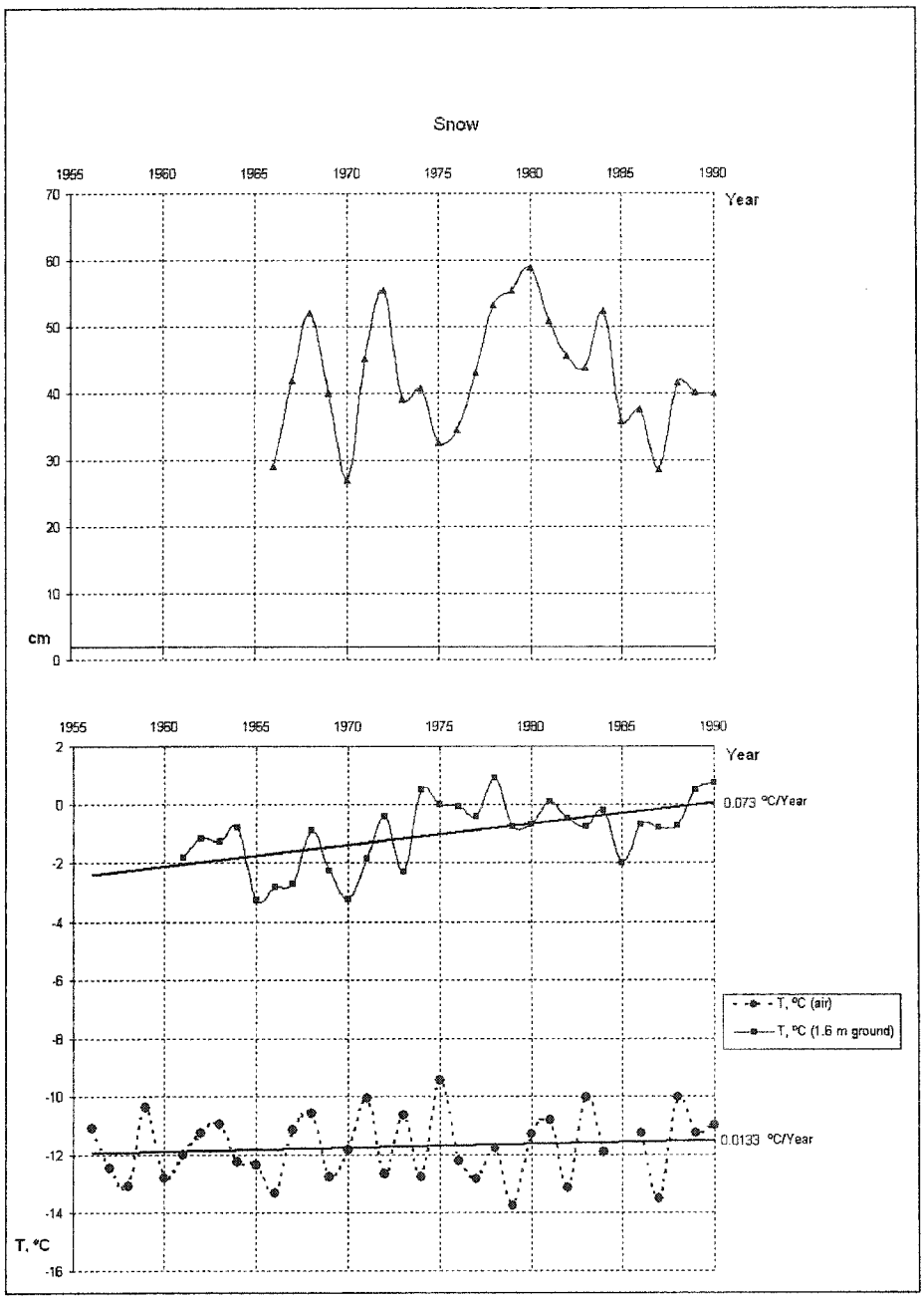

Figure 2.5: Mean winter snow thickness, mean annual air and ground (1.6 m) temperatures in Zhigansk, one of the locations where rates of ground warming exceeds the rate of warming air temperatures

Reproduced with permission of the copyright owner. Further reproduction prohibited without permission.

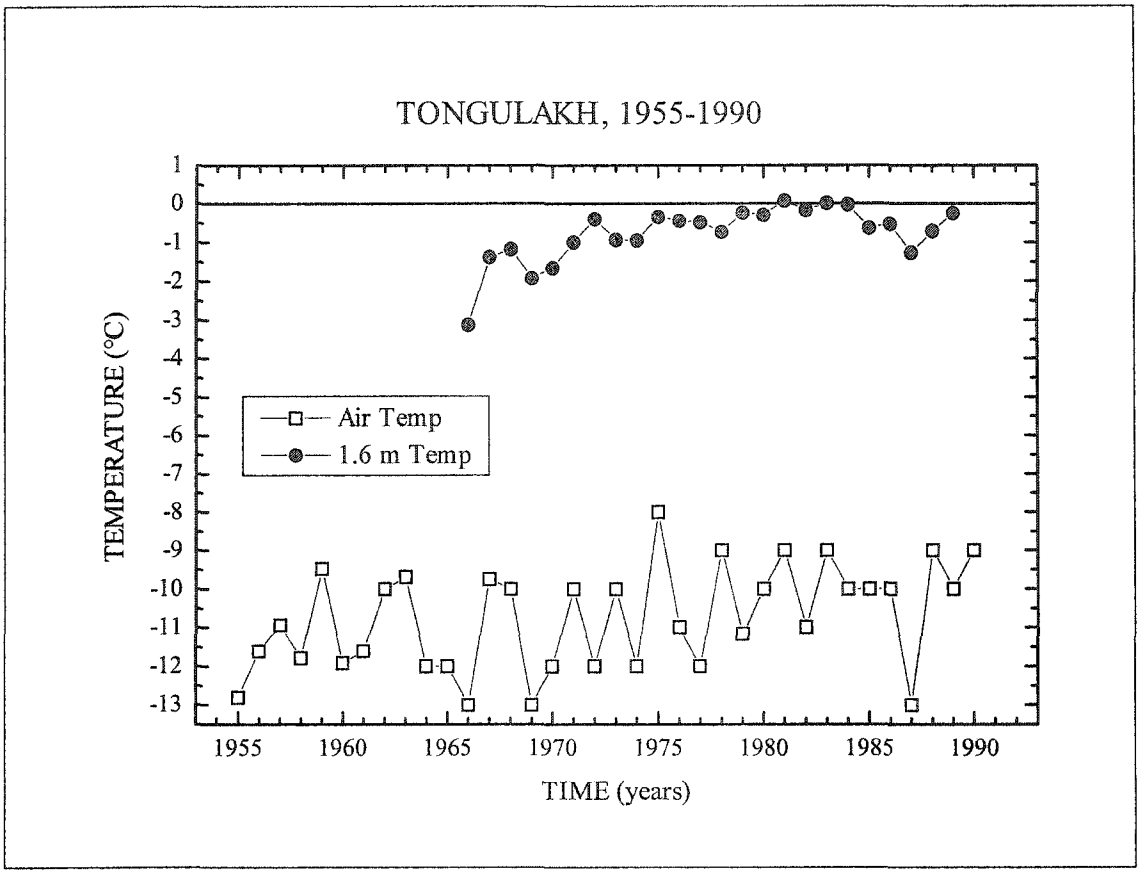

Figure 2.6: Mean annual air and ground (1.6 m) temperatures in Tongulakh, a site where permafrost degradation will occur if any more warming occurs.

Reproduced with permission of the copyright owner. Further reproduction prohibited without permission.

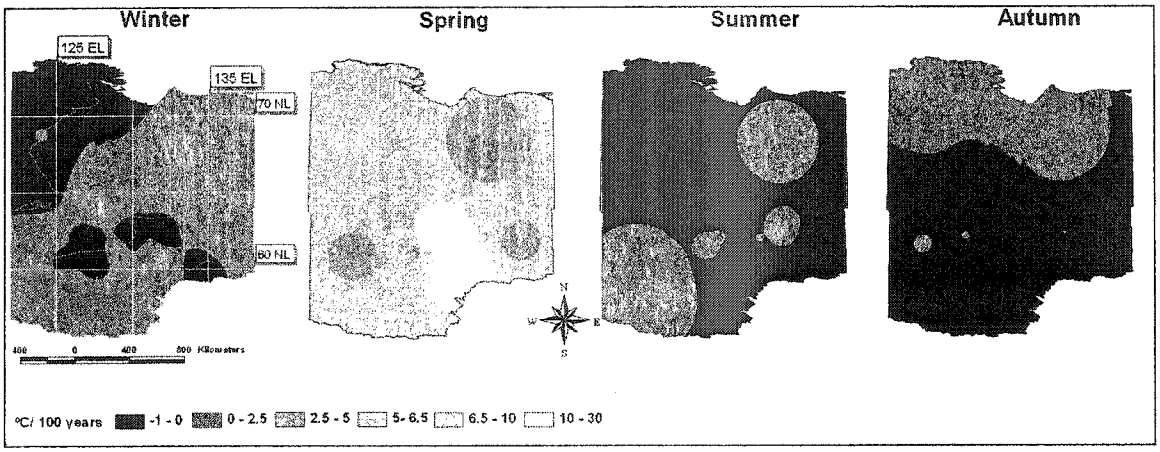

Figure 2.7.: Seasonal trends of air temperatures for the period of 1956 – 1990 along the East-Siberian transect.

Reproduced with permission of the copyright owner. Further reproduction prohibited without permission.

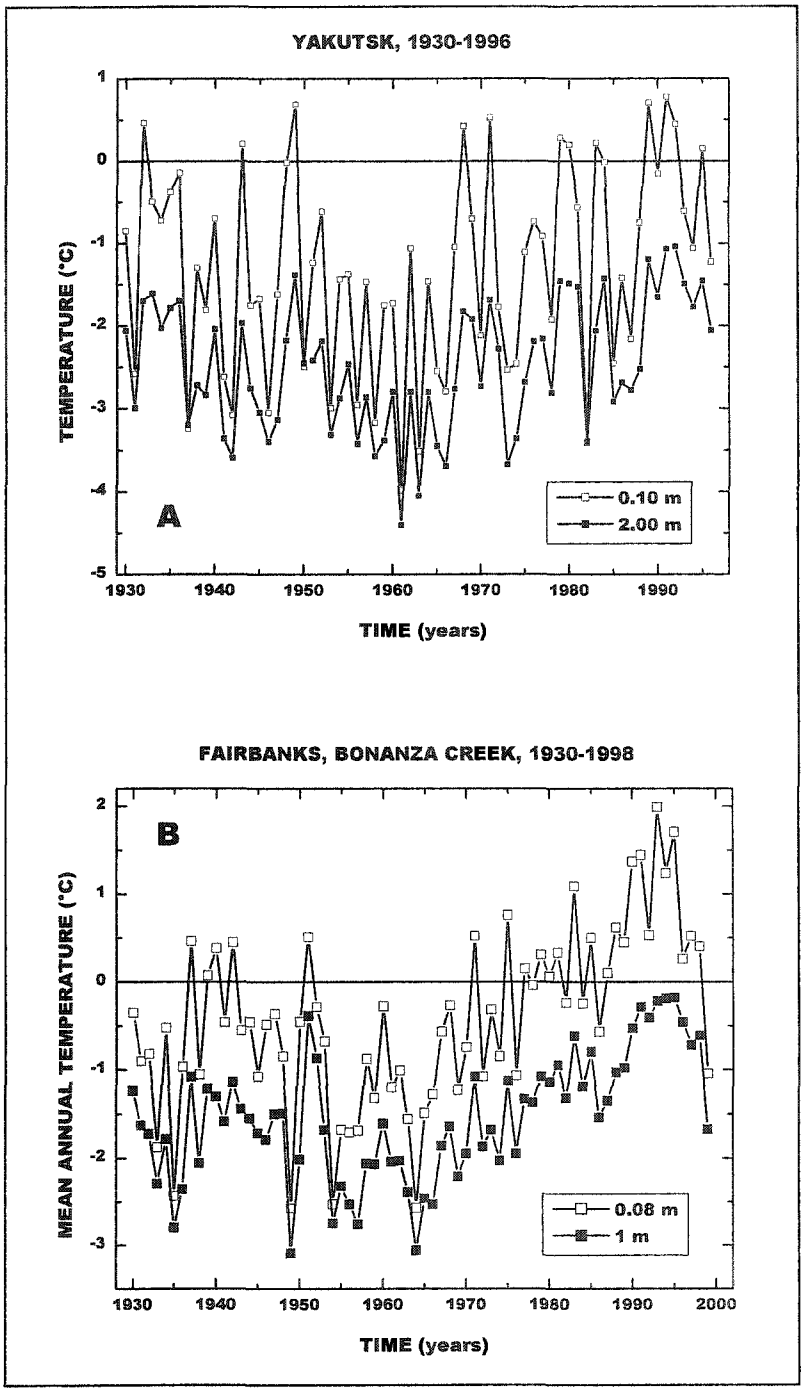

Figure 2.8: Calculated mean annual temperatures in active layer and near the permafrost surface in Yakutsk (A) and Fairbanks (B)

Reproduced with permission of the copyright owner. Further reproduction prohibited without permission.

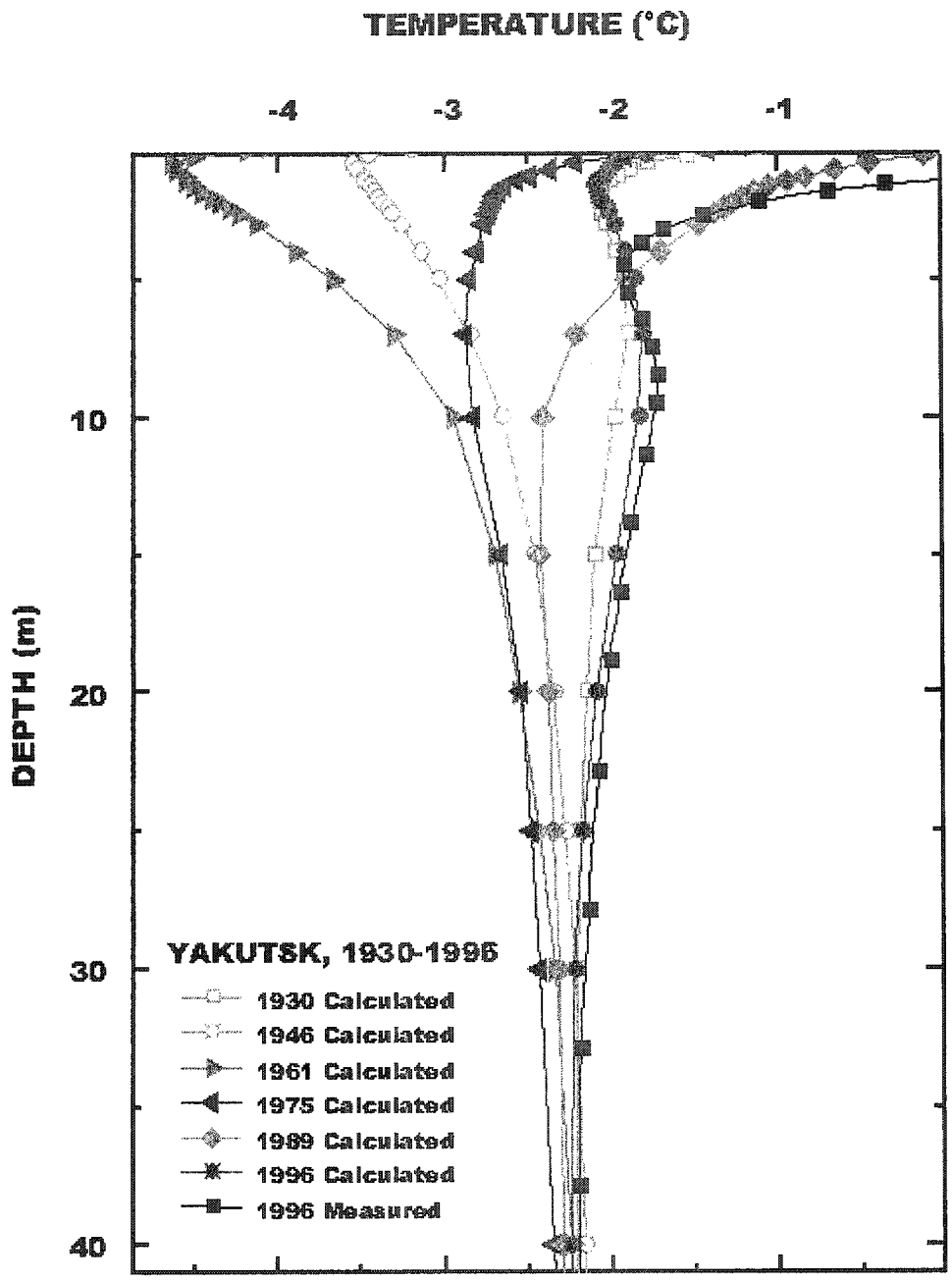

Figure 2.9: Temperature profiles in Yakutsk

Reproduced with permission of the copyright owner. Further reproduction prohibited without permission.

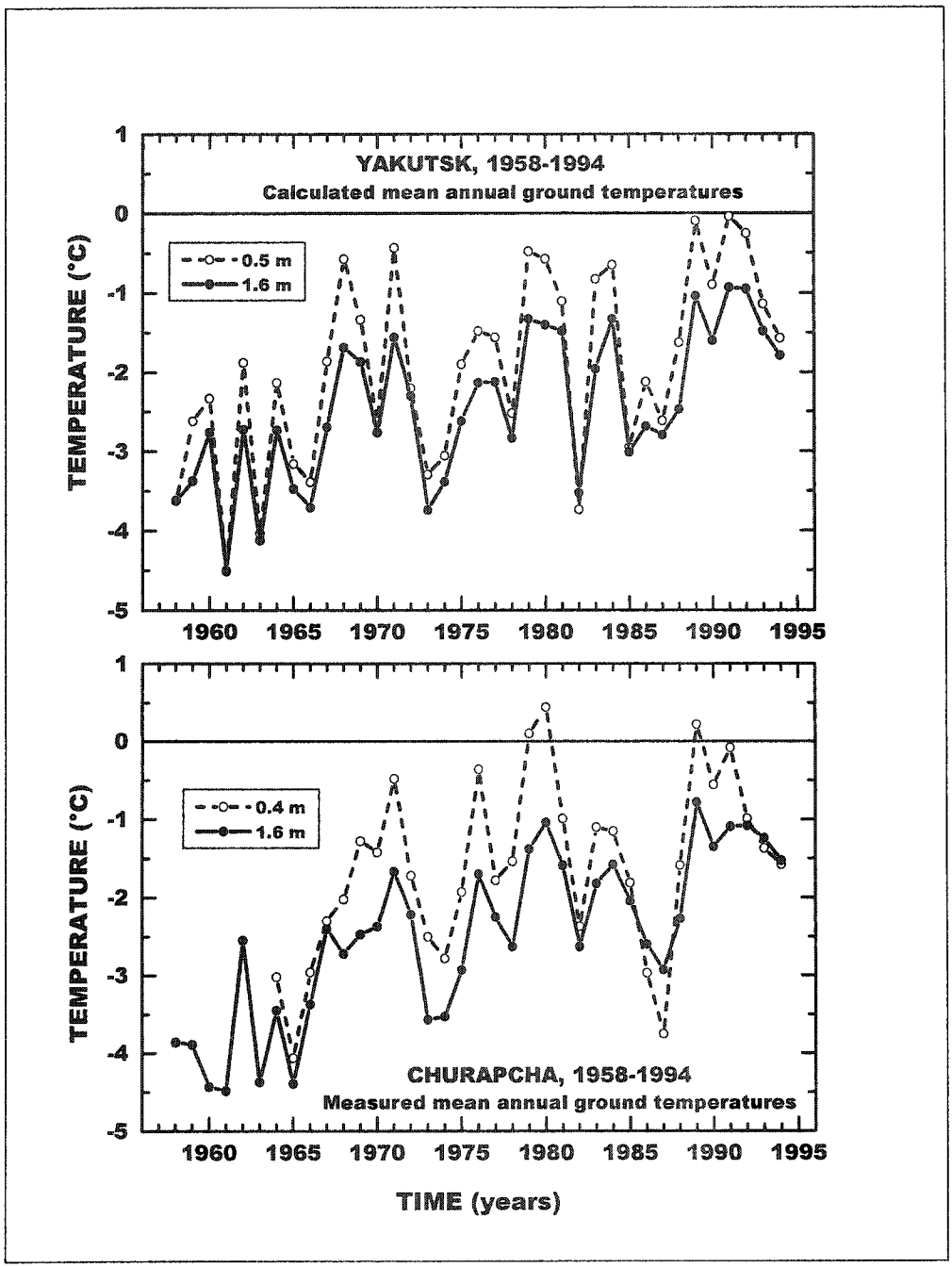

Figure 2.10: The comparison of calculated mean annual ground temperatures in Yakutsk with measured temperatures in Churapcha, about 100m from Yakutsk

Reproduced with permission of the copyright owner. Further reproduction prohibited without permission.

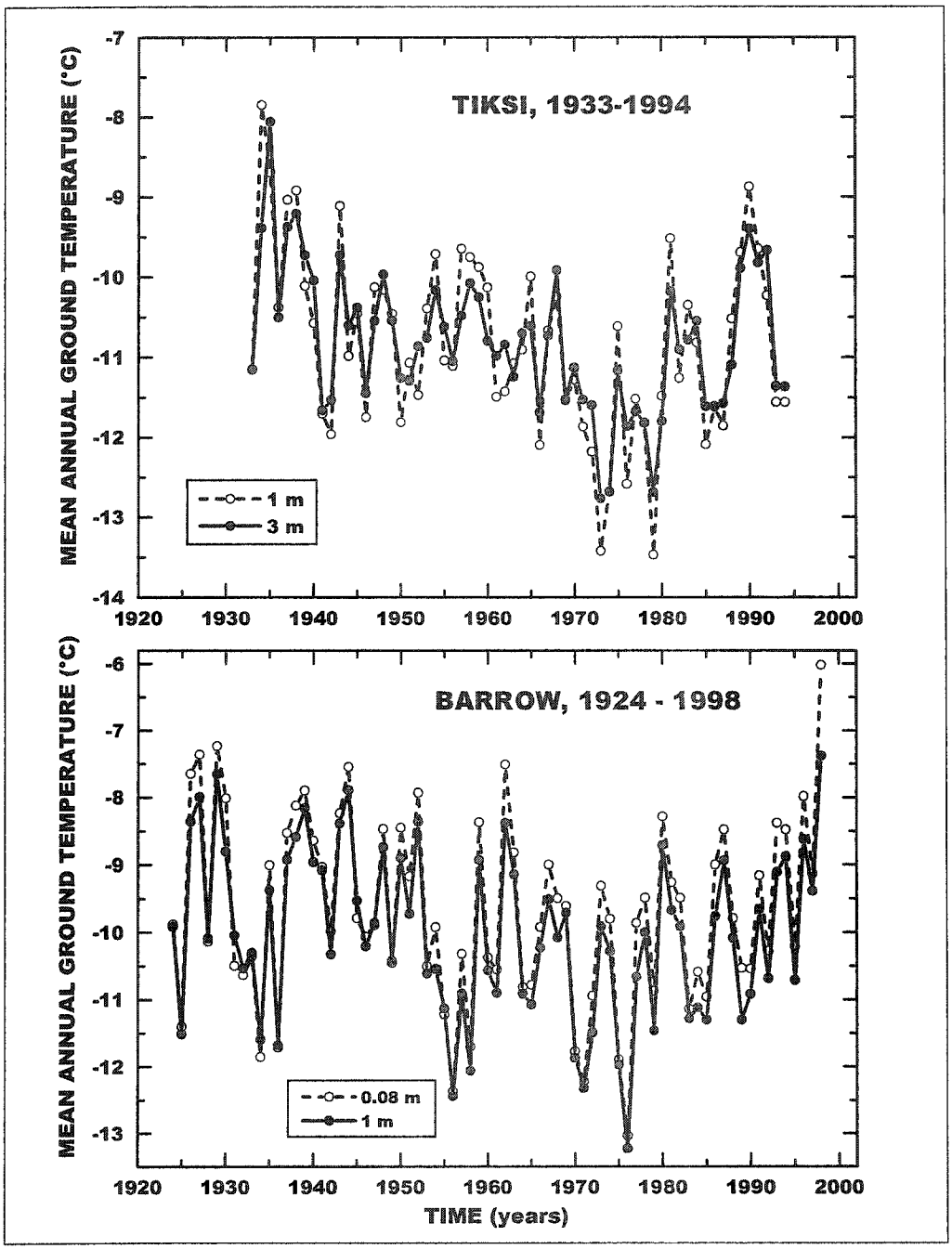

Figure 2.11: Calculated mean annual temperatures in active layer and near the permafrost surface in Tiksi and Barrow

Reproduced with permission of the copyright owner. Further reproduction prohibited without permission.

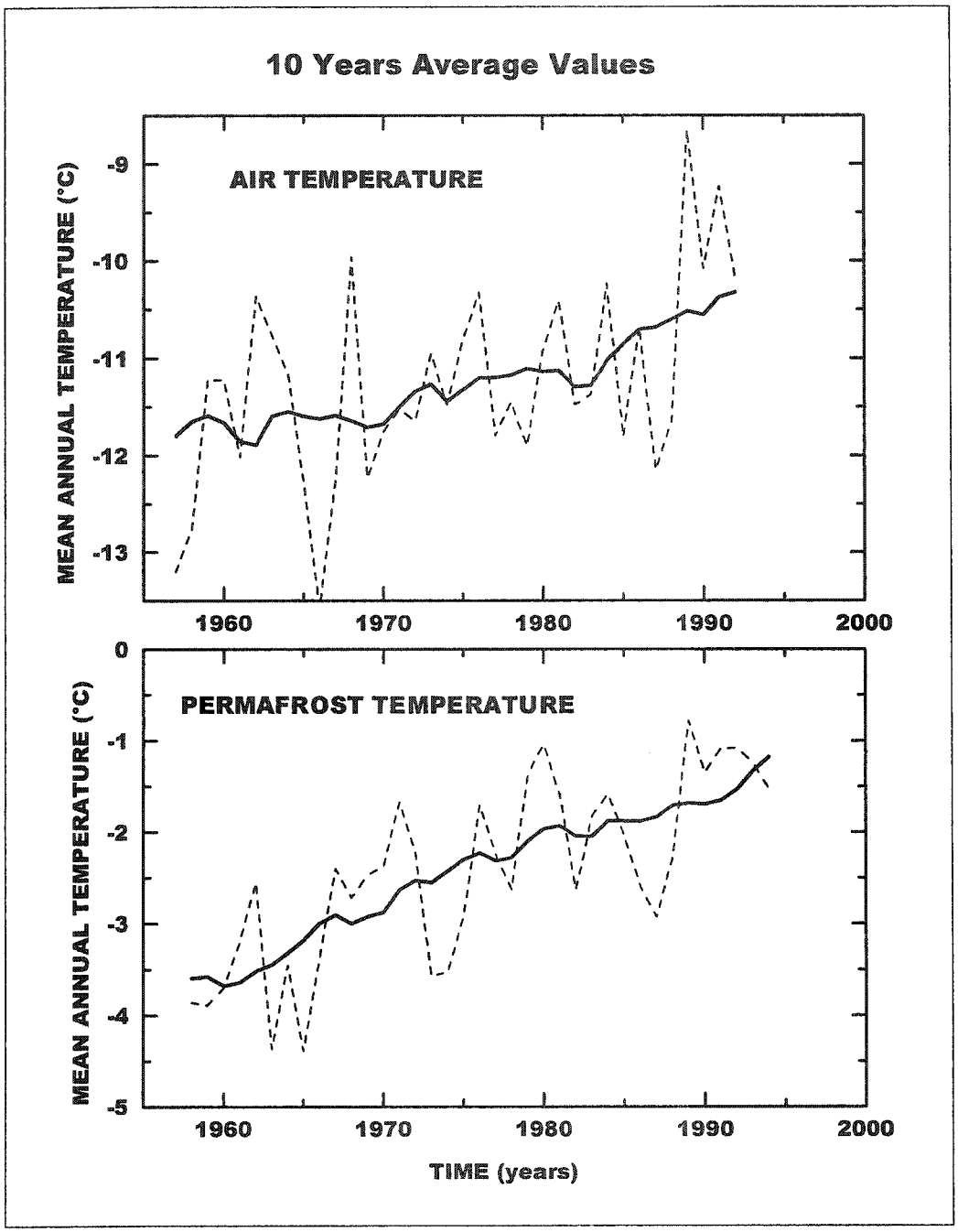

Figure 2.12: Measured mean annual air and permafrost (1.6 meters depth) temperatures (dashed line) and their 10-years running average values (solid line) at the Churapcha meteorological station, East Siberia.

Reproduced with permission of the copyright owner. Further reproduction prohibited without permission.

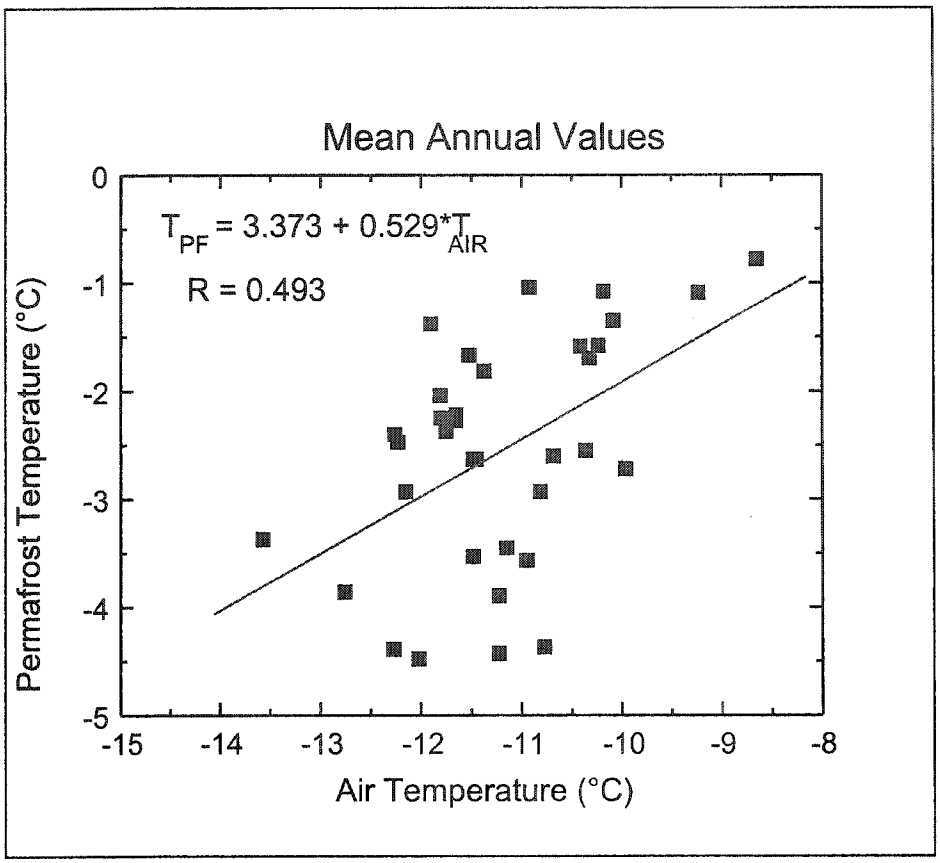

Figure 2.13: The correlation between permafrost and air temperatures in Churapcha

Reproduced with permission of the copyright owner. Further reproduction prohibited without permission.

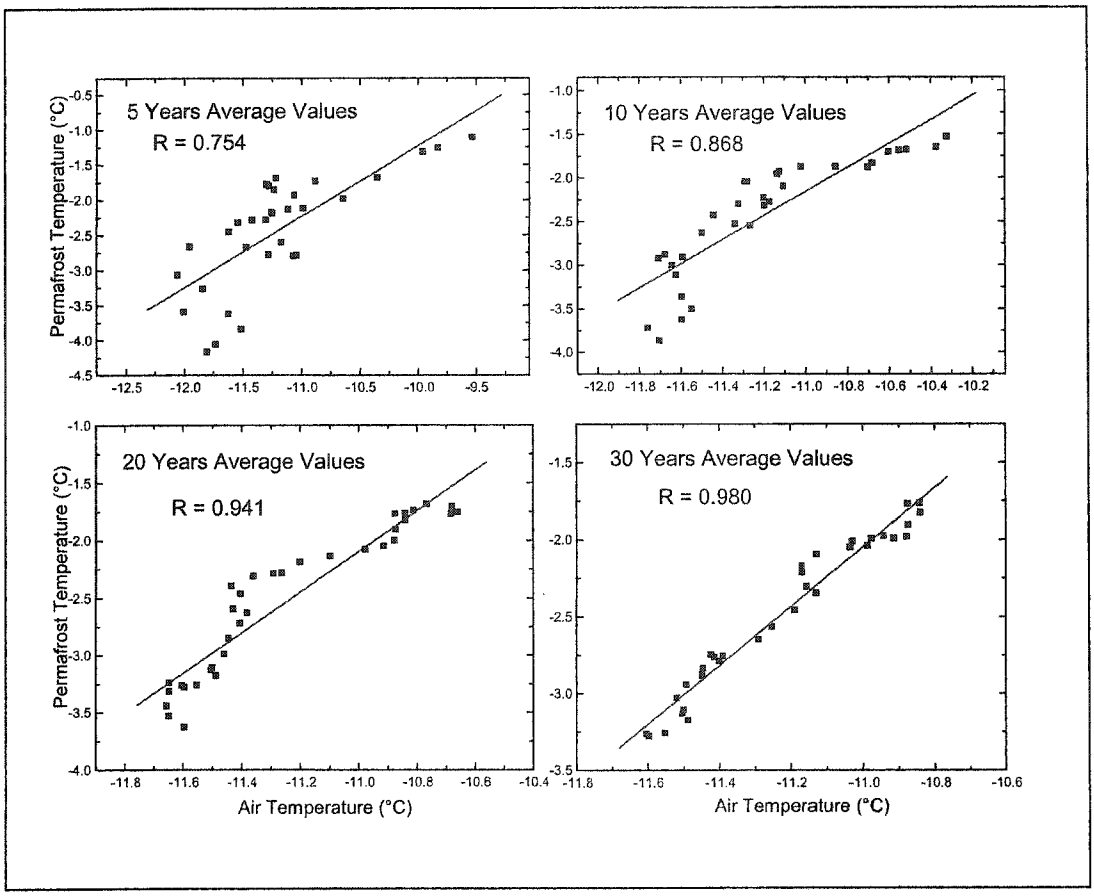

Figure 2.14: The correlation between averaged permafrost and air temperatures in Churapcha.

Reproduced with permission of the copyright owner. Further reproduction prohibited without permission.

Table 2.1: Trends in mean annual air and ground (1.6 m) temperatures within the East-Siberian transect

STATION	LATITUDE (DEGREES)	LONGITUDE (DEGREES)	PERIOD OF OBTAINED DATA (YEARS)	TREND IN AIR TEMPERATURES °C per 10 YEARS	TREND IN GROUND (1.6 m depth) TEMPERATURES °C per 10 YEARS
Kotelni	76.00	137.90	1933-2000	0.104	-
Tiksi	71.59	128.92	1956-1995	0.182	-
Dzhardzhan	68.73	124.00	1937-1992	0.130	-0.093
Verkhoyansk	67.55	133.38	1885-1994	0.290	0.043
Zhigansk	66.77	123.40	1936-1994	0.240	0.700
Bestyakhskaya Zveroferma	65.18	124.07	1959-1992	0.196	0.197
Sangar	63.97	127.47	1936-1994	0.224	0.054
Viluysk	63.77	121.62	1963-1994	0.476	0.540
Hatrik-Homo	63.57	124.50	1957-1991	0.255	-
Verkhneviluysk	63.27	120.19	1958-1990	0.509	0.710
Krest-Khal'dzhai	62.82	134.43	1960-1992	0.477	-0.186
Namtsy	62.73	129.67	1964-1994	0.590	0.312
Borogontsy	62.57	131.62	1959-1989	0.121	0.240
Ytyk-Kel'	62.37	133.55	1957-1994	0.173	0.613
Yakutsk	62.10	129.80	1882-1996	0.360	-
Churapcha	62.02	132.36	1936-1992	0.428	0.606
Okhotskiy Perevoz	61.87	135.50	1938-1992	0.200	-0.051
Tongulakh	61.55	124.33	1955-1990	0.517	0.650
Pokrovsk	61.48	129.15	1957-1994	0.190	-
Amga	60.90	131.98	1936-1994	0.349	-0.189
Isit'	60.82	125.32	1936-1994	0.362	0.155
Olekminsk	60.40	120.42	1882-1995	0.065	-
Ust'-Maya	60.38	134.45	1897-1992	0.344	0.147
Dobrolet	60.37	127.50	1959-1992	0.340	0.159
Saniyakhtat	60.35	124.04	1959-1994	-0.035 *	0.063
Tommot	58.58	126.16	1957-1990	0.408	0.440
Uchur	58.44	130.37	1957-1990	0.329	0.780
Nagorny	55.58	124.53	1955-1990	0.356	-

Reproduced with permission of the copyright owner. Further reproduction prohibited without permission.

Table 2.2: Trends in mean annual air temperatures within the Alaskan transect

STATION	LATITUDE (DEGREES)	LONGITUDE (DEGREES)	PERIOD OF DATA (YEARS)	TREND IN AIR TEMPERATURES °C per 10 YEARS
Barrow	71.18	156.47	1949-2001	0.316
Umiat	69.22	152.08	1949-2000	0.243
Bettles	66.55	151.31	1951-2001	0.597
Fairbanks	64.50	147.52	1949-2001	0.46
Eagle	64.46	141.12	1949-2001	0.279
Nome	64.30	165.26	1949-2001	0.393
Gakona 1N	62.19	145.18	1971-1989	0.316
Talkeetna	62.18	150.06	1949-2001	0.464
Glenhallen	62.07	145.32	1966-2000	0.469
Bethel	60.47	161.43	1949-2001	0.445
Cordova	60.30	145.30	1949-2001	0.334

Reproduced with permission of the copyright owner. Further reproduction prohibited without permission.

CHAPTER 3. A MODEL FOR REGIONAL-SCALE ESTIMATIONS OF TEMPORAL AND SPATIAL VARIABILITY OF THE ACTIVE LAYER THICKNESS AND MEAN ANNUAL GROUND TEMPERATURES *

ABSTRACT

High latitude ecosystems where the mean annual ground surface temperature is around or below 0°C are highly sensitive to global warming. This is largely because these regions contain vast areas of permafrost, which begins to thaw when the mean annual temperature rises above freezing. At the Geophysical Institute Permafrost Lab we developed a new GIS model to estimate the long-term response of permafrost to changes in climate. An analytical approach is used for calculating both the active layer thickness and the mean annual ground temperatures. Calibration of the model has shown a less than 33% relative error for mean annual ground temperatures and active layer thickness calculations. A spatial statistical analysis of the data from 32 sites in Siberia indicated a confidence level of 75% to have a deviation between measured and calculated mean annual ground temperatures of 0.2 -0.4°C. A detailed analysis has been performed for two regional transects in Alaska and Eastern Siberia which has validated the use of the model. This project has been a successful contribution to the Arctic Climate Impact Assessment project.

---

* Accepted under the same name with authors Tatiana S. Sazonova and Vladimir E. Romanovsky to Permafrost and Periglacial Processes.

Reproduced with permission of the copyright owner. Further reproduction prohibited without permission.

INTRODUCTION

There is an immediate need to evaluate climate dynamics and the respective impact on high-latitude ecosystems. The effects of global climate change are expected to be amplified in the Arctic, where a slight increase in mean annual air temperature can result in a change of state for large regions of frozen ground (Kattenberg et al., 1996; Anisimov et al., 2001).

Permafrost regions occupy about one quarter of the Earth's land surface (Pewe 1983; Zhang et al., 2000). The changing properties of permafrost play an important role in driving the ecosystem balance, and effecting the carbon and water cycles. Man made structures built on or near ice-rich permafrost have been known to be severely damaged by thaw-induced settling of the ground, which will accelerate if mean annual temperatures continue to rise (Osterkamp et al., 1997; Smith and Burgess, 1999). The carbon and water cycles can be dramatically affected by an increased thickness of the active layer which thaws seasonally.

The purpose of this research was to develop a model which can be used to evaluate active layer thickness and mean annual ground temperatures over large regions (such as the East-Siberian and Alaskan transects of International Geosphere-Biosphere Program (IGBP)). Sufficient accuracy and special resolution is required so that it can be applied effectively to current climatological and ecological models. Our model, the Geophysical Institute Permafrost Lab (GIPL) model was designed specifically to assess the effect of a changing climate on permafrost. The results have been used in the Arctic

Reproduced with permission of the copyright owner. Further reproduction prohibited without permission.

Climate Impact Assessment (ACIA) program (www.acia.uaf.edu), which was designed to investigate the various impacts of the future climate change on timescales of up to 100 years.

A transect approach is considered to be the most effective method for modeling permafrost dynamics because of problems with collecting data over large high-latitude regions. This method analyzes permafrost dynamics along several latitudinal transects where different types of environmental conditions exist. After analysis of these transects is complete, they can be used to interpolate the permafrost dynamics over other temporal and spatial domains leading eventually to circum-polar coverage.

The two transects we have analyzed differ significantly in the information available on climate, vegetation, and soil properties (Figure 3.1). Despite these differences, previous investigations and point by point comparisons of different sites have shown that variations in ground temperatures within the transects are consistent (Shender, et al., 1999; Romanovsky et al., 2001). The climatic parameters we used to evaluate permafrost dynamics in the future were provided by the ACIA program and were output from six Global Climate Models (GCMs).

A number of algorithms have been developed to determine the active layer thickness and the permafrost distribution. One such approach, based on Kudryavtsev's method, was developed to provide a spatially distributed analytical model that estimates the maximum annual thaw depth (active layer thickness). In this approach, Geographical Information Systems (GIS) were used to incorporate climate records, field data and digital mapping techniques to estimate active-layer thickness (Shiklomanov and Nelson,

Reproduced with permission of the copyright owner. Further reproduction prohibited without permission.

1999). This analysis was applied over a 22,300 sq. km. area in the Kuparuk River basin, north-central Alaska.

The introduction of GCMs made it possible to evaluate permafrost dynamics on a global scale. Anisimov and Nelson (1997) used the frost index (Nelson and Outcalt, 1987), coupled with three GCMs to develop the first GCM-based assessment of permafrost dynamics over the Northern Hemisphere. The results indicated that a large, nearly circumpolar zone of relict permafrost would develop by the end of the 21st century.

The most recent application of GCMs to determine permafrost dynamics has been done by Stendel and Christensen (2002). They calculated active layer thickness (ALT) using the modified Stefan's equation. The results of this work indicated that the ALT will increase by 30-40% by the end of the 21st century.

The models developed by Anisimov and Nelson, and Stendel and Christensen have a special resolution of about 2.5-5 degrees of latitude/longitude. This resolution does not allow for complex relief and vegetation patterns, and is a rough approximation for applications in ecosystem modeling and infrastructure risk assessment. For the purposes of this project, it was determined that a special resolution of 0.5 x 0.5 degrees would be appropriate for modeling on a regional scale. It should be mentioned that the authors never aimed at creating a highly accurate model, which is not feasible with the resolution scale of 0.5 x 0.5 degrees latitude/longitude. It was most important to create a physically-based model which will describe the temporal dynamic well.

Reproduced with permission of the copyright owner. Further reproduction prohibited without permission.

GIPL allows for the calculation of ALT and mean annual ground temperatures at the bottom of the active layer (MAGT). For the areas with permafrost, this temperature is the same as mean annual temperature at the permafrost table. Where permafrost is absent, MAGT is the mean annual temperature at the bottom of seasonally frozen layer. The MAGT is important because it reflects the existence and thermal stability of the permafrost. When MAGT becomes positive (above 0°C), the winter freezing front does not reach the surface of permafrost (permafrost table) by the end of cold season, resulting in a talik formation and the start of permafrost degradation. The permafrost degradation could also start with MAGT is still below 0°C. If the increasing ALT reaches the ice horizon, or the ground layer with high ice content, the ice begins to melt and the ground subsides. Surface water will flow into the deepening trough and can form pools and lakes. This new presence of water on the surface will help thermal energy to penetrate the ground faster, resulting in an acceleration of the permafrost degradation. In winter, more snow will settle into the deepening trough, which will additionally insulate the ground, resulting in an increased MAGT. This will prevent the winter freeze from penetrating to the permafrost table, further accelerating degradation (Kudryavtsev et al., 1974; Yershov, 1998). Because of these effects, once permafrost begins to thaw and a significant settlement of the ground surface occurred, the process would continue even through colder winters, which would otherwise be expected to resist the degradation process.

The GIPL model focuses on calculation of the ALT and MAGT, but does not calculate the depth of permafrost thawing from the surface. Other models need to be

Reproduced with permission of the copyright owner. Further reproduction prohibited without permission.

used to calculate the timing and dynamics of permafrost degradation (Kudryavtsev et al., 1974; Kane et al., 1991; Hinzman et al., 1997). The cross of the temperature threshold will have a crucial effect on the northern ecosystems through changes in thermal and hydrological conditions in soils, and can effect changes in the carbon cycle on a global scale.

This paper describes the basic concept and structure of the GIPL model. The calibration of the model and evaluation of the model's performance will be discussed to assess possible uncertainties associated with data handling and processing.

DESCRIPTION OF THE GIPL MODEL

The GIPL model consists of two parts: The GIS approach allows visual analysis of the spatial distribution of various geographical parameters. With this approach, the results from analytical or numerical models can be applied to evaluate permafrost parameters over large geographic areas. The second part of the model is an analytical solution which is used for the evaluation of the major permafrost properties, such as MAGT and the ALT.

Throughout the years, simplified analytical solutions for the ALT have been applied for structural engineering and other practical purposes. Most of these methods have been based on the Stefan solutions, and they do not yield a good level of accuracy (Romanovsky and Osterkamp, 1997). Two factors played the primary role in choosing a method for calculating the ALT: the model should be relatively simple and have a reasonable computation time, and must have an acceptable degree of accuracy. It was

Reproduced with permission of the copyright owner. Further reproduction prohibited without permission.

determined that the best method for computation of the ALT and MAGTs was a modified Kudryavtsev's approach (mKA) (Romanovsky and Osterkamp, 1997). The mKA approach is the core of the GIPL model.

In their work on the active layer thickness distribution, Shiklomanov, Nelson and Anisimov (1997) demonstrated that Kudryavtsev's approach works well. The research showed that the approach allows for consideration of variations in conditions such as snow cover and vegetation (Shiklomanov and Nelson, 1999). This approach had several shortcomings due to factors such as neglect of unfrozen water, and treating the ground as being homogeneous. Still, the method has shown to allow the estimation of permafrost temperatures to within 0.5°C.

Modified Kudryavtsev's Approach (mKA)

Kudryavtsev's approach is chosen because it effectively accounts for the effects of snow cover, vegetation, soil moisture, thermal properties, and regional climate variations. The approach was developed to find the MAGTs and the ALT while taking into account major geological and geographical factors, while assuming a periodical, steady-state temperature regime (Kudryavtsev et al., 1974).

The daylight surface (ground or vegetation surface during the summer and snow surface during the winter) temperature is assumed to behave in accordance with: $T(t) = T_a + A_a \sin\left(\frac{2\pi}{\tau}t\right)$, where A_a is the seasonal amplitude of air temperatures °C, T_a is the mean annual air temperature, τ is the period which is equivalent to one year, and t is time. The ground is assumed to have a homogeneous thermal conductivity. The

Reproduced with permission of the copyright owner. Further reproduction prohibited without permission.

effects of geothermal heat flux are ignored because it is considered to have a minimal contribution to the MAGT and ALT values.

Kudryavtsev introduced the idea of applying the Fourier temperature wave propagation theory on a medium with phase transitions, such as frozen ground (Tikhonov and Samarsky, 1966). Application of this approach resulted in the discovery of the thermal offset and an understanding of the laws that govern the dynamics of the ground thermal regime. These discoveries led to an understanding the effects that the thermophysical properties of the ground have upon the MAGTs and ALT, and how periodically varying climatic parameters effect permafrost dynamics. The output parameters of this method are given as annual averages. Input and output parameters are listed in Tables 3.1 and 3.2.

Kudryavtsevs's approach treats the complex system considering air, snow cover, surface vegetation, and active layer, as a set of individual layers with different thermal properties. In the regions of Alaska and East-Siberia that were analyzed, surface vegetation consists of lichens, grass, and moss (sphagnum or feather mosses) (Feldman et al., 1988; Brown and Kreig, 1983). The upper level of vegetation which consists of trees and shrubs (vegetation taller than 50 cm) was not considered in the computation. This upper level vegetation affects the thickness and density of the snow cover, along with the amount of solar radiation which is incident on the ground surface. In our study we considered only low-level of vegetation (surface vegetation) that is less than 0.5 meter high, because the information about higher vegetation such as trees and tall shrubs is already incorporated into the monthly surface air temperature data, which were used as

Reproduced with permission of the copyright owner. Further reproduction prohibited without permission.

input data in the model. Also, effective methods for calculating the thermal effects of vegetation are still under development (Potter et al., 2001; Friend et al., 1997).

Evaluation of the snow cover influence

Snow cover plays an important role in heat exchange processes between the surface of the ground and the atmosphere. Snow cover influence is complex, working as an insulator for the ground throughout the winter, effectively increasing the MAGT, but when snow remains on the ground after air temperatures rise above freezing, the seasonal thawing can be delayed.

The warming effect of the snow cover has been calculated using approximate formulas derived by Romanovsky (1987) and Lachenbruch (1959), which incorporate ground properties, vegetation cover, and their respective effect on heat turnovers through the snow. Heat turnovers are defined as the quantity of incident heat (during the heating period), or out going heat (during the cooling period) throughout the media over a given time interval (usually half year increments). So that the heat transport is $Q = \int_{t_1}^{t_2} q(t)dt$, where t_1 and t_2 are the times when the regime changes from the heating to cooling periods, or the cooling to heating periods, and $q(t)$ is the heat flux through the ground surface as a function of time.

The total thermal effect of snow cover on the seasonal amplitude of air temperatures ΔA_{sn} and mean annual air temperatures ΔT_{sn} is calculated as follows:

Reproduced with permission of the copyright owner. Further reproduction prohibited without permission.

(1-2) $\Delta A_{sn} = \Delta A \frac{\tau_1}{\tau}$ and $\Delta T_{sn} = \frac{2}{\pi} \Delta A_{sn}$, where τ is one year period, τ_1 - is the duration of winter period and

(3) $\Delta A = A_a (1 - \frac{1+\mu}{\sqrt{s}})$

Where s is the mean thermal effect of the snow cover, and is computed by:

(4) $s = e^{2H_{sn}\sqrt{\frac{\pi C_{sn}}{\tau K_{sn}}}} + 2\mu \cos\left(2H_{sn}\sqrt{\frac{\pi C_{sn}}{\tau K_{sn}}}\right) + \mu^2 e^{-2H_{sn}\sqrt{\frac{\pi C_{sn}}{\tau K_{sn}}}}$

μ is a dimensionless parameter that characterizes the contrast in the thermal properties between snow cover and the underlying material (such as vegetation or different types of soils), and reflects the influence of the underlying material on the insulating effect of snow cover. H_{sn} is the winter-averaged snow cover thickness, C_{sn} is the average snow heat capacity, and K_{sn} is the average snow thermal conductivity. μ can range from -1 to +1.

(5) $\mu = \frac{\sqrt{K_{sn}C_{sn}} - \sqrt{K_f C_{ef}}}{\sqrt{K_{sn}C_{sn}} + \sqrt{K_f C_{ef}}}$

where K_f is the frozen soil thermal conductivity and

(6) $C_{ef} = C_f \frac{\alpha - \beta}{(\alpha - \beta) - \ln\frac{\alpha+1}{\beta+1}}$, where C_f is the frozen soil heat capacity.

The parameter C_{ef} is the effective heat capacity of the substrate below the snow cover. C_{ef} was derived taking into account the heat turnover. The two dimensionless

Reproduced with permission of the copyright owner. Further reproduction prohibited without permission.

variables α and β are analogous to the Stefan number (which is the ratio of the sensible and latent heats) in the Neumann equation (Zarling, 1987)

(7) $\alpha = \frac{2A_a C_f}{L}$, (8) $\beta = \frac{2|T_a|C_f}{L}$, where L is the volumetric latent heat of the water fusion in the ground.

The result is that the mean annual temperature T_{vg} and the seasonal amplitude of temperatures A_{vg} on top of the vegetation cover are: $T_{vg} = T_a + \Delta T_{sn}$ and $A_{vg} = A_a - \Delta A_{sn}$

The thermal effects of surface vegetation cover

In our studies, only conductive heat transfer through the surface vegetation (lichens, moss, and grasses) was considered, even though this mechanism is a small part of the vegetation – ground interaction. The rate of heat turnovers between the ground and atmosphere have been shown to have a strong dependence on vegetation cover. In summer, surface vegetation prevents solar radiation from penetrating into the ground and warming it. In wintertime, surface vegetation acts as an insulator and keeps heat in the ground.

For the purposes of the GIPL model, we assumed that the thermal conductivity of moss is 0.2 W/(m*K) (Kudryavtsev, 1974) and for grass it is 0.3-0.5 W/(m*K). Heat capacities of moss and grass are about 2500-3000 kJ/m^3. The vegetation effect on the ground thermal regime was calculated using an algorithm suggested by Yershov (Yershov, 1998):

$$\tau_1 = \tau \cdot \left(0.5 - \frac{1}{\pi}\arcsin\frac{T_a}{A_a}\right), \quad \tau_2 = \tau - \tau_1,$$

Reproduced with permission of the copyright owner. Further reproduction prohibited without permission.

Where τ_1 and τ_2 are the winter cooling and the summer warming periods respectively. The vegetation cover thermal effect for winter ΔA_1, and for summer ΔA_2 are:

$$\Delta A_1 = \left(A_{vg} - T_{vg}\right) \cdot \left(1 - e^{-H_{vg}\sqrt{\frac{\pi}{D_{vf} 2\tau_1}}}\right),$$

$$\Delta A_2 = \left(A_a - T_a\right) \cdot \left(1 - e^{-H_{vg}\sqrt{\frac{\pi}{D_{vt} 2\tau_2}}}\right).$$

Average thermal effect for seasonal amplitude of temperature variations ΔA_v and for mean annual temperature ΔT_v are calculated from:

$$\Delta A_v = \frac{\Delta A_1 \tau_1 + \Delta A_2 \tau_2}{\tau}, \qquad \Delta T_v = \frac{\Delta A_1 \tau_1 - \Delta A_2 \tau_2}{\tau} \frac{2}{\pi}$$

From this result we can estimate the temperature on the surface of the ground T_{gs} and the seasonal amplitude of temperature variations at the ground surface A_{gs} as:

$$T_{gs} = T_{vg} + \Delta T_v, \text{ and } A_{gs} = A_{vg} - \Delta A_v$$

Calculating the Thermal Offset and MAGT at the Bottom of the Active Layer.

The seasonal freezing and thawing cycles cause changes in the thermal properties of soils within the active layer. Typically, this will lead to a decrease in MAGTs with depth. The thermal offset is defined as the difference between the mean annual temperature on the surface of the ground and the MAGT on the bottom of the active layer (Kudryavtsev et al., 1974; Goodrich, 1978; Burn and Smith, 1988). The thermal offset

Reproduced with permission of the copyright owner. Further reproduction prohibited without permission.

depends on soil moisture content and thermal properties, and has the most pronounced effect within the peat layer.

The analytical equation to estimate the thermal offset ΔT_k was given by Kudryavtsev (1981) (no derivation was published), and was formally derived by Romanovsky (Romanovsky and Osterkamp, 1995).

The equation for thermal offset gives:

$$\Delta T_k = I_t (K_t/K_f - 1)/\tau \qquad \text{for } K_t I_t \le K_f I_f \qquad (9)$$

and

$$\Delta T_k = I_f (1 - K_f/K_t)/\tau \qquad \text{for } K_t I_t > K_f I_f \qquad (10)$$

Where I_t and I_f are thawing and freezing indices at the ground surface. The freezing index is the absolute value of the sum of all negative mean daily ground surface temperatures (below 0°C) during the calendar year. Equation 9 is for a seasonally thawed active layer that has permafrost underneath, and equation 10 is for a seasonally frozen active layer that is on top of unfrozen ground. Seasonal temperature variation at the surface of the ground can be expressed by the harmonic function:

$T(t) = T_{gs} + A_{gs} \sin\left(\frac{2\pi}{\tau} t\right)$, and T_{ps} can be estimated by the formula

$$T_{ps} = \frac{0.5T_{gs}\left(K_f + K_t\right) + A_{gs}\frac{K_t - K_f}{\pi}\left[\frac{T_{gs}}{A_{gs}}\arcsin\frac{T_{gs}}{A_{gs}} + \sqrt{1 - \frac{T_{gs}^2}{A_{gs}^2}}\right]}{K^*}, \text{ where}$$

$$K^* = \begin{cases} K_f, if \quad numerator < 0 \\ K_t, if \quad numerator > 0 \end{cases}$$

Reproduced with permission of the copyright owner. Further reproduction prohibited without permission.

The Kudryavtsev's approach in calculating MAGT is the consecutive layer-by-layer introduction of thermal effects of snow, ground surface vegetation, and the soils within the active layer on mean annual temperatures and seasonal amplitudes at each considered level (snow surface, vegetation surface, ground and permafrost surfaces). However, this scheme is not totally additive because the estimation of the impact of each new layer already includes the thermal effects of all layers above it. Moreover, in the modified Kudryavtsev's approach, the thermal effect of snow reflects the thermal properties and temperature field dynamics in the subsurface layers through the heat turnover estimation (see the *Evaluation of the snow cover influence* Section). As a result, the modified Kudryavtsev's approach takes into account some negative and positive feedbacks between designated layers in the "atmosphere-permafrost" system.

Calculating Active Layer Thickness

Calculation of the ALT using Kudryavtsev's formula is the final step in the model (Romanovsky and Osterkamp 1997). The formula was derived for a homogeneous ground, but in actuality, even if the soil properties are the same throughout the active layer, the moisture content or mode of heat flow may vary significantly. This can make the active layer inhomogeneous with regard to its thermal properties. Also, the model does not take into account unfrozen water, which can exist in the frozen active layer even at relatively cold temperatures (-5°C or colder), and has a significant effect on the grounds thermal properties (Williams, 1964; Williams and Smith, 1989). The assumption of a periodically steady state temperature regime seems to be a good approximation when applied to the annual temperature cycle, which varies from year to year (Romanovsky

Reproduced with permission of the copyright owner. Further reproduction prohibited without permission.

and Osterkamp, 1997). Considering the advantages along with the shortcomings, the formula appears to give a good representation of the coupling between permafrost and the atmosphere.

Evaluating the Performance of the Modified Kudryavtsev Approach

Two methods have been applied to determine the accuracy of the mKA approach for ALT and MAGT calculations. First, the results of the mKA approach were compared with numerical model outcomes. Second, the analytical results were compared to measured ALT and MAGTs taken from sites along the East-Siberian and Alaskan transects.

Comparison of mKA approach to a numerical model

The numerical model chosen to compare to the mKA results was developed by G.S. Tipenko of the Geophysical Institute Permafrost Lab. This model solves the one-dimensional heat conduction equation in a non-homogeneous media, containing unfrozen water. The model was successfully used for the ground temperature regime reconstruction at the Barrow Permafrost Observatory during the period 1924-2001 (Romanovsky et al., 2002). The numerical model accounts for snow cover by treating it as part of the upper boundary conditions together with the air temperatures. This approach was applied to Barrow and Fairbanks in the Alaskan transect, and to Tiksi and Yakutsk in the East-Siberian transect. For each location, five different forecasts were done for the period of 2000-2099. Each of the forecasts used mean monthly air temperatures and snow thickness output from the respective GCMs. The five ACIA – designated GCMs are provided by the Canadian Center for Climate Modeling and

Reproduced with permission of the copyright owner. Further reproduction prohibited without permission.

Analysis (CCC model), the National Center for Atmospheric Research/Climate System Model (CSM model), the Geophysical Fluid Dynamics Laboratory (GFDL model), Hadley Climate Center (HadCM3 model), and the Max Plank Institute for Meteorology (ECHAM model).

The thermophysical properties of the ground that were used for the numerical model have been taken from previous studies (Romanovsky and Osterkamp, 1995; Romanovsky and Osterkamp, 2000; Romanovsky et al., 2001). These thermophysical properties have been averaged for the purposes of applying them to Kudryavtsev's formula. These averages take into account the thickness of each layer in the ground. The results are presented in Figures 3.2 through 3.5.

To evaluate how the mKA corresponds to the numerical model, a linear regression technique has been applied (Table 3.3). The slope of the least squares fit ranges from 0.6 to 1.35, and the slope of the ALT varies from 0.4 to 1.1. This shows a good agreement between the mKA and numerical models. The correlation coefficient and the P-value (probability that the correlation coefficient is zero) have also been calculated. The results show a strong correlation for the active layer thickness and the MAGTs between mKA and the numerical model, with correlation coefficients between 0.7-0.9 and a P-value close to 0.

The mKA and the numerical model show similar variations in ALT calculations (Figures 3.2 and 3.3). For all the scenarios that have been analyzed (excluding CSM), the differences in the calculated ALT on the 100-year interval did not exceed 0.3 m. For CSM, the difference between the two models was 0.48 m. The numerical model accounts

Reproduced with permission of the copyright owner. Further reproduction prohibited without permission.

for unfrozen water content, which results in phase transitions at temperatures less than 0°C. This results in the mKA giving deeper active layer values for most scenarios.

For most scenarios, the mKA approach gives slightly warmer temperatures than the numerical model for the years 2000-2050, and gives colder temperatures for 2050-2100 (Figure 3.4). Additional work will be needed to determine the nature of these biases. The steady-state periodical regime on the surface, which is one of the assumptions used in mKA, is one possible explanation for this. For all scenarios, the difference between MAGTs given in the mKA and the numerical model is within 0.3°C.

Comparison with measured MAGT

The next step was to compare the mKA values with measured MAGTs and ALT from data sites along the transects. There is a lack of long-term data (on the scale of 20-40 years) for the Alaskan transect, and an overall lack of ALT data from the East-Siberian transect. Because of this, only seven points were chosen from each transect to evaluate error in the MAGT and ALT calculations.

The monthly air temperatures and snow cover thickness were recorded for all points that have been chosen, but the thermophysical properties of the soils (Table 3.4) are not available for the individual sites. To account for the lack of soil properties, we used the "Geocryological Map of the USSR" for the East-Siberian transect, and properties of the Alaskan transect were taken from Brown and Kreig (1983).

The difference between the measured and calculated values of the MAGT can reach 1.5-2°C for certain years. When averaged over the entire time interval, the relative error does not exceed 33% (Table 3.5). The interval is different for each meteorological

Reproduced with permission of the copyright owner. Further reproduction prohibited without permission.

station, and ranges from 1970-1990 at Verkhoyansk, to 1935-1990 at Krest-Khaldzai. Generally, the mKA gives slightly colder temperatures for points within the East-Siberian transect (Table 3.5). The calculated MAGTs have shown a greater magnitude for internal fluctuations than the measured values yield (Figures 3.6 through 3.8).

The measured values of the ALT were supplied by the CALM network (www.geography.uc.edu/~kenhinke/CALM). Analysis shows that the relative error of the ALT calculations is lower than 32%. For about half of the points, the mKA gives a shallower active layer thickness than was measured (Table 3.6). The primary source of error might be the uncertainty in setting snow and vegetation cover parameters which were not known. This error is of particular concern with regard to the thermal diffusivity of the vegetation.

Geographic Information System (GIS) approach for evaluating the spatial dynamics of the ALT and MAGTs

Geographical Information Systems are widely used to store and analyze large volumes of data. They allow visualization of the spatial distribution of topographic features such as soil types, vegetation and climatic parameters, as well as the incorporation of modeling results. We have applied a GIS approach to evaluate the spatial dynamics of the ALT and MAGTs along the two transects.

Each database that was used contains layers representing soils, vegetation cover, meteorological data, rivers, elevation, permafrost distribution, etc (Romanovsky et al., 2001). Climate data, including mean annual air temperatures, the range of mean

Reproduced with permission of the copyright owner. Further reproduction prohibited without permission.

monthly air temperatures, and snow cover thickness and density from GCMs have been incorporated into these databases.

Once compiled, the datasets contain all the necessary parameters for calculation of ALT and MAGTs for the period from 1900-2100. Seasonal air temperature range, and average winter snow thickness and density were supplied by the GCMs, but there is not enough data available on vegetation cover changes and soil properties for the same time period. When calculating past and present ALT and MAGTs, we have assumed that these uncertainties are relatively small and do not have an effect on the permafrost dynamics of interest. The calculations for both transects were performed using a uniform special gird with a resolution of 0.5 x 0.5 degrees latitude/longitude. The special grids for the Alaskan and East-Siberian transects contain 517 and 1000 grid cells respectively. Figure 3.9 shows an example of the results obtained with GIPL using the HadCM2 GCM that was developed in Hadley Climate Center. Results using other GCM outputs can be obtained through the ACIA project.

The procedure used to calculate the active layer thickness and MAGTs for a given year is demonstrated by the block diagram (Figure 3.10). One external script and two internal scripts have been written to create a user-friendly interface for the evaluation of MAGT. The first internal script obtains information from the user for which year(s) the calculations should be performed. These input parameters are sent to the external script. The external script uses mKA to calculate ALT and MAGT for each point on the grid.

The first internal script activates the second internal script, which takes the results from the new file, which was created by the external script. The script then performs the

Reproduced with permission of the copyright owner. Further reproduction prohibited without permission.

interpolation between the points using an Inverse Distance Weighted (IDW) interpolator. Two gridded output files are created; one for the ALT and another for the MAGTs. The second internal script assigns a prescribed colorscale for visualization of each of the grid cells. Another important function of the second internal script is the extraction of the area where the MAGTs are positive (above 0°C). This is important because if an area has a positive MAGT, permafrost degradation has begun.

Through combination of Kudryavtsev's approach and the GIS method of data storing and processing, the quasi-two-dimensional, quasi-transitional, spatially distributed, analytical model for the ALT and MAGT calculations have been developed. This model has been called the GIPL model, and can be referred to as an interactive GIS because input parameters can be easily changed and yield new results instantly.

The Overall Performance of the GIPL Model

A method of statistical analysis has been applied to determine the overall performance of the model. Soil temperatures that have been measured daily and stored as monthly means at 52 different weather stations along the transect were used for the analysis. MAGTs at the bottom of the active layer were calculated for each station. These data are available from the Joint Office of Science Support (JOSS) and can be obtained at www.joss.ucar.edu ; the dataset name is ATLAS: 1899-1994, and contains the East-Siberian Transect – air and ground temperatures and snow depth (Romanovsky).

Originally, this dataset was compiled and digitized by our collaborators on this project from the Permafrost Institute in Yakutsk (group leader V. T. Balobaev) and at the Institute of Physicochemical and Biological Problems in Soil Science, Russian Academy

Reproduced with permission of the copyright owner. Further reproduction prohibited without permission.

of Sciences (group leader D. A. Gilichinsky) using published monthly meteorological regional reports (Klimatologicheskii spavochnik SSSR, 1961-1992). From those sites only 32 points were chosen on the basis of data quality and measurement consistency. Ground temperature measurements taken at a depth of 1.6 m during a 24-year period from 1966 – 1989 were used for comparison with the calculated MAGTs. Even though it would be better to compare with the temperatures measured deeper at 2.4 or 3.2 m, we chose the depth of 1.6 m because of the higher consistency of measurements and availability. At one third of the meteorological stations ground temperatures below 1.6 m were not measured. This particular depth matches very well the depth of the permafrost table at the most sites used in this research. Only eight out 32 sites show the active layer deeper than 1.6 meters and at only three of them the ALT was in excess of 2.4 meters. Because the most significant changes in MAGTs due to the thermal offset take place within the upper third of the active layer (Burn and Smith, 1988; Romanovsky and Osterkamp, 1995), the measured mean annual temperatures at 1.6 m can represent MAGTs very well even for the sites with deeper active layer. The long-term difference between mean annual temperatures at 1.6 m and 3.2 m will typically not exceed 0.3°C.

Air temperature measurements are available for all data sites, and the snow cover thickness is available for 8 of them. We have extrapolated snow thickness along the entire transect. The MAGTs were calculated using the GIPL model for each of the 32 sites for every year from the interval of 1966 to 1989, and these values were compared with the measured values. Two digital maps have been created using IDW interpolation between the points (Figure 3.11). It should be noted that most of the points are in the

Reproduced with permission of the copyright owner. Further reproduction prohibited without permission.

central and southern parts of the transect. This is probably why calculated MAGTs for the higher latitudes do not correlate well with the measured temperatures.

Differences between the measured and calculated values for MAGTs over a 24-year period varied from 0.2 to 0.6°C (Figure 3.11). In the southern regions of the transects, the GIPL model gives colder MAGTs while the model gives warmer than measured temperatures in the western part of the transect, with differences varying from 0.2 – 0.4 °C. When averaged over the entire 24-year period of calculations, the difference between the measured and calculated values did not exceed 0.6°C and is around 0.3°C for most base points.

In order to determine the uncertainty associated with the MAGT calculations, a confidence analysis was performed, which return the confidence interval for a population mean (in our case, averaged MAGT over a 24-year interval). The analysis was performed for 50%, 75%, and 95% levels of confidence (Figure 3.12). The interpretation of the results must include the confidence interval as it shows the range on either side of the MAGT averaged over the years 1966 – 1989.

The results of the confidence analysis show that with a 50% confidence, the calculated MAGT will not differ from measured temperatures by more than 0.1 – 0.2°C for the eastern, central, northern and southeastern parts of the transect. In the western part of the transect, the measured and predicted MAGTs do not differ by more than 0.2 – 0.3°C. For a 75% confidence level, we can expect that differences in calculated and measured temperatures range from 0.2 – 0.3°C for the eastern part of the transect (to the east from 130 EL) and in the range of 0.3 – 0.4°C for the western part. If confidence

Reproduced with permission of the copyright owner. Further reproduction prohibited without permission.

level is 95%, the difference between calculated and measured temperatures can reach up to 0.4 – 0.5°C for the eastern part of the transect, and 0.6 – 0.8°C for the western part.

The confidence analysis has shown that in the western part of the transect (roughly the area between 120 and 130 EL) a greater level of uncertainty and wider differences between calculated and measured MAGTs might be expected. For the eastern part of the transect, the range of differences between calculated MAGTs and measured values is not as large as in the western part of the transect. Additional investigations and data on snow and vegetation cover properties are required to explain the results of the confidence analysis more thoroughly. With the data that is currently available, the variance in the uncertainty between the eastern and western parts of the transect can be explained by deeper snow cover (0.4 – 0.8 m) and greater interannual variations in snow cover thickness in the western part of the transect. A level of confidence of 75% is considered to be appropriate for engineering and scientific purposes. We assume that calculated mean annual temperatures are equal to measured MAGTs with a 0.2 – 0.4°C uncertainty. Unfortunately, it was not possible to perform the same analysis for the active layer thickness for the East-Siberian transect due to the lack of active layer thickness measurements. Long-term data on the active layer thickness is available only for 10 points from the Alaskan transect and measurements were not taken consistently, so we could not perform the same statistical analysis. Instead, calculated and measured active layer thicknesses were compared (Table 3.6). From this analysis it is clear that the relative error of active layer thickness calculations does not exceed 33% with the most typical relative errors between 15 and 25%. These relative errors can be assumed to be

Reproduced with permission of the copyright owner. Further reproduction prohibited without permission.

acceptable for the regional scale analysis especially if very high natural variability in ALT will be taken into account. Our data from the North Slope of Alaska show that the natural variability in ALT within the 100x100 meters sampling grids is typically in the range of 15 - 35%.

CONCLUSIONS

Kudryavtsev's approach was chosen for active layer thickness and MAGT calculations. This approach shows an accuracy of $\pm$0.2-0.4°C for the mean annual ground temperatures and $\pm$0.1 – 0.3 m for the active layer thickness calculations. The relative error does not exceed 32% for the ALT calculations.

The comparison of Kudryavtsev's approach with numerical model shows good correlation. Small difference in estimation of permafrost parameters, attributed mostly to the limitations in Kudryavtsev's approach, result from not taking into account unfrozen water dynamics.

Calculations using Kudryavtsev's approach and measured permafrost parameters do not show good correlation. For some years difference between the two can be considerable (1.5 –2°C for MAGTs), but when averaged over the same period of time, the difference between the averaged values is relatively small (from 0.1 to 0.3°C). This inadequacy of measured and calculated parameters can be explained by errors in snow density estimations and approximations of thermophysical parameters of soils.

The spatial statistical evaluation of GIPL model using data from 32 sites within the East-Siberian transect showed that with 75% probability the confidence interval for

Reproduced with permission of the copyright owner. Further reproduction prohibited without permission.

averaged over 24 years MAGTs can deviate from the measured temperatures by not more than $\pm$0.3°C for the eastern part of the transect (to the east from 130 EL) and by not more than $\pm$ 0.4 °C for the western part.

The analysis performed for two transects validated the use of Kudryavtsev's approach and our GIPL model for calculating active layer thickness and MAGTs.

ACKNOWLEDGEMENTS

This research was funded by the Polar Earth Science Program and by ARCSS Program, Office of Polar programs, National Science Foundation (OPP-9870635, OPP-9721347, OPP-9732126), and by the State of Alaska. The temperature data used in this study are available to other researchers through the JOSS project (http://www.joss.ucar.edu) and NSIDC (http://nsidc.org). We would like to thank Dr. C. Burn and an anonymous reviewer for very helpful suggestions that were used to improve the manuscript.

Reproduced with permission of the copyright owner. Further reproduction prohibited without permission.

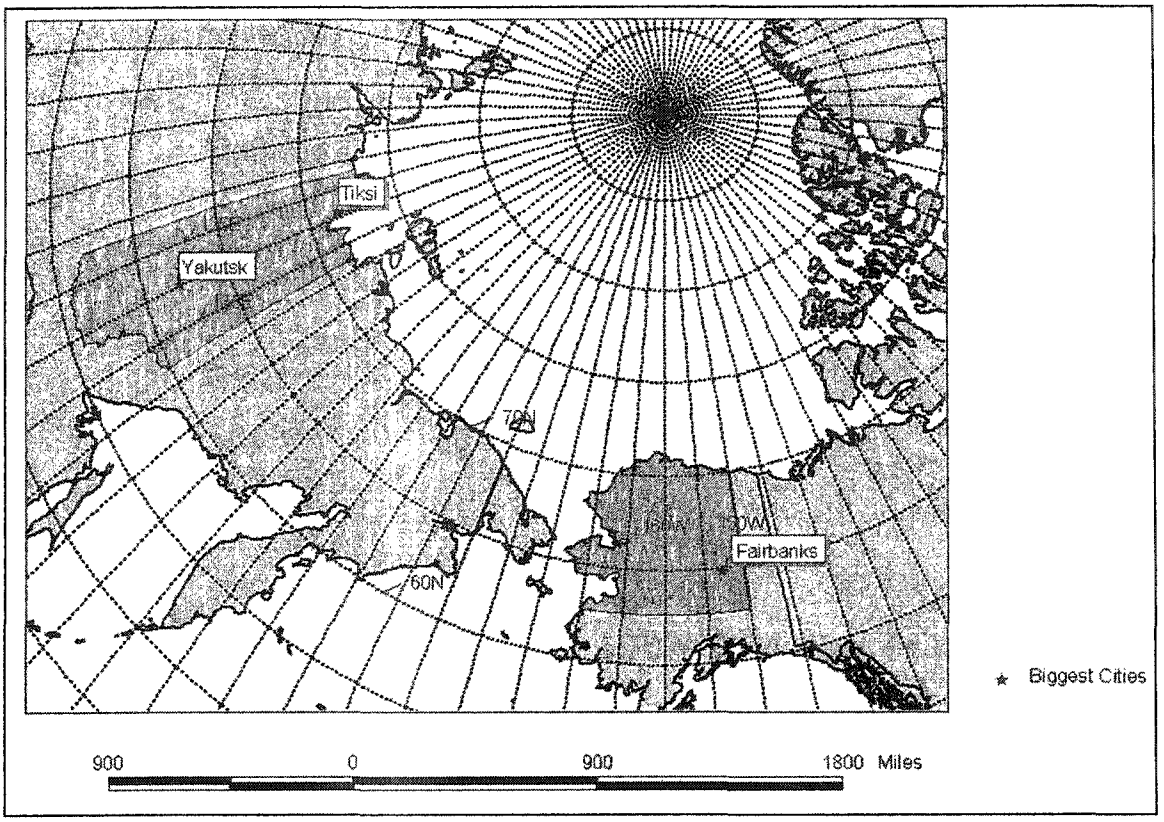

Figure 3.1: East-Siberian and Alaskan transects

Reproduced with permission of the copyright owner. Further reproduction prohibited without permission.

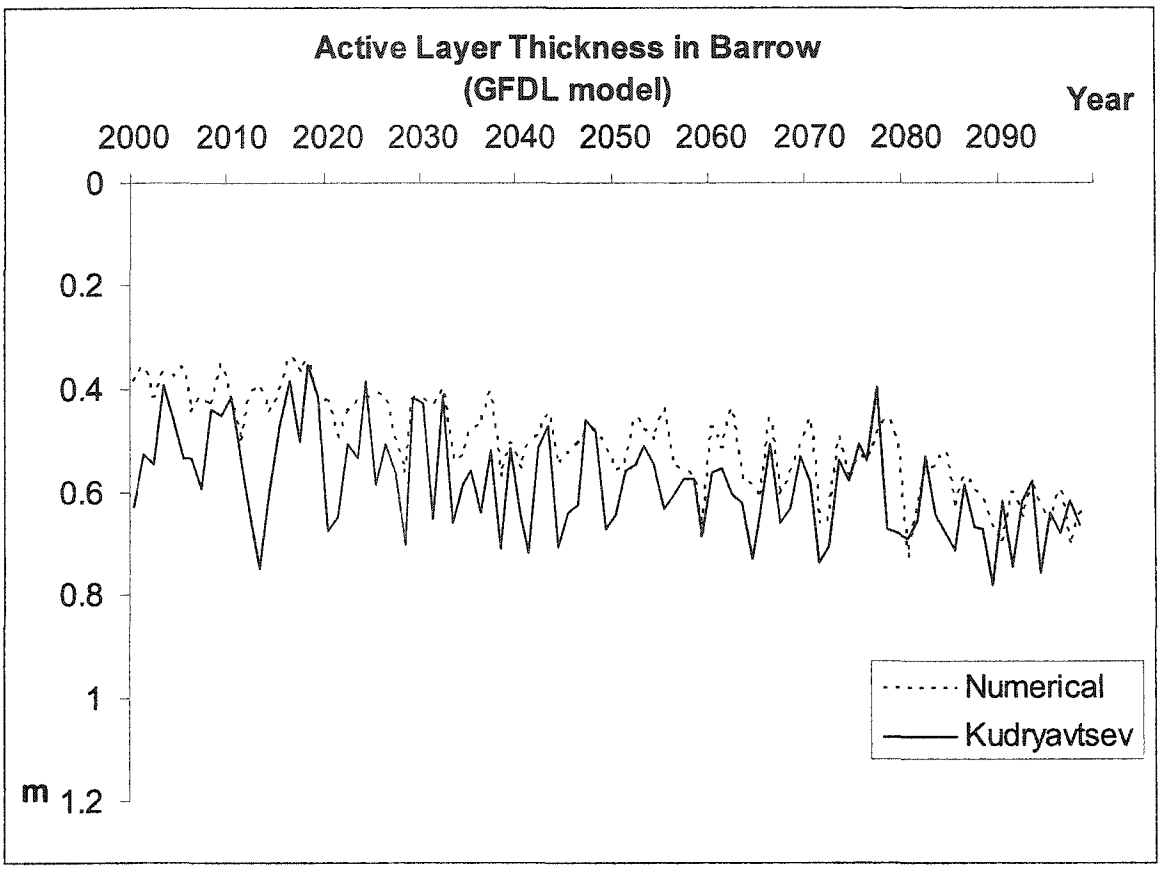

Figure 3.2: Active layer thickness calculated using numerical model and Kudryavtsev's method for Barrow

Reproduced with permission of the copyright owner. Further reproduction prohibited without permission.

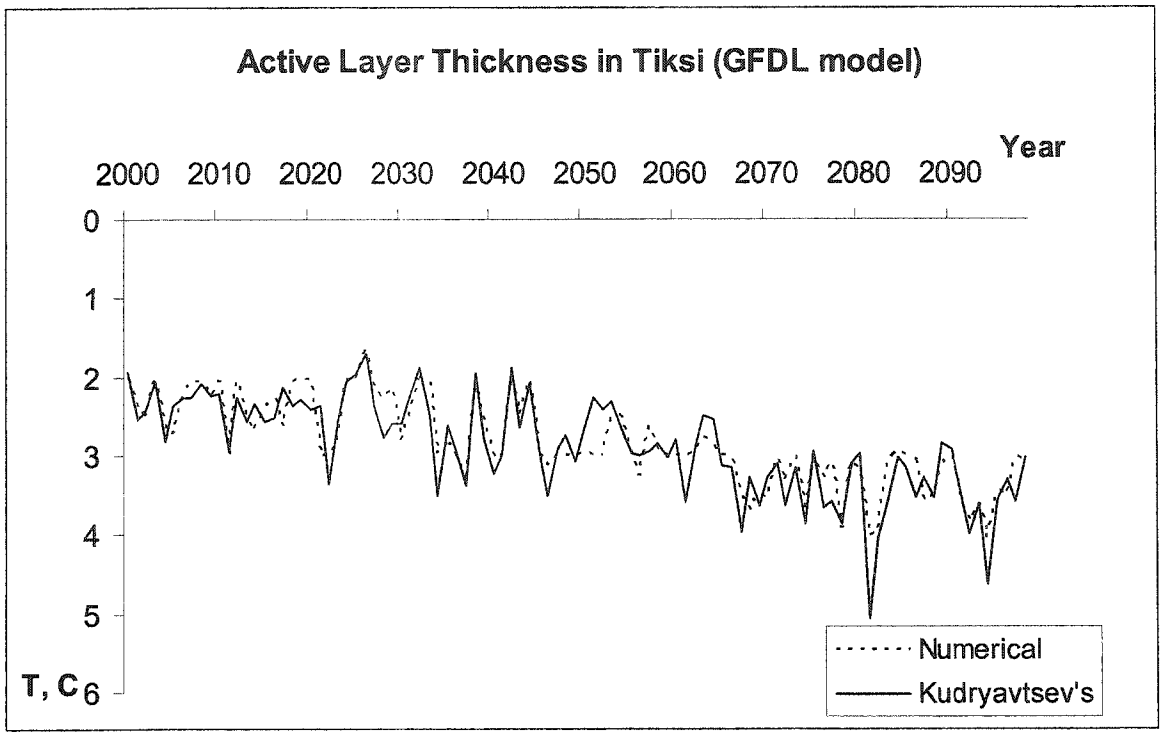

Figure 3.3: ALT calculated using numerical model and Kudryavtsev's method for Tiksi

Reproduced with permission of the copyright owner. Further reproduction prohibited without permission.

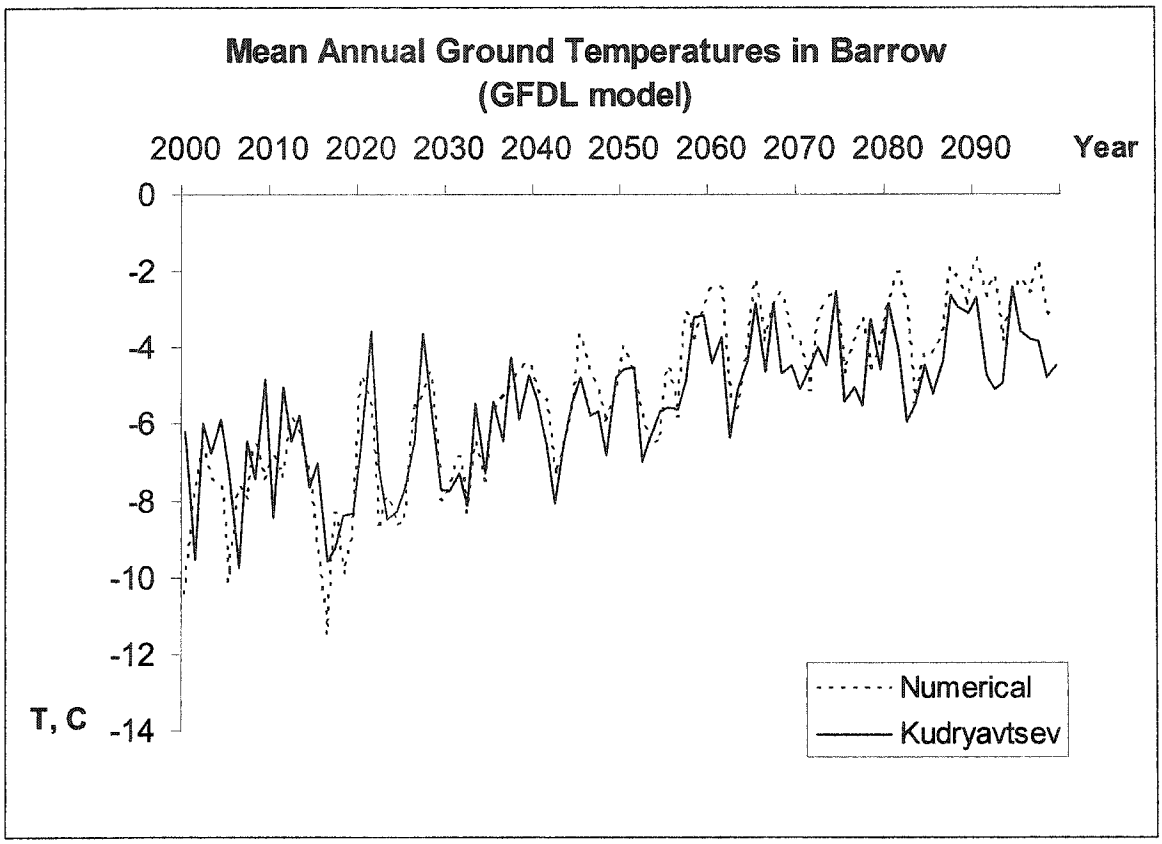

Figure 3.4: MAGTs calculated using numerical model and Kudryavtsev's method for Barrow.

Reproduced with permission of the copyright owner. Further reproduction prohibited without permission.

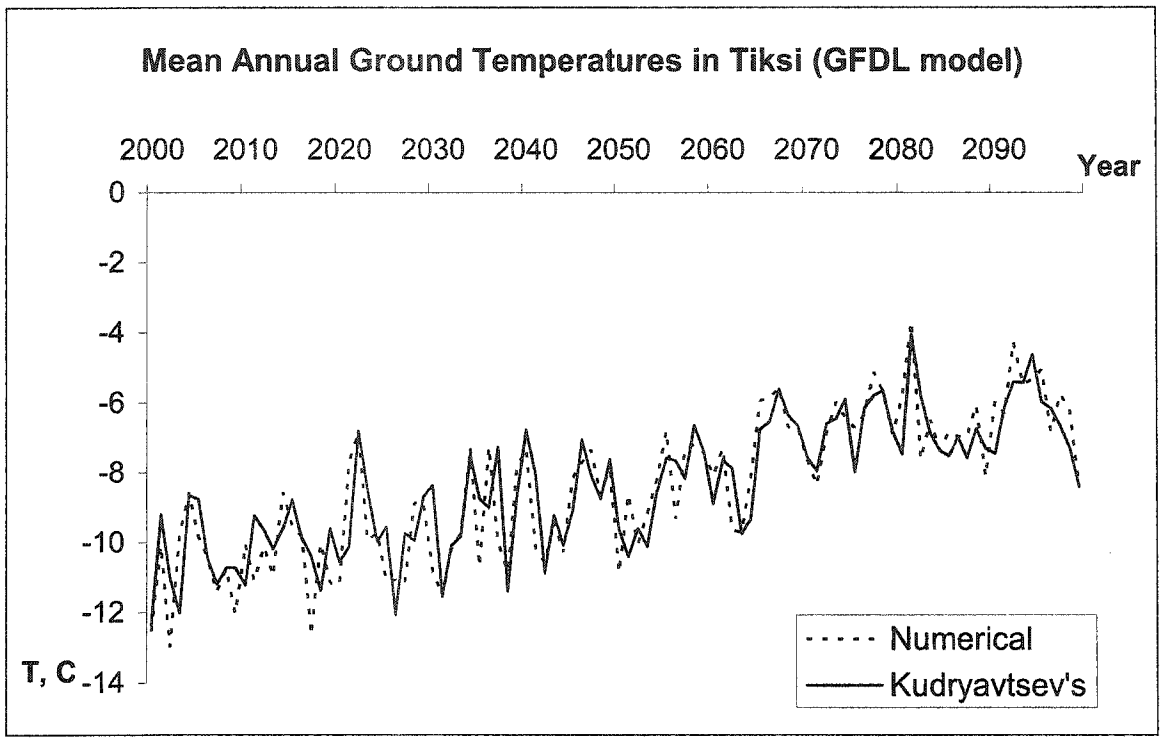

Figure 3.5: MAGTs calculated using numerical model and Kudryavtsev's method for Tiksi.

Reproduced with permission of the copyright owner. Further reproduction prohibited without permission.

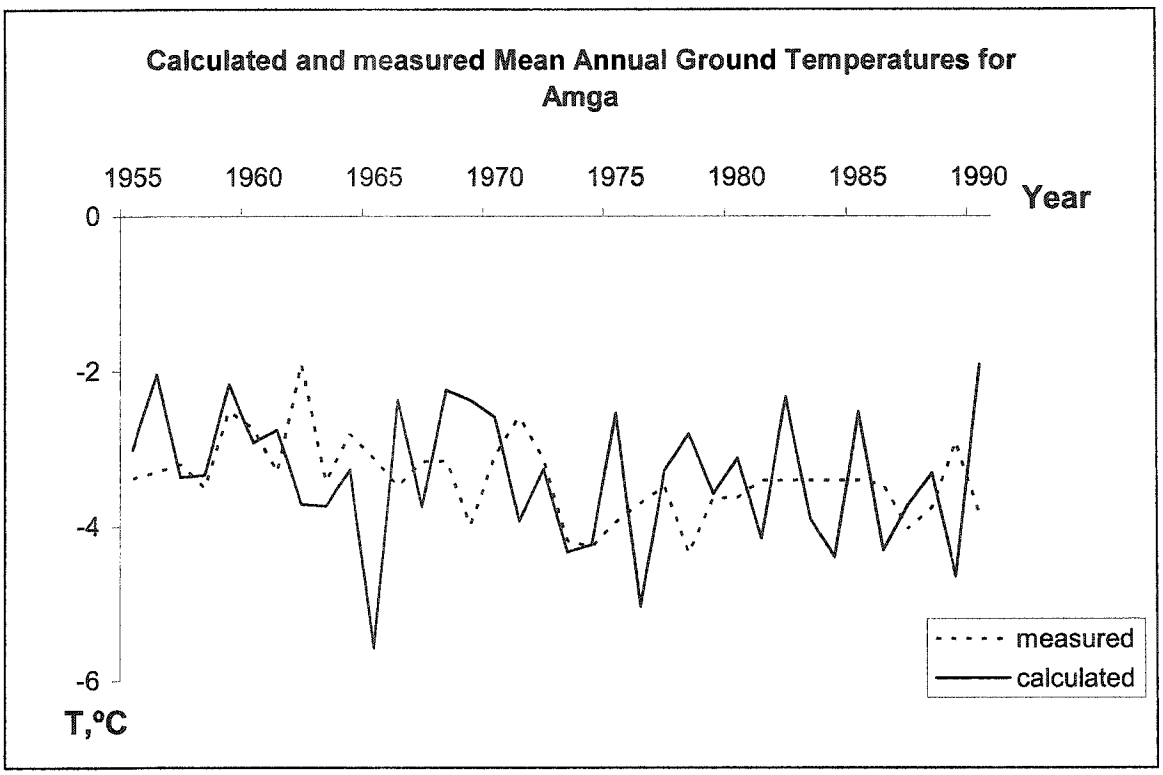

Figure 3.6: Measured and Calculated MAGTs for Amga

Reproduced with permission of the copyright owner. Further reproduction prohibited without permission.

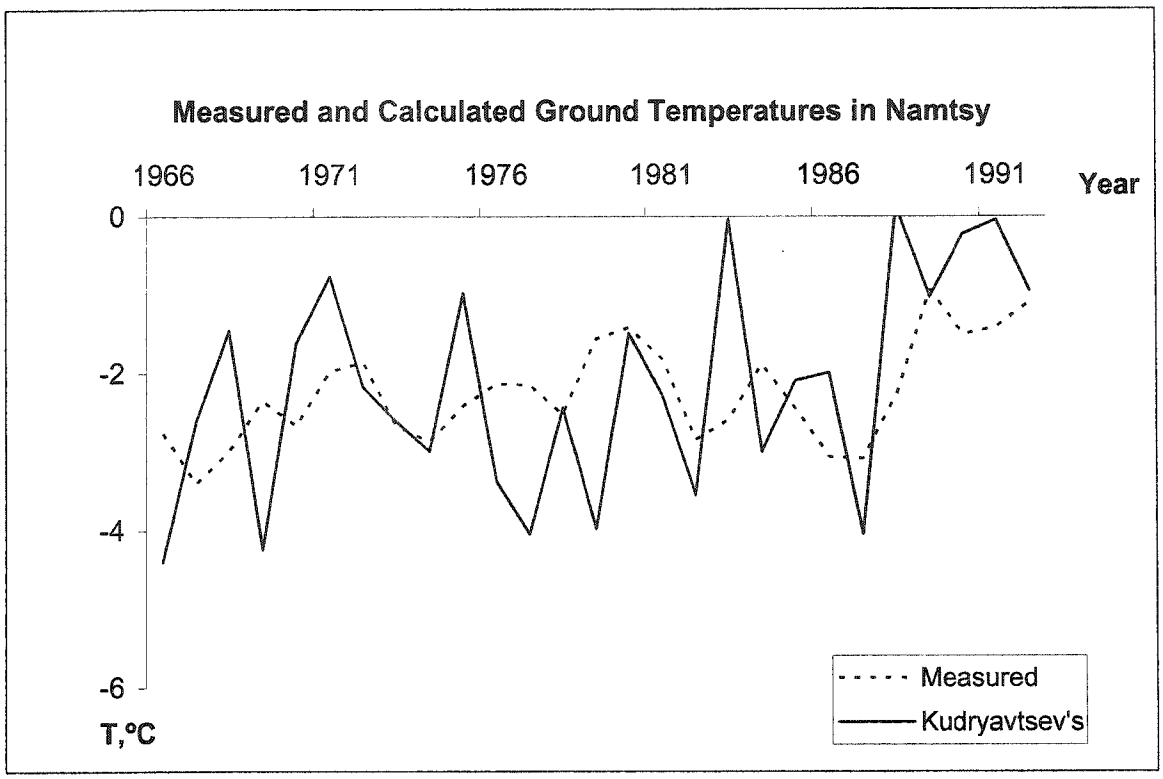

Figure 3.7: Measured and Calculated MAGTs for Namtsy.

Reproduced with permission of the copyright owner. Further reproduction prohibited without permission.

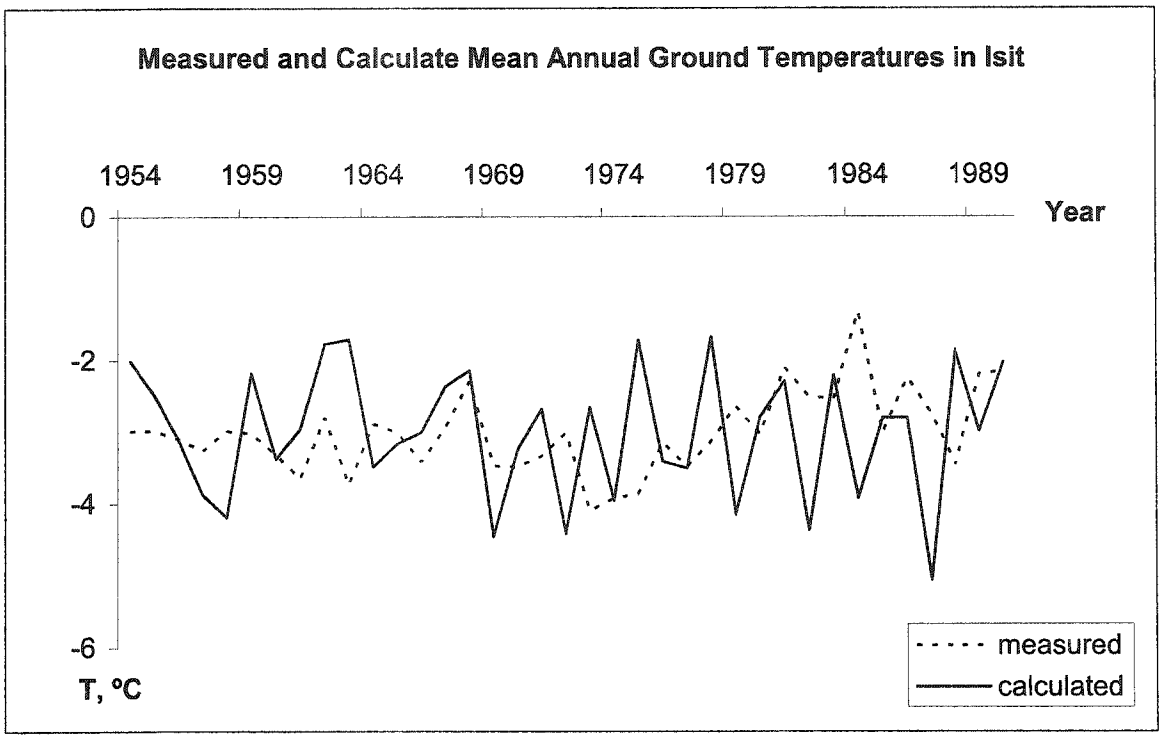

Figure 3.8: Measured and Calculated MAGTs for Isit.

Reproduced with permission of the copyright owner. Further reproduction prohibited without permission.

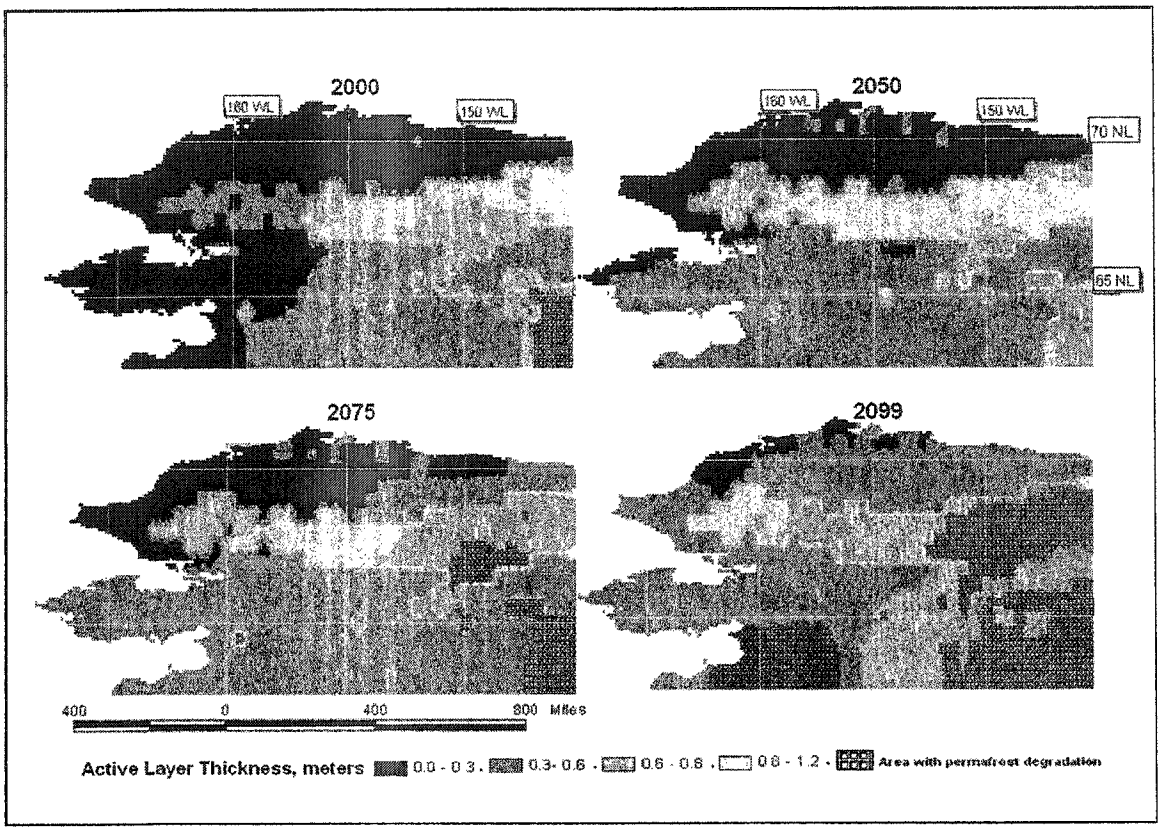

Figure 3.9: ALT for the Alaskan transect (Had CM2 GCM).

Reproduced with permission of the copyright owner. Further reproduction prohibited without permission.

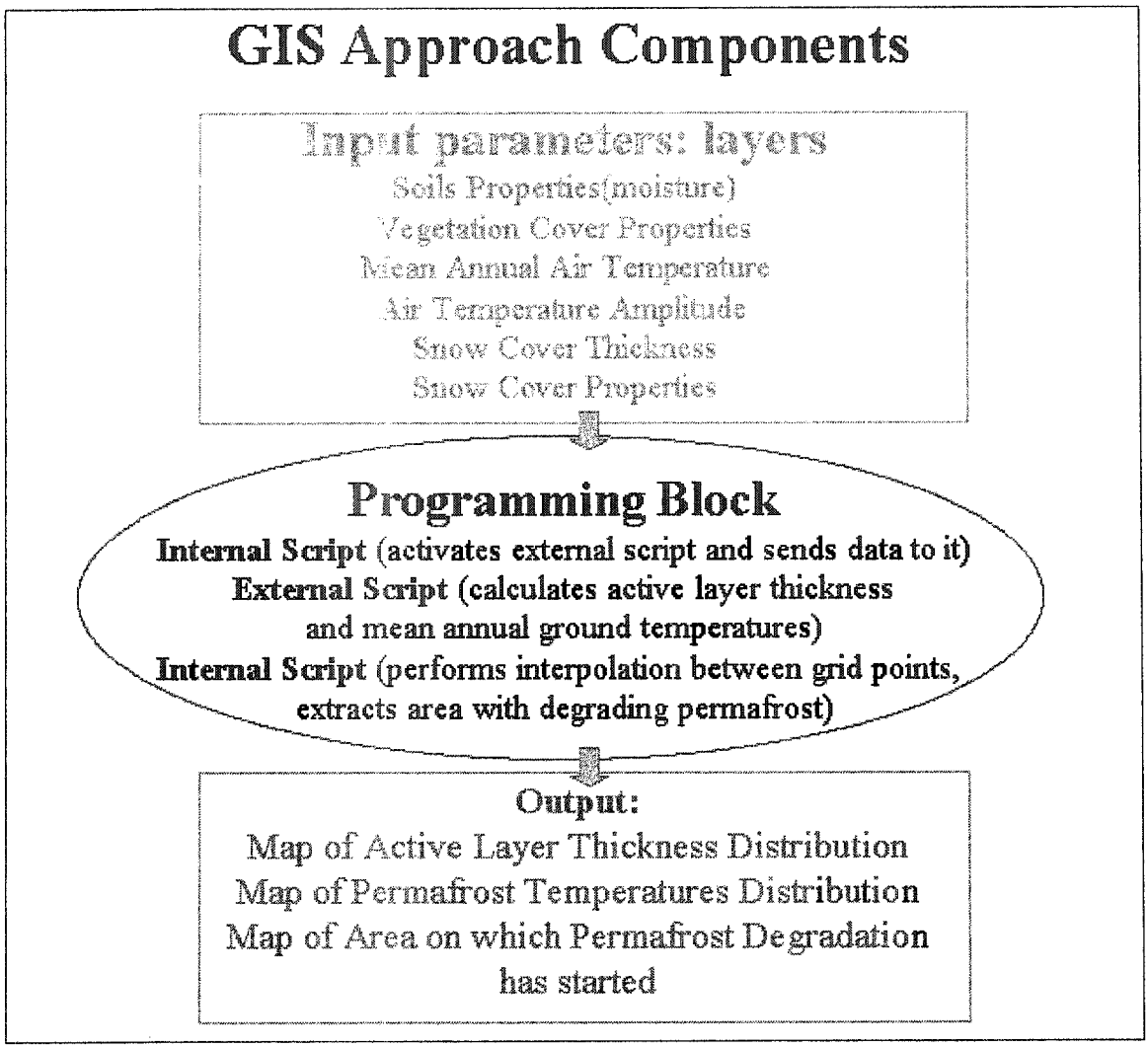

Figure 3.10: Block-Diagram of GIS Approach.

Reproduced with permission of the copyright owner. Further reproduction prohibited without permission.

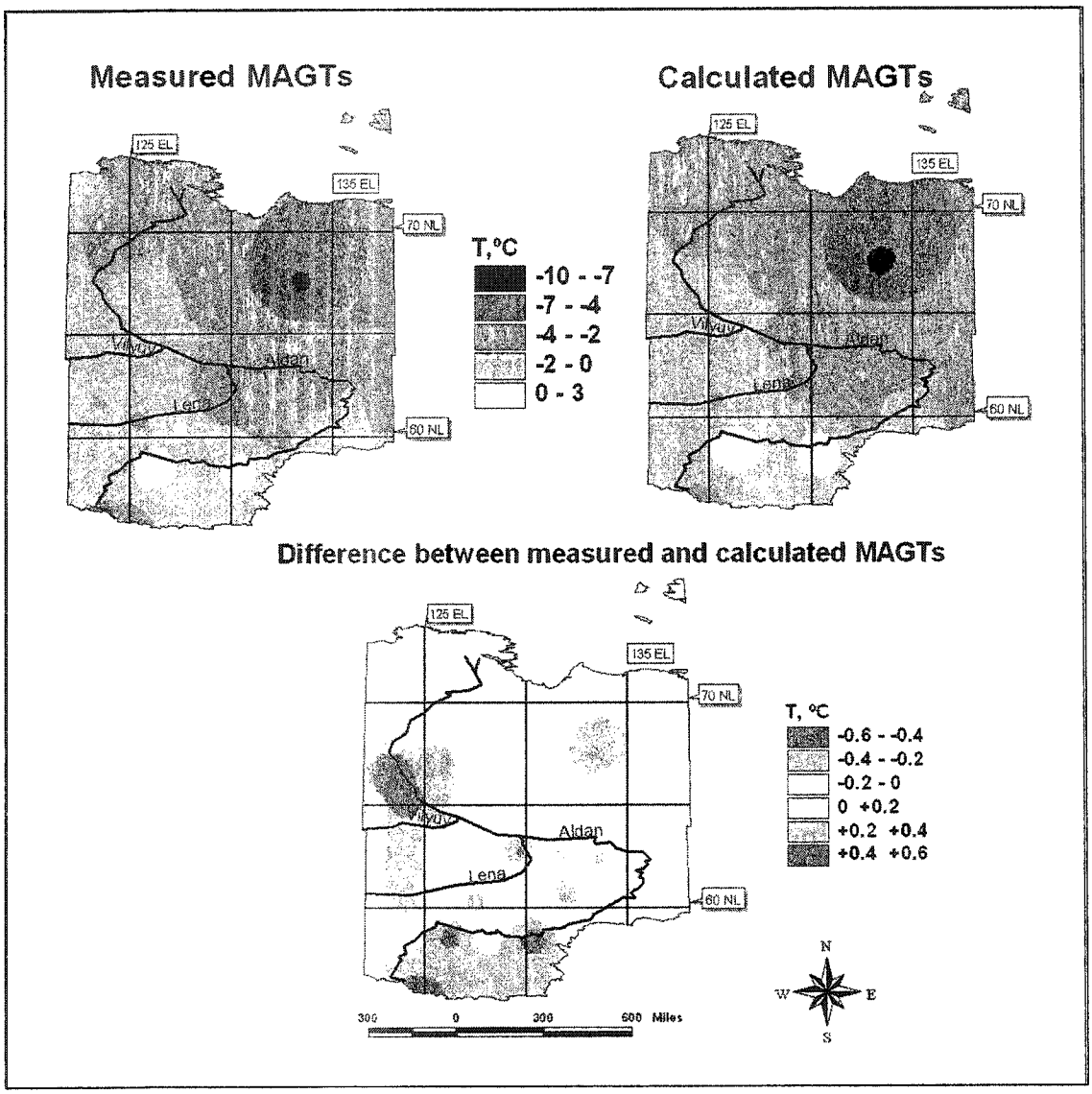

Figure 3.11: Calculated, measured MAGTs for the East-Siberian transect, averaged over the period of 1966 – 1989.

Reproduced with permission of the copyright owner. Further reproduction prohibited without permission.

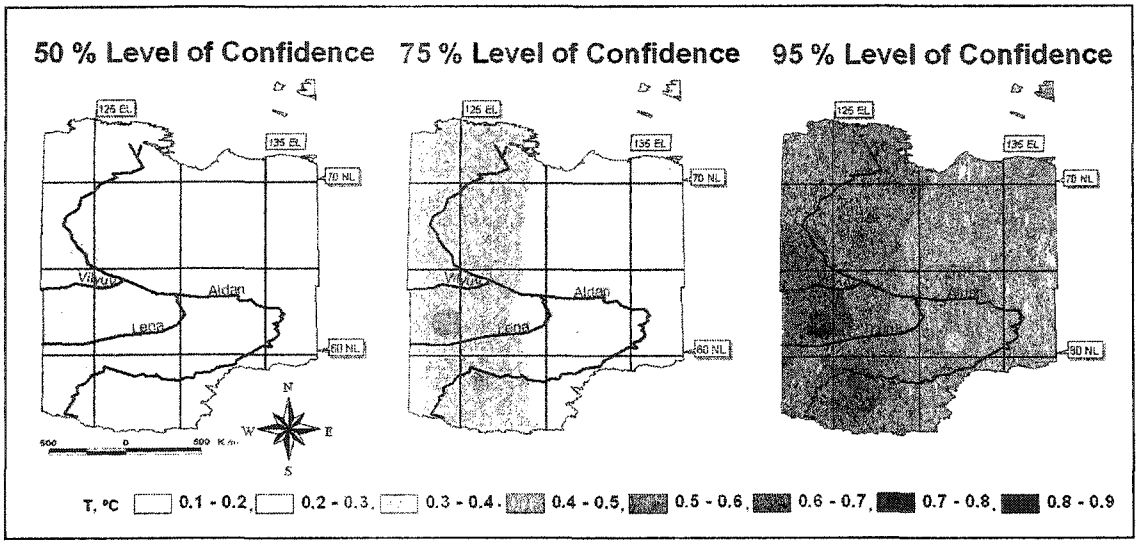

Figure 3.12: Ranges of variation of MAGTs with certain levels of confidence.

Reproduced with permission of the copyright owner. Further reproduction prohibited without permission.

Table 3.1: Input variables and parameters

Input Variables	Notation	Units
Seasonal range of air temperature variations	A_a	°C
Mean annual air temperature	T_a	°C
Mean annual snow thickness	H_{sn}	m
Snow density	ρ_{sn}	kg/m^3
Thermal conductivity of snow	K_{sn}	W/(m*K)
Height of vegetation cover	H_v	m
Thermal diffusivity of vegetation in frozen state	D_{vf}	m^2/s
Thermal diffusivity of vegetation in thawed state	D_{vt}	m^2/s
Thermal conductivity of frozen ground	K_f	W/(m*K)
Thermal conductivity of thawed ground	K_t	W/(m*K)
Volumetric water content	W_{vol}	Fraction of 1
Volumetric heat capacity of snow cover	C_{sn}	J/m^3K
Volumetric heat capacity of ground skeleton	C_{sk}	J/m^3K
Volumetric heat capacity of thawed ground	C_t	J/m^3K
Volumetric heat capacity of frozen ground	C_f	J/m^3K

Reproduced with permission of the copyright owner. Further reproduction prohibited without permission.

Table 3.2: Output variables.

Output Variables	Notation
Correction to T_a accounting for snow cover effect, °C	ΔT_{sn}
Correction to A_a accounting for snow cover effect, °C	ΔA_{sn}
Correction to T_a accounting for vegetation cover , °C	ΔT_v
Correction to A_a accounting for vegetation cover , °C	ΔA_v
Seasonal range of temperature variations at the ground surface, °C	A_{gs}
Mean annual temperatures at the ground surface, °C	T_{gs}
Thermal offset, °C	ΔT_k
MAGT , °C	T_{ps}
MALT ,m	X

Reproduced with permission of the copyright owner. Further reproduction prohibited without permission.

Table 3.3: Statistical analysis of Kudryavtsev's model correspondence with numerical model.

	MAGT				Active Layer Thickness			
Station, GCM	**Intercept**	**Slope**	**Correlation**	**P-value**	**Intercept**	**Slope**	**Correlation**	**P-value**
Barrow, CCC	-1.54	0.63	0.87	<0.0001	-0.20	0.94	0.85	<0.0001
Barrow, CSM	-1.90	0.79	0.71	<0.0001	0.13	0.72	0.32	0.00
Barrow, ECHAM	-1.81	0.78	0.92	<0.0001	0.22	0.91	0.82	<0.0001
Barrow, GFDL	-2.20	0.63	0.82	<0.0001	0.25	0.66	0.63	<0.0001
Barrow,HAD3	-1.77	0.67	0.87	<0.0001	0.23	0.82	0.74	<0.0001
Fairbanks, CCC	-0.13	1.35	0.85	<0.0001	-0.20	0.94	0.85	<0.0001
Fairbanks, CSM	-0.03	1.35	0.58	<0.0001	-	-	-	-
Fairbanks, ECHAM	-0.22	1.16	0.87	<0.0001	-	-	-	-
Fairbanks, GFDL	-0.22	1.16	0.84	<0.0001	-	-	-	-
Fairbanks, HAD3	-0.24	1.31	0.79	<0.0001	-	-	-	-
Tiksi, CCC	-1.17	0.83	0.94	<0.0001	-0.55	1.11	0.86	<0.0001
Tiksi, CSM	-1.19	0.91	0.88	<0.0001	-0.27	0.61	0.74	<0.0001
Tiksi, ECHAM	-1.24	0.83	0.94	<0.0001	-0.41	1.04	0.92	<0.0001
Tiksi, GFDL	-1.87	0.77	0.87	<0.0001	0.03	1.00	0.88	<0.0001
Tiksi,HAD3	-1.65	0.85	0.90	<0.0001	0.31	0.82	0.75	<0.0001
Yakutsk, CCC	-0.48	0.84	0.90	<0.0001	0.56	0.55	0.81	<0.0001
Yakutsk, CSM	-0.87	0.88	0.71	<0.0001	0.41	0.39	0.41	<0.0001
Yakutsk, ECHAM	-0.15	0.96	0.87	<0.0001	0.56	0.54	0.78	<0.0001
Yakutsk, GFDL	-1.02	0.76	0.86	<0.0001	0.30	0.67	0.79	<0.0001
Yakutsk, HAD3	-0.74	0.74	0.86	<0.0001	0.50	0.59	0.79	<0.0001

Reproduced with permission of the copyright owner. Further reproduction prohibited without permission.

Table 3.4: Thermophysical properties for the sites within East-Siberian transect

Station	Volumetric water content	Thermal conductivity of frozen soils W/(m*K)	Thermal conductivity of thawed soils W/(m*K)
Amga	0.20	2.36	1.91
Isit	0.65	1.37	0.96
Namtsy	0.20	1.39	0.88
Krest-Khaldzai	0.04	1.39	1.38
SanYahtat	0.20	1.95	1.43
Verkhoyansk	0.20	2.36	1.35
Nyurba	0.20	2.22	1.71

Reproduced with permission of the copyright owner. Further reproduction prohibited without permission.

Table 3.5: Comparison of calculated and measured active layer thickness for Alaskan transect.

Station	Years	Measured MALT, m	Calculated MALT, m	Relative error, %
Franklin Bluffs	1990-2000	0.6491	0.5909	9
Dead Horse	1990-2001	0.5973	0.4609	23
Happy Valley	1993-2000	0.4438	0.5863	32
Bonanza Creek	1990-2000	0.5040	0.5918	17
Barrow	1991-2000	0.3280	0.2610	20
Pearl Creek	1990-2000	0.6200	0.6691	8
Toolik Lake	1990-2001	0.3955	0.3336	16
Ivotuk 1	1999-2001	0.5933	0.4333	27

Reproduced with permission of the copyright owner. Further reproduction prohibited without permission.

Table 3.6: Comparison of calculated and measured MAGTs for East-Siberian transect.

Station	Years	Measured MAGT, °C	Calculated MAGT, °C	Relative error, %
Amga	1955-1990	-3.38	-3.34	1
Isit	1954-1990	-3.01	-2.99	0.4
Namtsy	1966-1992	-2.25	-2.16	4
Krest-Khaldzai	1970-1991	-3.80	-3.78	0.4
SanYakhtat	1963-1988	-0.46	-0.31	32
Verkhoyansk	1935-1990	-7.67	-7.43	3
Nyurba	1956-1990	-1.01	-0.75	26

Reproduced with permission of the copyright owner. Further reproduction prohibited without permission.

CHAPTER 4. PERMAFROST DYNAMICS IN 20TH AND 21ST CENTURIES ALONG THE EAST-SIBERIAN TRANSECT*

ABSTRACT

The East-Siberian transect, which has been designated by International Geosphere-Biosphere Program (IGBP) as its Far East Transect, has unique permafrost conditions. Not only does permafrost underlie the entire transect, but about one third of the region is underlain by an "Ice Complex", consisting of extremely ice-rich Late Pleistocene sediments. Given the possibility of global warming in the near future, an evaluation of the magnitude of changes in the ground thermal regime becomes desirable for assessments of possible ecosystem responses and impacts on infrastructure. A soil model developed at the Geophysical Institute Permafrost Lab was used to simulate the dynamics of the active layer thickness and ground temperature in this transect, both retrospectively and prognostically, using climate forcing from six Global Climate Models (GCMs). The analysis of future permafrost dynamics showed that, within the southwestern part of the transect, widespread permafrost thawing from the surface can begin as early as in 2050. The spatial extent and temporal dynamics of the zone with thawing permafrost vary significantly among the different GCMs. According to all the GCMs, the mean annual ground temperatures could rise by 2-6°C, and the active layer thickness could increase by 0.5 – 2 m everywhere within the transect by 2099.

---

* Submitted under the same title with authors Tatiana S. Sazonova, Vladimir E. Romanovsky, John E. Walsh, and Dmitri O. Sergueev to *Journal of Geophysical Research.*

Reproduced with permission of the copyright owner. Further reproduction prohibited without permission.

However, the increase in mean annual ground temperatures and the active layer thickness are not uniform in time. Relatively cold and warm periods associated with natural fluctuations in the air temperature and precipitations are superimposed on the background warming trend. The most significant increase in mean annual ground temperatures and in the active layer thickness are projected to occur in the southwestern part of the transect and in the areas with coarse-grained sediments, characterized by low water content and high thermal conductivity.

INTRODUCTION

Permafrost is a product of severe climate conditions and is one of the most sensitive parts of the Arctic System (UCAR, 1988). The active layer of permafrost is an upper layer that thaws every summer and re-freezes every winter. Due to the fact that almost all below-ground biological processes and activities take place within this layer, any changes in the active layer can affect the carbon cycle. When the annual mean temperature at the base of the active layer exceeds 0°C, the depth of thaw increases in successive summers and becomes greater than the depth of refreezing in the following winters. In this situation, known as "permafrost degradation", the thawing of the permafrost can significantly impact infrastructure, regional hydrology and ecosystems. Permafrost dynamics must be considered in order to understand changes in the active layer thickness and in mean annual ground temperatures.

Interactions between the atmosphere and permafrost are complex. They involve snow cover and vegetation, conduction through various soil types with varying ice

Reproduced with permission of the copyright owner. Further reproduction prohibited without permission.

content, and phase changes of water. Permafrost, in turn, influences the atmosphere by its effects on the surface heat fluxes, evaporation and runoff, and trace gas exchanges. As global climate models (GCMs) are increasingly used to project climate changes and to understand the impact of global climate change on the ecosystems, it will eventually be possible to address changes in permafrost and the role of permafrost in climate change over the entire circumpolar region.

At present, the data necessary for an evaluation of permafrost dynamics over the entire circumpolar region are not available. However, limited areas in both northern Asia and North America are amenable to the transect approach. The main idea of the transect approach is to study permafrost's spatial distribution and its temporal dynamics along latitudinal gradients in regions for which detailed information on climate, vegetation and soils is available (IGBP, 1996; McGuire et al., 2002). This approach represents an intermediate step between single-point studies and extrapolation/interpolation between transects to obtain a circumpolar picture of permafrost conditions and their dynamics.

For our studies, which are part of the Arctic System Science Program (ARCSS) of the National Science Foundation, we address permafrost conditions along two north-south transects – the Alaskan North Slope transect and the Tiksi-Yakutsk East Siberian transect (Figure 4.1). The two transects differ in the amount and form of available information. The Alaskan transect has been an area of intensive study during the last 15 to 25 years and especially during the last ten years (e.g., Romanovsky and Osterkamp, 1997). Most of the data gathered in these studies is stored electronically in the Geographic Information Systems (GIS) in the ARCSS database. Although the studies

Reproduced with permission of the copyright owner. Further reproduction prohibited without permission.

along the East Siberian transect have more than 40 years of history, this area has been studied less intensely than the Alaskan transect. In this paper we will focus on the East Siberian transect by presenting the results of our research on past, present and future permafrost conditions as well as on the permafrost dynamics of this region.

ENVIRONMENTAL AND PERMAFROST CONDITIONS ALONG EAST-SIBERIAN TRANSECT

Geographic location

The East-Siberian transect occupies almost the entire central part (between 120° and 140°E) of the Yakutia (Sakha) Republic in the eastern Siberia (Figure 4.1). The Laptev Sea of the Arctic Ocean borders the transect on the north. The territory of the transect is a land of mountains and plateaus, which occupy over 70 % of the area. The main rivers of the East- Siberian transect are the Lena River and its major tributaries, the Vilyuy River and the Aldan River. The Lena River watershed begins in the steep mountains that border the western shores of the Lake Baikal. Then the river meanders northeast and is joined by the Vitim River, followed by the Olyokma, Aldan, Amga, and Vilui Rivers before flowing through a wide delta and into the Arctic Ocean. The Lena River is over 4,000 km long, and its entire basin is 2.5 million sq. km.

Yakutia's greatest mountain range, the Verkhoyansk Range, runs parallel to and east of the Lena River (Figure 4.1), forming a great arch that begins in the Sea of Okhotsk and ends near the Laptev Sea (Arctic Ocean). This range has hundreds of small tributaries that feed the Lena River as it moves northward.

Reproduced with permission of the copyright owner. Further reproduction prohibited without permission.

Climate

The climate in the most parts of the East Siberian transect is extremely continental. The mean annual air temperature ranges from –10 to –15°C within the transect (Gavrilova, 1981). The Arctic Laptev Sea Lowlands (Figure 4.1) are characterized by an oceanic type of climate in their northern part and by a continental type farther south in their subarctic belt. The Arctic Ocean's influence makes the climate much less continental near the Arctic shore. The seasonal range of air temperature near the coast is 32-36°C, in comparison with 50-54°C within the inland parts of the Lowlands. Mean annual air temperatures in the Lowlands range from –13.5 to -15°C in the northeastern part to –11.6 to -13.5°C in the southern part. Total annual precipitation in the Arctic Lowlands ranges from 140-170 mm/year on the shoreline and on islands to 250-270 mm/yr in the interior. In spite of the low values of total annual precipitation, the ground (vegetation) surface is abundantly moist because evaporation rates are small. Winter snow thicknesses (or snow depths) generally decrease from 0.6 – 0.7 m in the foothills to 0.15-0.25 m near the Arctic shoreline and on the islands (Yershov, 1998). Snow density increases in the same direction due to the increase of winter wind speeds.

The Verhoyansk Range (with elevations up to 2500 m) is in the zone of severe continental climate with long cold winters and short hot summers. Seasonal temperature variations exceed 100°C (from +40°C during the summer to –60°C during the winter). This region is famous for being the coldest region of the Northern hemisphere during winter. The most extreme winter temperatures occur at Verkhoyansk, where the temperature can drop here as low as -71.2°C (Gavrilova, 1978).

Reproduced with permission of the copyright owner. Further reproduction prohibited without permission.

Smooth relief characterizes the Central Yakutian Lowlands, which represent a typical alluvial-lacustrine and erosion-denudation plain. High points reach 50-300 m above sea level. The climate within this territory is severely continental, with little precipitation and large seasonal variations in air temperatures (Climate of Yakutia, 1982). During winter, the center of the Siberian anticyclone is located within the Central Yakutian Lowlands, bringing clear skies and very cold air temperatures (–50 to –60°C). Mean January air temperatures decrease from –32°C in the west to –44°C in the east. Summer monthly mean temperatures are usually around 16-18°C. Mean annual air temperatures are –9 to –11°C and the range of seasonal variations is from 50 to 62°C. Winter inversions of air temperatures are very common in valleys. As a result, the air temperatures in valleys in wintertime can be as low as –70°C. Total annual precipitation does not exceed 250-300 mm, and the thickness of the winter snow cover typically ranges from 20 to 40 cm (Yershov ed., 1998).

Southern Yakutia is also characterized by a severe continental climate. Mean annual air temperatures vary from –6 to –15°C and depend on elevation (Southern Yakutia, 1975). Snow cover is comparatively thick (winter-average snow cover thickness is 0.6-0.8 m) and at the same time quite porous. Annual precipitation is 400-500 mm.

Permafrost and ground ice

The entire transect is located within the permafrost area. The Arctic Laptev Sea Lowlands are one of the most severe regions on Earth in terms of climatic conditions (not only at present, but also during the Pleistocene) (Danilova, 1989). Permafrost is continuous with mean annual ground temperatures in the range of –5 to –13°C (Figure

Reproduced with permission of the copyright owner. Further reproduction prohibited without permission.

4.2). Mean annual ground temperatures gradually decrease from south (–5°C) to north (–11 to –15°C). Through its insulating effect, the snow cover can increase mean annual ground temperatures by up to 8 °C and is therefore a major factor determining mean annual ground temperatures in this region (Gavrilova, 1978).

Active layer thickness ranges from 0.15-0.3 m in peat and in silty sediments with organic inclusions, to 0.9-1.5 m in sands and deluvial sediments (Dunaeva and Kondratieva, 1989). The active layer becomes gradually shallower from south to north due to the northward decrease in summer air temperatures. Permafrost thickness ranges from about 200 m under rivers beds and lakes to 500 m near the Arctic shoreline. The volumetric ice content of the soils ranges from about 30% (in sands) up to 70% (in silts) (Karpov, 1978).

Permafrost within the Verhoyansk Range is continuous with mean annual ground temperatures between –3°C and –9°C (Figure 4.2). Mean annual ground temperatures are warmer in valleys than on the ridges and mountaintops. Active layer thickness is generally less than 0.5 m in silt and 1.2 m in coarse-grain sediments (Gavrilova, 1978).

The thickness of permafrost is greatest (700-900 m and more) on ridges and mountaintops. In foothills, the permafrost thickness does not exceed 500-700 m, and in river valleys it is typically 100-300 m (Yakupov et al., 1984; Varlamov et al, 1993). The volumetric ice content in the frozen soils is typically 5 % to 10 %. Within the glacial sediments on slopes of the mountains, ice content can reach 20-30 % (Yershov, 1998).

Permafrost is continuous everywhere in the Central Yakutian Lowlands. Mean annual ground temperatures decrease gradually from south (-2 to –4 °C) to the north (–7

Reproduced with permission of the copyright owner. Further reproduction prohibited without permission.

to –9°C) (Figure 4.2). Within the Lena-Vilui Plain, the mean annual ground temperatures vary from +0.2 to –6°C. The mean annual ground temperatures are similar in Yakutsk. The warmest temperatures are observed in sandy-silt and sandy sediments with low ice content. Active layer thickness is about 1-2 m in sands and 0.5 –1 m in peat (Dunaeva and Kondratieva, 1989). The depth of permafrost ranges from about 100 m in the southern part (Olekminsk, Russkaya River) to about 400 m (Namtsy) in the northern part of the Plain.

In Southern Yakutia, there is a transition from continuous to discontinuous permafrost in spite of the fact that mean annual air temperatures are very close to those typical for Central Yakutia, which is in a zone of continuous permafrost. Southern Yakutia's uniqueness arises from the wide variety of climatic, geographical, hydrological and geological conditions. The combination enables large taliks (unfrozen ground occupying small areas and existing for more than a year (Yershov, 1998)) with mean annual ground temperatures around 0°C to coexist with 200-300 m thick permafrost (Southern Yakutia, 1975). Bedrock is often exposed and consists of gneises, crystallic schist, and carbonates.

The most peculiar feature of the East-Siberian transect is "Yedoma" or "Ice Complex". The Ice Complex occupies approximately 30 % of the transect (Figure 4.3). It can be described as syncryogenic ice wedges in a matrix of silt. The volumetric ice content can be as high as 60-80 percent (Soloviev, 1959; Tomirdiaro, 1980). The genesis of the Ice Complex is still an active topic of discussion and research. The most common theories about its origin can be categorized as alluvial, alluvial-lacustrine, glacial,

Reproduced with permission of the copyright owner. Further reproduction prohibited without permission.

deluvial and eolian (Tomirdiaro, 1980). At least some sections of the Ice Complex contain evidences of water sedimentation (Kaplina, 1981; Rozenbaum, 1976).

Ice complex is covered with a so called "protection layer", usually silt or sandy silt that often contains significant amounts of organic material (Karpov, 1984). The thickness of the protection layer does not exceed 2.8 m and is usually 1.5 – 2.0 m (Balobaev et al, 1996). If seasonal thawing reaches the ice horizon or if mean annual ground temperature exceeds 0°C, long-term thawing will start from the surface and thermokarst development will accompany the process of permafrost degradation.

Soils and Their Thermophysical Properties

Thermophysical properties of soils and rocks are among the crucial initial parameters for calculating the active layer thickness and ground temperatures. These properties include thermal conductivity, volumetric heat capacity and the latent heat of changes of water phase. The thermophysical properties of soils depend on factors such as texture, structure, mineral composition, organic content, water content (ice content), density, salt content and temperature (Feldman et al, 1988). All these factors are the result of the geological history of the sediment formation and the present-day landscape type and climate. Within the East-Siberian Transect, most of the soils formed during the Quaternary and overlay Mezozoic and Paleozoic bedrock. Bedrock can be highly weathered and is visible on the surface in some places (Hrutskyi and Derevyagin, 1981). Quaternary deposits have alluvial, eluvial-deluvial, glacial, lacustrine and fluvioglacial genesis. Alluvial sediments consist of sands with different grain size, sandy-silts and silts, and gravel and boulders in sandy or silt matrices in some places. In alluvial silty-organic

Reproduced with permission of the copyright owner. Further reproduction prohibited without permission.

sediments, which are sometimes up to 100 meters thick, one can often find massive underground ice (Ivanov, 1984). Eluvial-deluvial, glacial and fluvioglacial sediments often consist of crumbly-detritus in different matrices (Elovskaya et al, 1978).

It is practically impossible to distinguish the thermophysical properties of all genetically different types of soils, even for a small area. For regional studies and for engineering purposes it is sufficient to distinguish between the following types of soils: peat, sand, sandy silt, silt, soils with organic, gravel and bedrocks (Feldman et al, 1988).

Special consideration must be given to peat. The thermal properties of peat have major effects on mean annual ground temperatures and active layer thickness (Yershov, 1998). Peat is very common in tundra and in marshes within the taiga zone. The thickness of a peat layer can be as large as 40-50 cm, and in some places can exceed 1 m. Within the East-Siberian transect peat can be found in the valleys of all major and small rivers (Figure 4.4). In the north, it is found within the deltas of the Lena and Yana Rivers and on the Arctic Lowlands of Northern Yakutia. The thermal conductivity of the unfrozen peat varies from 0.29 to 0.52 W/(m °K) (Gavriliev, 1998); the volumetric heat capacity varies from 1760 to 3780 kJ/(m^3 °K); the thermal conductivity of frozen peat can reach 1.3 W/(m °K).

Most alluvial sediments within the East-Siberian transect can be put into three categories: sand, sandy silt and silt (Table 4.1, Figure 4.4). Thermal conductivity, heat capacity and latent heat vary significantly within each category, depending on grain size, water content, presence of organic material and genesis. The presence of organic material in soils can alter the physical and thermophysical properties of the soils (Yershov, 1998).

Reproduced with permission of the copyright owner. Further reproduction prohibited without permission.

The majority of alluvial soils within the transect contain organic material (Yershov ed., 1989; Elovskaya et al., 1978). For most of the territory, the quantity and character of the organic is not known.

Gravel and coarse-grained sediments of glacial, fluvial glacial or deluvial origin can be found in mountainous and uplands regions (Figure 4.4). Those sediments are characterized by low water and ice content and by high thermal conductivity (up to 3 W/(m*K)) (Feldman et al., 1988). The thermophysical properties chosen for our calculations were adopted from Feldman et al. (1988) and are averaged characteristics for each group.

THE DESCRIPTION OF THE MODEL AND THE INPUT PARAMETERS USED FOR THE HINDCAST AND THE PROJECTION OF THE PERMAFROST DYNAMICS

The Geophysical Institute Permafrost Lab (GIPL) model was used to simulate the spatial and temporal dynamics of permafrost in the East-Siberian transect for the past and the future. This model is a quasi-two-dimensional, quasi-transitional, spatially distributed, physically based analytical model for the calculation of active layer thickness and mean annual ground temperature. Details of the formulation are provided by Sazonova and Romanovsky, 2003. The core of GIPL is a modification of the formulations of Kudryavtsev et al. (1974), Romanovsky (1989), and Romanovsky and Osterkamp (1995 and 1997) for calculating mean annual ground temperatures and active layer thickness. Input parameters for the calculations are stored in GIS format for a series of layers. Digital maps of mean annual ground temperatures and active layer thickness

Reproduced with permission of the copyright owner. Further reproduction prohibited without permission.

(ALT) are the output of the model. The combination of GIS and a modified Kudryavtsev approach can be referred to as an interactive GIS. The calculations of the ALT and mean annual ground temperatures were performed on a grid consisting of 1000 grid cells with spatial dimensions of 0.5° latitude x 0.5° longitude.

The strategy that was followed in this study included the use of a reference simulation of permafrost dynamics in the East Siberian transect. This reference simulation consists of a hindcast for the 20th century blended with a projection (forecast) for the 21st century. The hindcast simulation, for the period 1900-1966, was forced by observationally-based monthly grids of surface air temperature (Jones, 1994, updated; Leemans and Cramer 1991) and precipitation (Hulme, 1994, updated), gridded to 0.5° resolution in latitude and longitude, as described by McGuire et al. (2001). For the period 1966-1994, the observational grids were blended, by the procedure of McGuire et al. (2001), with the monthly simulated fields of surface air temperature and precipitation from a HADCM2 GCM for the same period to provide the upper boundary conditions for GIPL (Figure 4.5). The boundary conditions for 1994-2100 were obtained directly from the output of the HadCM2 global climate model, forced by prescribed values of greenhouse gas concentrations and sulfate aerosols (e.g., Johns et al., 1997). The observational data were also used to establish the credibility of HadCM2, as described in the following section. The reasoning behind this strategy is that a hindcast simulation that captures present-day climate characteristics reasonably accurately can provide a 21st-century reference scenario against which other simulations, forced by climate output from different climate models, can then be compared.

Reproduced with permission of the copyright owner. Further reproduction prohibited without permission.

Boundary conditions and input parameters for period 1901-2000.

Climatic parameters

The climatic parameters used to drive GIPL include mean annual air temperatures, seasonal range of air temperatures, snow thickness and snow density. We note here that GIPL requires utilizes only a single (winter average) snow thickness for each year. The seasonal variation of this thickness is included implicitly through the use of air temperature's annual range, which is one of the three GCM output parameters used in driving GIPL. The annual range of air temperature effectively introduces into the permafrost simulation the effects of the seasonality of the snow cover. Because of the air temperature and snow cover simulated by HADCM2 are essential to the GIPL simulation beyond the late 20^{th} century, we first summarize HADCM2's configuration and then examine the air temperature and snow distributions simulated by HADCM2 over the East Siberian transect.

The HADCM2 GCM was developed in the Hadley Center (formerly the UK Meteorological Office) in 1994 as a modification of the Unified Model (Gullen, 1993). A coupled, ocean-atmosphere GCM, HADCM2 was among the first to be used in historical climate change experiments forced by past concentrations of greenhouse gases. HADCM2 has been run with a spatial resolution of 2.5 x 3.75 degrees of latitude/longitude, corresponding to approximately 295 km x 278 km at 45° N and S. This GCM has 19 levels representing the atmospheric components. The equilibrium climate sensitivity of HADCM2, which is the global-mean temperature response to a doubling of effective CO_2 concentration, is in the mid-range of estimates for the real climate system

Reproduced with permission of the copyright owner. Further reproduction prohibited without permission.

behavior (Johns et al., 1997; Mitchell et al., 1995) and is approximately 3.0°C (www.cru.uea.ac.uk/).

The mean annual air temperatures simulated by HADCM2 generally decrease northward and eastward in the East Siberian transect. The warmest (–8 to –5°C) air temperatures are in the southern part of the transect (between 55° and 60°N), while the coldest mean annual air temperatures (down to –16°C) are in the northernmost parts of the transect (the Lena River delta and Arctic Lowlands) and along the eastern slope of the Verkhoyansk Range (Figure 4.5). Mean annual air temperatures are generally colder in the eastern part of the transect (east of 130°E) than in the western part. Interannual variations of mean annual air temperatures are 3 to 4°C (Figure 4.6).

The seasonal range of air temperatures has been derived from the mean monthly values. The average magnitude of the seasonal range is about 60-65°C. The lowest seasonal range of air temperatures is in the northernmost and southernmost parts of the transect (up to 35-40°C).

HADCM2 as well as other GCM's used for the hindcast and forecast provide the snow-water equivalent instead of snow thickness and snow density. The latter two important parameters for the ground thermal regime were derived from snow-water equivalents by the relation $W_{eq} = \rho_{sn} H_{sn}$ (where w_{eq} is snow-water equivalent in mm of water, ρ_{sn} is the snow density in kg/m^3, and H_{sn} is the snow cover thickness in meters), together with data from meteorological stations and Feldman et al.'s (1988) method based on an analysis of snow cover properties measured at 166 meteorological stations

Reproduced with permission of the copyright owner. Further reproduction prohibited without permission.

within Yakutia. The processing and analysis of the measured data permitted a grouping of the meteorological stations (five groups altogether) on the basis of the relation $\rho_{sn}(H_{sn})$, which in general form can be represented as:

$\rho_{sn} = a_i + b_i H_{sn} + c_i H_{sn}^2$, where

a_i, b_i, c_i are coefficients that are specific to each group of meteorological stations, i = 1,…,5.

For each group, the following relationships between snow density and snow thickness have been established (Feldman et al, 1988):

1st group $\rho_{sn} = 140 + 628 H_{sn} - 457 H_{sn}^2$

2nd group $\rho_{sn} = 100 + 414 H_{sn} - 267 H_{sn}^2$

3d group $\rho_{sn} = 120 + 171 H_{sn}$

4th group $\rho_{sn} = 120 + 160 H_{sn}$

5th group $\rho_{sn} = 170 + 100 H_{sn}$

A spatial interpolation between meteostations was then performed to obtain the spatial extent for each group, and each grid cell was assigned to a particular group (Figure 4.7). The largest portion of the transect area belongs to the fourth group with relatively low snow density. Low snow density together with thick (0.3 – 0.5 m) snow cover can warm the mean annual ground temperatures by up to 6-8°C (Feldman et al, 1988). By using HADCM2's and the observationally-based snow-water equivalents (W_{eq}), the relation $W_{eq} = \rho_{sn} H_{sn}$, and the linear or quadratic polynomials listed above, one

Reproduced with permission of the copyright owner. Further reproduction prohibited without permission.

can solve two equations for the two unknowns (ρ_{sn} and H_{sn}), thereby obtaining the snow thickness for each grid cell for each year of the calculation.

The northern part of the transect, including the Lena River delta and the Arctic Lowlands, is in the first group, for which snow thickness is generally smaller and snow density is relatively high. As a result, the warming effect of the snow in these areas is as small as 2-4°C. The high snow density can be explained by high moisture content in the air and in the snow during autumn and early winter, and by strong winds that cause the snow to compact.

Validation of the HADCM2 GCM

The measured air temperatures and snow thickness from 32 sites within the East-Siberian transect were used for the comparison with the outputs of HADCM2 model for the period 1966-1989. Snow cover thickness is available from 8 of the 32 sites. HADCM2's output climatic parameters (courtesy of David McGuire) were interpolated over the entire transect. The same interpolation has been done for observed climatic data. The results are shown in Figure 4.5.

For most parts of the transect, the simulated and observed mean annual temperatures are within 2°C of each other. For the northernmost and southernmost parts, this difference can increase to 4-5 °C. The difference between measured and calculated temperatures also decreases when approaching a data site, implying that the error between measured and calculated temperatures can be partially explained by errors in the spatial interpolation of the measure data.

Reproduced with permission of the copyright owner. Further reproduction prohibited without permission.

The model's seasonal range of air temperature is smaller than observed over the most of the transect. For the central part, the difference between observed and modeled seasonal ranges is as large as 20°C (Figure 4.5). This difference can lead to an error of up to 0.2 m in the estimate of the active layer thickness. The observed and modeled snow cover thicknesses are similar, except for the northernmost parts of the transect.

Overall, the validation of HADCM2 showed that this model can serve as a useful benchmark for comparisons with other GCMs and can be used to hindcast mean annual ground temperatures and active layer thickness for the 1900-2000 period, subject to small errors resulting from differences in the observed and simulated values of certain climatic parameters.

Vegetation and soils thermal properties

The thermal effects of surface vegetation depend on vegetation type, the presence of water and the season (Tyrtikov, 1974). Moss is one of the most important and widespread surface vegetation types (Beringer et al., 2001). Because moss has a large capacity for retaining moisture, the wintertime thermal conductivity of moss is high, sometimes as large as 1.8 W/(m*K) (Feldman et al., 1988). Hence moss allows the effects of cold waves to penetrate deep into the ground. During summer, when evaporation rates are high, moss loses moisture and its thermal conductivity can decrease to 0.2 W/(m °K) and possibly even lower (Feldman et al., 1988; Beringer et al., 2001). For this reason, moss is an effective insulator during summer. Consequently, permafrost is more stable and the active layer is shallower in areas with moss.

Reproduced with permission of the copyright owner. Further reproduction prohibited without permission.

Shrubs, grass and lichens generally, but not always, act like insulators in winter and in summer. Shrubs play an important role in snow distribution and redistribution (Sturm et al., 2001). In the presence of shrubs, the ground temperatures are warmer and the active layer is usually thicker. The only exception occurs in the presence of very thick shrubs, which create shadows and thus lead to a cooling of the surface during summer (Yershov, 1998).

In our study we considered only low-level of vegetation that is less than one meter high, because the information about higher vegetation such as trees and tall shrubs is already incorporated into the monthly surface air temperature output from GCMs. Our vegetation typing was based on a dataset for the East-Siberian transect created in GIS format by D.O. Sergueev using a Top-Soil Cover vegetation map from the Global Characteristics Database (edcdaac.usgs.gov/glcc/globdoc2_0.html). Surface vegetation was generalized into 6 classes: sparse moss or lichen, moss or lichen, moss with grass tussocks , moss or lichen with grass, sparse grass, and dense grass. Surface vegetation affects the ground temperature and is very important for the active layer thickness.

Soils properties such as moisture content, thermal conductivity in frozen and thawed state, heat capacity for frozen and thawed soils, and volumetric water content were assigned to each grid cell. The thermophysical properties assigned to each group of soils, discussed previously, are shown in Table 4.1.

Permafrost Dynamics Within The East-Siberian Transect During 1900-2000

The active layer thickness (ALT) and the mean annual ground temperatures are highly variable parameters, and the interannual range of the variations in the simulated

Reproduced with permission of the copyright owner. Further reproduction prohibited without permission.

time series can be considerable (0.5 m for the ALT and 3-4°C for the mean annual ground temperatures). Over decadal time scales (10-20 years), the mean annual ground temperatures can vary by as much as 5-6°C, while variations in the ALT can be as large as 1.5 m (Dunaeva and Kondratieva, 1989).

The distribution of the ALT for the sample year of 1905 (Figure 4.8) shows that the soil thermophysical properties are the major factor affecting ground thermal regime. The largest ALT can be found in mountains and uplands with glacial-fluvioglacial sediments and eluvial sediments consisting mostly of sand, pebbles, and cobbles, with inclusions of silt (Figure 4.4). Sand, pebbles and cobbles have high thermal conductivity and relatively low volumetric ice content (15-25 %). The shallowest ALT usually occurs in areas with significant peat or organic material content in soils and with a moss cover on the ground surface. In northern parts of the transect, the active layer is also shallow due to very low mean annual air temperatures and cold summers.

The retrospective analysis of the dynamics of the ALT and the mean annual ground temperatures shows periods of relative warming of ground temperatures and accompanying increases in the ALT, as well as periods with relative cooling in mean annual ground temperatures and decreases in the ALT. The first relatively warm period in the model period 1900-2000 occurred during approximately 1930-1940 (Figure 4.8). In comparison with the model's initial state, the ALT was deeper everywhere in the East-Siberian transect during that time. The most significant increase took place in uplands and mountainous areas (up to 1 m for the ALT and up to 3°C for mean annual ground temperatures). In the lowlands, near the coastline and adjacent regions, the increase in

Reproduced with permission of the copyright owner. Further reproduction prohibited without permission.

the ALT was much smaller, typically less than 0.3 m. The zone of the shallow ALT, where thickness does not exceed 0.3 m, shifted to the north and contracted.

After the warm period of 1930-1940, a relatively cold period occurred in the simulation during 1960-1970, when the ALT decreased and mean annual ground temperatures decreased (Figure 4.8). The area with shallow ALT moved southward, and the ALT did not exceed 2 m anywhere in the transect. The most significant changes in the ALT and in the mean annual ground temperatures again took place in uplands and mountainous regions.

The next warm period in the simulation occurred in 1990-2000, which was warmer than the 1930-1940 year period. The increase in mean annual air temperatures caused a deepening of the ALT (Figure 4.8) and an increase in the mean annual ground temperatures.

The analysis of the ALT and mean annual ground temperatures for the past 100 years (1900-2000 years) showed that, under the influence of natural variability of mean annual air temperatures (e.g., Polyakov et al., 2002), significant changes occurred in the ALT ($\pm$ 1 m) and in the mean annual ground temperatures ($\pm$ 3-4°C) of the East-Siberian transect. In the period since 1900, there were two warm subperiods during which the ALT was deeper and mean annual ground temperatures were higher. Those two warm periods were separated by a cold period, during which the mean annual ground temperatures were cooler and ALT was shallower.

Boundary conditions and parameters for the forecast for the period 2000-2099

Reproduced with permission of the copyright owner. Further reproduction prohibited without permission.

Climatic output parameters from five GCMs, in addition to HADCM2, were used as upper boundary conditions to obtain 21st-century projections of ALT and ground temperatures. The five additional GCMs were all designated for use by to the Arctic Climate Impact Assessment program (ACIA) (www.acia.uaf.edu).

The ACIA is using simulations forced by the B2 scenario (IPCC, 2000), which is a "moderate" scenario of CO_2 increase in the atmosphere. The outputs of 21st-century simulations (through 2100) forced by the B2 scenario were used here as input to the GIPL permafrost model.The five ACIA-designated GCMs are those of Canadian Center for Climate Modeling and Analysis (CCC), the National Center for Atmospheric Research/Climate System Model (CSM), Geophysical Fluid Dynamics Laboratory (GFDL), Hadley Climate Center's Version 3 (HadCM3) and the Max Planck Institute for Meteorology (ECHAM). The spatial resolution of each model, together with a reference for each, is shown in Table 4.2. In order to incorporate climatic data from each GCM into GIPL, the climatic outputs were formatted and interpolated to fit the 0.5° x 0.5° latitude/longitude grid of the GIPL.

The various GCMs differ significantly in terms of their projected mean annual temperatures, amplitudes of seasonal variations of temperature, and snow thickness for the period 2000-2099. The increase in mean annual air temperatures by the end of the year 2100 ranges from 2 to 9 °C among the models. The largest increase is projected to occur in high latitudes (to the north of 65° N).

The CCC simulation provides a good approximation to mean annual air temperatures of the reference (HADCM2) simulation in 2000. Latitudinal and

Reproduced with permission of the copyright owner. Further reproduction prohibited without permission.

longitudinal zonality is present. The CCC model's coldest mean annual air temperatures (–14 to –16°C) are in the western part of the Lena River delta; the warmest region (–8 to –6°C) is the southern (south of 60° N) part of the transect. The CCC model gives generally warmer (about 1-2 °C) mean annual air temperatures for the central and southern parts of the transect in comparison with HADCM2. Interannual variations of mean annual air temperatures are typically 2 to 4°C, and the magnitudes become smaller by the year 2100 (Figure 4.9). CCC projects increases in mean annual air temperatures by up to 3-4°C, which puts this simulation in the category of a moderate warming. The seasonal range of CCC air temperatures (35-55°C) is 10-20°C smaller than in the reference simulation over much of the transect. This difference in amplitude can lead to an error of up to 0.2 – 0.3 m in the estimated ALT.

The CSM (Figure 4.10) can be categorized as a "cold" model. The warmest mean annual air temperatures (–12 to -10°C) are in the far southwestern part of the transect. The coldest temperatures (–20 to –18°C) occupy a wide zone between 70° and 75 °N. In the central part of the transect, mean annual air temperatures do not exceed –12°C. In comparison with reference data, this GCM gives much colder (by up to 4°C) mean annual air temperatures. The variation of the CSM temperatures in the East Siberian transect is almost entirely zonal, i.e., the temperatures vary with latitude but only negligibly with longitude. The interannual variability of mean annual air temperatures is high (5 to 7°C), with a slight decrease towards 2100. CSM projects increases in mean annual air temperatures of up to 4-6°C by 2100. The seasonal range of air temperatures in this model is low (35-50°C) in comparison with the reference simulation. Because of its low

Reproduced with permission of the copyright owner. Further reproduction prohibited without permission.

mean annual air temperatures and small seasonal range, CSM predicts very cold summers. In the northern parts of the transect, the model simulates no summer at all, with snow cover persisting through the summer. The snow thickness is low in comparison with the reference, with a range from 0.1 to 0.3 m over much of the transect.

The annual mean air temperatures simulated by the Geophysics Fluid Dynamics Laboratory (GFDL) model are generally colder than those of HADCM2 by 1-3 °C in 2000. For most parts of the transect, the mean annual air temperatures range from –10°C to –14°C (Figure 4.11). There is a slight longitudinal variation of the simulated temperatures. The warmest temperatures are to the south of 60° N and do not exceed –10°C. Interannual variability of mean annual air temperatures reaches 6-8°C. In comparison with other models, there is no decrease in interannual variability by the end of the 21st century. Mean annual air temperatures increase by 5 - 7°C during the 2000-2100 simulation period. The seasonal range of air temperatures is realistic, 60-65 °C over most of the transect. This model's snow cover is very thick, ranging from 0.4 m in the far north to 0.8 m in the central and southern parts of the transect.

HADCM3 is the second GCM from Hadley Climate Center used for our East Siberian climatic forcing. In comparison with reference HADCM2, it gives slightly colder air temperature and a shallower snow cover. Mean annual air temperatures generally show a realistic variation in latitude and longitude (Figure 4.12). The coldest temperatures are in the northernmost part of the transect and range from –14 to –18°C. The warmest temperatures (–5 to –10°C) are in the southern and central parts. The interannual variability of temperatures is low (2 to 4°C).

Reproduced with permission of the copyright owner. Further reproduction prohibited without permission.

The ECHAM GCM developed at the Max Planck Institute for Meteorology produces what can be called the "worst case scenario" for permafrost. The increase in mean annual air temperatures for the period 2000-2100 is large, typically 8 - 11°C. Mean annual air temperatures are in good agreement with the reference values everywhere except in the northernmost part of the transect and in the Arctic lowlands, where the model's temperatures are warmer than the reference values (Figure 4.13). Mean annual air temperatures vary realistically with latitude and longitude. The warmest mean annual air temperatures (–5 to –8°C) occupy the southwestern part of the transect, while the coldest air temperatures (–14 to –16°C) are found in the center of the easternmost part of the transect. Averages for the central portion range from –10 to –14°C. The interannual variability of the air temperatures is 3 - 4°C. The seasonal range of air temperature, generally from 40° to 60°C, is slightly lower than the corresponding reference values. The highest amplitudes are in the central and western parts of the transect. Snow cover thickness is 0.2 m to 0.3 m for the entire transect. There is no zonality in the snow cover distribution.

The surface air temperature and snow cover from the models described above provided the climate forcing data for the GIPL model. Other parameters for the GIPL simulations, including soil properties and vegetation types, were the same as for the HADCM2 hindcast in all the permafrost simulations.

PROJECTIONS OF PERMAFROST DYNAMICS FOR THE PERIOD OF 2000-2099

Reproduced with permission of the copyright owner. Further reproduction prohibited without permission.

The ALT distributions for 2000 (Figure 4.14) permit evaluations of the different GCMs relative to the reference HADCM2 simulation. In comparison with this reference simulation, CSM gives a very shallow active layer (ALT less than 1.5 m) in the central part, where HADCM2 simulates an ALT of 2-3 m. In contrast, CCC and GFDL give generally larger values of the ALT. ECHAM and HADCM3 are the closest to the reference GCM.

According to all models, the smallest ALT occurs in the valleys of large rivers, where soils are composed of silt with peat, and in the colder northern parts of the transect (to the north of 70°N). CSM gives the largest zone with a shallow active layer (less than 0.6 m) to the north of 70°N; in the simulations by the other models, this zone includes only the Lena River delta and the Arctic Lowlands. The deepest (up to 2 – 3 m) ALT is simulated within territory occupied by glacial, fluvioglacial coarse deposits. Within the Central Yakutian lowlands, the ALT ranges from 1.2 m to 2.4 m according to all GCMs.

By 25 years after the beginning of the forecast, almost all GCMs, except for CSM, show that the mean annual ground temperatures will be warmer by up to 1-2°C and the ALT will be deeper by up to 1 m (Figure 4.15). CSM predicts a cooling in 2020-2030. According to this model, the zone with the shallowest ALT (less than 0.6 m) occupies most of the eastern part of the transect; in the rest of the area, the ALT simulated by CSM does not exceed 1.8 m. On average, the decrease in CSM's ALT ranges from 0.2 to 0.4 m. Mean annual ground temperatures are projected to be colder as well. In comparison with the reference model, ECHAM and CCC produce a larger

Reproduced with permission of the copyright owner. Further reproduction prohibited without permission.

increase of ALT by up to 1 m in the southwestern part of the transect. GFDL and HADCM3 produce ALT values that remain the closest to the reference GCM.

By 50 years after the beginning of the forecast (Figure 4.16), all the models predict an increase of 0.5-1 m in the ALT but, in comparison with the reference simulation, only ECHAM predicts a zone with thawing permafrost. The reference model and ECHAM predict the formation of a zone with widespread permafrost degradation (annual mean temperature at the base of the active layer exceeds 0°C) in the southwestern part of the transect, where uplands are widespread. According to ECHAM, this zone will be twice as large as in the reference model. CCC and ECHAM give the largest increases in the ALT (up to 1-2 m) in the central and southern parts of the transect. CSM predicts a northward shift of the zone with shallowest ALT, with a net increase of the ALT by up to 0.8-1 m. All the GCMs predict that the shallowest ALT will be in the Lena River delta and in the valleys of large rivers. The deepest ALT (from 1.2 m to 3.6 m) will be in the southwestern part of the transect. ECHAM gives the deepest ALT (3.6 m). The most significant increase in the ALT will take place in the areas with coarse-grained soils and in the southern part of the transect.

By 75 years after the beginning of the forecast, the ECHAM and CSM models indicate that there will be a relatively cold period, during which the zone with permafrost degradation that existed in 2050 (ECHAM) will totally disappear (Figure 4.17). The ALT will decrease by up to 1 m according to ECHAM and CSM. According to the CSM scenario, the zone with shallowest ALT will shift farther south. Other GCMs predict an increase in mean annual ground temperatures up to 2-3°C, together with a deepening of

Reproduced with permission of the copyright owner. Further reproduction prohibited without permission.

the ALT. A zone with permafrost degradation appears by 2075 in the CCC-driven simulation. This zone occupies the central part of southeastern uplands. According to the reference model, the zone where permafrost degradation has begun will progress farther and almost triple in size.

By the year 2099 (Figure 4.18), which is the end of the forecast, the zone with thawing permafrost will be widespread in the southwestern upland part of the transect, according to all simulations except CSM. ECHAM predicts the largest zone, which expands almost to the Vilui River and occupies approximately 19% from the total area of the transect. The reference model gives a smaller zone with permafrost degradation (about 10 % of the transect area). CCC and HADCM3 give even smaller areas of thawing permafrost. ECHAM, CCC, GFDL and HADCM3 predict deep ALT for uplands in the southwestern and central parts of the East-Siberian transect. In these simulations, the ALT ranges from 3 to 4 m in central part of the transect where coarse-grained sediments are found. CSM produces comparably smaller values of the ALT. According to this model, the deepest ALT is found in the southwestern part of the transect, and the depth will not exceed 2.4 m.

CONCLUSIONS

The primary conclusions are the following:

1. CCC, HADCM3, HADCM2 and ECHAM predict that a zone with permafrost degradation will develop within the southwestern part of the transect. The starting point in time and the character of dynamics of this zone vary among the models. ECHAM and

Reproduced with permission of the copyright owner. Further reproduction prohibited without permission.

HADCM2 predict that this zone will develop by 2050. According to HADCM2, this zone grows continuously through time and will reach its maximum (11% from the total area of the transect) in 2099. ECHAM indicates that the dynamics of the zone with permafrost degradation varies non-uniformly in time -- in 2075, this zone totally disappears due to a relatively cold period, but it forms again and reaches almost 25 % of the total area by 2099. According to CCC, this zone will develop by 2075 and will double in size by 2099. HADCM3 predict that permafrost degradation will not start until the 2080s.

2. All GCMs except CSM predict that the ALT will deepen by 0.5 – 2 m everywhere within the transect, and that mean annual ground temperatures will rise by 2-6°C. However, the increase in mean annual ground temperatures and the ALT will not be uniform in time. There will be relatively cold and warm periods caused by natural variations of air temperatures. These variations will be superimposed on the background warming trend. The timing of cold and warm periods varies among the GCMs. For example, the 2020s and 2030s are relatively cold according to CSM and GFDL, and the 2070s and 2080s according to ECHAM and CSM.

3. The most significant increase in mean annual ground temperatures and in the ALT take place in southwestern part of the transect and in the areas with coarse-grained sediments, which are characterized by low water content and high thermal conductivity. Such thermophysical properties allow those soils to respond quickly to changes in air temperature.

Reproduced with permission of the copyright owner. Further reproduction prohibited without permission.

ACKNOWLEDGEMENTS

This research was funded by ARCSS Program and by the Polar Earth Science Program, Office of Polar Programs, National Science Foundation (OPP-9721347, OPP-9732126, OPP-9870635), and by the State of Alaska. The temperature data used in this study are available to other researchers through the JOSS project (http://www.joss.ucar.edu) and from NSIDC (http://nsidc.org).

Reproduced with permission of the copyright owner. Further reproduction prohibited without permission.

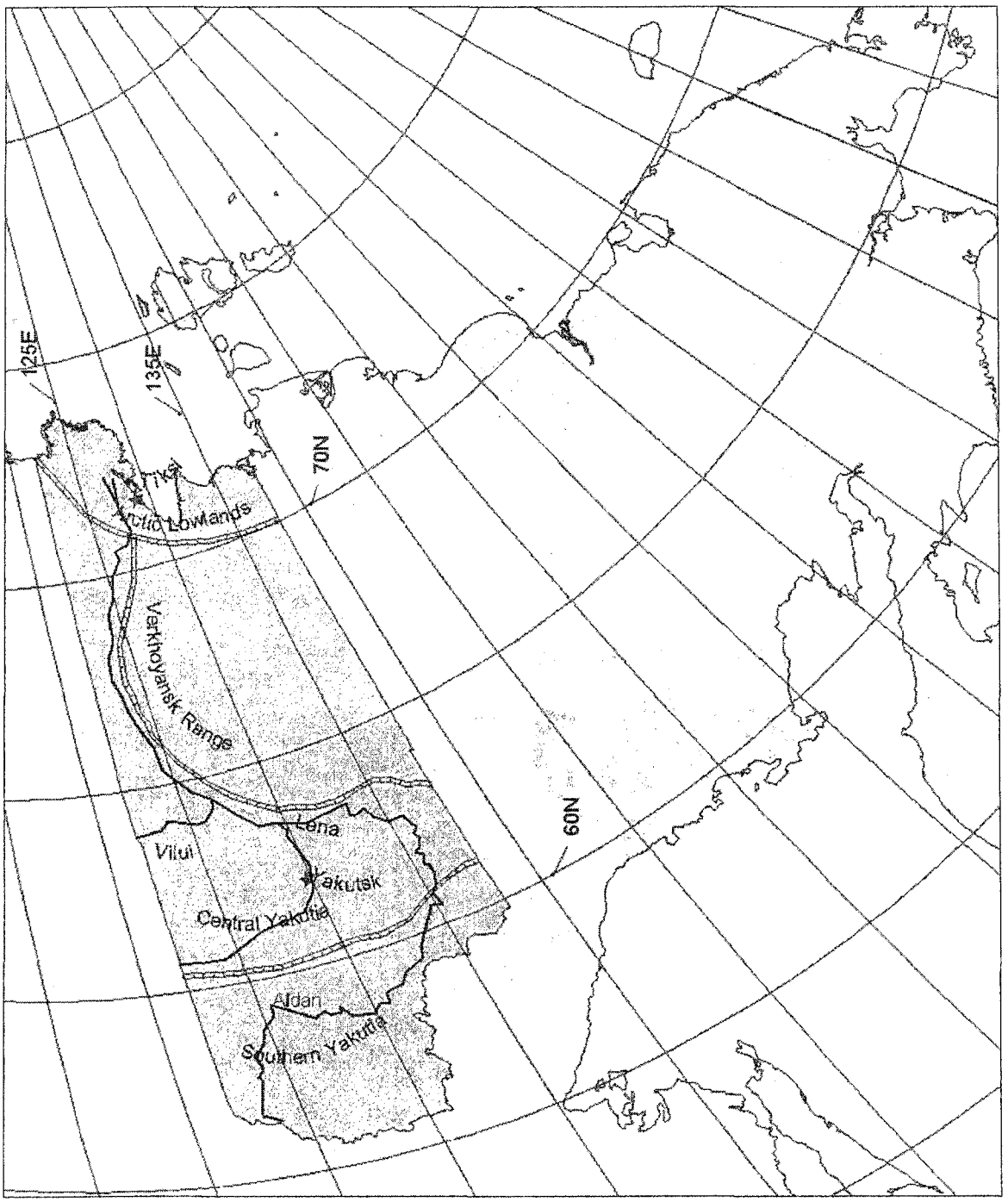

Figure 4.1: The geographic location of the East-Siberian transect showing the major rivers and the physiographic provinces.

Reproduced with permission of the copyright owner. Further reproduction prohibited without permission.

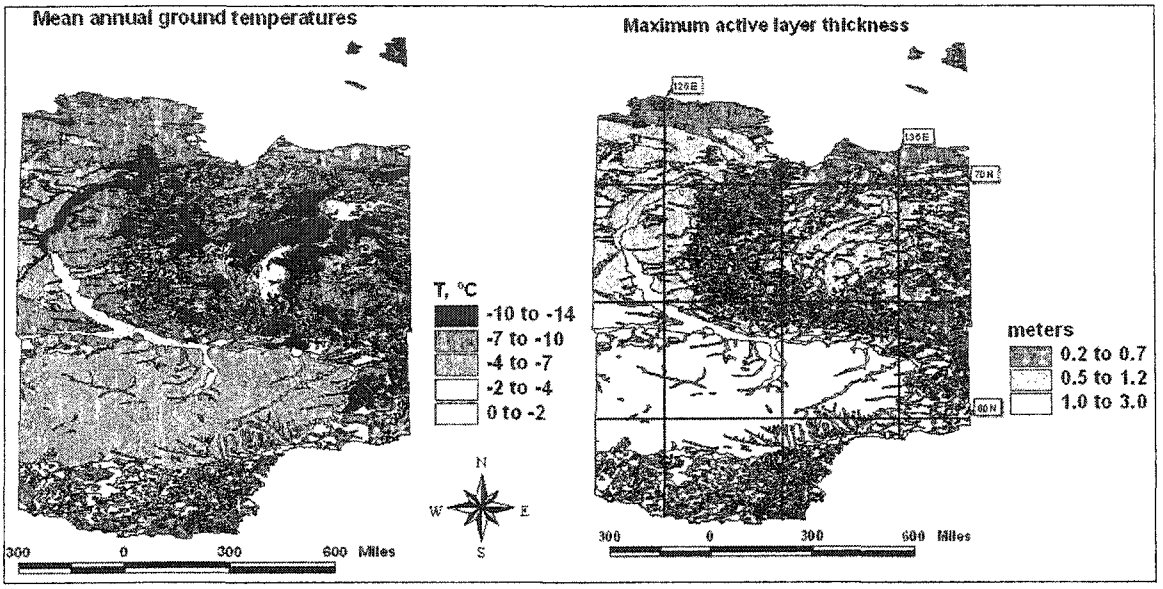

Figure 4.2: Active layer thickness and mean annual ground temperatures within the East-Siberian transect. Derived form the Map of Landscapes and Permafrost Conditions in Yakutia (scale 1: 2500 000), Academy of Science of USSR, Siberian Branch, Institute of Permafrost, P.I.Melnikov ed. Digitized by the Permafrost Lab, GI, UAF

Reproduced with permission of the copyright owner. Further reproduction prohibited without permission.

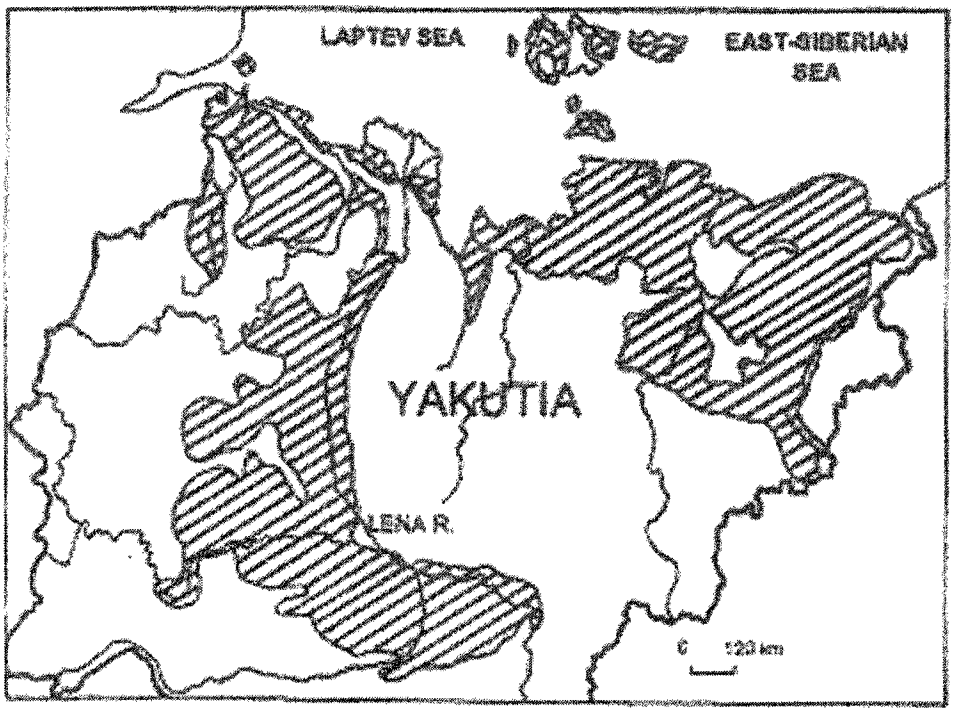

Figure 4.3: Schematic Map of Ice Complex distribution within the East-Siberian Transect (Courtesy of M.N. Grigoriev).

Reproduced with permission of the copyright owner. Further reproduction prohibited without permission.

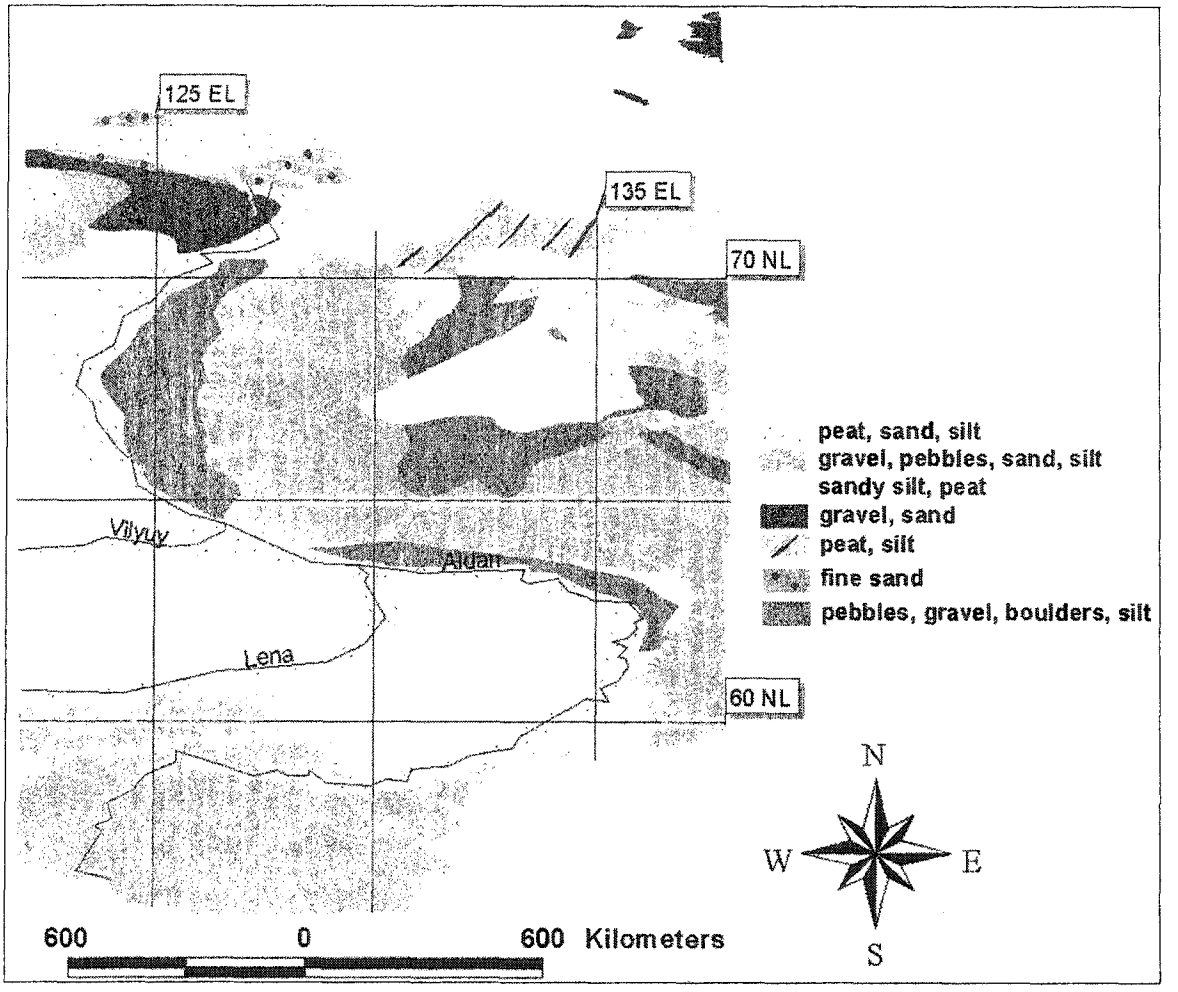

Figure 4.4: Soil types within the East-Siberian transect derived using (Elovskaya et al, 1978) and (Krasnyi, 1978).

Reproduced with permission of the copyright owner. Further reproduction prohibited without permission.

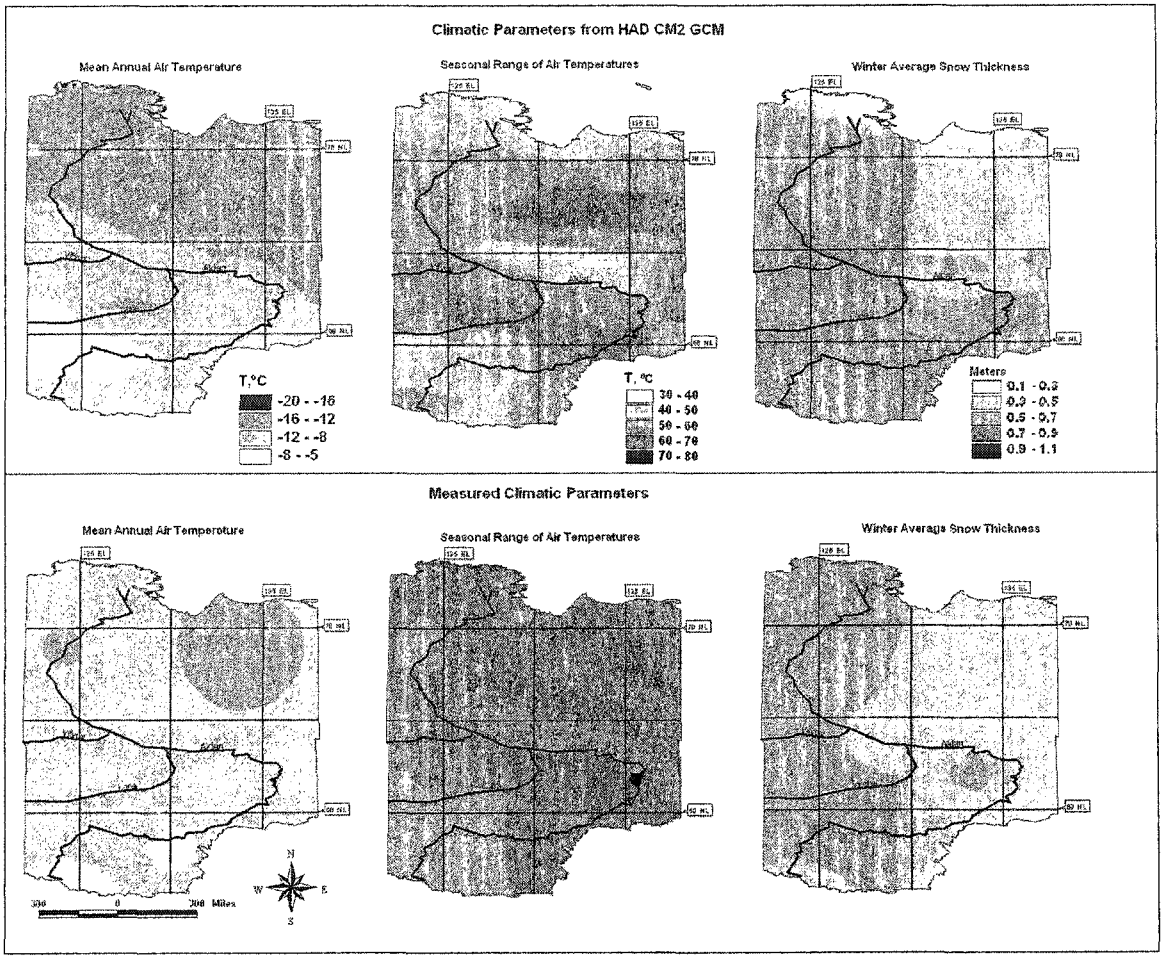

Figure 4.5: Comparison between measured and modeled using HAD CM2 GCM mean annual air temperatures, seasonal range of air temperatures and snow cover thickness (averaged for the period of 1966-1989).

Reproduced with permission of the copyright owner. Further reproduction prohibited without permission.

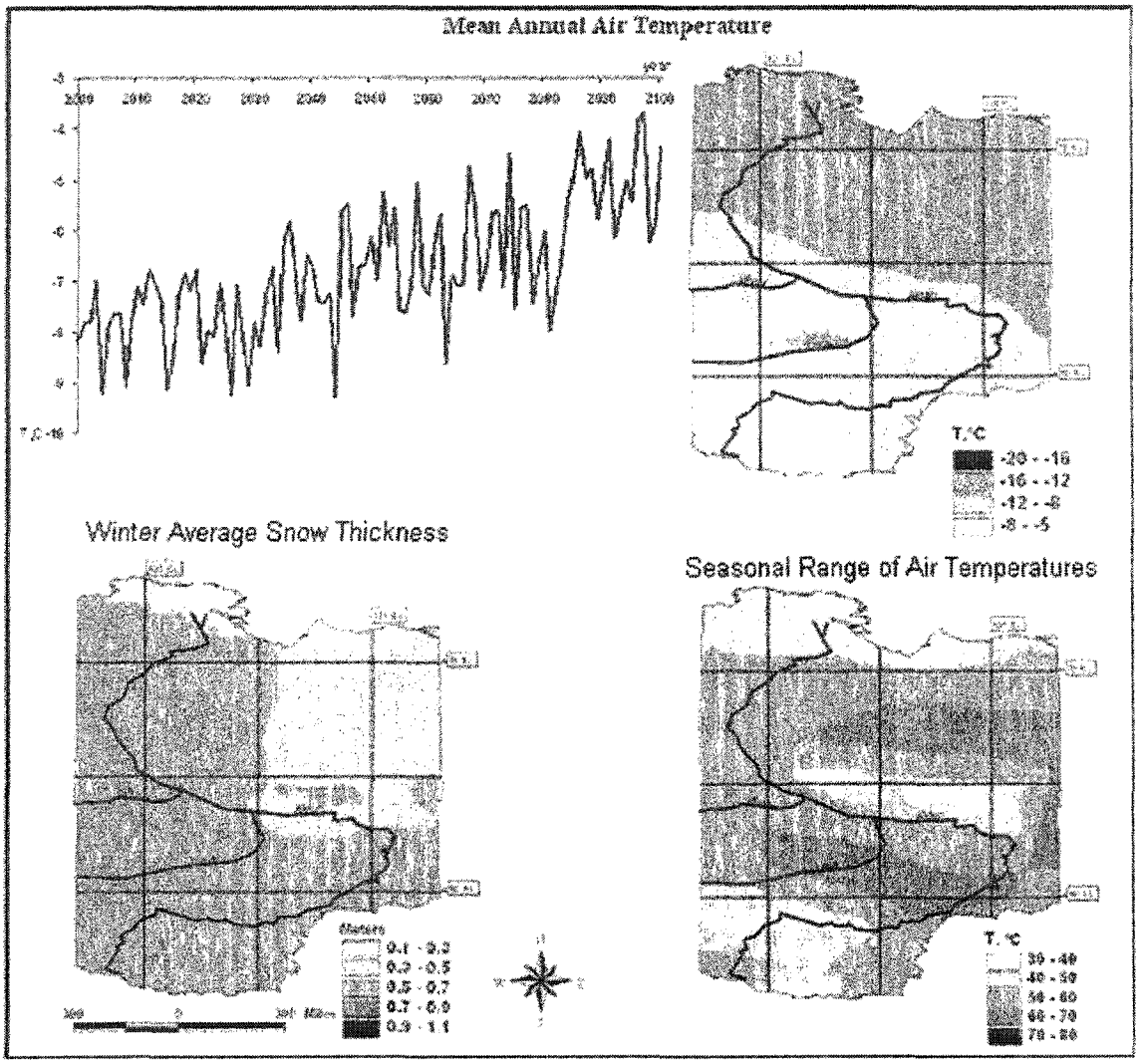

Figure 4.6: Output climatic parameters from HadCM2 GCM for the year 2000

Reproduced with permission of the copyright owner. Further reproduction prohibited without permission.

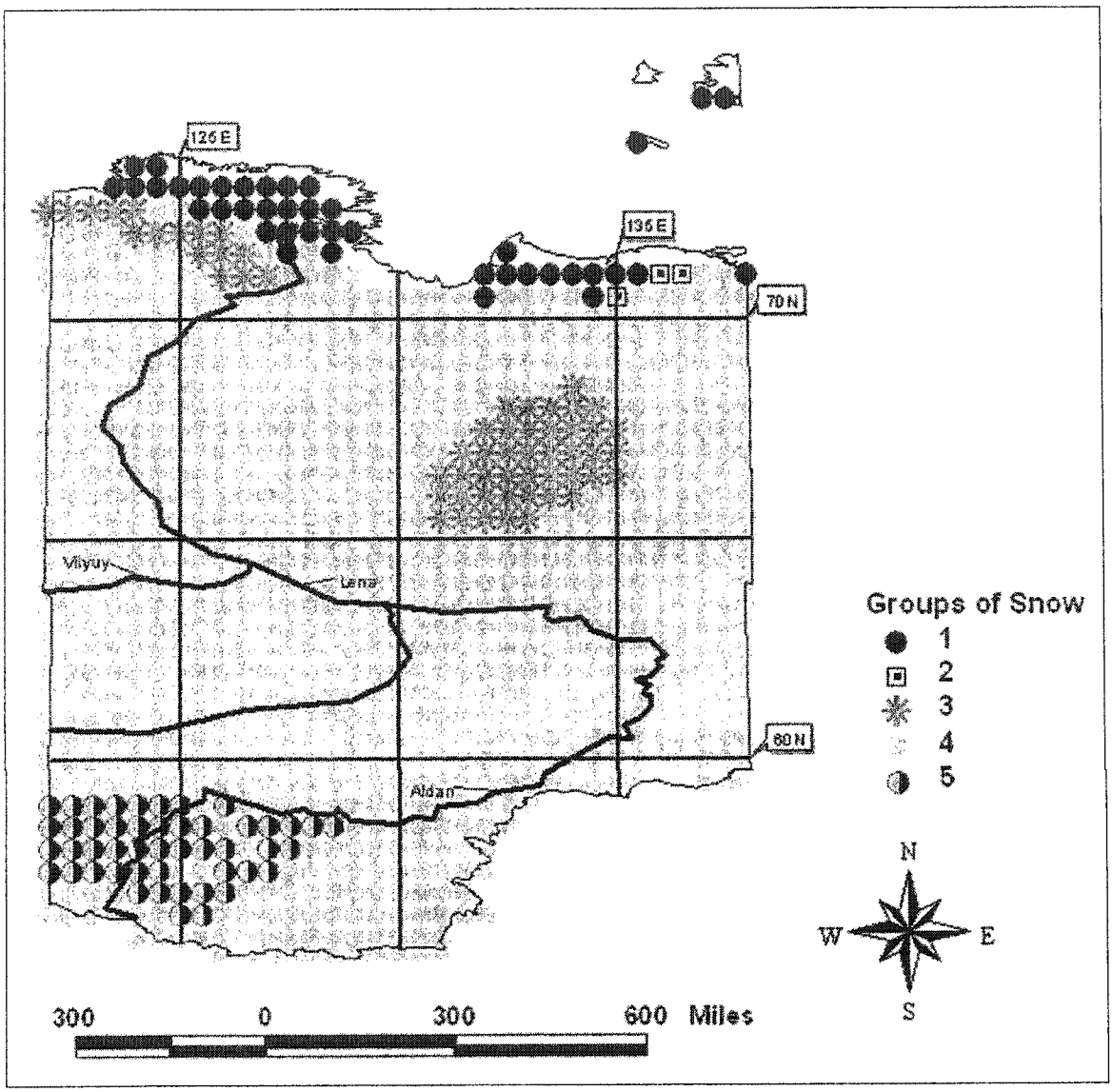

Figure 4.7: Snow cover types distribution derived from a snow density classification (after Feldman et al., 1998)

Reproduced with permission of the copyright owner. Further reproduction prohibited without permission.

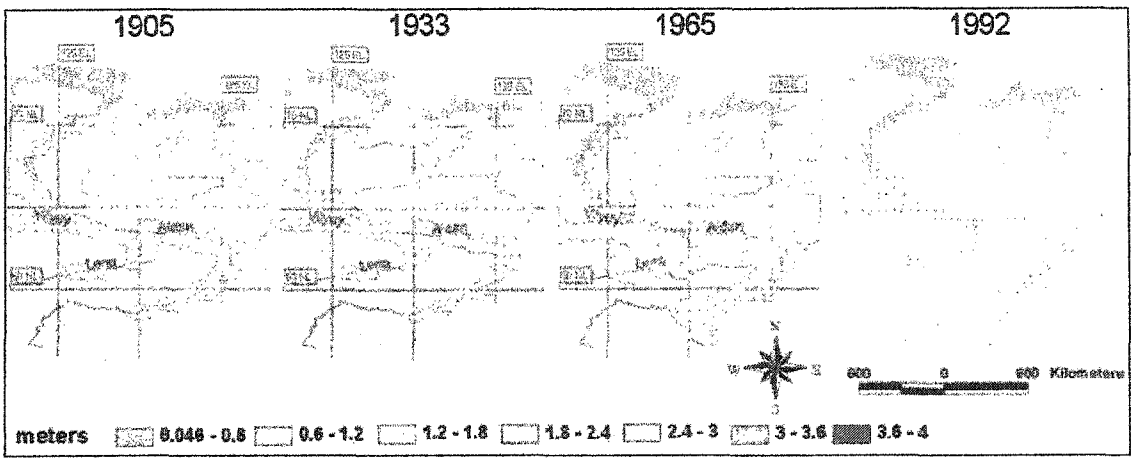

Figure 4.8: The active layer thickness dynamics within the East-Siberian transect in 20th century calculated using climatic parameters from HadCM2 GCM

Reproduced with permission of the copyright owner. Further reproduction prohibited without permission.

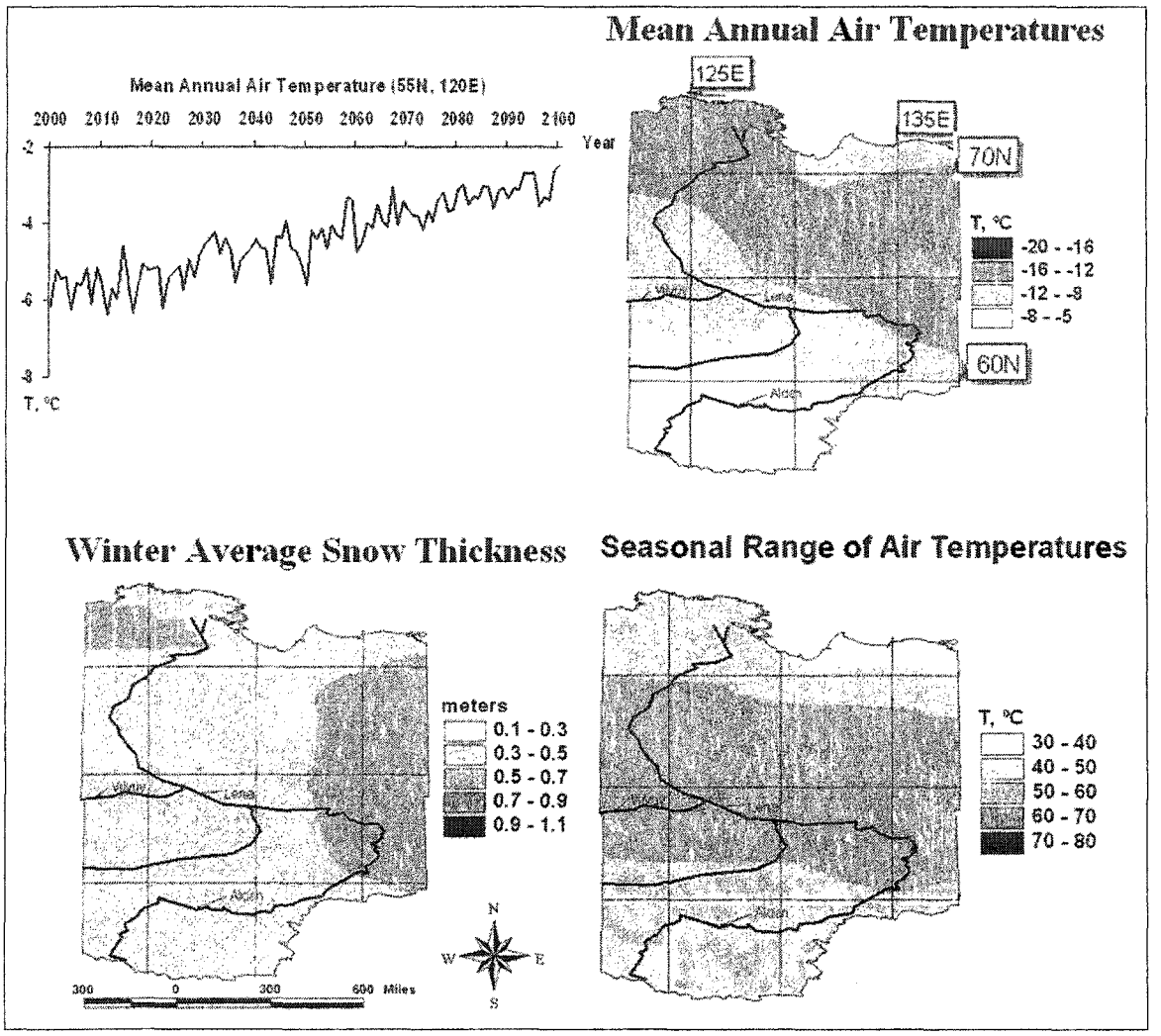

Figure 4.9: Output climatic parameters from CCC GCM for the year 2000.

Reproduced with permission of the copyright owner. Further reproduction prohibited without permission.

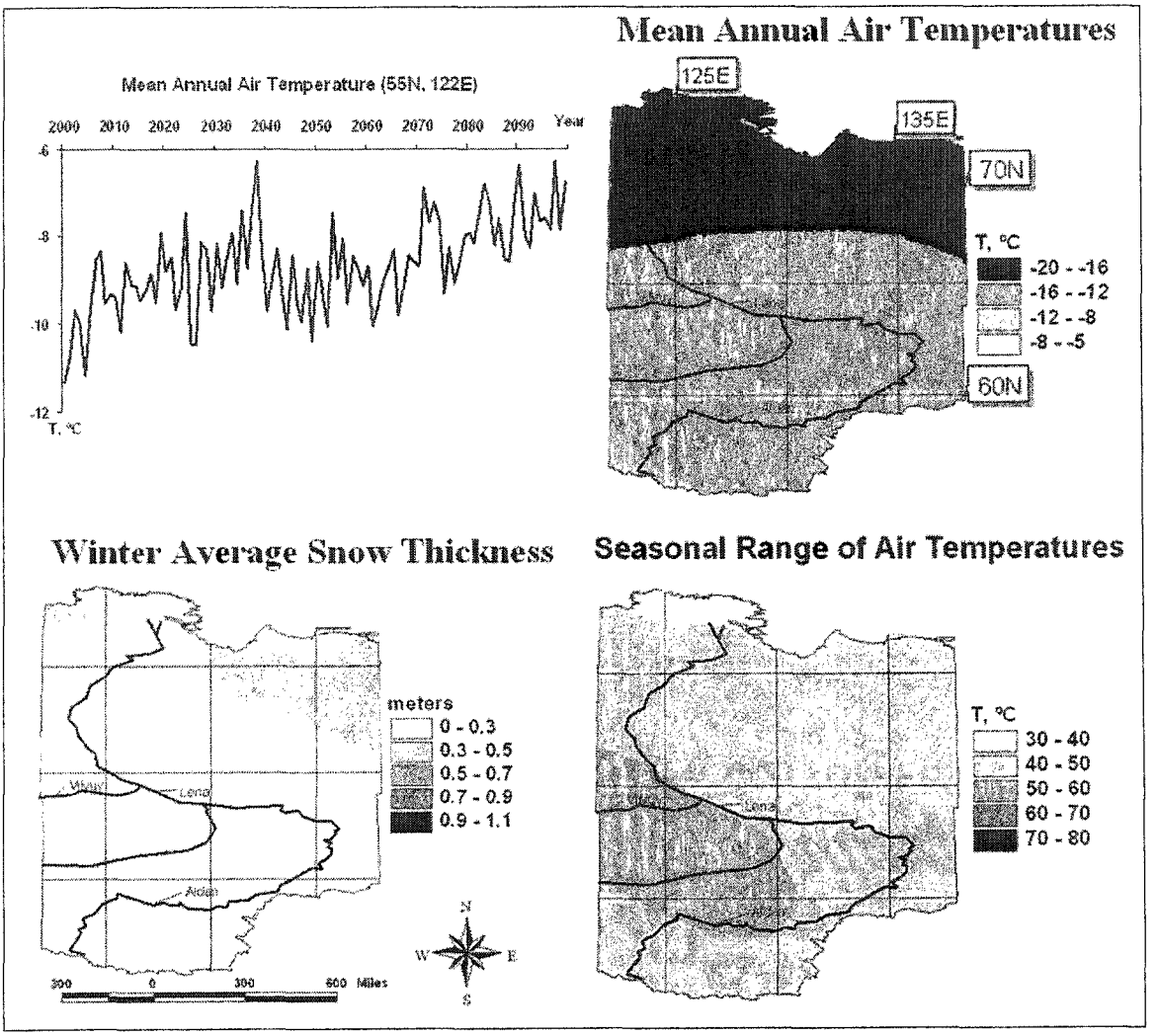

Figure 4.10: Output climatic parameters from CSM GCM for the year 2000.

Reproduced with permission of the copyright owner. Further reproduction prohibited without permission.

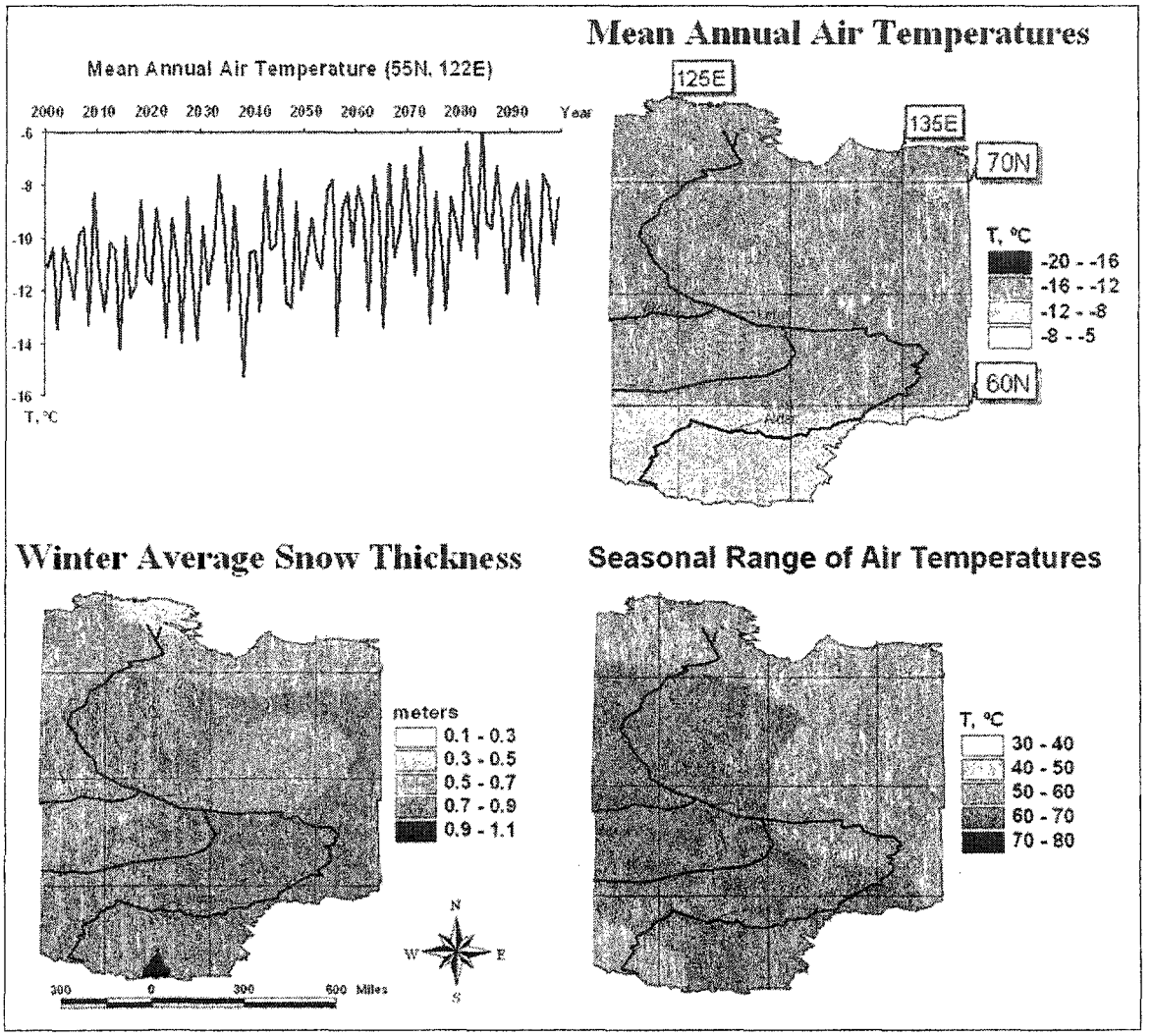

Figure 4.11: Output climatic parameters from GFDL GCM for the year 2000

Reproduced with permission of the copyright owner. Further reproduction prohibited without permission.

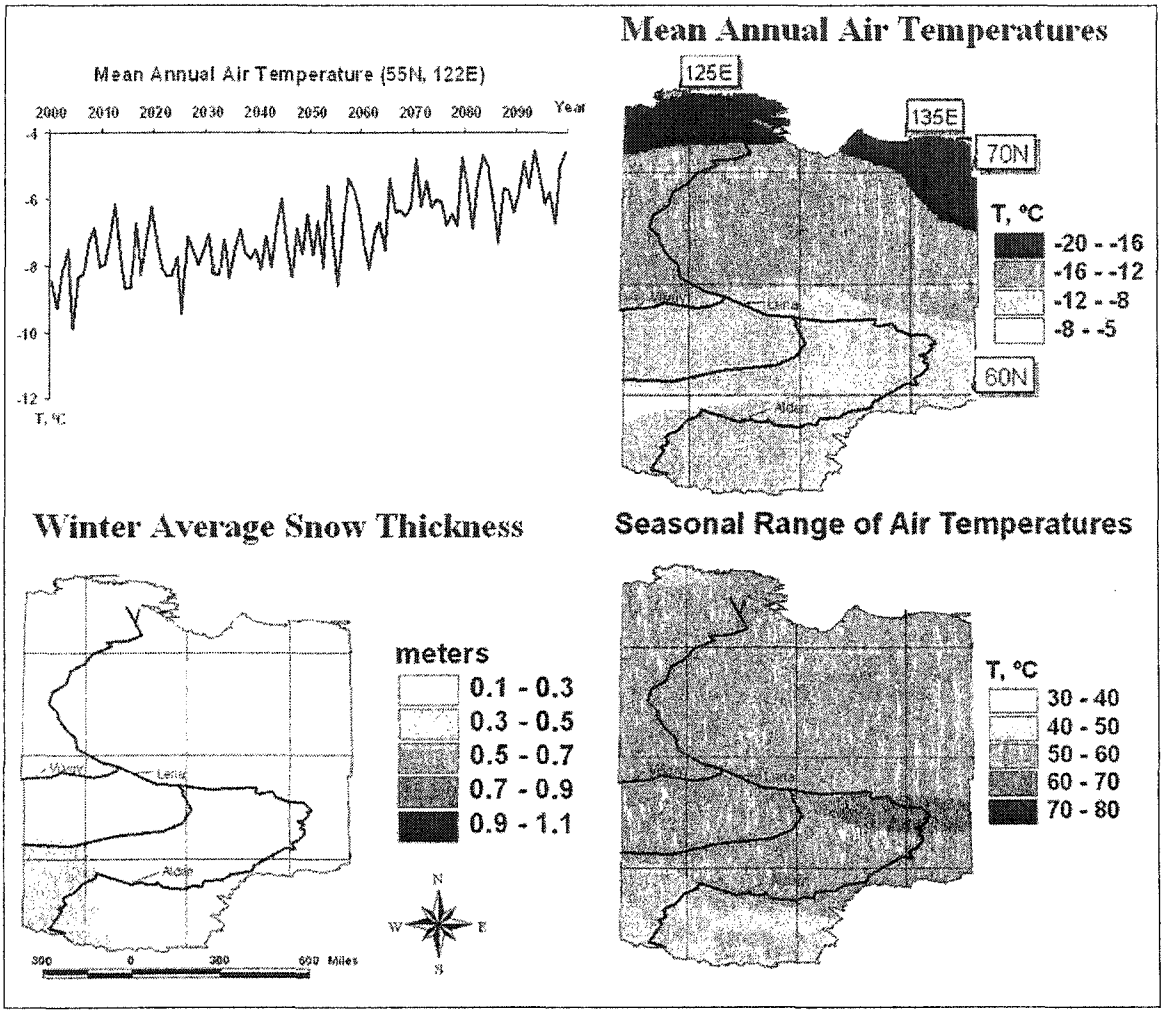

Figure 4.12: Output climatic parameters from HadCM3 GCM for the year 2000.

Reproduced with permission of the copyright owner. Further reproduction prohibited without permission.

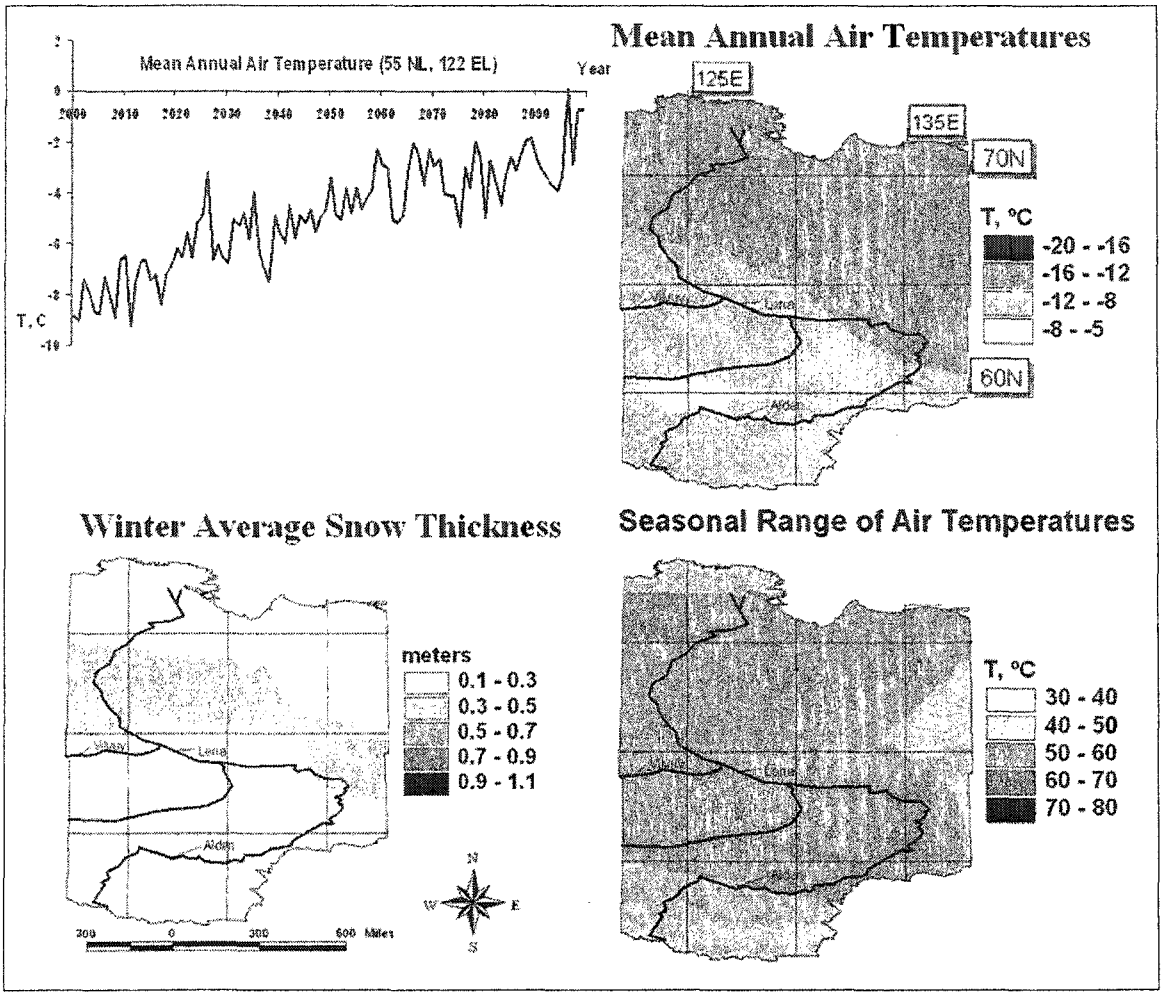

Figure 4.13: Output climatic parameters from ECHAM GCM for the year 2000.

Reproduced with permission of the copyright owner. Further reproduction prohibited without permission.

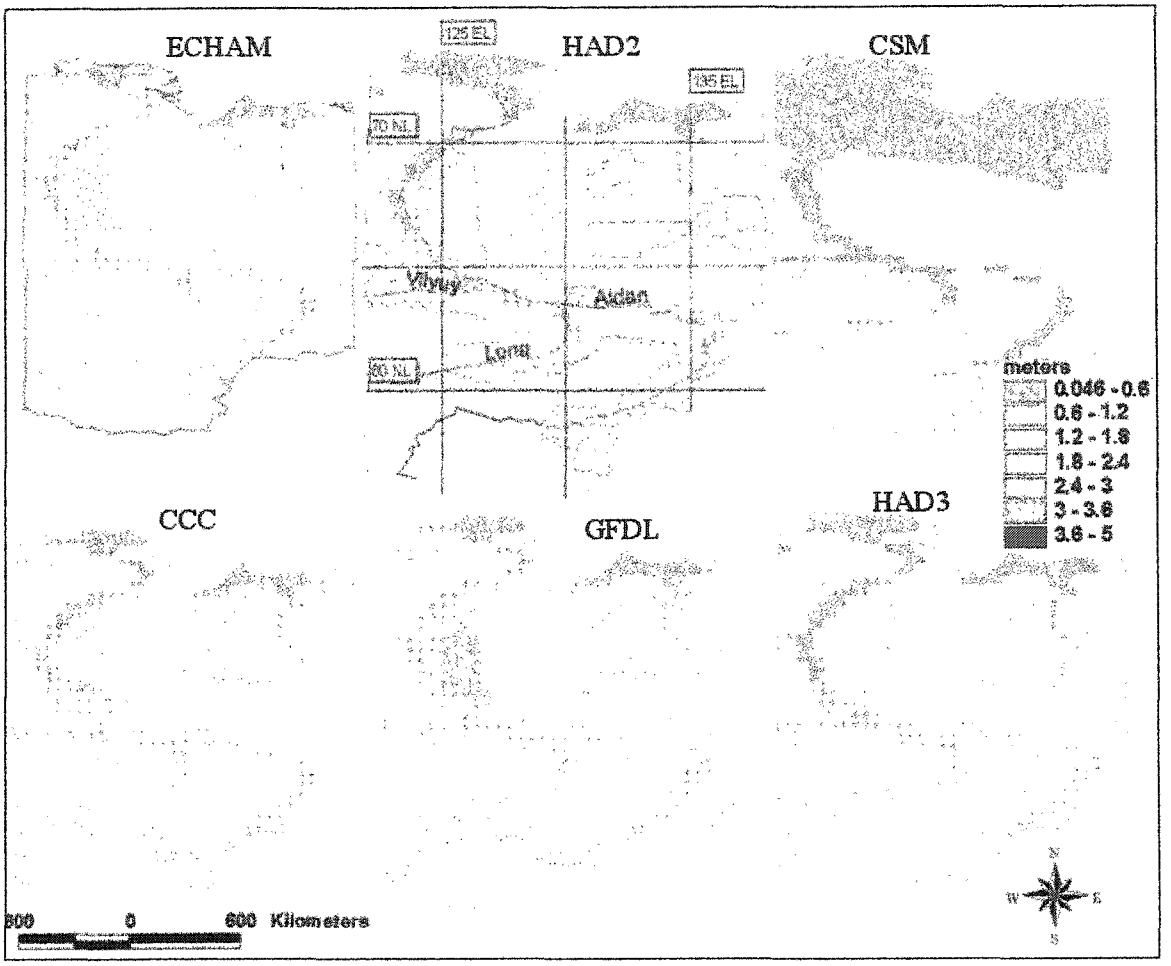

Figure 4.14: The active layer thickness distribution for the year 2000 according to six GCMs used in the forecast

Reproduced with permission of the copyright owner. Further reproduction prohibited without permission.

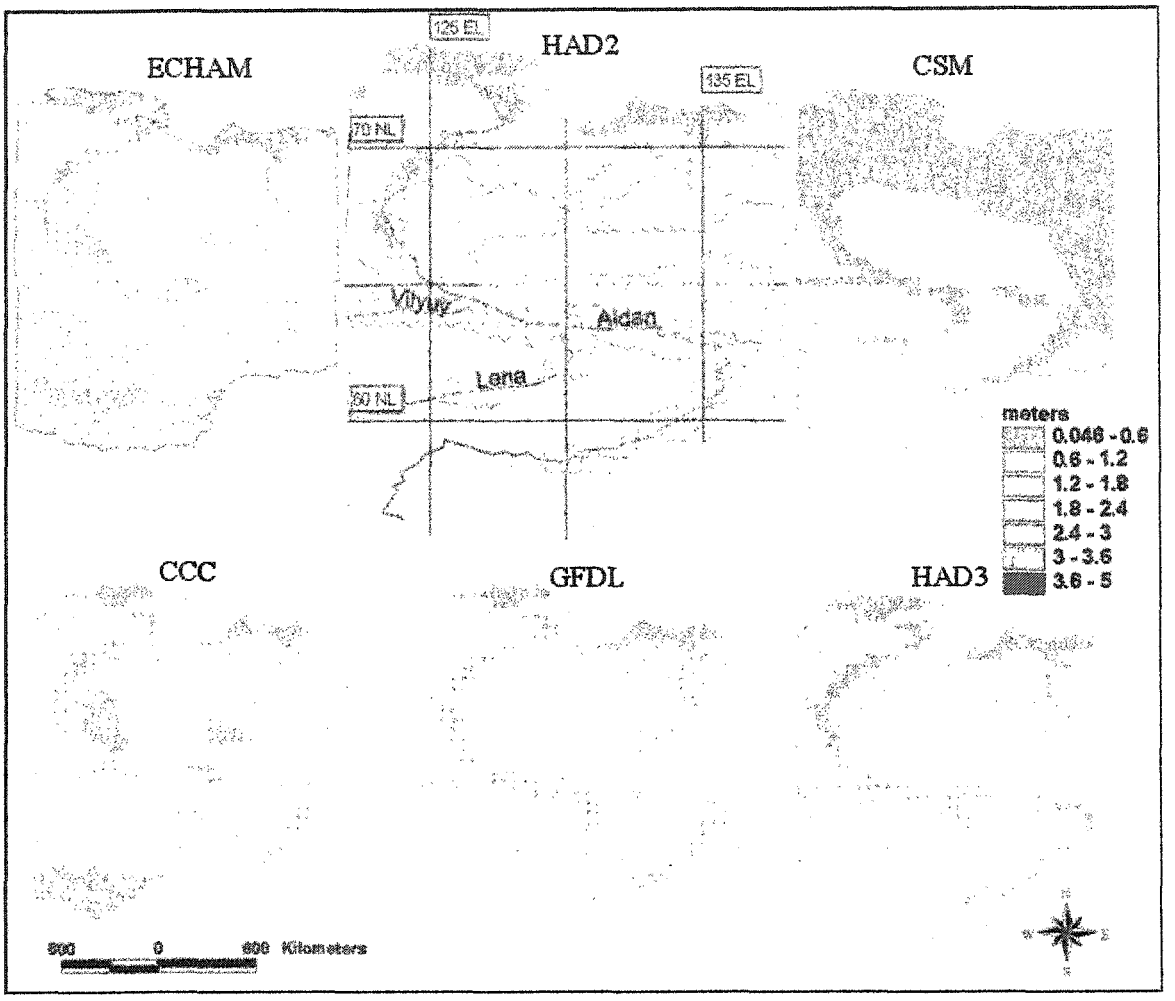

Figure 4.15: The active layer thickness distribution for the year 2025 according to six GCMs used in our forecast

Reproduced with permission of the copyright owner. Further reproduction prohibited without permission.

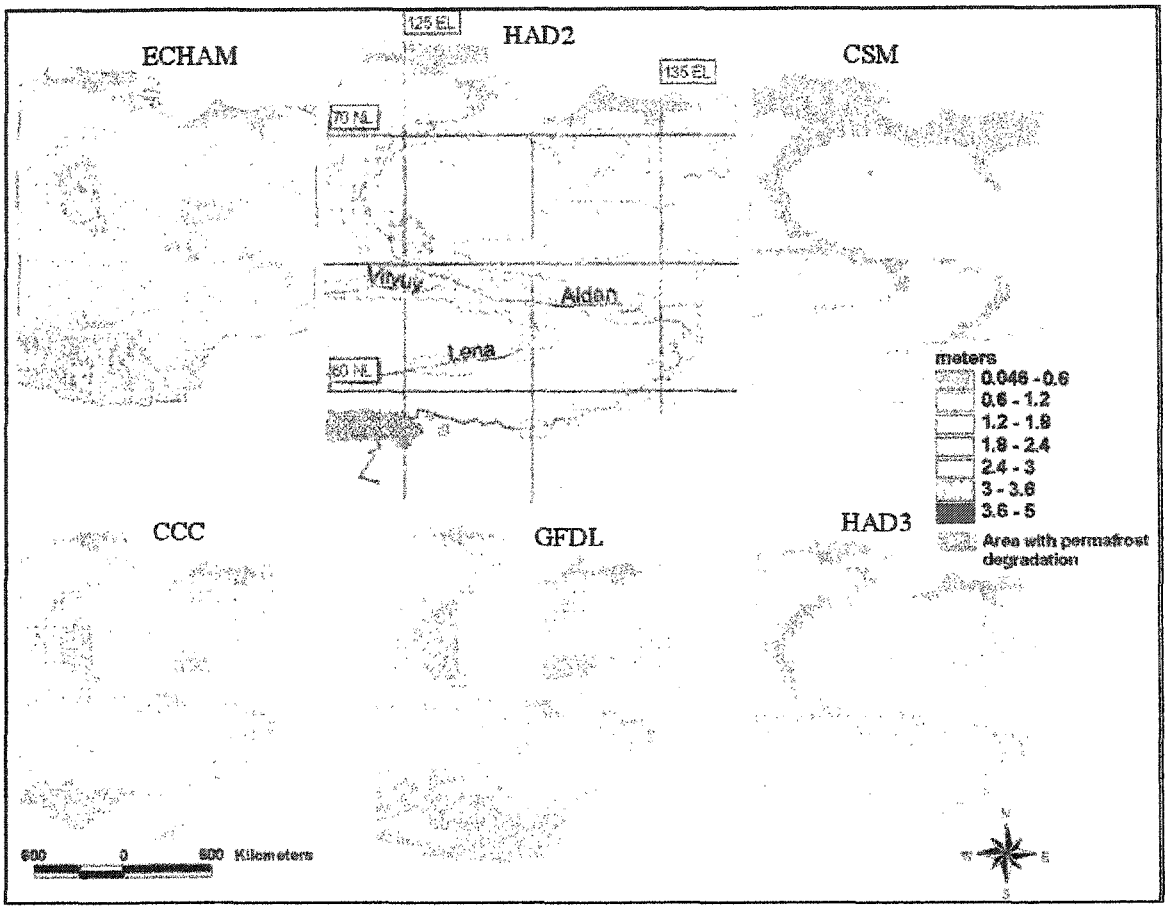

Figure 4.16: The active layer thickness distribution for the year 2050 according to six GCMs used in our forecast

Reproduced with permission of the copyright owner. Further reproduction prohibited without permission.

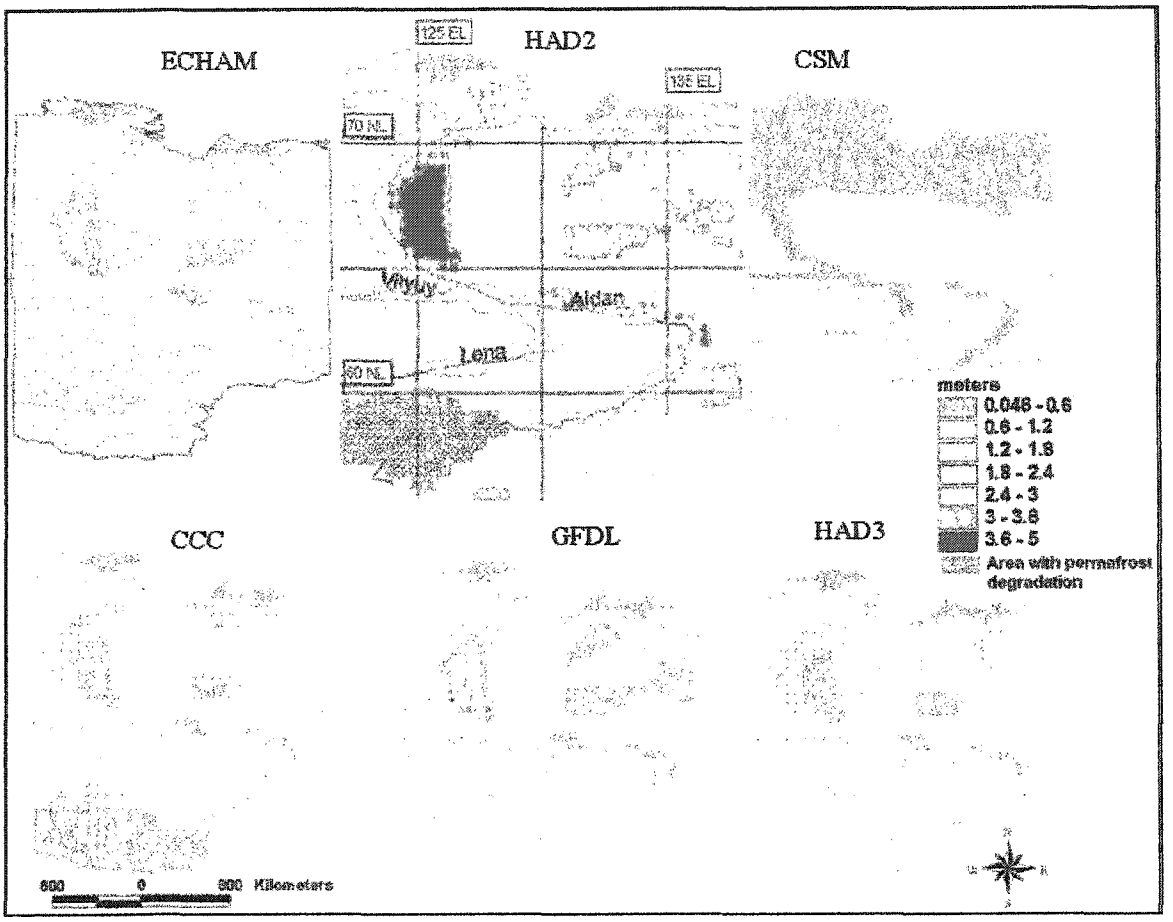

Figure 4.17: The active layer thickness distribution for the year 2075 according to six GCMs used in our forecast

Reproduced with permission of the copyright owner. Further reproduction prohibited without permission.

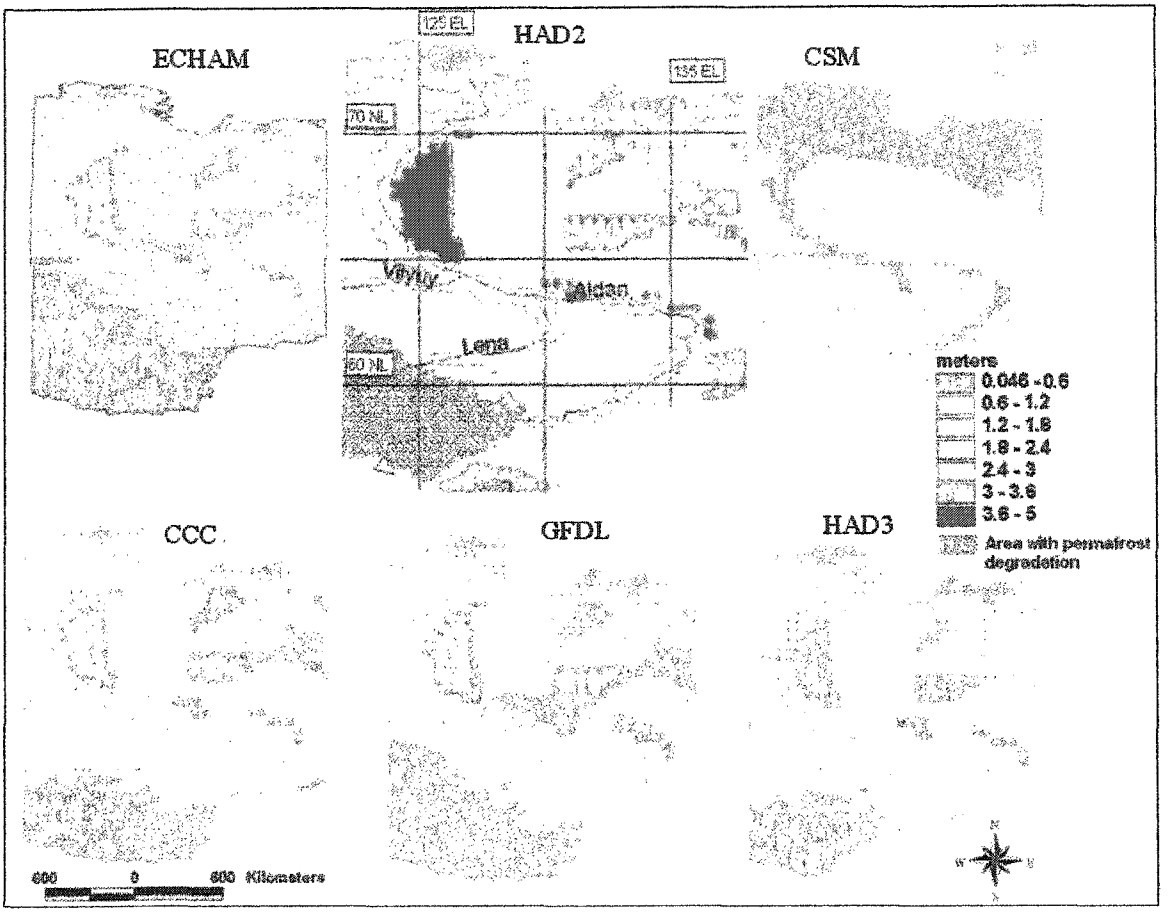

Figure 4.18: The active layer thickness distribution for the year 2099 according to six GCMs used in our forecast

Reproduced with permission of the copyright owner. Further reproduction prohibited without permission.

Table 4.1: Thermal properties of soils within East-Siberian transect (adopted from Feldman et al., 1988)

Groups of Soils	Volumetric water content	Thermal conductivity of frozen soils W/mK	Thermal conductivity of thawed state W/mK
Pebbles, gravel, boulders, silt	0.10	2.80	2.45
Fine sand	0.17	2.04	1.68
Sandy-silt with peat	0.15	2.48	1.52
Peat with silt	0.40	0.46	0.37
Gravel, sand	0.20	2.48	1.52
Gravel, pebbles, sand, silt	0.20	2.36	1.35

Reproduced with permission of the copyright owner. Further reproduction prohibited without permission.

Table 4.2. ACIA-designated GCMs

Full model name and (model "ID" for ACIA)	*Centre, country*	*Reference*	*Atmospheric resolution*	*Ocean resolution*
CGCM2 (**CGC**)	CCCma, Canada	Flato et al., 2000	T32 (3.8 x 3.8) L10	1.8 x 1.8 L29
CSM 1.4 (**CSM**)	NCAR, USA	Boville et al., 2001	T42 (2.8 x 2.8) L18	2.0 x 2.4 L45
ECHAM4/ OPYC3 (**ECH**)	MPI, Germany	Roeckner et al., 1999	T42 (2.8 x 2.8) L19	2.8 x 2.8 L11
GFDL_R3 0_c (**GFD**)	GFDL, USA	Knutson et al., 1999	R30 (2.25 x 3.75) L14	2.25 x 1.875 L18
HadCM3 (**HAD**)	UKMO, UK	Gordon et al., 2000	2.5 x 3.75 L19	1.25 x 1.25 L20

Reproduced with permission of the copyright owner. Further reproduction prohibited without permission.

CHAPTER 5. PERMAFROST DYNAMICS ALONG THE ALASKAN TRANSECT*

ABSTRACT

Ecosystems and infrastructure within the Alaskan transect, which spans almost the entire state of Alaska, are strongly dependent on permafrost, which occupies the entire transect. When facing the possibility of climate change in the future it becomes important to evaluate the impact of those changes on permafrost and consequently ecosystems and infrastructure. The spatial and temporal dynamics of the active layer thickness (ALT) and the mean annual ground temperatures (MAGTs) for 20th and 21st centuries has been analyzed by using the model developed at Geophysical Institute Permafrost Lab (GIPL) (Sazonova and Romanovsky, 2003) and the outputs of six Global Climate Models (GCMs) as driving forces. The results show that the natural variation of mean annual air temperatures in 20th century can cause changes in MAGTs of 3 to 4 °C and ALT up to 0.5 m. The permafrost degradation from the surface will start as early as 2025 and will progress to 2099 according to the CCC, GFDL, HADCM2, HADCM3, and ECHAM models. The spatial dynamics of the permafrost degradation will not be uniform in time. There will be cold and warm time periods on the background of the trend of the mean annual air temperature warming. HADCM2, HADCM3 and GFDL predict that the area with the permafrost degradation will be in the south-eastern part of the transect. The area will be within the Brooks Range and in the Interior according to CCC and ECHAM.

* In preparation for the submission under the same title with authors Tatiana S. Sazonova, Vladimir E.

Reproduced with permission of the copyright owner. Further reproduction prohibited without permission.

The relative increase in MAGTs will be from 1 to 6 °C by the end of 21st century. The ALT will be up to 0.5 m deeper by the year 2099.

INTRODUCTION

Most scenarios of climate change, based on CO_2 concentration increase, predict a significant warming of mean global air temperature by the year 2100. This warming will be amplified in the high latitudes (Houghton et al., 1996). Consequently, the MAGTs and the ALT could experience a systematic and widespread increase over the next 100 years (Anisimov et al., 1997). This increase can result in subsidence-induced damage to the human infrastructure (e.g., Lyons et al., 1995; Anisimov and Nelson, 1996) and release of organic carbon presently stored in the upper permafrost to the atmosphere and hydrosphere (Michaelson et al., 1996). Release of this carbon in the form of carbon dioxide (Oechel et al., 2000) and methane (Reeburgh, 1993), could produce positive feedbacks to the atmosphere warming (Weller et al., 1995).

The three quarters of the area of the state of Alaska is occupied by permafrost (Osterkamp and Lachenbruch, 1990), which makes the Alaskan ecosystems extremely vulnerable to climate change. Permafrost dynamics can trigger vegetation change, particularly the conversion of tundra to boreal forest causing potentially large effects on global climate (Bonan et al., 1993). The permafrost degradation, followed by the thaw settlement and the development of thermokarst, will destroy the substrate on which

---

Romanovsky, John E. Walsh and Dmitri O. Sergueev to *Journal of Geophysical Research.*

Reproduced with permission of the copyright owner. Further reproduction prohibited without permission.

ecosystems rest, altering the nature of the ecosystems (Osterkamp et al., 1997; Romanovsky and Osterkamp, 2001).

In our research we conducted the modeling of ALT and MAGTs for the Alaskan IGBP (International Geosphere – Biosphere Programme) transect (Figure 5.1), using climatic parameters from six GCMs as a forcing data. The similar analysis has been performed for the IGBP Far East Siberian transect (Sazonova et al., 2003). The results of the modeling of the permafrost dynamics within the Alaskan transect will be discussed in this paper.

ENVIRONMENTAL AND PERMAFROST CONDITIONS ALONG THE ALASKAN TRANSECT.

Alaskan transect occupies almost 2/3 of the State of Alaska. It is bounded by the Bering Sea and the Chukchi Sea from the west and Beaufort Sea from the north. The eastern boundary is 145 WL and southern is 55 NL. The area of the transect is approximately 148,252 sq. mi. The major geographical divides within the transect are the Brooks and the Alaska mountain ranges (Figure 5.1).

The flat lowlands to the north from the Brooks Range are called Arctic Lowlands. The Arctic Lowlands is a flat plain, with a relative elevation from 0 to 30 m (Brown and Kreig, 1983). There are many meandering rivers and creeks. The Brooks Range is the natural continuation of the Cordelier's mountain range (Kondratieva, 1998). The range consists of ridges covered by different types of glaciers and deeply cut by mountain river valleys.

Reproduced with permission of the copyright owner. Further reproduction prohibited without permission.

The area bounded by the Brooks Range from the north, by the Alaska Range from the south, and by the US – Canada border on the east and the Seward Peninsula on the west is the Interior Alaska region.

The Seward Peninsula lays between 64.5 NL and the Arctic Circle and separates the Chukchi Sea on the north from the Bering Sea on the south. Near-shore parts of the peninsula are typical lowlands consisting of numerous lakes and marshes. When moving towards the central part, the lowlands are gradually replaced by uplands and mountains with elevations around 1000 m (Brown and Kreig, 1983).

Two major rivers within the transect are the Yukon and the Tanana Rivers. The Yukon River flows from north-east to south-west. The Yukon River valley is flat lowland, with numerous meandering tributary river beds and lakes. The Tanana River is the left tributary of the Yukon River. The Tanana valley, which starts right after the Tanana joining the Yukon River, is the wide, flat lowland. The width of the Tanana valley is 13-15 km.

Climate

Generally speaking, the climate within the Alaskan transect can be characterized as severe. The proximity of the Arctic Ocean is the major factor affecting the climate within the transect.

The Arctic Lowlands and the Arctic foothills are characterized by moderate-maritime and moderate continental types of climate (Haugen and Brown, 1980). Those regions experience extremely low winter temperatures, low summer temperatures, and relatively low precipitation. Wind is a major environmental factor throughout much of

Reproduced with permission of the copyright owner. Further reproduction prohibited without permission.

the year. Winds cause considerable drifting of snow and severe wind - chill factor during the coldest months (Searby and Hunter, 1971). Mean annual air temperatures ranges from -11.8 °C in Umiat to -12.2 °C at Point Barrow. The total annual precipitation does not exceed 175 mm. The winter average snow thickness can be from 10 – 20 cm and up, reaching 80 cm and more due to wind transferring the snow into the valleys (Zhang et al, 1997; McFadden et al., 2001, Benson and Sturm, 1993).

The climate within the Brooks Range varies significantly depending on the elevation. The vertical gradient of mean annual air temperatures is 0.4 °C/100 m on average (Haughen, 1982). Consequently, the mean annual air temperatures are -14 to -15°C at 1000 m, -18 to -19 °C at 2000 m, and -21 to -23 °C at 2800 m (Kondratieva, 1998). The winter average snow thickness is 0.2 to 0.5 m. Annual total precipitation ranges from 140 mm at Sagwon to more than 400 mm in the Atigun Pass - Chandalar Shelf area (Brown and Kreig, 1983).

The Interior is an area of air temperature extremes and of relatively high precipitation (up to 300 mm) and its climate can be put into the category of continental type. The mean annual air temperatures vary from -6°C to -2 °C. Most precipitation occurs during the summer. During the winter, the Interior is dominated by relatively dry continental polar air masses, and sinking cold air creates high atmospheric pressure (Bilello, 1974). Winter average snow thickness is from 0.3 m to 0.7 m, very seldom reaching 1 m.

The climate within the Seward Peninsula is quite severe. Mean annual air temperatures are from -3.3 °C in Nome up to -6.5 ° in Candle. Annual total precipitation

Reproduced with permission of the copyright owner. Further reproduction prohibited without permission.

is from 370 – 400 mm in the lowlands, reaching 1000 – 1200 mm in the central part (Hopkins and Sigafoos, 1951).

Vegetation

The two major units of vegetation encountered within the transect are tundra and boreal forest. The boreal forest can be subdivided into bottomland spruce-poplar forests, upland spruce-hardwood forests, and lowland spruce hardwood forests (Brown and Kreig, 1983).

Bottomland spruce-forest is a tall, relatively dense forest along the rivers and streams, consisting of white spruce and balsam poplar. The ground surface vegetation includes bent reed grass, shrubs, and thick mat of feather mosses. This forest grows on flood plains, low river terraces, and on south-facing slopes of major river valleys in the Interior.

Upland spruce-hardwood forest is composed of white spruce and black spruce with paper birch, and aspen. The surface ground vegetation usually represented by mosses and low shrubs. This forest is everywhere between the Yukon River and Fairbanks (Pewe, 1982).

Lowland spruce-hardwood forest consists of dominating black spruce with some paper birch, balsam poplar, and aspen. The surface ground vegetation is composed of shrub birch, blueberry, sedge, and bog moss. This forest can be found within the lowlands on peat, glacial deposits, outwash plains, and alluvial valleys bottoms.

Reproduced with permission of the copyright owner. Further reproduction prohibited without permission.

The tundra is divided into wet tundra, moist tundra, and alpine tundra and barren ground. Wet tundra is common in the coastal area and is represented by an almost continuous cover of grasses and sedges, rooted in mosses and lichens.

The moist tundra exists north of the Brooks Range. The tundra vegetation consists of cottongrass tussocks, sedges and dwarf shrubs. Mosses and lichens grow between the tussocks. At present the moist tundra is subdivided into the acidic and the nonacidic types on the basis of plant diversity and biomass supported. The acidic/nonacidic boundary extends all along the northern front of the Arctic Foothills (Walker et al., 2003). To the south of the boundary, within the moist acidic tundra, soils have thick organic soil horizon and higher moisture content, plant production is larger, and the ALT is shallower in comparison with nonacidic tundra (39 cm vs. 52 cm). Moist nonacidic soils support lower biomass, higher plant diversity, and more frost boils (Walker et al., 2003).

Alpine tundra occupies mountainous areas and well-drained rocky ridges at elevations between 600 m and 1,250 m within the tundra and boreal forest zones (Brown and Pewe, 1973; Pewe, 1983). Dryas, lichens, low-growing herbs, grasses, and sedges are the major vegetation types.

Soils

On the Arctic Lowlands, soils contain organic materials of variable thickness, overlying silt –loam mineral horizons. Within the Arctic Foothills, soils generally consist of silt loam and silty clay loam with thin organic horizon (Brown and Kreig, 1983). In the Brooks Range, most soils are coarse-grained colluvial deposits (Figure 5.2).

Reproduced with permission of the copyright owner. Further reproduction prohibited without permission.

Between the Yukon River and the Brooks Range, in highlands, loess is a significant component of soils, which are fine-texture silts overlying weathered bedrock fragments. Loess can also be found within the uplands and hilly terrain to the south from the Yukon River, on the Seward Peninsula, and on the Arctic Lowlands (Figure 5.3). The thickest loess can be found at the eastern part of the Yukon River. Organic soils are usually developed on the top of loess.

In the Interior, on flood plains and terraces, fibrous organic soils and half bog soils with a thick (more than 20 cm) organic surface horizon lay over silty or fine-sandy subhorizons. In the valleys soils are fine-grained, silt with organic components (Pewe, 1982). Within the drainageways and tussock meadows, organic soils or mineral soils with thick organic horizons are very common (Brown and Kreig, 1983).

Permafrost conditions

Permafrost occupies about three quarters of the entire state of Alaska (Osterkamp and Lachenbruch, 1990). The thickest permafrost more than 600 m can be found at the Arctic Lowlands and the Arctic foothills (Lachenbruch et al., 1987).

Permafrost is continuous north of Atigun Pass and discontinuous in much of interior Alaska to the south, including areas within the valleys south of the Continental Divide in the Brooks Range (Figure 5.2).

Within the Arctic foothills (the area between the Brooks Range and the Arctic Lowlands) and the Arctic Lowlands long-term MAGTs are typically from -4 °C at the Galbraith Lake, to -9.9 °C at Point Barrow (Lachenbruch et al., 1982; Brown and Pewe, 1973; Zhang et al., 1997; Romanovsky and Osterkamp, 1995; Romanovsky et al., 2002;

Reproduced with permission of the copyright owner. Further reproduction prohibited without permission.

Romanovsky et al., 2003). The permafrost thickness ranges from 140 m in Galbraith Lake up to 630 m in Prudhoe Bay (Lachenbruch et al., 1987; Osterkamp and Payne, 1981). The taliks (the ground with positive MAGTs surrounded by permafrost and existing for 2 years or longer) can only be found underneath the wide, deep lakes and river beds (Black, 1949).

The Brooks Range is characterized by complex permafrost conditions. The thickness of permafrost and the MAGTs depend on the elevation and on the exposition. The thickness of the permafrost varies from 100 m up to 700 – 900 m (Kondratieva, 1998). Within the Brooks Range, the presence of the hydrothermal high-mineralized springs creates favorable environment for the taliks to exist (Black, 1949).

On the Seward Peninsula, uplands and mountains are underlain by discontinuous permafrost. The lowlands are underlain by moderately thick to thin permafrost in areas of fine grained deposits (MAGTs are -3 °C to -5 °C) and by discontinuous or isolated masses of permafrost in areas of coarse grained deposits (Hopkins, 1951).

The border between areas with continuous and discontinuous permafrost passes the foothills of the southern slopes of the Brooks Range and northern foothills of Seward Peninsula uplands (Figure 5.2).

The Interior is characterized by discontinuous permafrost, with MAGTs from -4 ° to 0 °C (Pewe, 1983). The thickness of permafrost can reach up to 120 m and more. The sediments with extremely high volumetric ice content (up to 80%) are common for the Interior. Excess ice inclusions in permafrost are usually in the form of ice wedges or massive ice layers in the loess and fine-grained matrix (for example, in the eastern part of

Reproduced with permission of the copyright owner. Further reproduction prohibited without permission.

the transect, along the Yukon and Tanana Rivers) (Figure 5.3) (Pewe, 1982). The protection layer above the ice usually consists of silt and its thickness is from 1 to 2 m.

In the Interior, the presence of permafrost and the thickness of the active layer are closely related to slope angle and aspect, vegetation, and drainage. Vegetation is a general indicator of permafrost conditions. Within the regions, black spruce, larch, and bogs nearly always indicate the presence of permafrost within 0.6 m of the surface (Pewe, 1983). White spruce and aspen usually indicate an area that is free of permafrost or that has an active layer 1 m or thicker (Brown and Kreig, 1983). The Tanana River flood plain is in the area of discontinuous permafrost (Figure 5.2). Massive taliks are present beneath existing or recently abandoned river channels, sloughs, and lakes. The thickness of permafrost on flood plains varies considerably from 0.3 m up to 90 m (Pewe and Reger, 1983).

THE DYNAMICS OF THE ALT AND THE MAGTS FOR THE 20th and 21st CENTURIES ALONG THE ALASKAN TRANSECT.

The Geophysical Institute Permafrost Lab (GIPL) model was used to simulate the spatial and temporal dynamics of the permafrost for the future and past within the Alaskan transect. The GIPL is the modified Kudryavtsev's approach (Romanovsky and Osterkamp, 1997) incorporated into GIS database (Sazonova and Romanovsky, 2003). The soils and vegetation datasets are stored in GIS format in form of layers and used as input parameters for the calculations. Digital maps of MAGTs and the ALT are the outputs of the model. The GIPL was successfully applied for the simulation of the

Reproduced with permission of the copyright owner. Further reproduction prohibited without permission.

permafrost dynamic analysis along the IGBP Far East-Siberian transect (Sazonova et al., 2003).

The strategy that was used for the East-Siberian transect was followed in this study as well. It includes the use of the reference scenario, which consists of hindcast for 1901 – 2000 and forecast for 2001 – 2100 and was obtained from HADCM2 GCM output. The reasoning behind choosing this particular GCM is that the credibility of HADCM2 was established in our previous studies (Sazonova et al., 2003).

The ALT and MAGTs were calculated on a grid consisting of 517 grid cells (spatial dimensions of 0.5 x 0.5 degrees of latitude/longitude).

Boundary conditions and input parameters for period 1901 – 2000

Climatic parameters

In order to evaluate permafrost dynamics along Alaskan transect for the past 100 years, climatic parameters from HADCM2 GCM output has been used as upper boundary conditions. Climatic parameters include mean annual air temperatures, seasonal range of air temperatures, winter average snow thickness and snow density. According to HADCM2 in 20th century there were two relatively cold periods (1910 – 1920 and 1960 - 1980) when mean annual air temperatures were close to -13°C and two relatively warm periods (1930 – 1950 and 1990 - 2000) with the temperatures around -9°C (Figure 5.4). On the background of interchanging cold and warm periods interannual variations of mean annual air temperatures took place. The magnitudes of these variations range from 2°C to 5°C. Mean annual air temperatures in the year 2000 (Figure 5.5) were generally 1 to 2°C colder in comparison with those observed in the Interior and the Seward Peninsula

Reproduced with permission of the copyright owner. Further reproduction prohibited without permission.

(Table 5.1). In the Arctic Foothills and Arctic Lowlands mean annual air temperatures are slightly warmer (from 0.3 to 1°C) in comparison with the observed (Table 5.1).

Unfortunately HADCM2 GCM does not provide acceptable values for winter average snow thickness for the Alaskan transect. The dataset for winter average snow thickness and density was derived from Chang Monthly Nimbus-7 SMMR Derived Global Snow Cover and Snow Depth Data Set (OCT 1978 - AUG 1987) (Chang et al., 1987; Chang et al., 1990), and snow course data from125 meteorological stations (Figure 5.6) in Alaska (www.ak.nrcs.usda.gov/snow/). This dataset contains mean monthly values of snow thickness for the period of October, 1978 to August, 1987. The winter average snow – water equivalent and snow thickness for the period 1978-1987 were measured at meteorological stations. The snow cover density for each meteorological station was calculated from these two snow cover parameters. We averaged mean monthly values of snow depth from the dataset to obtain winter average snow thickness at the Nimbus-7 grid points. The values of winter average snow thickness from this dataset were interpolated and assigned to the closest meteorological station. Then linear regression analysis was performed to find the correlation between measured and the Nimbus-7 dataset values of winter average snow thickness for each meteorological station. Standard deviations of measured winter average snow thickness and density for the period 1978 - 1987 were calculated for each meteorological station to obtain natural variability of snow cover parameters.

Winter average snow thickness from the Nimbus-7 dataset was adjusted to match measured snow thickness and interpolation has been performed to assign winter average

Reproduced with permission of the copyright owner. Further reproduction prohibited without permission.

snow thickness and snow cover density for the each grid point used for the retrocast and the forecast of permafrost dynamics within the Alaskan transect. As a result the new dataset containing winter average snow thickness and snow density for the period of 1978 – 1987 was developed.

To perform the retrocast (for the period 1901 - 1978) and the forecast (for the period of 1987 – 2100) of winter average snow thickness and densities for each grid point, the random numbers generator from IMSL(R) (Fortran 90 MP Library ,Version 3.0) was used.. The random number generator applies the pre-defined standard deviation, obtained from analysis of measured winter average snow thickness, to generate the numbers within the range of snow parameters natural variability. The final dataset consists of 517 grid points. For each grid point the winter average snow thickness and snow density for the period of 1901 – 2099 were calculated.

Parameters used for the retrocast include vegetation cover thermal properties and soils thermophysical properties and moisture content of soils. Climate data from GCM outputs already include the information about upper cover of the vegetation. So, only the lower level vegetation (up to 50 cm from the ground surface), which is essential for the MAGT regime and the active layer depth, was used for the calculations. For this purposes vegetation was subdivided into 4 classes (Figure 5.2): moss, grass, and moss with grass in equal proportion and grass with 30 % of the moss.

Soil types and genesis vary significantly within the Alaskan transect. Unfortunately, it is rather difficult to include such a variety in a model. Thus we put all soils in two categories (Figure 5.2). They are mostly organic soils with high moisture

Reproduced with permission of the copyright owner. Further reproduction prohibited without permission.

content (65%) and low thermal conductivity (0.4 W/m*K in thawed state and 0.6 W/m*K in frozen state), and coarse-grained sediments also containing some organic material – with relatively high thermal conductivity (1.2 W/m*K in thawed state and 1.6 W/m*K in frozen state) and low moisture content (20 %).

The permafrost dynamics in 20th century

The initial year for the hindcast was 1901. MAGT distribution shows strong south-to-north latitudinal trend of cooling. There is also longitudinal trend revealed by colder MAGTs within the western part of the transect compared to warmer eastern part. The coldest ground temperatures are on the Arctic Lowlands; they range from –10 °C up to –7 °C (Figure 5.7). The warmest MAGTs are in the southeastern part of the transect and ranges from –2 °C to 0 °C. ALT is relatively shallow up to 0.5 m for entire transect, except for the southeastern part and eastern part of the Brooks Range, where it reaches 1.5 -1.8 m, due to the presence of coarse-grained soils. Shallow ALT is caused by presence of organic material in silty soils and extensively distributed moss cover (Walker et al., 2003).

In comparison with MAGTs for 1901, the period of 1920-1930 years was a relatively warm period. The ALT net increase was up to 0.2 m for the most parts of the transect. On the North Slope MAGTs were from –4°C to –7 °C. In the south-eastern part of the Interior MAGTs became positive and some partial permafrost degradation from the surface started (Figure 5.7). Permafrost degradation takes place when the active layer, developed during the summer does not freeze all the way from the surface down during the following winter. If ALT reaches an ice horizon or a ground layer with high ice

Reproduced with permission of the copyright owner. Further reproduction prohibited without permission.

content, ice begins to melt and the ground subsides. Rain water and surface water will flow into the deepening holes and form water pools and lakes. The presence of water on the surface helps summer warm temperatures penetrate deeper and faster into the ground. In winter time, because of wind transition of the snow cover, snow will be the thickest within the deepening and will contribute the increase in MAGTs (Kudryavtsev et al., 1974; Yershov, 1998). As a result, process of thawing permafrost will be progressing in spite of cold winter which might slow it down to some degree. Our model is limited to calculating only ALT and MAGTs, but not the depth of permafrost thawing from the surface. The other methods could be used to calculate timing and the dynamics of permafrost degradation (Kudryavtsev et al., 1974; Hinzman et al., 1997; Kane et al., 1991).

The 1950 - 1960 period was relatively cold (Figure 5.7). The area with permafrost degradation completely disappeared. MAGT became about 2°C to 4 °C colder and ALT decreased up to 0.3 m. The most significant cooling occurred in the central and southeastern parts of the transect (up to 2-3 °C).

The period of 1970 – 1980 was colder for northern part of the transect and warmer for central and southeastern parts of the transect. At the north, MAGTs become considerably (2 to 4 °C) colder in comparison with the period of 1950 - 1960. Active layer thickness decreased as well. The zone with shallow (up to 0.3 m) ALT has expanded to 66 NL in the western part of the transect. In southeastern part of the transect the warming of the air temperatures led to an increase in MAGTs (1 to 2 °C) and to the deepening of the ALT.

Reproduced with permission of the copyright owner. Further reproduction prohibited without permission.

The next relatively warm period took place in 1990 – 2000, with the maximum around 1991-1992. Relative increase in MAGTs was 2°C to 4°C in the southeastern part of the transect and around 1°C to 3°C on the rest of the territory. In the southeastern corner of the transect MAGTs became positive at some locations and permafrost degradation from the surface has started (Figure 5.7). Recent observations of permafrost degradation in many locations within the south-eastern part of the transect support the results of our calculations (Jorgenson et al., 2001; Osterkamp et al., 2000).

Boundary conditions used for the forecast of the permafrost dynamics

Climatic parameters, such as mean annual air temperatures, seasonal amplitudes and winter average snow thickness were used as upper boundary conditions in our modeling. All those parameters were taken from six GCMs. The five ACIA-designated GCMs are those of Canadian Center for Climate Modeling and Analysis (CCC), the National Center for Atmospheric Research/Climate System Model (CSM), Geophysical Fluid Dynamics Laboratory (GFDL), Hadley Climate Center's Version 3 (HadCM3) and the Max Planck Institute for Meteorology (ECHAM). The sixth model was the HADCM2 model, which was used as the reference for the evaluation of the other GCMs.

Climatic parameters from the five GCMs were formatted and interpolated to fit the 0.5° x 0.5° latitude/longitude grid and then incorporated into GIPL. The various GCMs differ significantly in terms of their projected mean annual temperatures, amplitudes of seasonal variations of temperature, and winter average snow thickness for the period 2000-2099. The increase in mean annual air temperatures by the end of the year 2100 ranges from 2 to 6 °C among the

Reproduced with permission of the copyright owner. Further reproduction prohibited without permission.

models. The largest increase is projected to occur in high latitudes (to the north of 65° N).

The winter average snow thickness was derived using winter average snow - water equivalent and snow density values. The winter average snow - water equivalent is given by the five respective GCM models, and snow density is derived from the Nimbus-7 dataset. The snow density values were taken from the Nimbus-7 because of the limited data available on the complex relationship between snow cover thickness and density in Alaska (Sturm et al., 1994).

The comparative analysis of all GCMs outputs for the year 2000 has been performed using HADCM2 as a reference GCM. The results are presented in Table 5.2. The analysis has been done for three climatic parameters (mean annual air temperatures, seasonal range of air temperatures and winter average snow thickness) used in the modeling of the ALT and MAGTs. When comparing mean annual air temperatures, a special consideration was given to the presence or absence of the latitudinal gradient. Latitudinal south-to-north gradient of the decrease in mean annual air temperatures is the major characteristic showing the reliability of the GCM.

The CCC gives warmer mean annual air temperatures in comparison with the reference (HADCM2) in the Brooks Range (Figure 5.8). In the Interior and on the Seward Peninsula, air temperatures are very similar to HADCM2. The coldest mean annual air temperatures (from -8°C to -12°C) are on the North Slope and within the Arctic Lowlands. The warmest temperatures (from -5°C to -8 °C) are distributed evenly over the Brooks Range, the Interior, and the Seward Peninsula. Interannual variations of mean

Reproduced with permission of the copyright owner. Further reproduction prohibited without permission.

annual air temperatures are typically 2 to 3°C (Figure 5.9). The CCC projects increases in mean annual air temperatures by up to 4 – 6°C, and gives a good approximation of the seasonal range of air temperatures to the reference. The spatial distribution is different from the reference and does not follow latitudinal or longitudinal zonality. The magnitude of seasonal variations of air temperatures ranges from 30 to 40°C within the Arctic Lowlands, eastern part of the Brooks Range, and the Interior, up to 40°C to 50°C in the northern part of the Seward Peninsula and the western part of the Brooks Range. The winter average snow is deeper in the western part of the transect and ranges from 0.5 to 1.1 m. Overall, the spatial distribution of winter average snow thickness follows wedge shaped profile facing west.

The CSM model approximates mean annual air temperatures well. The spatial distribution of temperatures follows latitudinal and longitudinal profiles. The coldest temperatures -12°C to -16°C are in the very north of the transect (to the north from 70°NL). The area with mean annual air temperatures in the range of -8°C to -12°C occupies the Arctic Lowlands and the Arctic foothills (Figure 5.10). The Interior, the Brooks Range, and the Interior are characterized by mean annual temperatures from -5°C to -8°C. The interannual variability of mean annual air temperatures is from 2°C to 4°C. On the decadal scale, the variations in mean annual air temperatures can be up to 7°C (Figure 5.11). The CSM simulation indicates that during 21st century relatively cold and warm periods with typical duration around 5 – 15 years will take place on the background of warming trend (3°C to 5°C per 100 years) in mean annual air temperatures. The magnitude of the decadal fluctuation will decrease toward the end of the century. The

Reproduced with permission of the copyright owner. Further reproduction prohibited without permission.

magnitude of seasonal range of air temperatures is from 30°C to 40°C everywhere. The winter average snow thickness is from 0.1 to 0.3 m everywhere within the transect and by 0.2 to 0.3 m smaller in the Interior in comparison with the reference HADCM2. The CSM does not predict summer even in southern part of the transect during relatively cold periods.

Mean annual air temperatures simulated by GFDL are generally 3°C to 4°C warmer than those of HADCM2 in the Brooks Range and the Arctic foothills. The coldest temperatures are within the Arctic Lowlands and do not exceed -12°C (Figure 5.12). In the Brooks Range, Seward Peninsula, and in the Interior mean annual air temperatures are in the range of -5°C to -8°C. The projected for 2000 – 2100 increase in mean annual air temperature are from 4°C to 5°C (Figure 5.13). The magnitude of the interannual fluctuations of the temperatures is the largest in comparison with other GCMs and ranges from 4°C to 6°C. Seasonal range of air temperatures is from 30°C to 40°C in the eastern part of the transect and 40°C to 50°C in the western part. Winter average snow thickness is from 0.1 m to 0.3 m almost everywhere, except small areas at the north and in the Interior where winter average snow thickness reaches 0.5 – 0.7 m.

The HADCM3 model predicts the spatial distribution of climatic parameters which does not follow any latitudinal or longitudinal pattern and can not be explained by any combination of environmental parameters. The coldest mean annual air temperatures are in the north-east and the very north-west of the transect and do not exceed -16°C (Figure 5.14). The area with temperatures in the range of -8°C to -12°C occupies the most territory and has complex shape. The area crosses the Brooks Range and goes far to the

Reproduced with permission of the copyright owner. Further reproduction prohibited without permission.

south in the central part of the transect. The warmest temperatures -5°C to -8°C occupy the Seward Peninsula and the eastern part of the Interior. The projected for 2000 - 2100 increase in mean annual air temperatures is 5°C to 6°C (Figure15). The interannual variations of mean annual air temperatures do not exceed 2 °C to 3°C. The seasonal range of air temperatures is from 30°C to 60°C in general. The highest magnitudes (50 – 60°C) of the seasonal variations dominate in the eastern part of the transect. In the western part 30°C to 40°C seasonal ranges of air temperatures prevail. The HADCM3 gives complex pattern of winter average snow thickness distribution for the Alaskan transect. The deepest snow up to 1.1 m is in the north – west and fills stripe-like area in the eastern part of the transect. The shallowest winter average snow thickness is in the north-east of the transect and bounded by the stripe of deep snow from the west. In the rest of the territory, winter average snow thickness is from 0.3 to 0.9 m.

The ECHAM model, the most recent of all GCMs, approximates mean annual air temperatures very closely to reference HADCM2. The temperatures follow the latitudinal and longitudinal pattern, with the coldest temperatures (from -12°C to -16°C) in the very north of the transect (Figure 5.16). The area with the coldest temperatures does not form a continuous zone but patches instead. The temperatures in the range from -8°C to -12°C form a continuous triangle shaped zone. The zone includes the Arctic Lowlands and the Brooks Range. In the Interior and on the Seward Peninsula simulated mean annual air temperatures do not exceed -5°C. The projected increase in mean annual air temperatures are up to 6°C to 8°C (Figure 5.17). The interannual variations of mean annual air temperatures are in the range of 2°C to 4°C. The predicted seasonal range of air

Reproduced with permission of the copyright owner. Further reproduction prohibited without permission.

temperatures is from 30 to 40°C in the southeastern corner and within the northern part of the Arctic Lowlands, up to 50°C in the Brooks Range, the Interior, and the Seward Peninsula. The ECHAM gives deeper winter average snow thickness in comparison with HADCM2. The deepest snow is in the eastern part of the Interior and ranges from 0.7 m to 0.9 m. In the Brooks Range and the Arctic Lowlands winter average snow thickness does not exceed 0.7 m.

The forecast of the permafrost dynamics along the Alaskan transect for the period of 2000-2099.

Year 2000 was the first year of the forecast. The HADCM3 predicts very warm ground temperatures from 0°C to 1°C and permafrost degradation in the south-eastern part of the transect (Figure 5.18). The area with permafrost degradation occupies approximately 5% of the entire transect. In the Brooks Range, Seward Peninsula and the Arctic Lowlands MAGTs are in the range of -4°C to -10°C, with the coldest temperatures in the very north of the transect. The ALT is shallow and does not exceed 0.3 m within the Seward Peninsula and Arctic Lowlands. In the Brooks Range ALT ranges from 0.3 – 0.6 m in the western part, and up to 1.2 m in the central and eastern parts. The ALT and MAGTs simulated by the HADCM3 are not in a good agreement with the reference HADCM2.

CCC and ECHAM give very warm ground temperatures within the entire transect in comparison with the reference HADCM2. In terms of the ALT, CCC and GFDL are the closest to the reference HADCM2. ECHAM gives deeper ALT for the entire transect.

Reproduced with permission of the copyright owner. Further reproduction prohibited without permission.

In the 25 years after the beginning of the forecast, CCC, HADCM2, and GFDL predict the formation of the zone with permafrost degradation in the south-eastern part of the transect (Figure 5.19). HADCM3 shows that the zone with permafrost degradation will double in size. According to HADCM2 and HADCM3 the relative increase in MAGTs will be about 2 to 3 °C and will lead to up to 0.3 m increase in ALT on the Seward Peninsula and in the Interior. In the Brooks Range and the Arctic Lowlands those two GCMs predict the cooling of MAGTs and decrease in ALT.

ECHAM and CSM models do not predict the permafrost degradation anywhere. According to CSM, the 2020s and 2030s will be relatively cold. CCC predicts the warming of the MAGTs (3 to 4 °C) and the deepening of the ALT within the Arctic Lowlands.

In 50 years, the relative increase in the MAGTs in comparison with the beginning of the forecast will be 2°C to 3°C in the southern parts of the transect and up to 5°C in the northern parts of the transect, according to HADCM2 and ECHAM. GFDL and CSM show that MAGTs will be warmer and ALT will be deeper within the entire transect. HADCM3 predict relative decrease in MAGTs which leads to shrinking of the area with permafrost degradation and in the shallowing of the ALT throughout the transect (Figure 5.20). HADCM2, CCC, ECHAM and GFDL predict the formation of the zone with permafrost degradation in southern part of the transect. According to reference HADCM2 model, this zone doubled in size in comparison with 2025.

The comparison of the distributions of the MAGTs and the ALT for the final (2099) and the first year of the forecast (2000) (Figures 5.18 and 5.21), indicates that the

Reproduced with permission of the copyright owner. Further reproduction prohibited without permission.

significant warming of MAGTs (2 to 6 °C) and the deepening of the ALT (0.2 to 0.5 m) will take place throughout 2000-2099 according to all six GCMs. CCC, CSM, GFDL, HADCM2 and HADCM3 predict that the area with the permafrost degradation will be formed (Figure 5.21). HADCM2 and GFDL predict that this area will be confined within the south-eastern part (the Interior) of the transect. According to CCC the area will be located in the central part of the transect in the Brooks Range and several small patches will be formed in the Interior. ECHAM predicts that the zone will occupy south- eastern and southwestern parts of the Interior, the western part of the Brooks Range, and the southern half of the Seward Peninsula. According to HADCM3, the area with permafrost degradation will occupy eastern part of the Brooks Range, and the south-eastern and south-western parts of the Interior. HADCM2 shows the area with the permafrost degradation will occupy almost one third of the Alaskan transect, the largest area in comparison with other models.

CONCLUSIONS

The analysis of the permafrost dynamics during the last century shows that natural variations of mean annual air temperatures can cause changes in MAGTs and ALT. The magnitude of these variations could reach 3 to 4 °C for the MAGTs and up to 0.5 m for the ALT.

The ALT and the MAGTs dynamics had a cycle-like character and these changes were not uniform in space. Different parts of the Alaskan transect experience cooling or warming for the same time period (for example 1970 – 1980 period, when the northern

Reproduced with permission of the copyright owner. Further reproduction prohibited without permission.

parts of the transect was undergoing the relative decrease in MAGTs, but the central and southern parts were getting warmer). There were time periods, when cooling or warming happened everywhere within the transect, e.g. the period of 1990 – 2000 was the warm period for the entire transect.

The analysis of GCMs showed that CSM, ECHAM and GFDL are the closest to the reference HADCM2 GCM in terms of mean annual air temperatures.

The permafrost degradation from the surface will start as early as 2025 and will progress to 2099 according to the CCC, GFDL, HADCM2, HADCM3, and ECHAM models. The dynamics of the area with permafrost degradation will not be uniform. There will be cold and warm time periods on the background of the trend of the mean annual air temperatures warming. HADCM2 and GFDL predict that the area with the permafrost degradation will be in the south-eastern part of the transect. This area will be within the Brooks Range and the Interior according to CCC, ECHAM, and HADCM3.

According to the GCMs the relative increase in MAGTs will be from 2 to 6 °C by the end of 21st century. This increase will cause a deepening of the ALT by up to 0.5 m.

Reproduced with permission of the copyright owner. Further reproduction prohibited without permission.

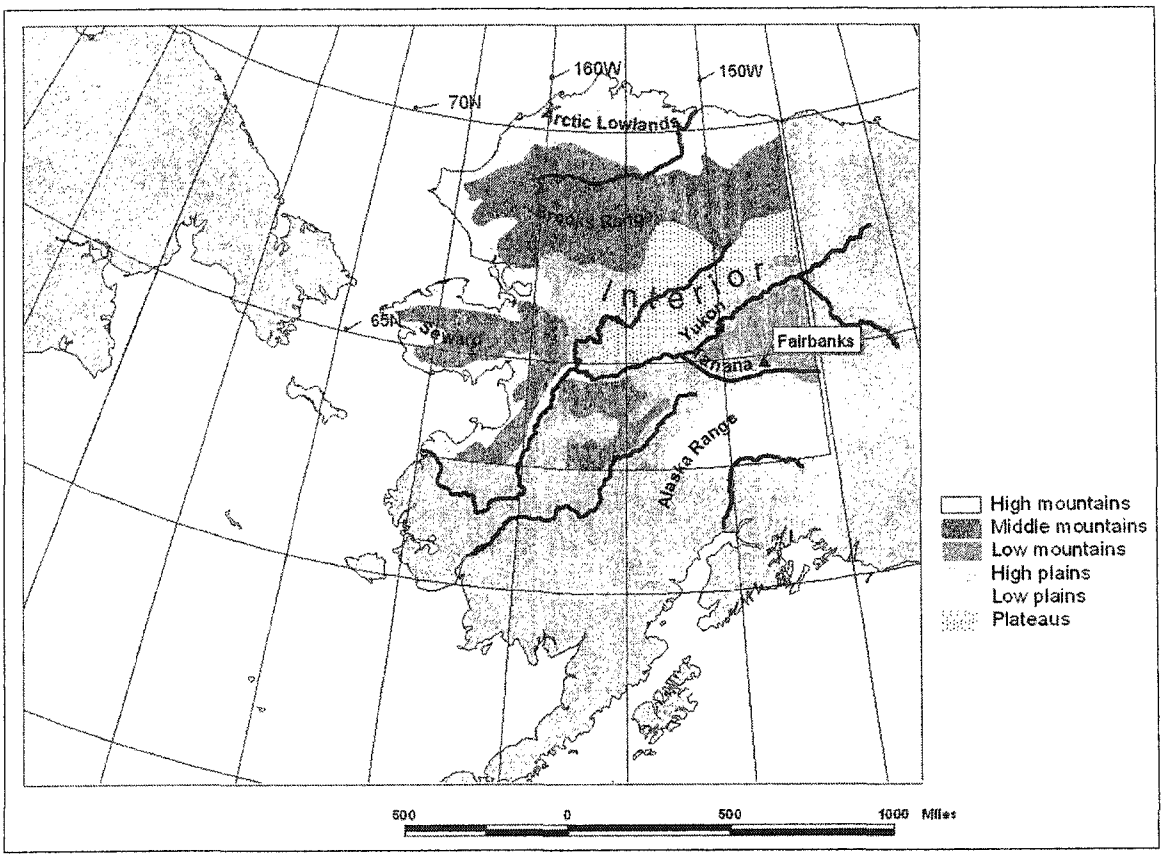

Figure 5.1: The Alaskan transect, major geographical regions, and topography (modified from ESRI topographic map).

Reproduced with permission of the copyright owner. Further reproduction prohibited without permission.

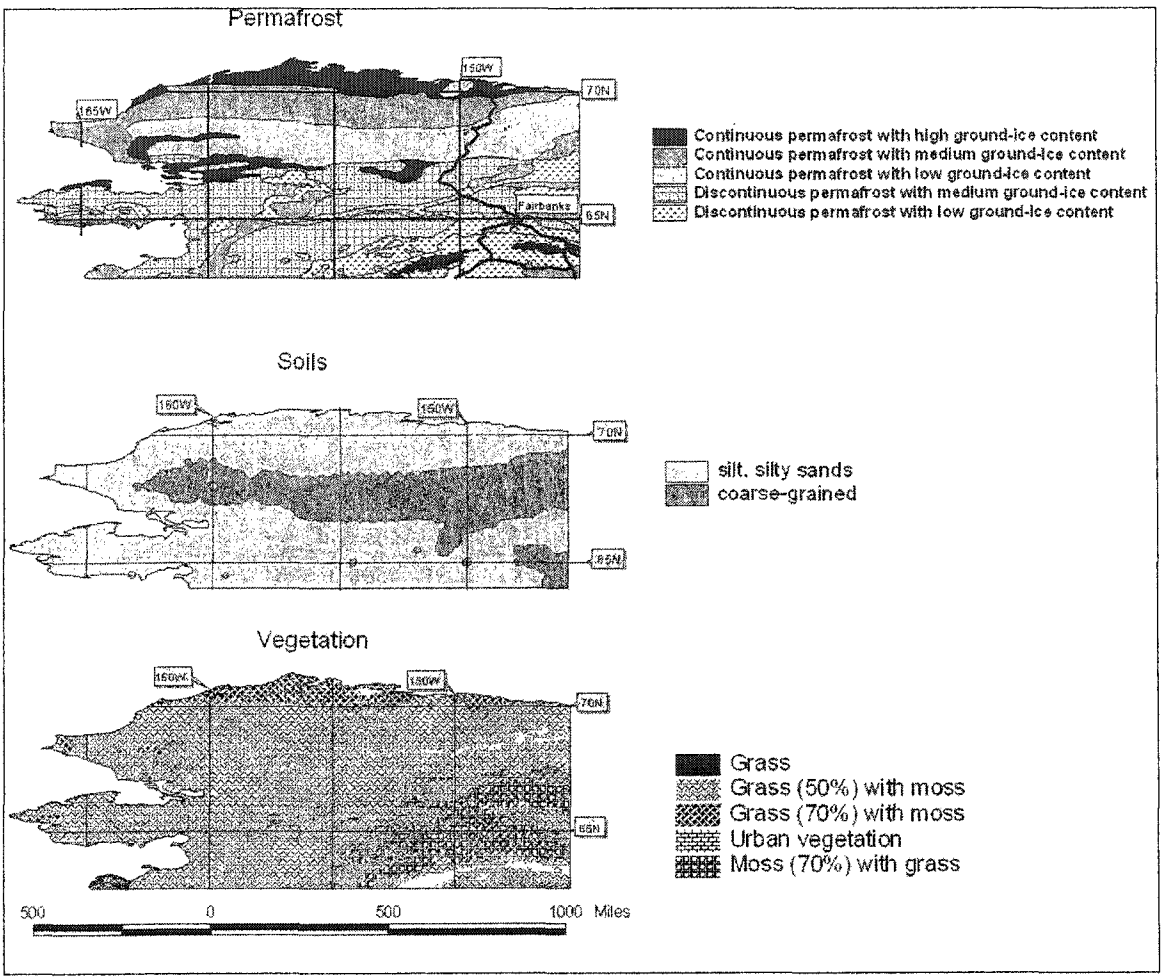

Figure 5.2: Permafrost distribution (Circum-Arctic Map of Permafrost and Ground Ice Conditions, 1997). The soils within the Alaskan transect (derived from the State Surficial Geology Map of Alaska, www.nps.gov/akso/gis). The major types of vegetation (from the Top - Soil Cover vegetation map using Global Characteristics Database, edcdaac.usgs.gov/glcc/globdoc2_0.html).

Reproduced with permission of the copyright owner. Further reproduction prohibited without permission.

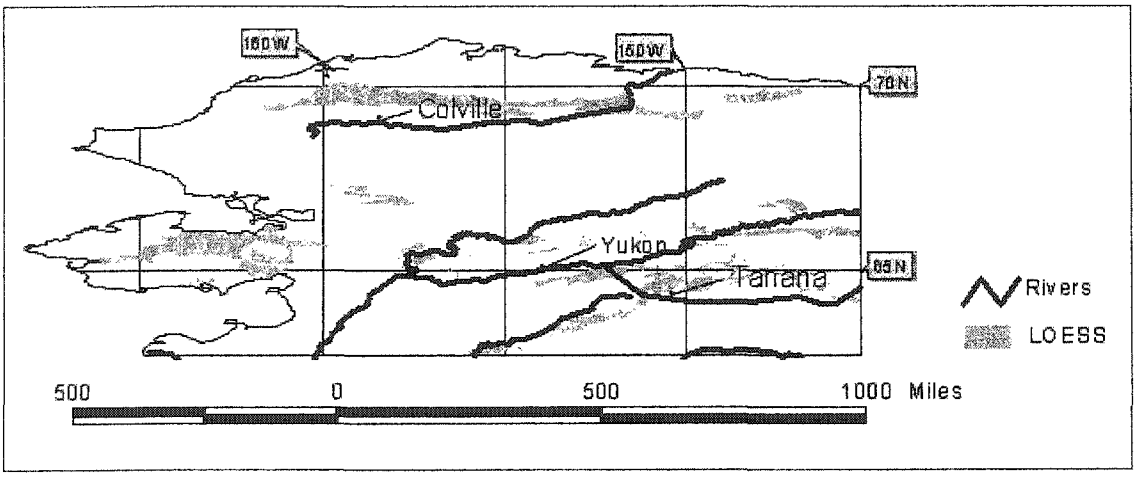

Figure 5.3: The map of the loess deposits locations. (modified from State Surficial Geology Map of Alaska, www.nps.gov/akso/gis). Gray color indicates areas with loess.

Reproduced with permission of the copyright owner. Further reproduction prohibited without permission.

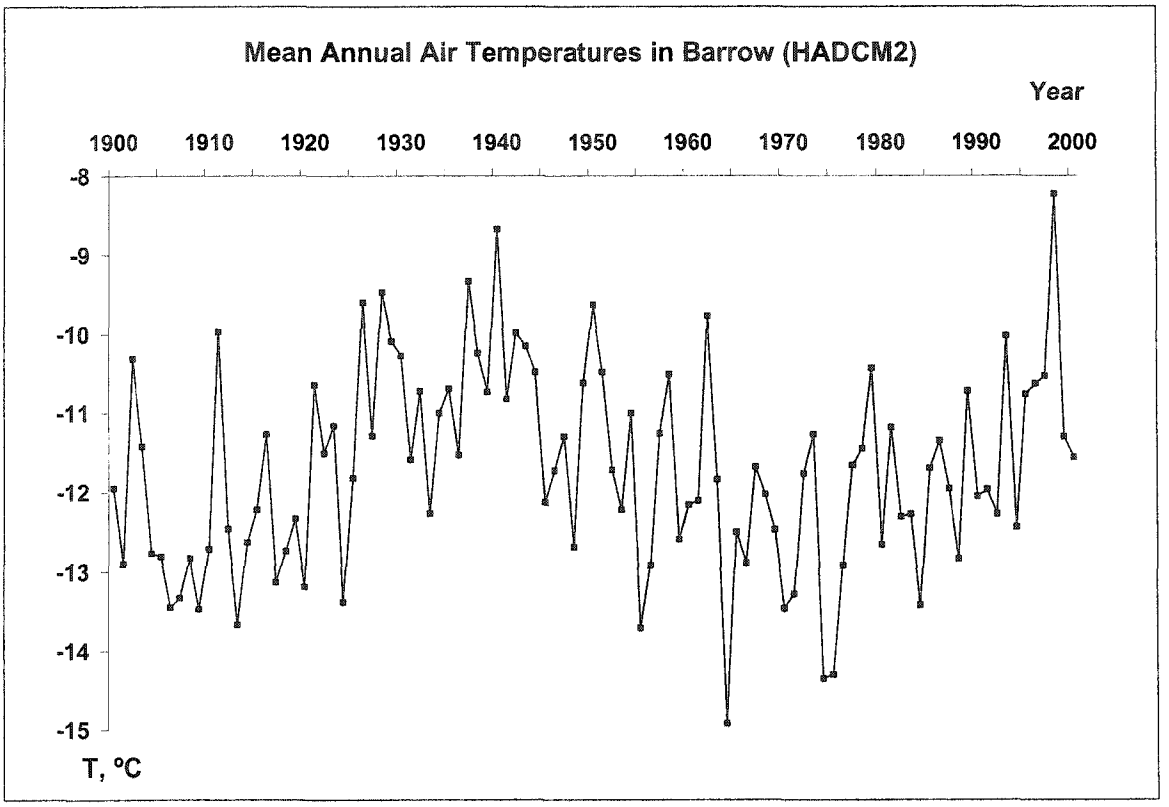

Figure 5.4: Mean annual air temperatures in Barrow, according HADCM2 GCM

Reproduced with permission of the copyright owner. Further reproduction prohibited without permission.

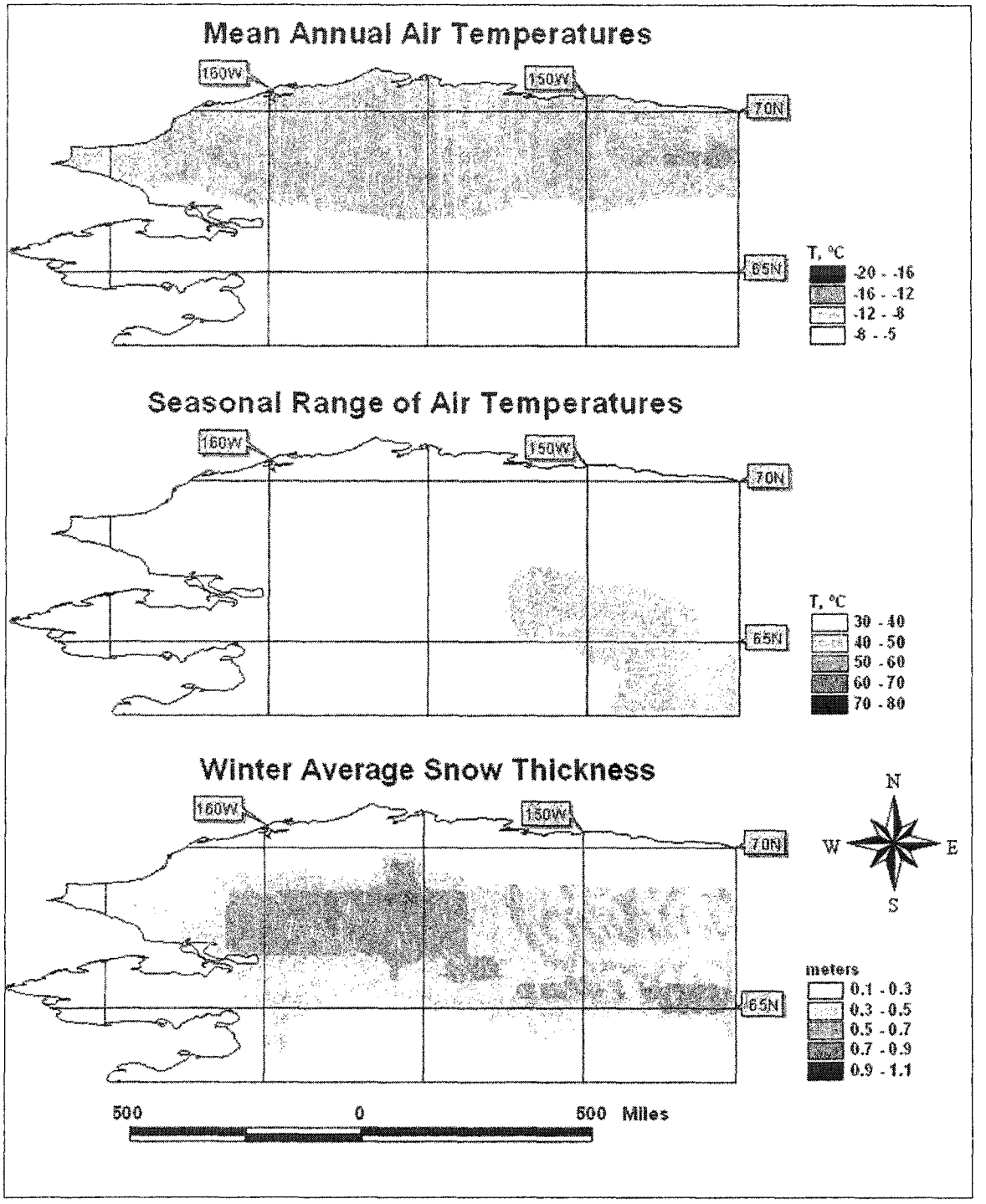

Figure 5.5: Winter average snow thickness; mean annual air temperature and seasonal range of air temperatures according to HADCM2 GCM for the year 2000.

Reproduced with permission of the copyright owner. Further reproduction prohibited without permission.

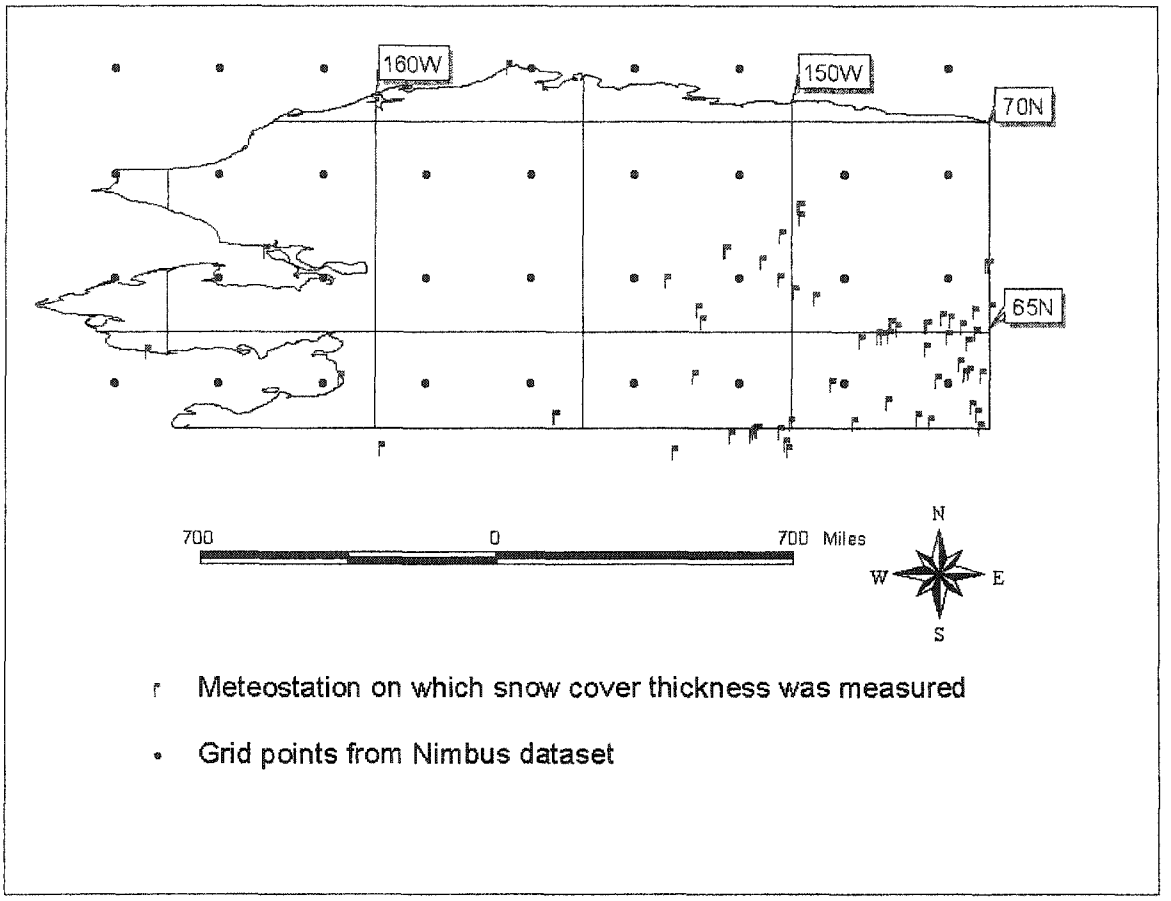

Figure 5.6: Grid points of Nimbus 7 dataset, and meteorological stations used for the correction of satellite data.

Reproduced with permission of the copyright owner. Further reproduction prohibited without permission.

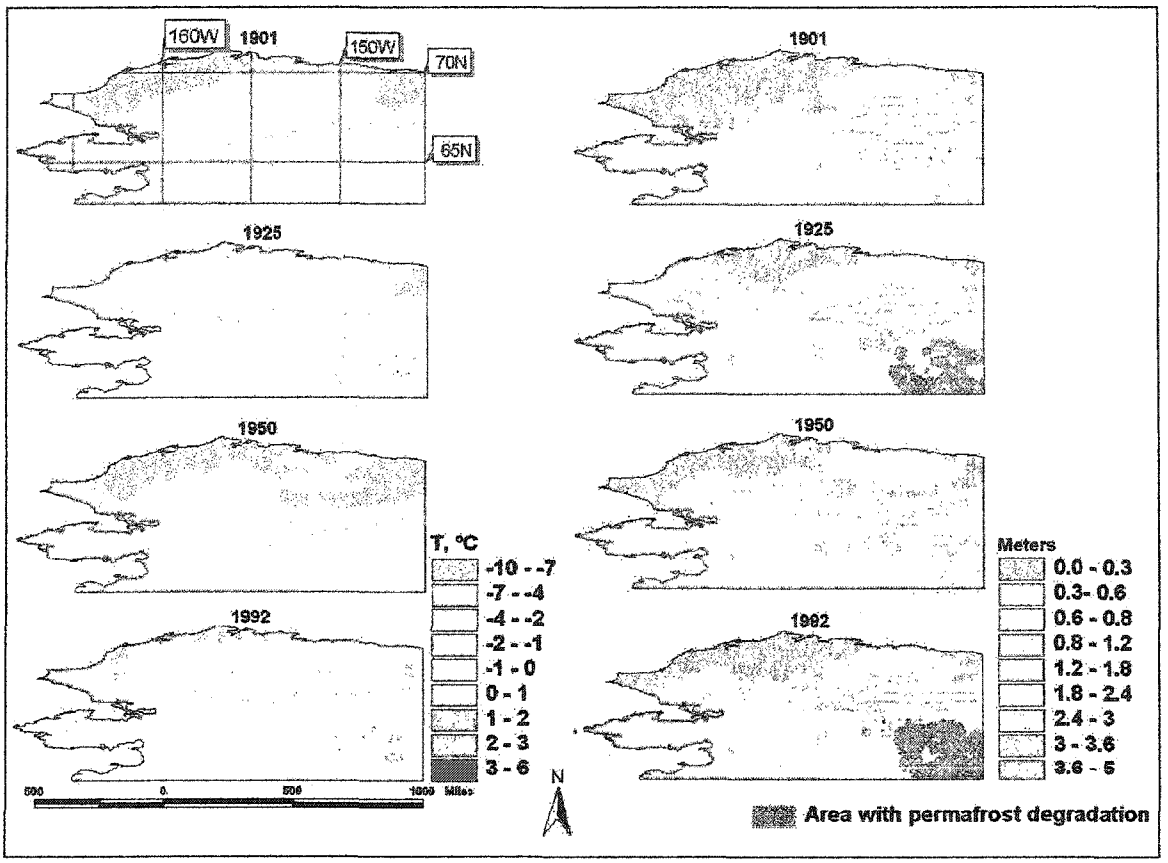

Figure 5.7: Mean annual ground temperatures and the ALT dynamics in 20th century.

Reproduced with permission of the copyright owner. Further reproduction prohibited without permission.

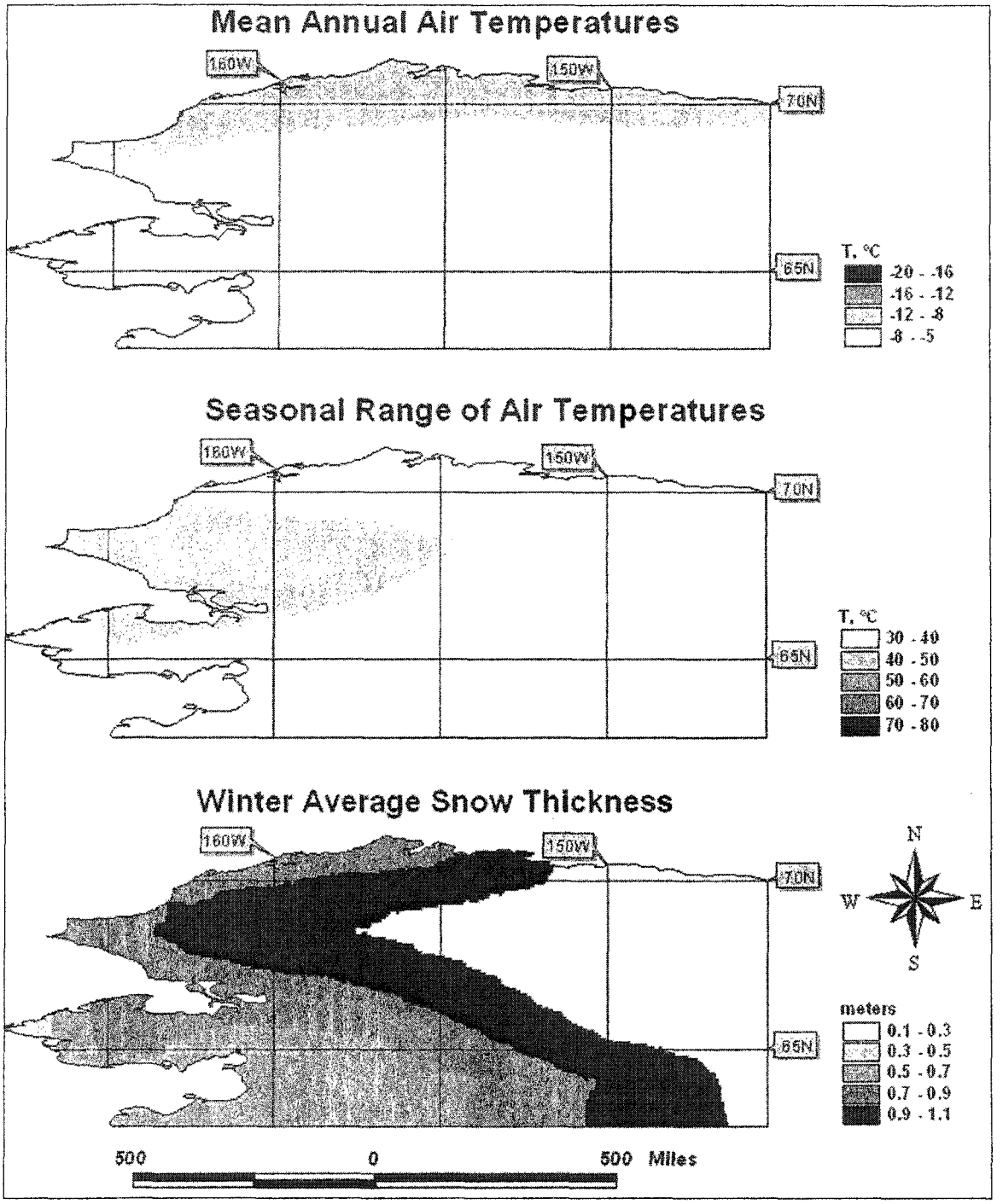

Figure 5.8: Winter average snow thickness; mean annual air temperature and seasonal range of air temperatures according to CCC GCM for the year 2000

Reproduced with permission of the copyright owner. Further reproduction prohibited without permission.

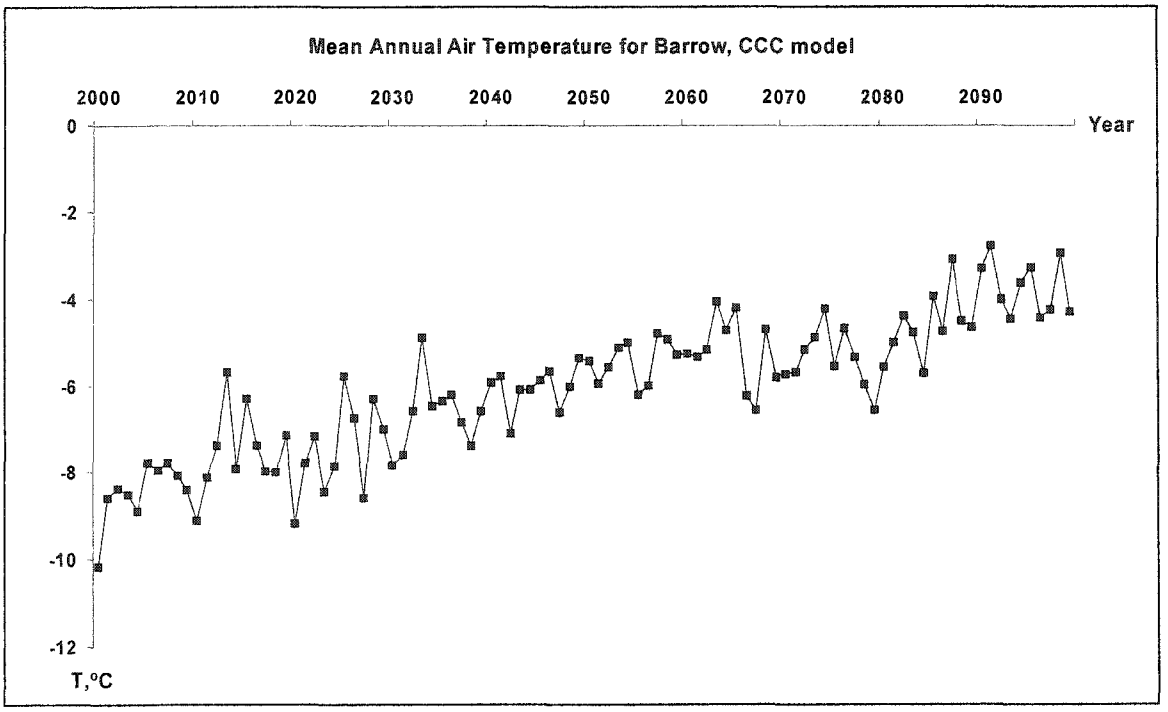

Figure 5.9: Mean annual air temperatures in Barrow, according CCC GCM

Reproduced with permission of the copyright owner. Further reproduction prohibited without permission.

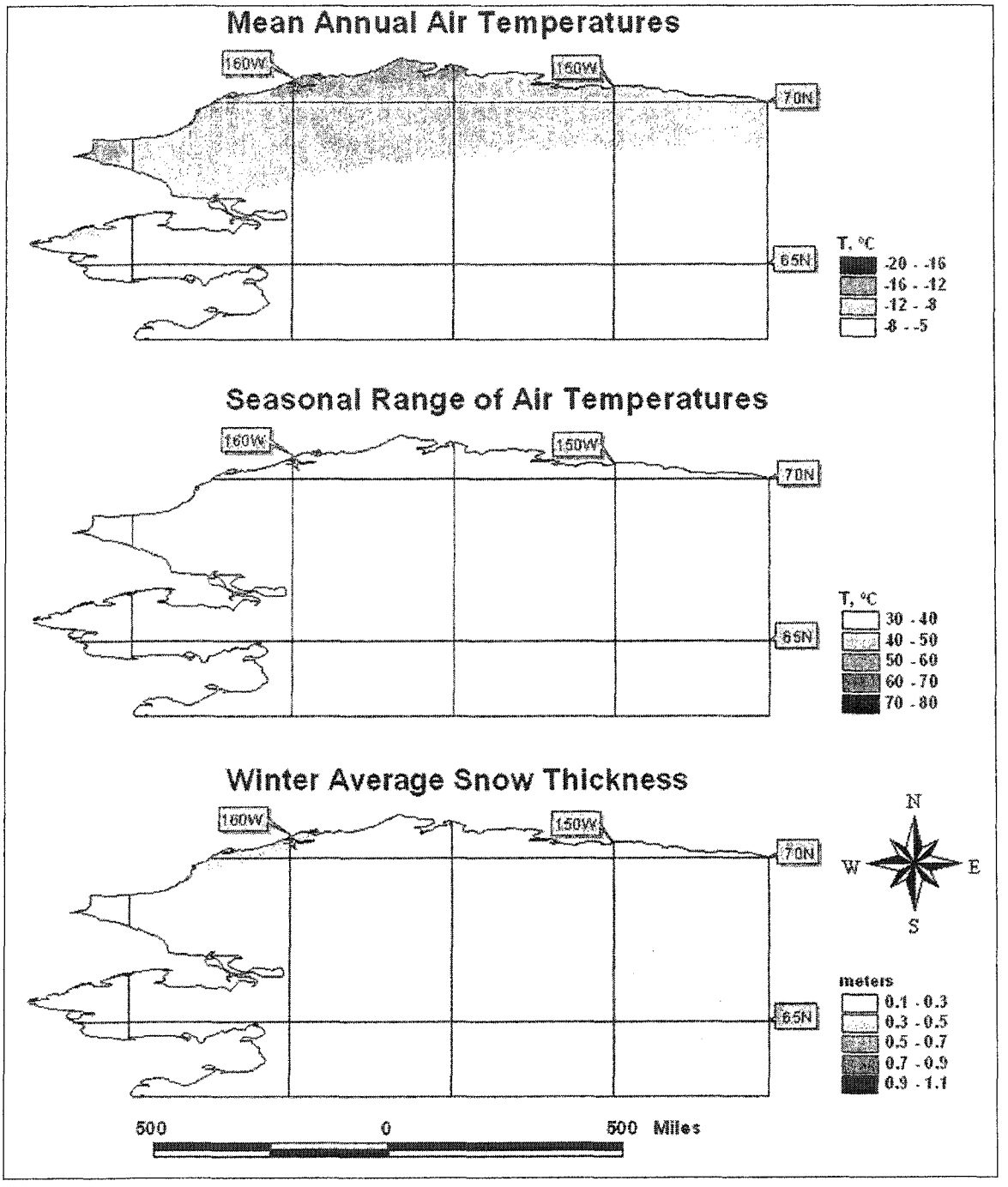

Figure 5.10: Winter average snow thickness; mean annual air temperature and seasonal range of air temperatures according to CSM GCM for the year 2000

Reproduced with permission of the copyright owner. Further reproduction prohibited without permission.

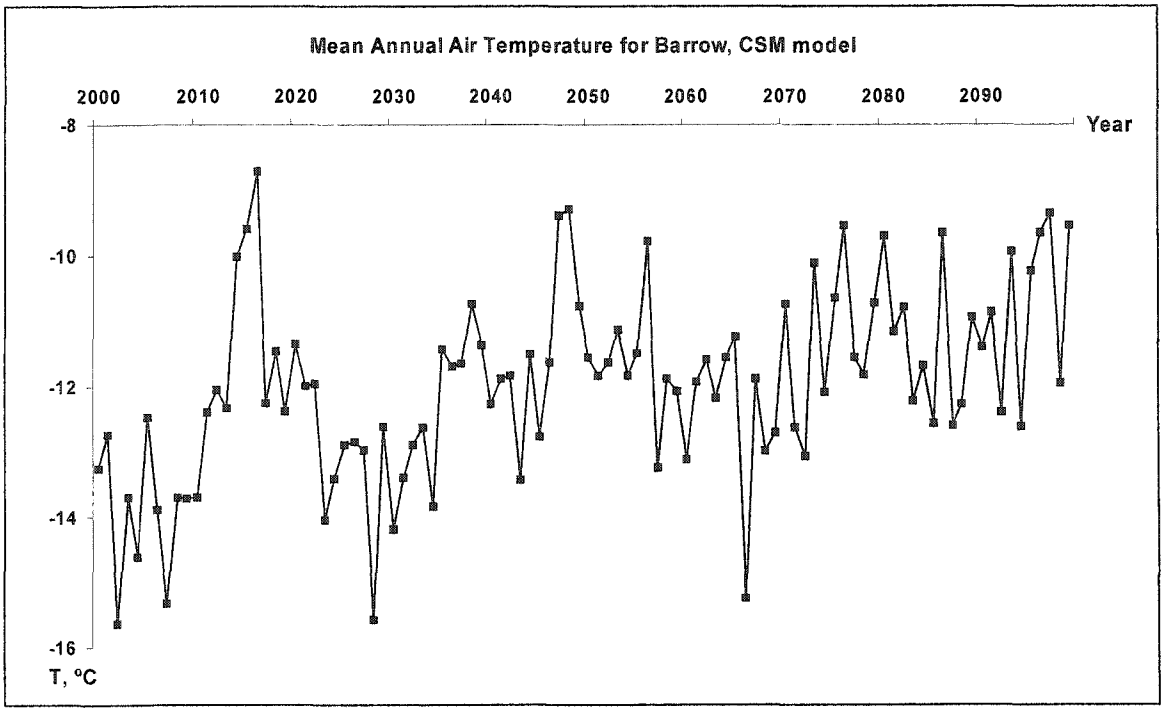

Figure 5.11: Mean annual air temperatures in Barrow, according CSM GCM.

Reproduced with permission of the copyright owner. Further reproduction prohibited without permission.

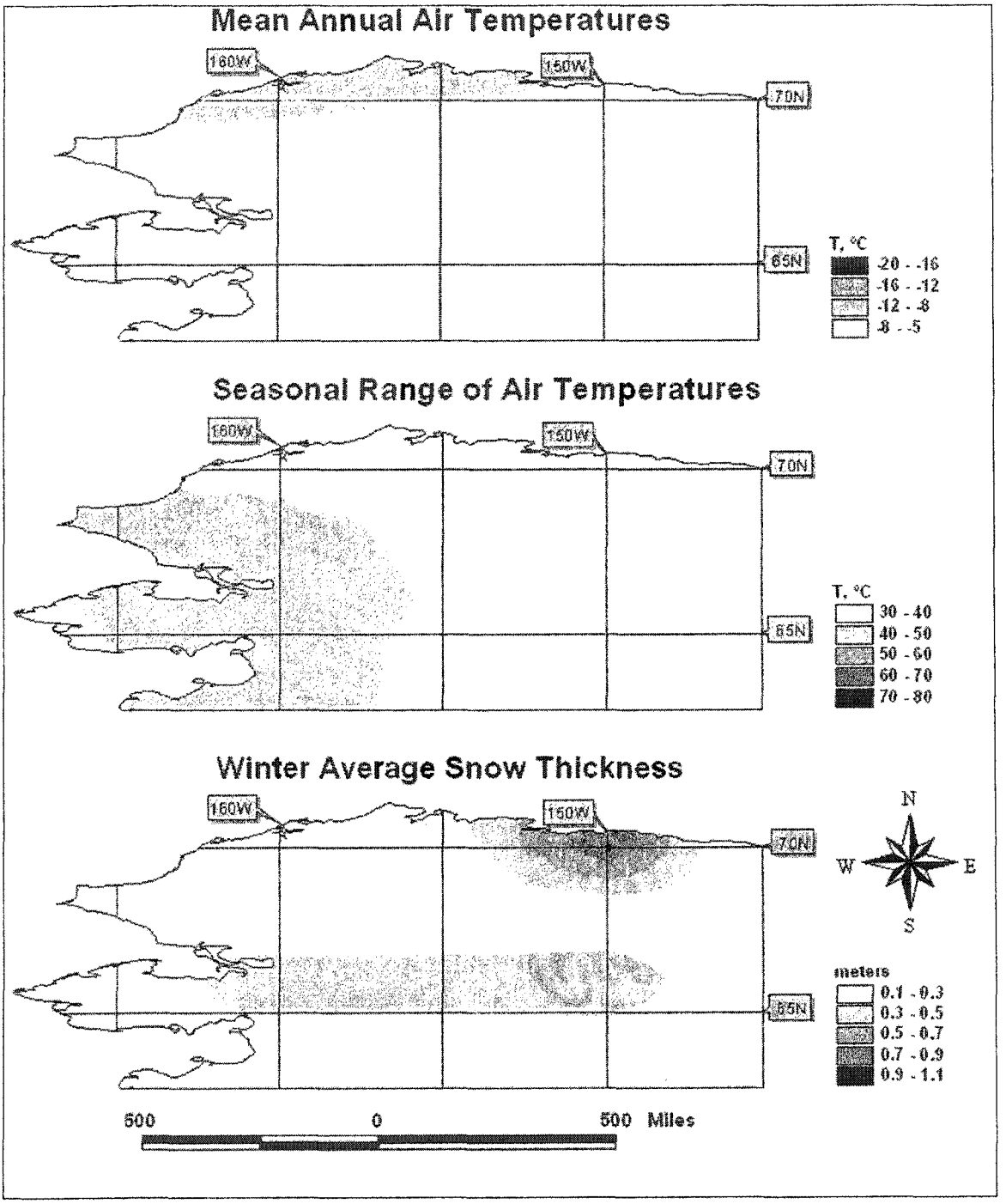

Figure 5.12: Winter average snow thickness; mean annual air temperature and seasonal range of air temperatures according to GFDL GCM for the year 2000.

Reproduced with permission of the copyright owner. Further reproduction prohibited without permission.

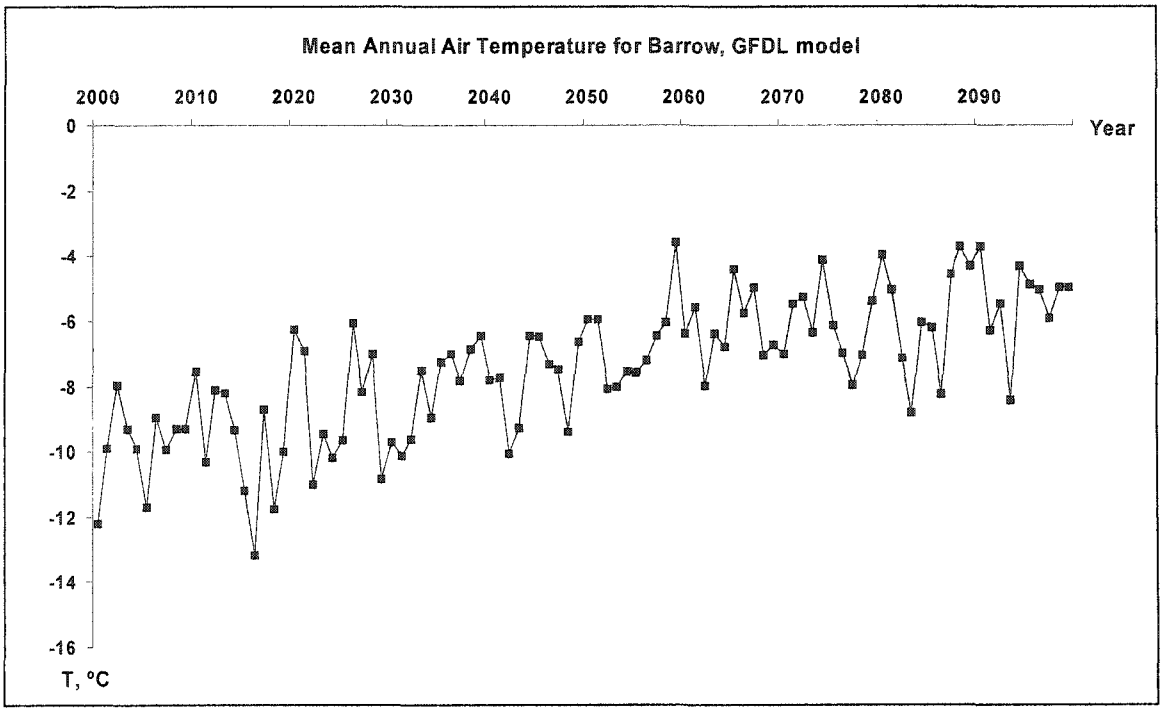

Figure 5.13: Mean annual air temperatures in Barrow, according GFDL GCM.

Reproduced with permission of the copyright owner. Further reproduction prohibited without permission.

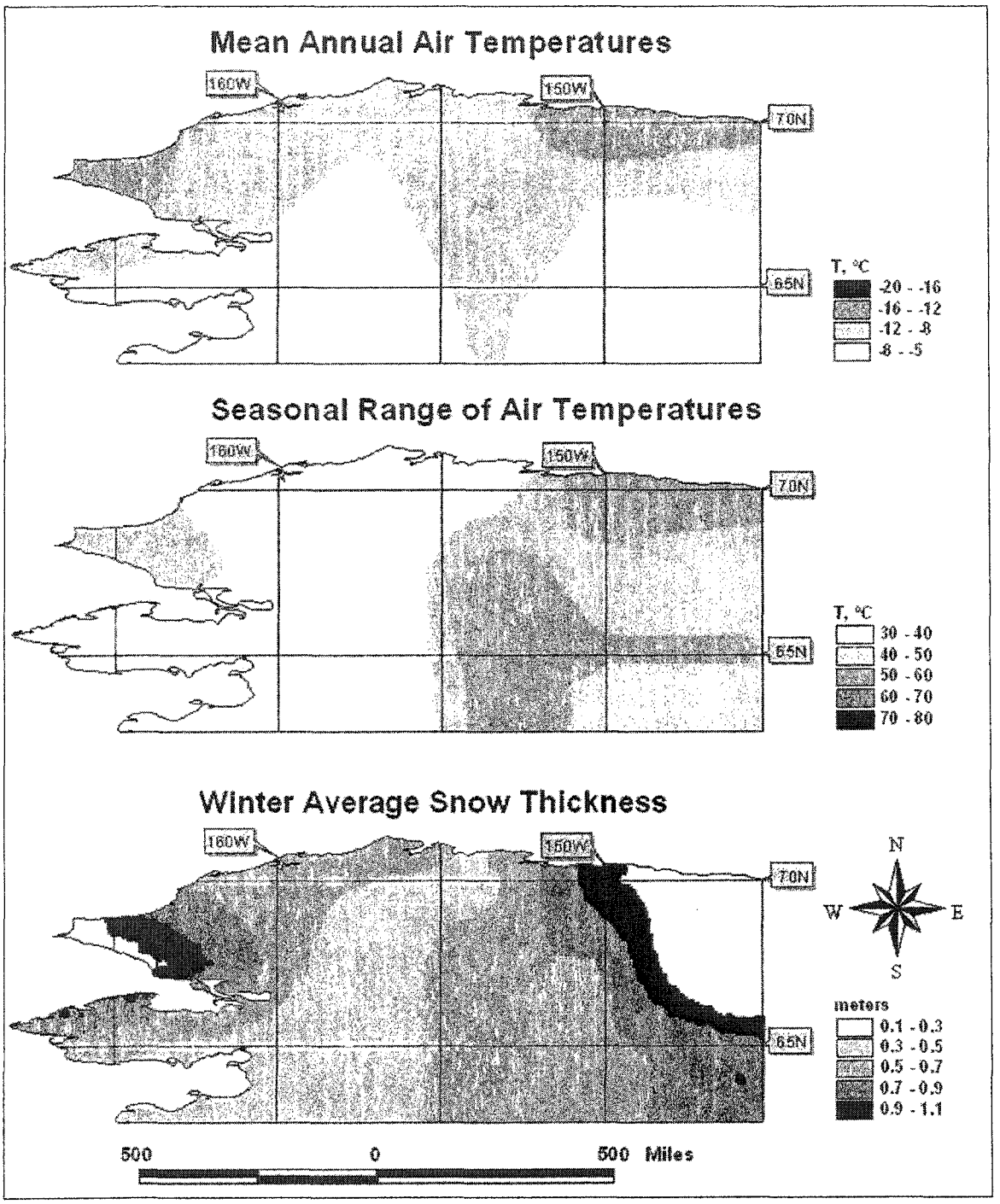

Figure 5.14: Winter average snow thickness; mean annual air temperature and seasonal range of air temperatures according to HADCM3 GCM for the year 2000.

Reproduced with permission of the copyright owner. Further reproduction prohibited without permission.

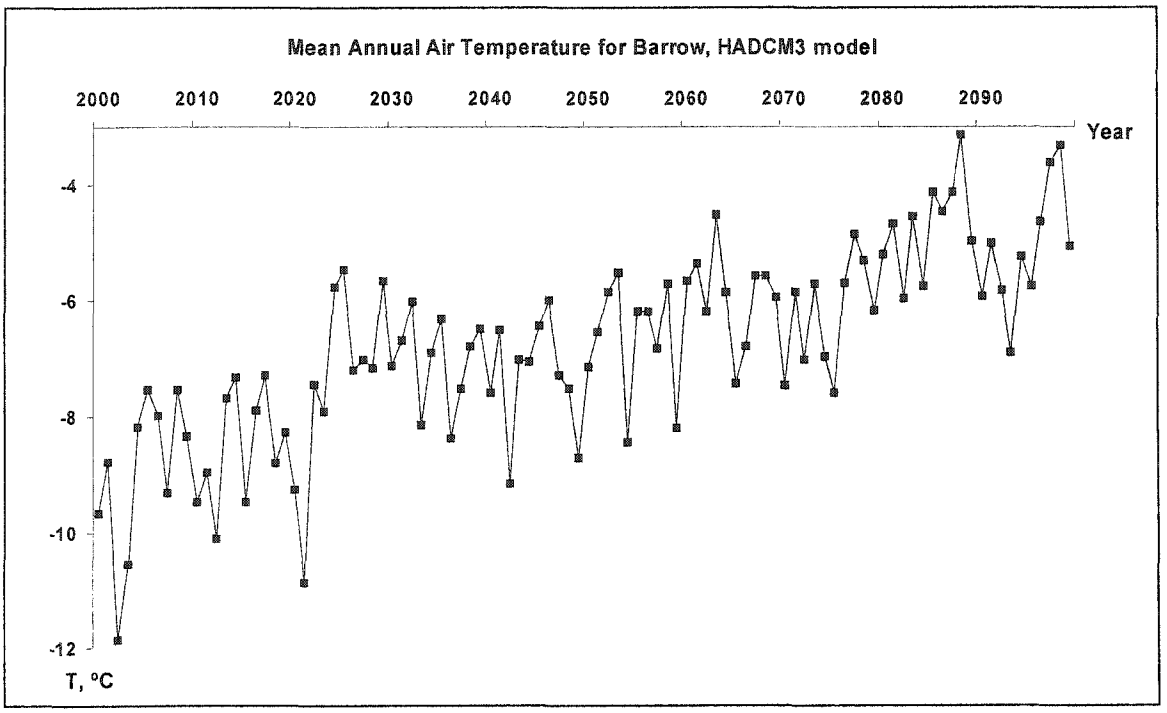

Figure 5.15: Mean annual air temperatures in Barrow, according HADCM3 GCM.

Reproduced with permission of the copyright owner. Further reproduction prohibited without permission.

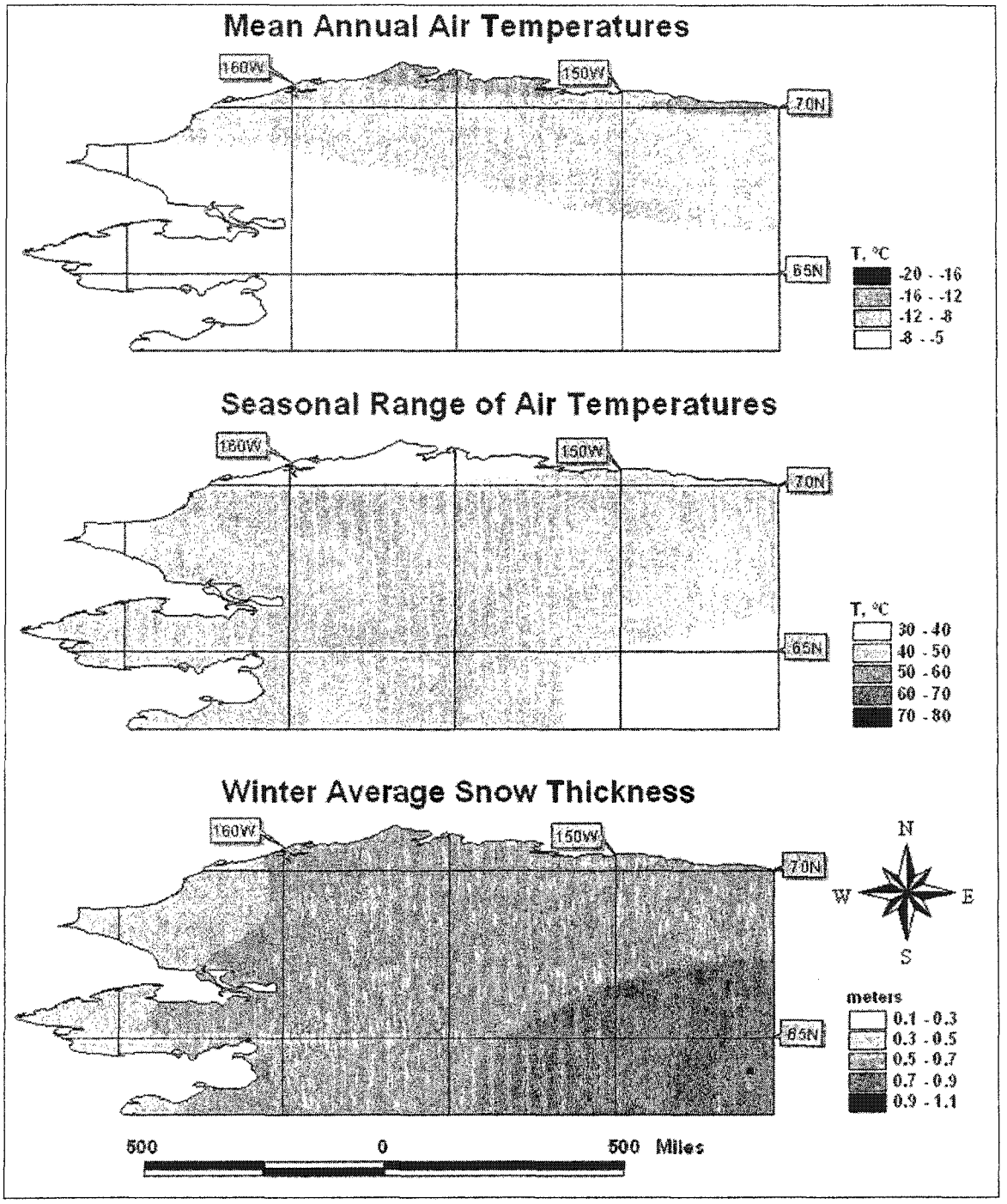

Figure 5.16: Winter average snow thickness; mean annual air temperature and seasonal range of air temperatures according to ECHAM GCM for the year 2000

Reproduced with permission of the copyright owner. Further reproduction prohibited without permission.

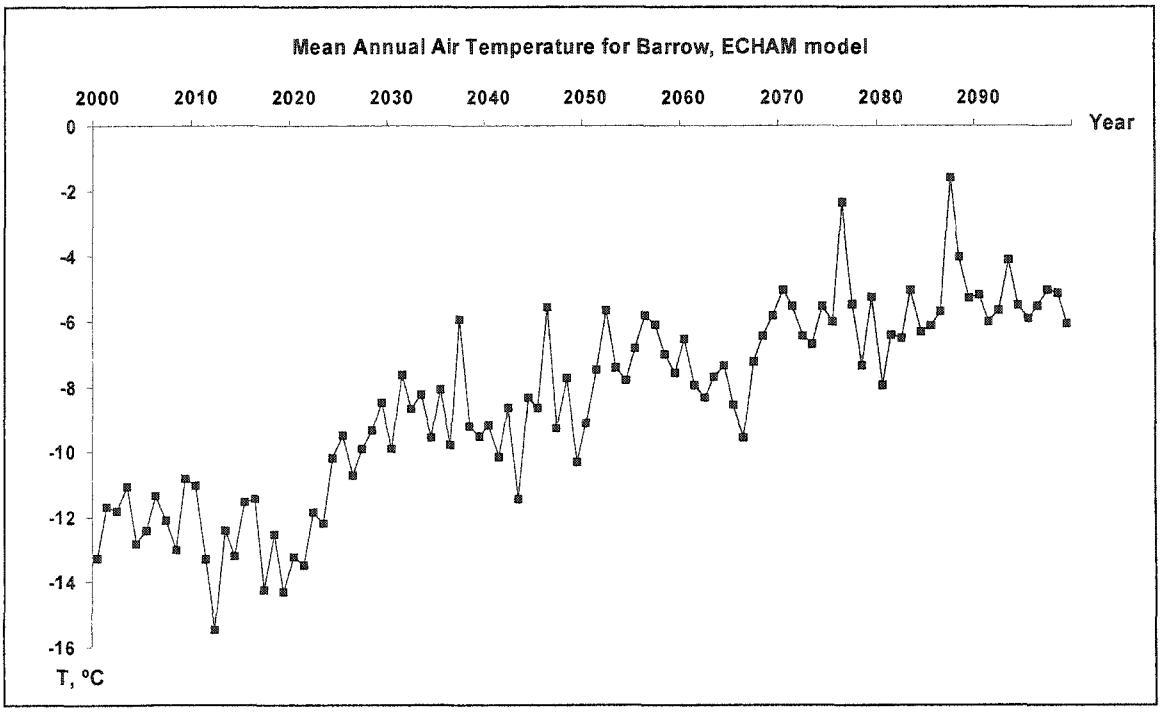

Figure 5.17: Mean annual air temperatures in Barrow, according ECHAM GCM

Reproduced with permission of the copyright owner. Further reproduction prohibited without permission.

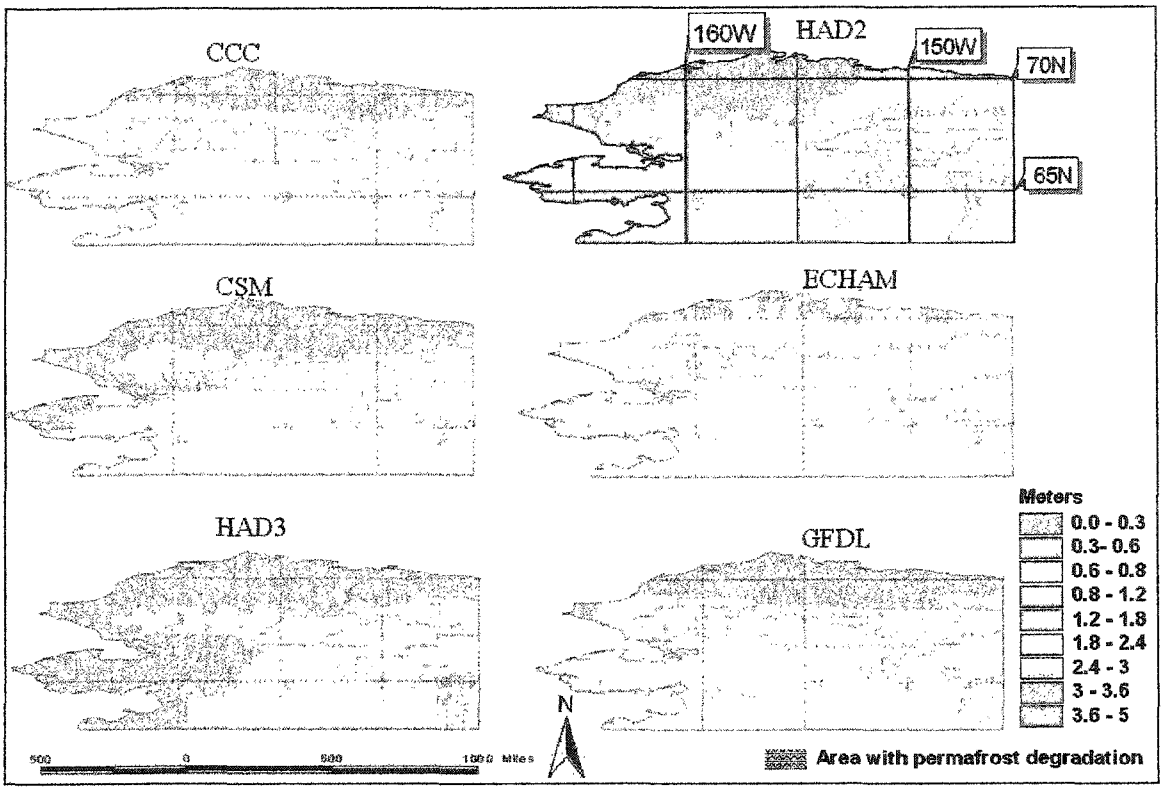

Figure 5.18: The ALT distribution for the year 2000, according to six GCMs.

Reproduced with permission of the copyright owner. Further reproduction prohibited without permission.

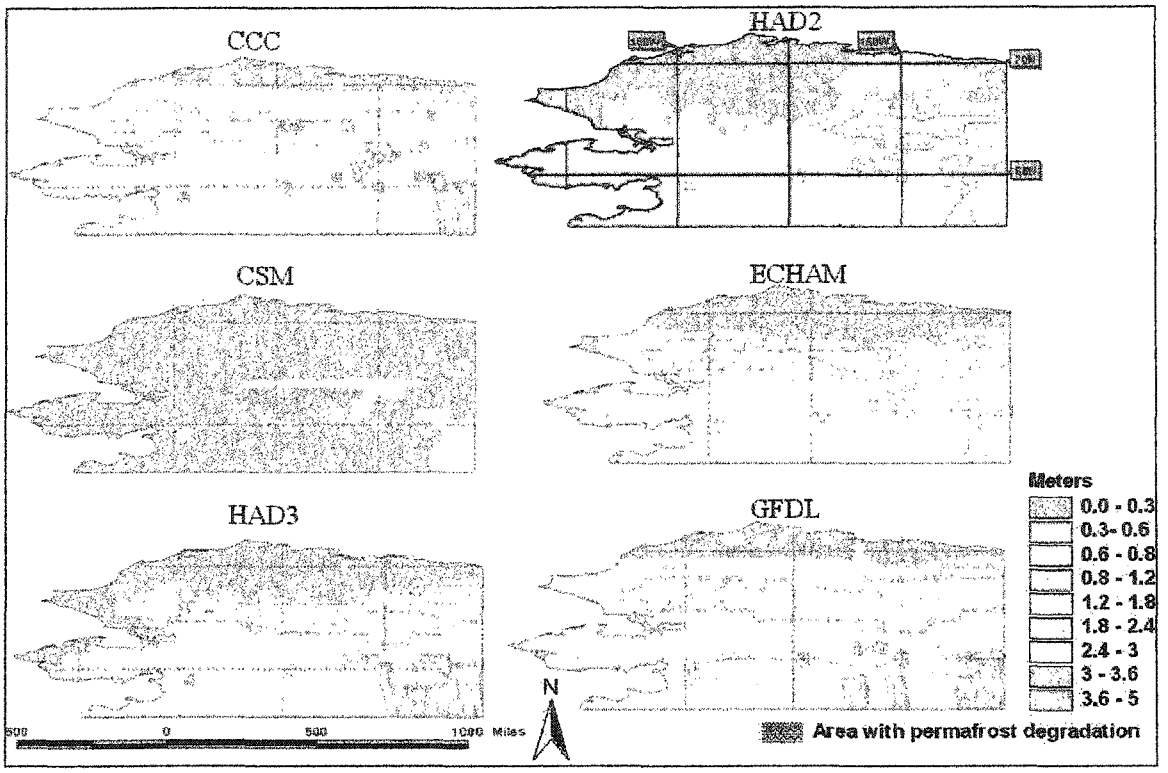

Figure 5.19: The ALT distribution for the year 2025, according to six GCMs.

Reproduced with permission of the copyright owner. Further reproduction prohibited without permission.

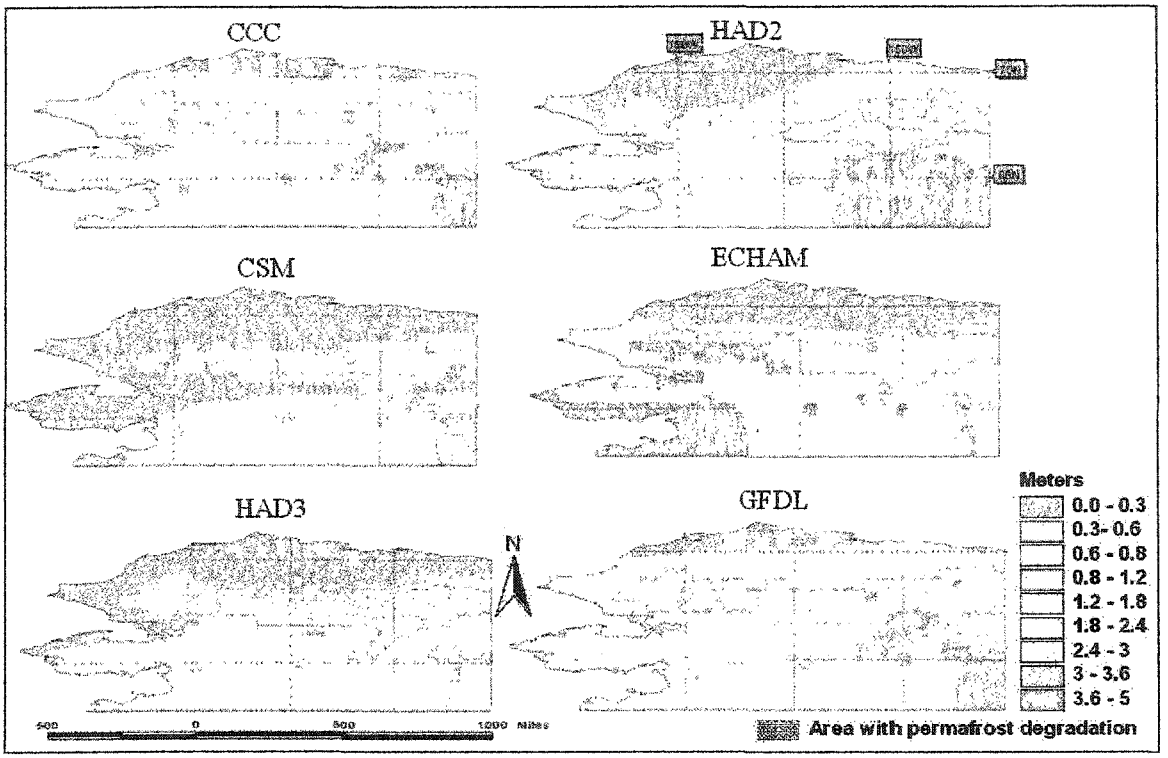

Figure 5.20: The ALT distribution for the year 2050, according to six GCMs.

Reproduced with permission of the copyright owner. Further reproduction prohibited without permission.

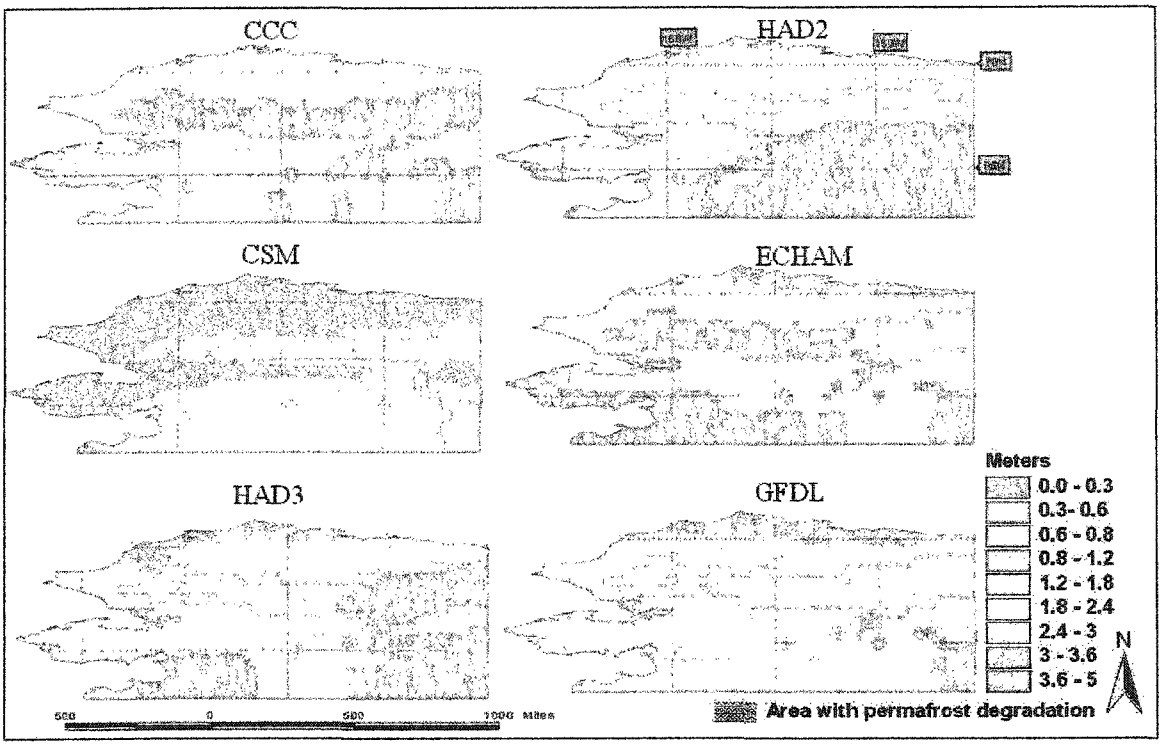

Figure 5.21: The ALT distribution for the year 2099, according to six GCMs.

Reproduced with permission of the copyright owner. Further reproduction prohibited without permission.

Table 5.1: Comparison of measured (www.wrcc.dri.edu/summary/climsmak.html) and simulated (HADCM2) mean annual air temperatures for the year 2000.

Name	**T,°C measured**	**T,°C HADCM2**
Barrow	-11.79	-11.44
Umiat	-10.12	-8.90
Kotzebue	-5.01	-6.12
Bettles	-4.53	-5.26
Nome	-1.33	-3.96
Tanana	-3.69	-3.86
Fairbanks	-2.21	-3.32
Nenana	-4.14	-4.02

Reproduced with permission of the copyright owner. Further reproduction prohibited without permission.

Table 5.2: Comparative analysis of five GCMs using HADCM2 as a reference for the year 2000.

GCM	Mean annual air temperatures	Seasonal range of air temperatures	Winter average snow thickness
CCC	Latitudinal gradient is present. Warmer (3 °C) in the Brooks Range and the Arctic Lowlands. Colder (1 to 3°C) in the Interior	No latitudinal gradient and decreasing of magnitude towards the shore lines. Smaller magnitudes (10 to 15 °C) in the Interior.	20 to 1m thicker for the entire transect
CSM	Latitudinal gradient is present. This GCM is very close to the reference.	No latitudinal gradient. Smaller magnitudes (5 to 15°C) in the entire territory of the transect.	20-30 cm shallower almost everywhere
GFDL	Latitudinal gradient is present. Warmer temperatures (3 to 4°C) on the Arctic Lowlands. In the rest of the territory is the closest to the reference.	Smaller magnitudes (20 to 25 °C) in the Interior.	30-40 cm deeper in the Arctic Lowlands.
HADCM3	Generally colder in the Arctic Lowlands, Seward Peninsula and the Interior.	No latitudinal gradient. Larger magnitudes (10 to15 °C) in the eastern part of the transect (to the east from 155 WL) and smaller (10 to 15°C) in the western part.	20 – 40 cm thicker for the entire transect
ECHAM	Latitudinal gradient is present. 3to 4 °C colder within the Brooks Range, and 2 to 3 °C colder in the Interior.	Larger magnitudes (10 to 20 °C) in Seward Peninsula and in the western part of the transect. Smaller (10 to 15°C) in the Interior (south-eastern part of the transect).	Deeper up to 1m, almost everywhere

Reproduced with permission of the copyright owner. Further reproduction prohibited without permission.

CHAPTER 6.GENERAL CONCLUSIONS

Spatial and temporal dynamics of permafrost along the East-Siberian and Alaskan transects has been evaluated and discussed in previous chapters. This evaluation is a first component of the transect approach widely used now by scientific communities to assess the consequences of the global climate change (McGuire et al., 2002). The second step of the approach is an attempt to compare the transects and find differences and similarities in permafrost dynamics. This analysis allows creating a basis for the extrapolation of the permafrost parameters between the two transects. The spatial dynamics of the ALT and MAGTs within the transects was compared using the results of 2000 – 2100 forecast for the East-Siberian (Chapter 4) and the Alaskan (Chapter 5) transects.

THE COMPARISON OF THE EAST-SIBERIAN AND ALASKAN TRANSECT IN TERMS OF SPATIAL AND TEMPORAL DYNAMICS OF PERMAFROST

To make the comparison of two transects, the ALT and MAGTs have been calculated for each transect, using six GCMs (ECHAM, HADCM2, HADCM3, GFDL, CCC and CSM) for the 2000 – 2100 time interval. To evaluate the changes in MAGTs and ALT averages for 2000 – 2004 and 2096 – 2100 time intervals were calculated and differences between these two intervals were found. The results, which represent relative changes in MAGTs and ALTs for the period of 2000 - 2100, are presented in Figures 6.1 through 6.4.

The spatial dynamics of MAGTs

Reproduced with permission of the copyright owner. Further reproduction prohibited without permission.

MAGTs within the East-Siberian and Alaskan transects according to all scenarios will be 2°C to 5°C warmer (Figures 6.1 and 6.2) by the end of 21st century. ECHAM predicts the most increase in MAGTs over the entire area of the East-Siberian and Alaskan transects. Within the uplands in the southwestern part of the East-Siberian transect MAGTs will exceed 0°C and permafrost degradation from the surface will start. MAGTs will become positive and the degradation of permafrost will start in the western part of the Brooks Range, southern part of the Seward Peninsula, and in the most parts of the Interior, within the Alaskan transect. The area with permafrost degradation will occupy approximately 35% of total area of the Alaskan transect and about 16% of the East Siberian transect.

HADCM3 projected increase in MAGTs will be up to 5°C for the most territory of the Alaskan transect (Figure 6.2), and for the northern part of the East-Siberian transect (Figure 6.1). MAGTs will exceed 0°C in the eastern and south-western parts of the Alaskan transect, and permafrost degradation will start within these areas, which will occupy almost 30% of the total area. In the East-Siberian transect the permafrost degradation will start only in the uplands within the south-western part of the transect.

HADCM2 shows that MAGTs within the most parts of the East-Siberian and Alaskan transects will be 3 to 4°C warmer by the end of 21st century. The most significant increase (up to 5°C) will take place in the northern parts of the East-Siberian transect and in the Brooks Range in Alaska (Figures 6.1 and 6.2). Permafrost degradation will start in the uplands within the East-Siberian transect and in the Interior within the Alaskan

Reproduced with permission of the copyright owner. Further reproduction prohibited without permission.

transect. The area with permafrost degradation will be approximately 10% of total area in the East-Siberian transect and almost 40% of the total area in the Alaskan transect.

According to GFDL, the increase in MAGTs will range from 2°C to 4°C for both transects. The most significant increase (up to 4°C) will take place within the entire area of the East-Siberian transect and in the Brooks Range and in the western part of the Alaskan transect (Figures 6.1 and 6.2). Permafrost degradation will not start in the East-Siberian transect. In the Alaskan transect, MAGTs within the small area in the south-eastern part of the Interior will become positive and permafrost degradation from the surface will start.

MAGTs calculated using outputs from CCC and CSM will be 1 to 4°C warmer in the transects. The most increase (up to 4°C) will take place within the northern and northwestern parts of the transects. CCC predicts the permafrost degradation by the end of 21st century. The area with permafrost degradation will be the Brooks Range and the Interior, and occupy approximately 30% of the total territory of the Alaskan transect. In the East-Siberian transect, permafrost degradation will start in the south-western uplands. According to CSM, permafrost degradation from the surface will not start.

The spatial dynamics of ALT and the areas with permafrost degradation.

By the end of 21st century, according to all scenarios, ALT will become deeper within the East-Siberian and Alaskan transects, except for the areas where permafrost degradation will start from the surface. Within these areas a seasonally frozen layer will develop during cold seasons (when ground surface temperatures are colder than 0°C) and

Reproduced with permission of the copyright owner. Further reproduction prohibited without permission.

will thaw every consecutive summer. The areas with permafrost degradation and seasonally frozen layer formation were excluded from the analysis of ALT dynamics.

Within the East-Siberian and Alaskan transects, ALT will be up to 0.5 m and in some areas by 2 m deeper by the end of 21st century (Figures 6.3 and 6.4). The most increase in ALT can take place within the East-Siberian transect (up to 2 m) and especially in regions with coarse-grained soils. Those areas include uplands within the south-western part and several patches in the central part of the transect. This deepening of the ALT can be explained by high thermal conductivity and low moisture content of the soils, which make them respond quicker and more significantly to changes in climate.

In other places within the East-Siberian and Alaskan transects, where relatively fine –grained soils prevail (silt for example, or sandy silt) the deepening of the ALT does not exceed 1 m and is less than 0.5 m on average. The 0.5 to 1 m deepening is in the limits of long-term natural variability of the ALT.

ECHAM projects the most increase in the ALT (up to 1-2 m) within the regions to the east from the Lena River, in the central part of the transect and in the south-western uplands. The ALT will be 0.5 to 1 m deeper almost everywhere except the river valleys and the Arctic Lowlands, where the deepening will be less than 0.5 m. In the Alaskan transect, the most increase (from 1 to 2 m) will take place within the eastern part of the Brooks Range, on the rest of territory the deepening will be less than 0.5 m.

According to HADCM3 the most significant increase in the ALT (up to 2 m) will take place on the small oblong area along the 125 EL within the Verkhoyansk Range in the East-Siberian transect. In the central and most southern parts of the transect, the ALT

Reproduced with permission of the copyright owner. Further reproduction prohibited without permission.

will be 0.5 to 1 m deeper by the end of 21st century. Within the Arctic lowlands, the Central Yakutian Lowlands, and the river valleys, the increase in thee ALT will be less than 0.5 m. In the Alaskan transect within the central and western parts of the Brooks Range the ALT will be 0.5 to 1 m deeper. Everywhere else the relative increase will not exceed 0.5 m.

HADCM2 predicts the 1 to 2 m deepening of the ALT within the small regions in the central part of the East-Siberian transect. The soils in these regions are dominated by coarse-grained sediments. The largest region is located to the east from the Lena River between 65 and 70 NL. On the rest of the territory of the East-Siberian transect, except the river valley and the Arctic Lowlands, the relative increase in the ALT will range from 0.5 to 1 m. The ALT within the Alaskan transect will be from 0.5 m to 1 m deeper in the Brooks Range, and less than 0.5 m in the Arctic Lowlands, Interior and the Seward Peninsula.

According to GFDL, the ALT will be 1 to 2 m deeper within the small region in the central and south-western parts of the East-Siberian transect. The predicted deepening of the ALT ranging from 0.5 to 1 m will take place in the areas to the east from the Lena River and in the southern and south-western parts of the East-Siberian transect. In the Arctic Lowlands, the western part of the transect, the Central Yakutian Lowlands, and in the Yana River Valley, the deepening of ALT will no exceed 0.5 m. Almost everywhere in the Alaskan transect, the ALT will be up to 0.5 m deeper. In some places in the north-western part of the transect, the ALT can be up to 1 m deeper.

Reproduced with permission of the copyright owner. Further reproduction prohibited without permission.

CCC predicts from 1 to 2 m increase in the ALT in the central, and south-western parts of the East-Siberian transect. On the rest of the territory of the transect the deepening of the ALT will be less than 0.5 m. Everywhere within the Alaskan transect, the relative increase in the ALT will be 0.2 m on average and will not exceed 0.5 m.

According to CSM, the most significant increase in the ALT (from 0.5 to 1 m) will take place in the small regions between 65 and 70 NL to the east from the Lena River, and in the south-western uplands within the East-Siberian transect. On the rest of the territory the relative deepening of the ALT will be less than 0.5 m (about 0.2 - 0.3 m on average). The Alaskan transect will experience less than 0.5 m increase in the ALT.

Within the East-Siberian transect the permafrost degradation from the surface will start in 2050 according to HADCM2 and ECHAM. HADCM2 projects the steady development of the zone with permafrost degradation, which will double in size by 2075 (5% of the total area), and reach maximum in 2099 (almost 10% of the total area). ECHAM predicts the permafrost aggradation by 2075 and total disappearance of the zone, with following reanimation by 2099 (Figure 6.5). The zone with permafrost degradation will occupy 15% of the total area of the East-Siberian transect. CCC shows the beginning of the permafrost degradation in 2075 with further development and reaching the maximum (6% of the total area) by 2099. Permafrost degradation can start in 2099 according to HADCM3 and occupy less than 5% of the total area.

In the Alaskan transect the zone with permafrost degradation will develop earlier and be considerably larger in comparison with the East-Siberian transect. The permafrost degradation predicted by HADCM3 model started as early as 2000 and was almost 3% of

Reproduced with permission of the copyright owner. Further reproduction prohibited without permission.

the total area. By 2025, this zone will be doubled in size and totally disappear by 2050 (Figure 6.6). But by 2075, the zone with permafrost degradation will be developed once more and progress throughout 2075 – 2099, reaching 30% of the total area of the transect by the end of 21st century.

HADCM2 predicts the start of the permafrost degradation within the Alaskan transect by 2025 and steady increase in the area during 2025 – 2099. By 2099, the area occupied by thawing permafrost will reach 35% of the total area. CCC predicts the beginning of the permafrost thawing in 2025, but in comparison with HADCM2 the area occupied by this zone will not change till the very end of the forecast. The area will be almost 26% of the total area in 2099. According to GFDL, permafrost degradation from the surface will start in 2025 as well and take almost 7% of the total area. The following years, the area occupied by this zone will become smaller and be less than 5% by 2099. ECHAM predicts that the area with permafrost degradation will start in 2050 and reach 15% of the total area of the Alaskan transect, with following decrease in the area by 2075. However, by 2099 the area with permafrost degradation will occupy approximately 33 % of the total area (Figure 6.6).

THE ICE COMPLEX IN THE EAST-SIBERIAN AND ALASKAN TRANSECTS.

The Ice Complex described in Chapters 4 and 5 occupy about 30% of the East-Siberian and 10% of the Alaskan transect. Unfortunately, a very little information is available on the Ice Complex in Alaska and not enough research has been conducted on the composition and structure of the complex. Therefore in this section only the Ice

Reproduced with permission of the copyright owner. Further reproduction prohibited without permission.

Complex within the East-Siberian transect will be discussed. The Ice Complex contains massive ice wedges in the fine-grained, usually silty matrix. The so-called protection layer is 1.5 to 2.8 m deep and prevents ice from thawing (Figure 6.7). When the ALT exceeds the thickness of the protection layer and reaches icy sediments; the long term thawing will start. The process of the thawing will not be uniform in time and will most probably accelerate because of the thermokarst processes and changes in the landscape associated with the thawing of the underground ice.

The results of the described above analysis of the relative changes in MAGTs and ALTs can be applied to see if the massive destruction of the East-Siberian Ice Complex will start in the 21st century. The Ice Complex occupies the northern and north-western (to the west from 125 WL) parts of the transect and the most of the Central Yakutian Lowlands (Figures 6.1 and 6.2). Measured MAGTs in the north-western part are in the range from -7 to -10°C in the western part of the Verkhoyanks Range, up to -4 to -7°C in river valleys and in to the west from the Lena River. The relative increase of MAGTs prescribed by different GCMs within the north-western part can reach 2 to 5°C and lead to permafrost degradation from the surface and to the start of Ice Complex destruction in some limited areas.

Relative deepening of the ALT is from 0.5 m in river valleys up to 2 m in the Verkhoyansk Range. If superimposed on the measured ALT, which ranges from 0.5 to 1.2 m, by the end of 21st century the ALT will exceed the protection layer at some places. MAGTs measured at Central Yakutian Lowlands are from -7 to -2°C. The relative increase of MAGTs predicted by GCMs ranges from 2 to 5°C. The relative deepening of

Reproduced with permission of the copyright owner. Further reproduction prohibited without permission.

the ALT according to GCMs can reach almost 1 m there and will exceed the thickness of the protection layer. Therefore regions with the Ice Complex will be subject to thermokarst, land subsidence, soilfluction and other processes associated with thawing of the ice-rich sediments by the end of 21st centuries.

The environmental impact of Ice Complex destruction can be extremely severe and lead to changes in hydrology, carbon cycle, and destruction or major changes in ecosystems, which will lead to significant shift in carbon cycle and increase in green house gases emissions into the atmosphere.

ENVIRONMENTAL IMPACT CAUSED BY PERMAFROST DYNAMICS.

The vast majority of possible impacts can be subdivided into three groups: 1) feedback mechanism of permafrost –atmosphere interaction 2) ecosystem impacts, and 3) engineering impacts.

Permafrost –Atmosphere interaction

Almost 2/3 of the approximately 750 Gt of the atmospheric CO_2 is stored in the northern ecosystems, which include arctic, boreal forest, and northern bogs (Miller, 1981; Miller et al., 1983; Gorham, 1991; Oechel and Billings, 1992). About 83% of this carbon is preserved as dead organic matter within the active layer, and in the upper parts of permafrost. Northern ecosystems have been always considered as a carbon sink (Schell 1983; Schell and Ziemann 1983; Marion and Oechel 1993; Miller *et al.*, 1983; Gorham, 1991). When facing the future conditions of elevated concentration of CO_2 and climate change, most of the scientists agree that northern ecosystems could become a carbon source and constitute a positive feedback (Billings, et al., 1982; Post, 1990; Oechel et al.,

Reproduced with permission of the copyright owner. Further reproduction prohibited without permission.

2000). The mechanism behind this process is the change in thermal regime of permafrost and variation in ALT. Thermal regime of the permafrost effects the organic decomposition rates and moisture regime, and ALT controls surface hydrology, soils moisture content, aeration conditions, and the depth of soils involved into carbon cycle (Silvola, 1986; Gorham, 1991; Billings et al., 1983; Billings and Peterson, 1990). The permafrost degradation can lead to release of the carbon into atmosphere and contributing to a green house effect.

Impacts on ecosystems

Northern ecological systems depend on permafrost conditions. Permafrost controls plant communities and biomass production by temperature, moisture content, presence of unfrozen water, and surface hydrology. The change of permafrost thermal regime can affect plant diversity and biomass (Walker et al., 2003).

The thawing of the ice–rich permafrost can lead to destruction of the substrate and major changes in ecosystems. Those changes can result in replacement of the boreal forest with wetlands, and damaging wildlife habitats (Osterkamp et al., 2000; Jorgenson et al., 2001).

Permafrost degradation can have a strong impact on shoreline stability, erosion rates and sediment redistribution and the implications on coastal ecosystems, coastal communities, infrastructure and human activities such as transportation and shipping.

Impacts on the infrastructure

The impact of ALT or MAGT changes can be significant even if those changes do not lead to the permafrost degradation. Mechanical strength, compressive and shear

Reproduced with permission of the copyright owner. Further reproduction prohibited without permission.

strength of the ground are temperature and moisture dependent and controlled by the permafrost temperature regime (Osterkamp et al., 1997).

Structures built on ice reach permafrost are especially vulnerable to permafrost dynamics. Subsidence and deformation of the ground beneath the individual structures (Figure 6.8) and/or turning the ground surface into irregular thermokarst terrain can be the consequences of the changes in permafrost thermal regime (Nelson et al., 2001).

The deepening of the ALT or warming of the MAGTs within the hilly terrains can result in development of mechanical discontinuities in the substrate, leading to slides, flows and slumps (Figure 6.9).

PRIMARY CONCLUSIONS OF THIS RESEARCH

This research is the first that combined three major approaches to the present day global change studies: 1) the regional scale introduced allows for incorporating the measured data on soils, air and ground temperatures, vegetation, and complex terrain, 2) the development of interactive GIS (the GIPL model) which incorporates relatively simple and accurate model for the evaluation of the permafrost dynamics, 3) incorporation and evaluation of GCM outputs on a regional scale.

The development of the GIPL model is the most significant achievement of this research. This model is a quasi-two-dimensional, quasi-transitional, spatially distributed, physically based analytical model for the calculation of maximum active layer thickness and mean annual ground temperature. Calibration of the model has shown a less than 33% relative error for mean annual ground temperatures and maximum active layer thickness calculations. A spatial statistical analysis of the data from 32 sites in Siberia

Reproduced with permission of the copyright owner. Further reproduction prohibited without permission.

indicated a confidence level of 75% to have a temperature interval of 0.2 -0.4°C. A detailed analysis has been performed for two regional transects in Alaska and Eastern Siberia which has validated the use of the model.

The hindcast in 20th century and forecast for the 21st century of permafrost dynamics for the East-Siberian and Alaskan transects have been performed, using the GIPL model, and climatic parameters from HADCM2 model for the hindcast, and climatic outputs from HADCM2 along with five ACIA – designated GCMs for the forecast.

The analysis of the permafrost dynamics in the 20th century showed that, under the influence of natural variability of mean annual air temperatures in the HADCM2 simulation, significant changes occurred in the MALT (ranging from less than 0.5 m up to 1 m) and in the mean annual ground temperatures (± 3-4°C) of the East-Siberian and Alaskan transects.

In the 21st century the ALT will deepen by 0.5 – 2 m everywhere within the East-Siberian transect, and that mean annual ground temperatures will rise by 2-6°C according to all GCMs except CSM. However, the increase in MAGTs and the ALT will not be uniform in time. There will be relatively cold and warm periods caused by natural variations of air temperatures. These variations will be superimposed on the background warming trend. In the Alaskan transect, the relative increase in mean annual ground temperatures will be from 2 to 6 °C by the end of 21st century. This increase will cause the deepening of the ALT up to 0.5 m.

Reproduced with permission of the copyright owner. Further reproduction prohibited without permission.

The forecast showed that the permafrost degradation from the surface will start as yearly as 2025 and will progress to 2099 according to the CCC, GFDL, HADCM2, HADCM3, and ECHAM models in the Alaskan transect. The dynamics of the area with permafrost degradation will not be uniform. There will be cold and warm time periods on the background of the trend of the mean annual air temperatures warming. HADCM2 and GFDL predict that the area with the permafrost degradation will be in the south-eastern part of the transect. The area will be within the Brooks Range and the Interior according to CCC, ECHAM, and HADCM3. In the East-Siberian transect the permafrost degradation from the surface will start in the southwestern part of the transect according to CCC, HADCM3, HADCM2 and ECHAM. The starting point in time and the character of dynamics of this zone vary among the models.

In conclusion, the finding presented in this thesis shows that the spatial and temporal dynamics of the permafrost is an extremely complex process. Three environmental factors including climate, soils, and vegetation have a most significant influence on the permafrost characteristics. The comparison of the East-Siberian and Alaskan transects revealed differences and similarities in the permafrost dynamics in the past and in the future. Even though, we can not extrapolate permafrost data between them at present time, in the future, if additional transect between them will be analyzed, this extrapolation will become possible.

We hope that this research will continue and a number of other longitudinal transect will be considered and as a result the dynamics of permafrost over the entire circumpolar region will be reconstructed and forecasted.

Reproduced with permission of the copyright owner. Further reproduction prohibited without permission.

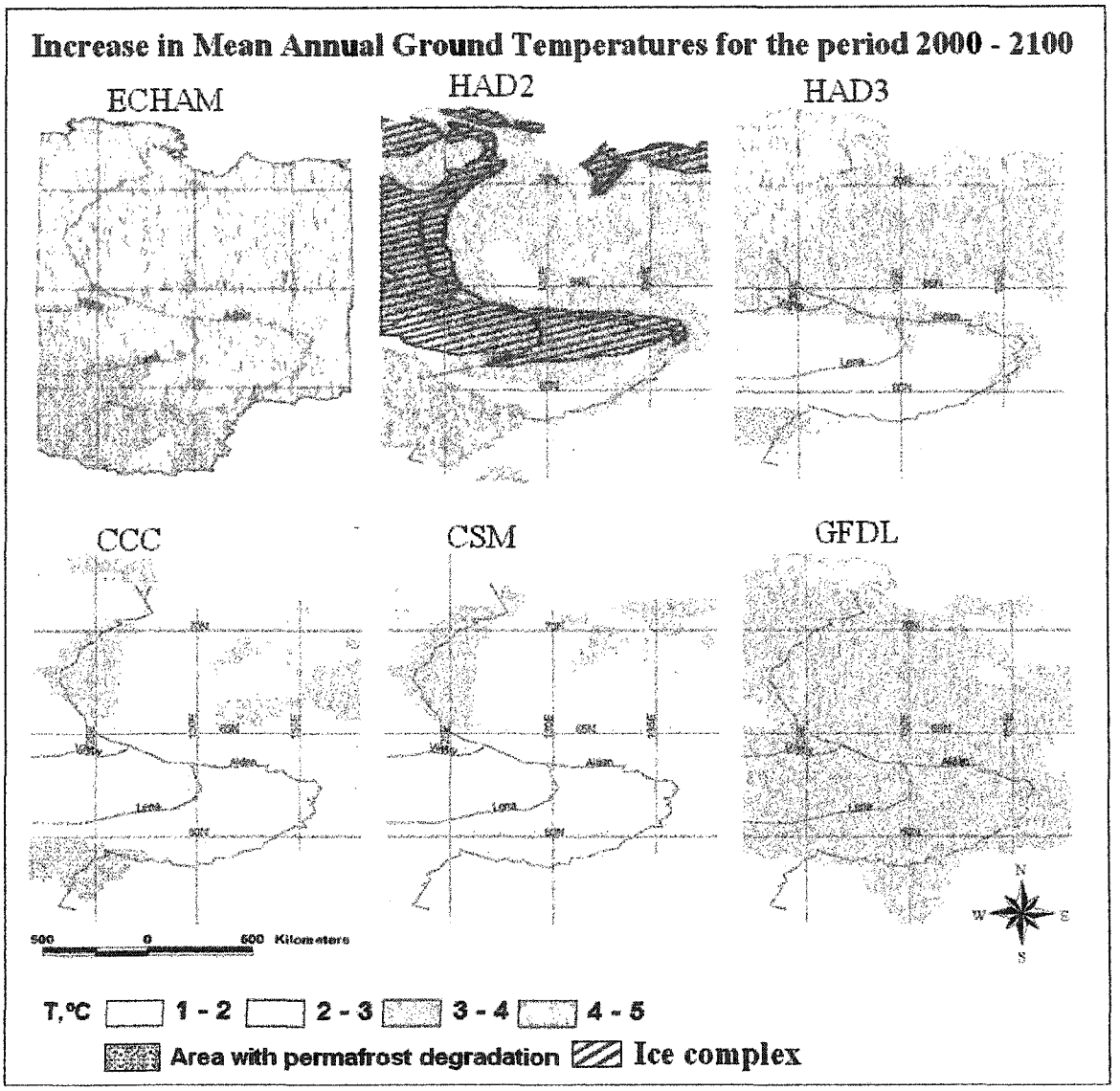

Figure 6.1: The relative increase in MAGTs for the East-Siberian transect according to six GCMs

Reproduced with permission of the copyright owner. Further reproduction prohibited without permission.

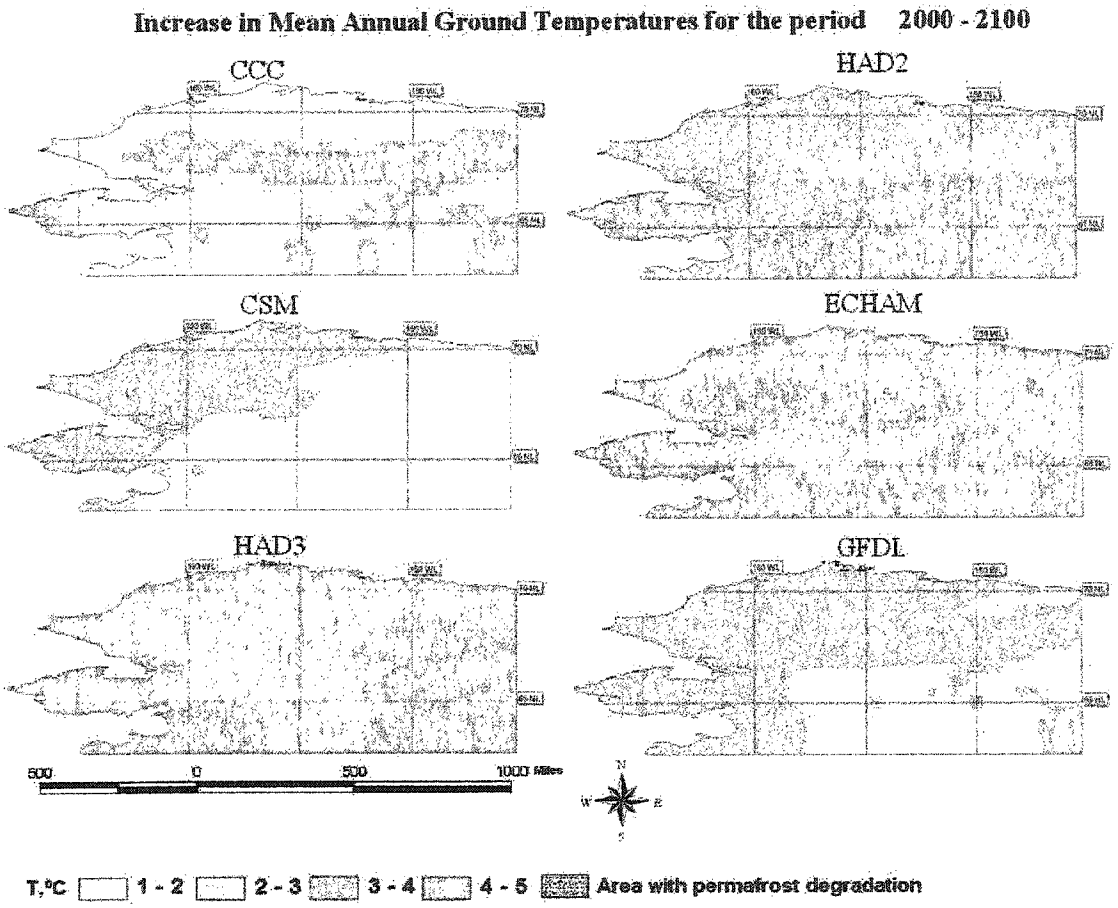

Figure 6.2: The relative increase in MAGTs for the Alaskan transect according to six GCMs.

Reproduced with permission of the copyright owner. Further reproduction prohibited without permission.

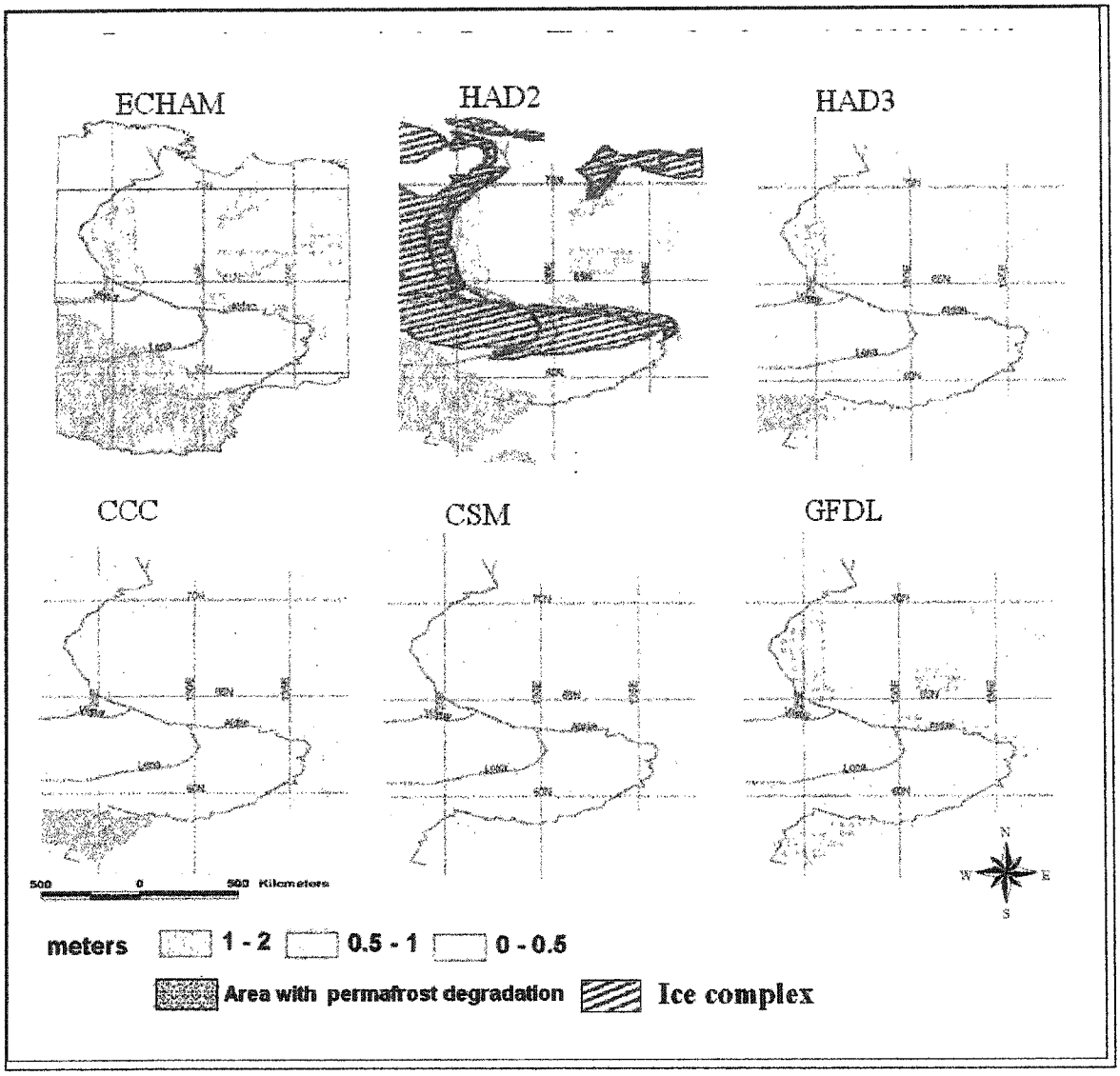

Figure 6.3: The relative increase in ALTs for the East-Siberian transect according to six GCMs

Reproduced with permission of the copyright owner. Further reproduction prohibited without permission.

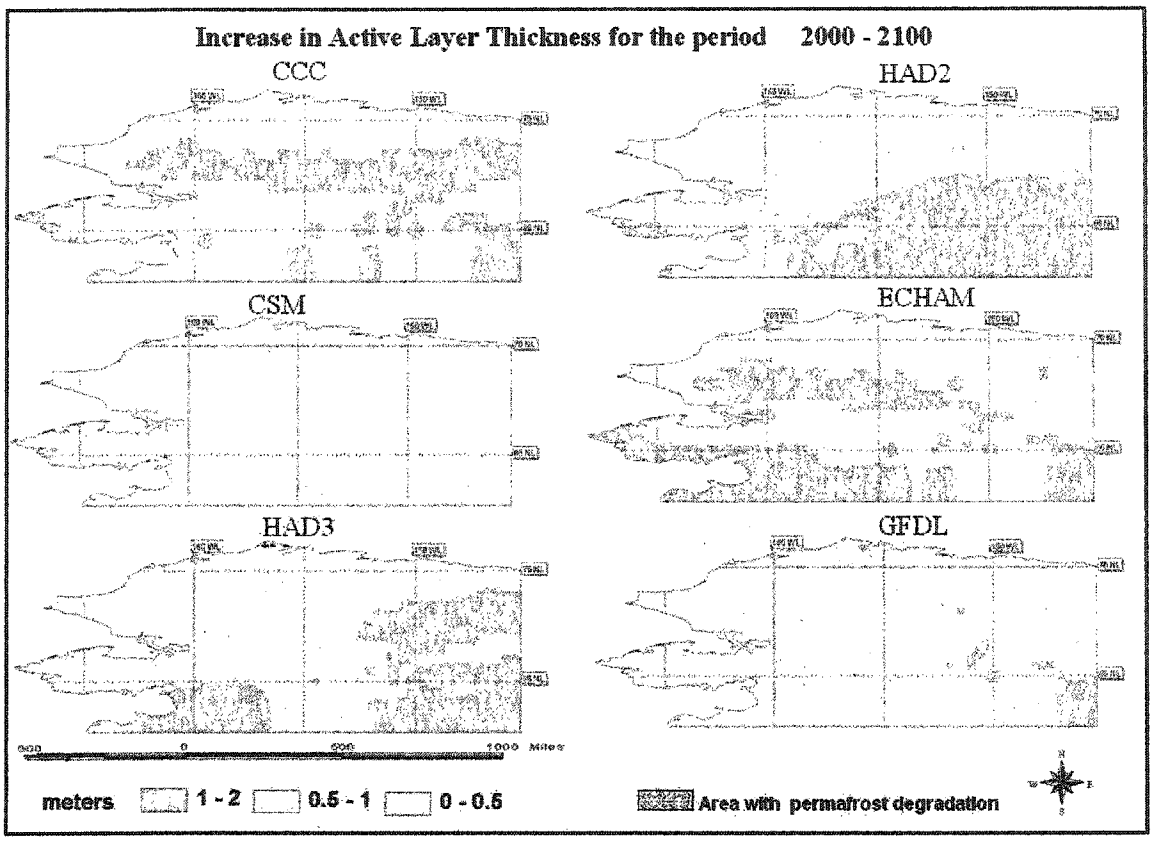

Figure 6.4: The relative increase in ALTs for the Alaskan transect according to six GCMs

Reproduced with permission of the copyright owner. Further reproduction prohibited without permission.

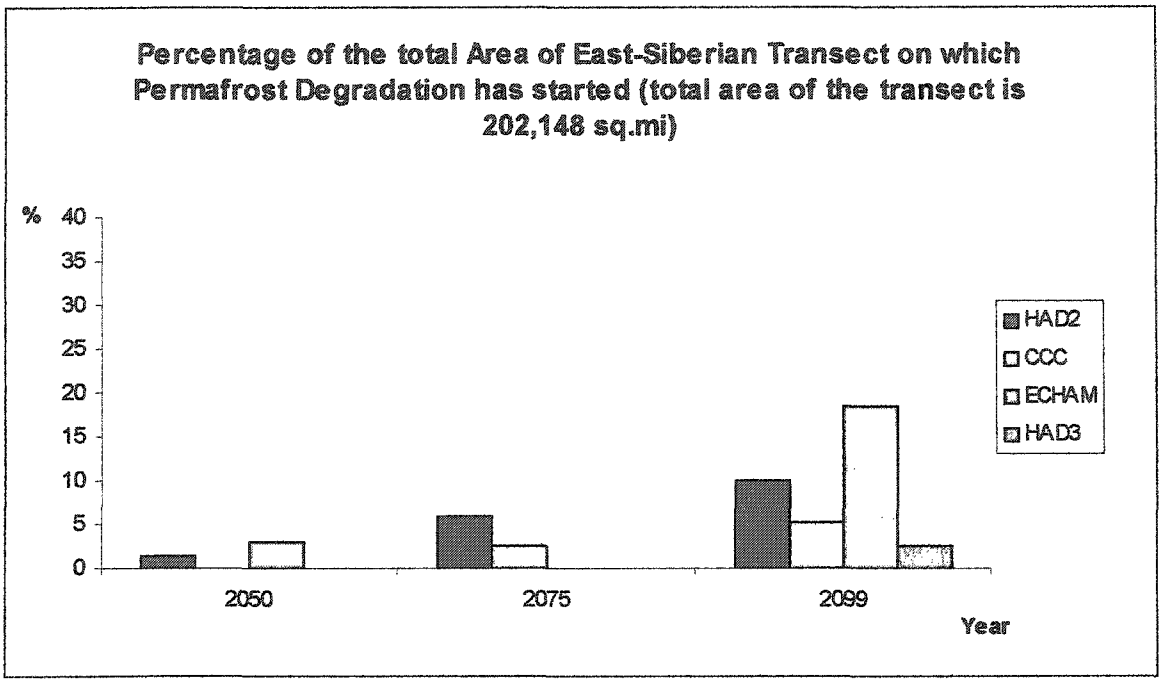

Figure 6.5: Percentage of the total area of the East-Siberian transect where permafrost degradation has started.

Reproduced with permission of the copyright owner. Further reproduction prohibited without permission.

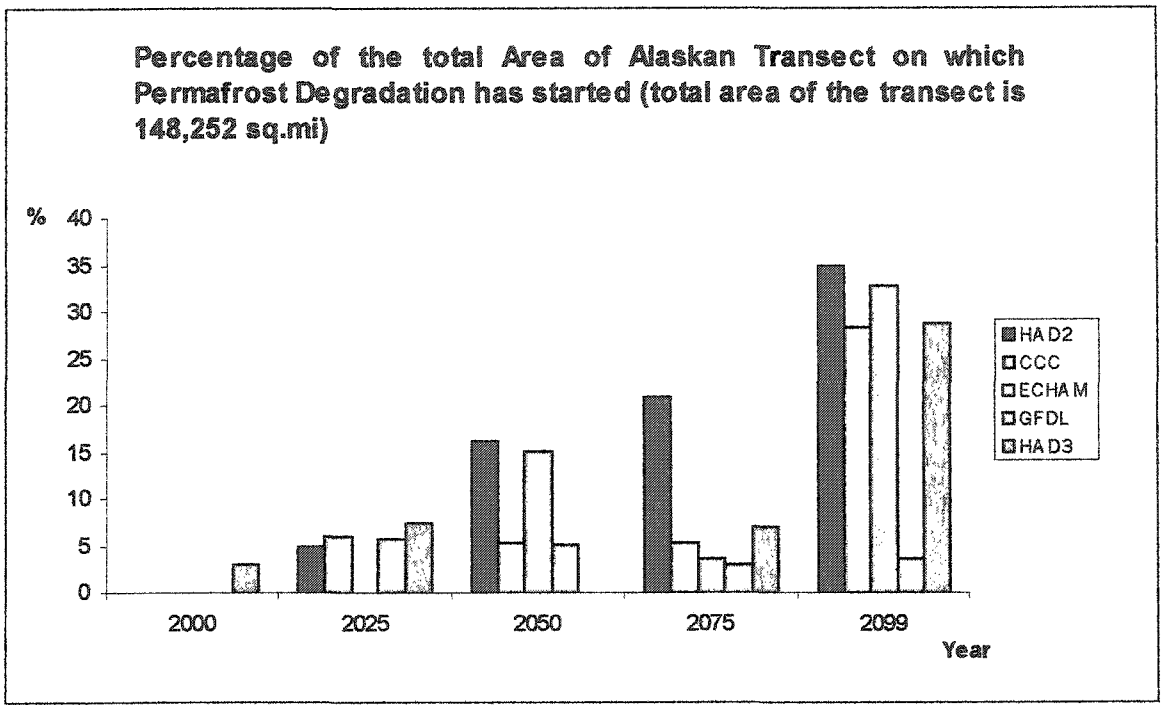

Figure 6.6: Percentage of the total area of the Alaskan transect where permafrost degradation has started.

Reproduced with permission of the copyright owner. Further reproduction prohibited without permission.

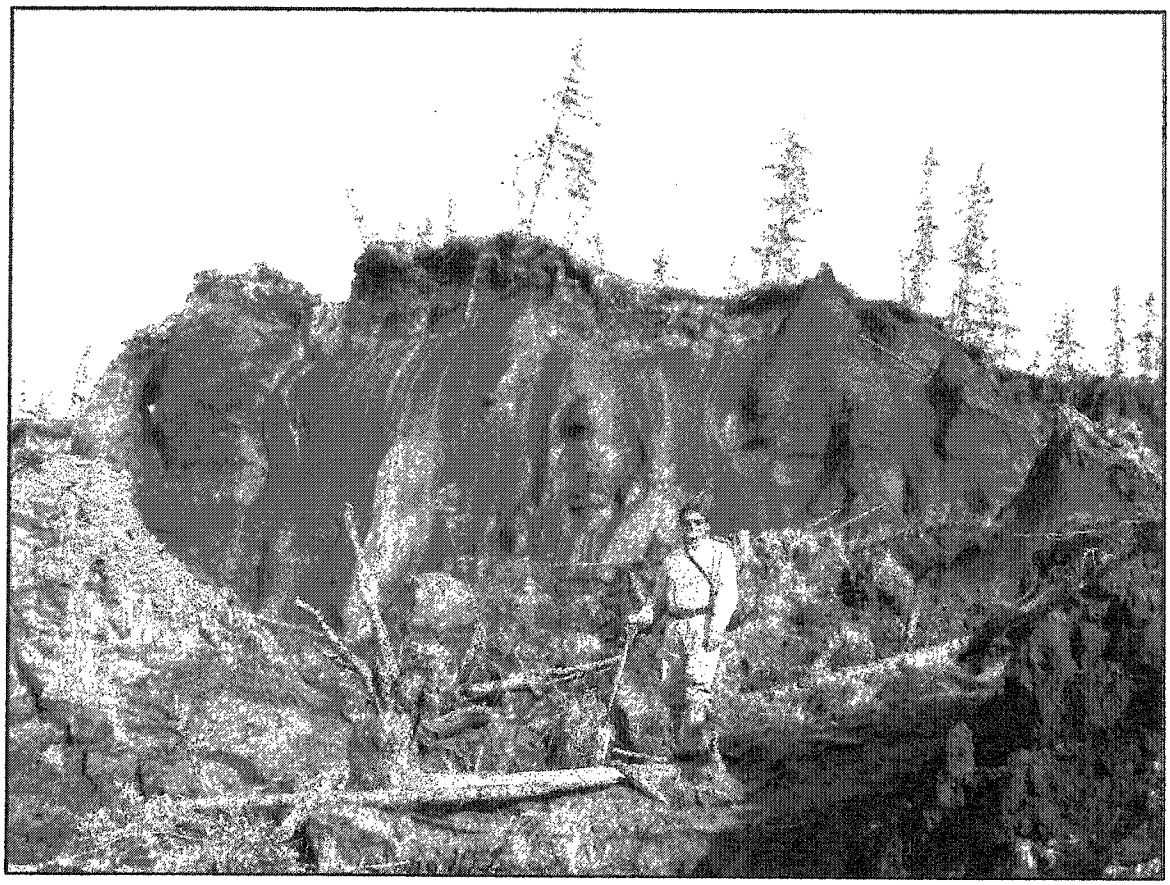

Figure 6.7: The Ice Complex in Duvanyi Yar, Eastern Siberia. (Photo taken by S. Davidov)

Reproduced with permission of the copyright owner. Further reproduction prohibited without permission.

Figure 6.8: The destruction of the four stores building in Cherskyi, Eastern Siberia, as a result of thermokarst processes beneath the building. (Photo was taken by V.Romanovsky)

Reproduced with permission of the copyright owner. Further reproduction prohibited without permission.

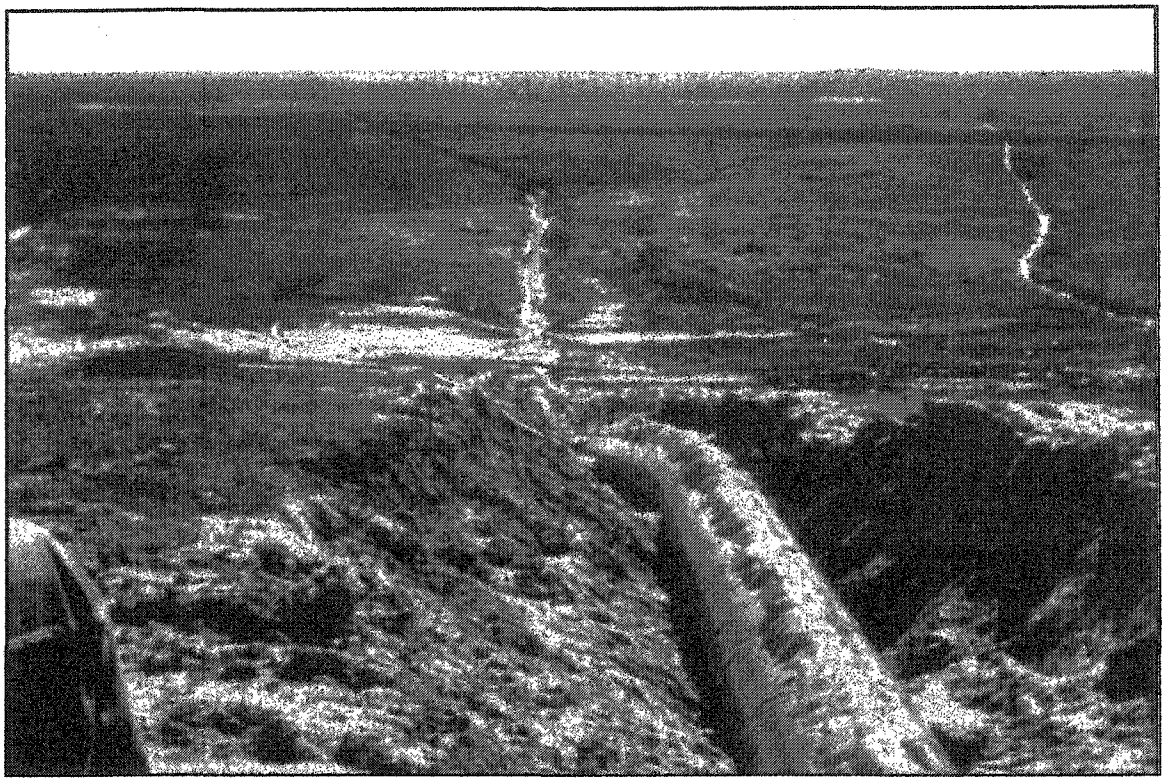

Figure 6.9: The damage of the pipeline in Western Siberia caused by heat flow from the pipeline and permafrost thawing. (Photo taken by S.Yu. Parmuzin).

Reproduced with permission of the copyright owner. Further reproduction prohibited without permission.

References Cited

Anisimov, O.A. and Nelson, F.E. (1997). *Influence of climate change on continental permafrost in the northern hemisphere.* Meteorologiya i Gidrologiya 1997/5: pp.71-80 (In Russian; English translation appears in *Russian Meteorology and Hydrology* 1997/5).

Anisimov, O.A. and Nelson, F.E. (1996). *Permafrost distribution in the Northern Hemisphere under scenarios of climatic change.* Global and Planetary Change 14(1): pp. 59-72.

Anisimov, O.A., N.I. Shiklomanov and F.E. Nelson, (1997): *Effects of global warming on permafrost and active-layer thickness: results from transient general circulation models*. Global Planetary Change, 61, pp. 61-77.

Anisimov, O., B. Fitzharris, J. O. Hagen, R. Jeffries, H. Marchant, F. E. Nelson, T. Prowse, and D. G. Vaughan, (2001): *Polar Regions (Arctic and Antarctic)*, in: Climate Change: Impacts, Adaptation, and Vulnerability, the Contribution of Working Group II of the Intergovernmental Panel on Climate Change, Third Assessment Review, Cambridge: Cambridge University Press, pp.801-841.

Balobaev V.T. ed. (1996), *Climate influence on permafrost in Central Yakutia.* (in Russian), Yakutsk.

Benson, C. S. & Sturm, M. (1993), *Structure and wind transport of seasonal snow on the Arctic slope of Alaska*, Annals of Glaciology, 18, pp. 261-267.

Beringer, J., A.H. Lynch, F.S. Chapin, III, M. Mack, and G.B. Bonan. (2001). *The representation of arctic soils in the Land Surface Model (LSM)*: The importance of mosses. Journal of Climate 14: pp. 3324-3335.

Reproduced with permission of the copyright owner. Further reproduction prohibited without permission.

Bilello, M.A., (1974), *Air masses, fronts, and winter precipitation in central Alaska*: U.S. Army Cold Regions Research and Engineering Laboratory Special Report 319, 58 pp.

Billings WD, Peterson KM (1990). *Some possible effects of climatic warming on arctic tundra ecosystems of the Alaskan North Slope.* In: Consequences of the greenhouse effect for biological diversity (eds Peters RL, Lovejoy T). Yale University Press, New Haven, Connecticut, USA, pp. 200 – 204.

Billings WD, Luken JO, Mortensen DA, Peterson KM (1982). *Arctic tundra: a source or sink for atmospheric carbon dioxide in a changing environment?* Oecologia (Berlin), 53, pp. 7-11.

Billings WD, Luken JO, Mortensen DA, Peterson KM (1983) *Increasing atmospheric carbon dioxide: possible effects on arctic tundra.* Oecologia (Berlin), 58, pp. 286-289.

Black, R.F., and Barksdale, W.L., (1949), *Oriented lakes of northern Alaska*: Journal of Geology, v. 57, no. 2, pp. 105-118.

Bonan, G. B., D. Pollard, and S. L. Thompson, (1993). *Influence of subgrid-scale heterogeneity in leaf area index, stomatal resistance, and soil moisture on grid-scale land-atmosphere interactions*, Journal of Climate, 6, pp.1882.

Boville, B.A.; Kiehl, J.T.; Rasch, P.J.; Bryan, F.O.,(2001): *Improvements to the NCAR CSM-1 for Transient Climate Simulations*, Journal of Climate, vol. 14, no. 2, pp.164-179.

Brown, J. and Kreig, R.A. (1983) *Guidebook to permafrost and related features along the Elliot and Dalton highways, Fox to Prudhoe Bay, Alaska.* Proceedings of Fourth International Conference on Permafrost. 18 - 22 July 1983, University of Alaska, Fairbanks, Alaska Division of Geological and Geophysical Surveys, 230 pp.

Reproduced with permission of the copyright owner. Further reproduction prohibited without permission.

Brown R. J. E. and Pewe T. L., (1973). *Distribution of permafrost in North America and its relationship to the environment: a review.* 1963-1973. Permafrost Second International Conference, Washington, D.C., pp. 71-100.

Burn, C. R., and Smith, C. A. S. (1988). *Observations of the 'Thermal Offset' in Near-Surface MAGTs at Several Sites near Mayo, Yukon Territory, Canada.* Arctic 41 (2) (June): pp.99-104.

Chang, A.T.C., Foster, J.L., Hall, D.K., Powell, H.W., and Chien, Y.L. (1990). *Nimbus-7 SMMR Derived Global Snow Cover and Snow Depth Data Set Documentation, Product Description, and User's Guide*, Unpublished Manuscript.

Chang, A.T.C., Foster, J.L., and Hall, D.K. 1987. *Nimbus-7 SMMR derived global snow cover parameters.* Annals of Glaciology. 9, pp. 39-44.

Circum-Arctic Map of Permafrost and Ground Ice Conditions. (1997).*Published by the USGS.*

Climate of Yakutsk (1982). (in Russian). Saint-Petersburg, Gydrometeoizdat, 248 pp.

Danilova N.S. (1989). *Major features of natural conditions in Middle Siberia during permafrost formation*, (in Russian) in-Geocrylogy of USSR, Moscow "Nedra, pp. 230 – 240.

Dobrovol'skii, G. V., Urusevskaya, I. S. and Rozov, N. N., (1984). *The map of soil-geographical regionalization of Russia.* Moscow: GUGK.

Dunaeva E.N., Kondratieva K.A.(1989), *Seasonal freezing and thawing of soils*, in-Middle Siberia, Geocrylogy of USSR (in Russian), Moscow "Nedra", pp.68-71

Reproduced with permission of the copyright owner. Further reproduction prohibited without permission.

Eisched, J. K., Baker, C. B., Karl, T. R. and H. F. Diaz, 1995. *The quality control of long-term climatological data using objective data analysis*, Journal of Applied Meteorology 34, pp. 2787-2795.

Elovskaya, L. G., Petrova, E. I. and Teterina, L. V. (1978). *Soil map of Yakutia 1;5,000,000 scales*. Yakutsk.

Fedorov, A. N., 1996. *Effects of Recent Climate Change on Permafrost Landscapes in Central Sakha*, Polar Geography. 20, pp. 99-106.

Feldman G.M., Tetelbaum A.S., Shender N.I., Gavriliev R.I. (1988) *The guidebook for temperature regime forecast in Yakutia* (in Russian), Yakutsk, 240 pp.

Flato, G., Boer, G. J., Lee, W. G., McFarlane, N. A., Ramsden, D., Reader, M. C., and Weaver, A. J. (2000). *The Canadian Centre for Climate Modelling and Analysis global coupled model and its climate.* Climate Dynamics, 16, pp. 451-468.

Friend, A. D., A. K. Stevens, R. G. Knox and M. G. R. Cannell,(1997) *A process-based, terrestrial biosphere model of ecosystem dynamics (Hybrid v3.0)*, Ecological Modeling, 95, pp. 249-287.

Gavriliev R.I. (1998) *Thermophysical properties of soils and soils' covers within cryolithozone*, (in Russian), Novosibirsk., 220 pp.

Gavrilova M.K. (1978) *Climate and long-term freezing of soils*. (in Russian). Novosibirsk, Nauka, 214 pp.

Gavrilova M.K. (1981) *Contemporary climate and permafrost on the continents*, (in Russian). Novosibirsk, Nauka. 112 pp.

Reproduced with permission of the copyright owner. Further reproduction prohibited without permission.

Goodrich, L.E. (1978). *Some results of numerical study of ground thermal regime.* Proceedings of the Third International Conference on Permafrost. National Research Council of Canada, Ottawa, vol.1, pp. 29-34.

Gordon, C., C. Cooper, C.A. Senior, H.T. Banks, J.M. Gregory, T.C. Johns, J.F.B. Mitchell, and R.A. Wood, (2000): *The simulation of SST, sea ice extents and ocean heat transports in a version of the Hadley Centre copled model without flux adjustments.* Climate Dynamics, 16, pp. 147-168.

Gorham E, (1991) *Northern peatlands: role in the carbon cycle and probable responses to climatic warming.* Ecological Applications, 1:(2), pp. 182-195.

Gullen M.J.P. (1993) *The Unified forecast/climate model.* The Meteorological Magazine Vol. 122, pp.81- 95

Hamilton, T. D., (1965). *Alaskan temperature fluctuations and trends: Analysis of recorded data*, Arctic, 18(2), pp. 105-117.

Hansen, J. and Lebedev, S., (1987). *Global trends of measured surface air temperatures*, Journal of Geophysical Research, 92(D11), pp.13,345-13,372.

Haugen, R.K. (1982) *Climate of Remote Areas in North-Central Alaska*, 1975-1979, Summary. CRREL Report 82-35.

Haugen, R.K. and Brown, J. (1980). *Coastal-inland distribution of summer air temperatures and precipitation in northern Alaska.* Arctic and Alpine Research, 12(4), pp. 403-412.

Hinzman, L.D., D.J. Goering, S. Li and T.C. Kinney. 1997. *Numeric Simulation of Thermokarst Formation During Disturbance.* Crawford, R. M. M. Ed., Disturbance and

Reproduced with permission of the copyright owner. Further reproduction prohibited without permission.

recovery in Arctic lands: an ecological perspective Kluwer Academic Publishers, Dordrecht, the Netherlands,V. 25, pp. 191 – 211.

Hopkins, D.M., and Sigafoos, R.S., (1951), *Frost action and vegetation patterns on Seward Peninsula, Alaska*: U.S. Geological Survey Bulletin 974-C, 101 pp.

Houghton, J. T., Filho, L. G. M., Callander, B. A., Harris, N., Kattenberg, A., and Maskell, K., (1996). *Climate Change 1995 - the Science of Climate Change: Contribution of WGI to the Second Assessment Report of the Intergovernmental Panel on Climate Change*, Intergovernmental Panel on Climate Change, Cambridge University Press,Cambridge (UK). 100 pp.

Hrutskyi C.F., Derevyagin A.U. (1981), *Cryolitological characteristics of upper part of Anabarskyi-Olenekskyi plate cryolithozone.*-in Problems of cryolithology (in Russian). No.IX, Moscow, pp.139-141

IGBP (1996), *Northern Eurasia Study: Prospectus for an integrated Global Change Research Project.* Report No. 37., Stockholm, 95 pp.

IPCC (2000) Special Report on Emission Scenarios: A Special Report of Working Group III of the Intergovernmental Panel on Climate Change (Nakicenovic N. J., Alcamo J., Davis G., and 25 co-authors, Eds.), Cambridge University Press, Cambridge, U.K.

Ivanov M.S. (1984), *Cryogenic structure of Quaternary deposits in Leno-Aldanskaya depression.*(in Russian). Novosibirsk, "Nauka".

Johns T.C., Carnell R.E., Crossley J.F., Gregory J.M., Mitchell J.F.B., Senior C.A., Tett S.F.B. and Wood R.A. (1997) The Second Hadley Centre coupled ocean-atmosphere GCM: Model description, spinup and validation. Climate Dynamics 13, pp.103-134

Reproduced with permission of the copyright owner. Further reproduction prohibited without permission.

Jones, P. D., (1994). *Hemispheric surface air temperature variations: a reanalysis and an update to 1993,* Journal of Climate 7, 1794-1802.

Jorgenson, M. T., C. H. Racine, J. C. Walters, and T. E. Osterkamp, (2001). *Permafrost degradation and ecological changes associated with a warming climate in central Alaska.* Climatic Change, 48(4), pp. 551-571.

Kane, D.L., L.D. Hinzman and J.P. Zarling. (1991). *Thermal Response of the Active Layer in a Permafrost Environment to Climatic Warming.* Cold Regions Science and Technology, 19(2): pp.111-122.

Kaplina T.N. (1981). *The Late Cenozoic history of permafrost in northern Yakutia.* In book: The history of permafrost dynamics in Eurasia, (in Russian). Moscow, Nauka, pp.153-181

Karpov E.G. (1984) *Genesis of thick ice complex in Enisei lowlands.-in Geology and Geophysics,*(in Russian) , No.1, pp.118-123

Karpov E.G. (1978) *Morphology and temperature of contemporary permafrost on shoreline and shallow parts of Eniseisko-Pyasinskyi northern rivers*-in Geocryological and hydrogeological research in Yakutia (in Russian), Yakutsk, pp.105-114

Kattenberg, A., F. Giorgi, H. Grassl, G.A. Mechl, J.F.B. Mitchell, R.J. Stouffer, T. Tokioka, A.J. Weaver, and T.M.L. Wigley, (1996) *Climate Models-Projections of Future Climate. In:* Houghton, J.T., L.G. Meira Filho, B.A. Callander, N. Harris, A. Kattenberg, and K. Maskell (eds.), Climate Change 1995, The Science of Climate Change, Contribution of Working Group I to the Second Assessment of the Intergovernmental

Reproduced with permission of the copyright owner. Further reproduction prohibited without permission.

Panel on Climate Change (Ch. 6), Cambridge University Press, Cambridge, U.K., pp. 289-357.

Klimatologicheskii spravochnik SSSR, (1963) vypusk 24,*po Yakutskoi ASSR, severnoi chasti Khabarovskogo kraya,Magadanskoi oblasti i severnoi chasti Kamchatskoi oblasti.Meteorologicheskie dannye za otdel'nye gody, chast' VII,Temperatura pochvy, tumany, grozy, meteli i grad.*Gidrometeoizdat, Leningrad,(In Russian).

Knutson, T. R., Delworth, T. L., Dixon, K. W., and Stouffer, R. J. (1999). *Model assessment of regional surface temperature trends (1949-1997).* Journal of Geophysical Research, 104, pp. 30981-30996.

Kondratieva, K.A., (1998). *Alaska.* In: Fundamentals of Geocryology, V.3, Regional and historical geocryology of the world, pp. 442 - 467

Krasnii, L. I. ed. (1978).*Geological map of Yakutia 1:1,500,000 scale.* Moscow: GUGK.

Kudryavtsev, V. A., Garagula, L. S., Kondrat'yeva, K. A. and Melamed V. G. (1974). *Osnovy merzlotnogo prognoza* (in Russian). MGU (431 pp.) [CRREL Translation: V. A. Kudryavtsev et al., *Fundamentals of Frost Forecasting in Geological Engineering Investigations*, CRREL Draft Translation 606, 1977, 489 pp.]

Lachenbruch, A. H. (1959). *Periodic heat flow in a stratified medium with application to permafrost problems*, US Geological Survey Bulletin, 1083-A, 36 pp.

Lachenbruch A. H., Sass J.H., Marshall B.V., Moses T.H. Jr. (1982) *Permafrost, heat flow and the geothermal regime at Prudhoe Bay, Alaska.* Journal of Geophysical Research. 87. B11. pp. 9301 – 9316.

Reproduced with permission of the copyright owner. Further reproduction prohibited without permission.

Lachenbruch, A.H., J.H. Sass, L.A. Lawver, and M.C. Brewer (1987): *Temperature and depth of permafrost on the Alaskan arctic slope*, in Tailleur, I. and P. Weimer, eds., Alaskan North Slope Geology, Bakersfield, Calif., Society of Economic Paleontologists and Mineralogists, Pacific Section, vol. 2, pp. 545-558.

Lachenbruch, A.H., J.H. Sass, L.A. Lawver, M.C. Brewer, G.V. Marshall, R.J. Munroe, J.P. Kennelly, Jr., S.P. Galanis, Jr., and T.H. Moses, Jr. (1982): *Temperature and depth of permafrost on the arctic slope of Alaska*, in Gryc, G., ed., Geology and Exploration of the National Petroleum Reserve in Alaska, 1974-1982, U.S. Geological Survey Professional Paper 1399, pp. 645-656.

Lyons, W.B. / Howard-Williams, C. / Hawes, I. (eds): (1997) *Ecosystems processes in Antarctic ice-free landscapes* - Proceedings of an international workshop on polar desert ecosystems, Christchurch, 1-4 July 1997, 294 pp.

Marion GM, Oechel WC, (1993) *Mid- to late-Holocene carbon balance in arctic Alaska and its implications for future global warming.* The Holocene 3, 3, pp. 193-200.

Maxwell, B. (1992). Arctic climate: potential for change under global warming. In: Chapin FS III, Jeffries RL, Reynolds JF, Shaver GR, Svoboda J (eds) *Arctic Ecosystems in a Changing Climate*. Academic Press, San Diego, pp. 11-34.

McFadden, J.P., Liston, G.E., Sturm, M., Pielke, R.A., Chapin, F.S. III, (2001). *Interactions of shrubs and snow in arctic tundra: measurements and models* . Proceedings of a symposium held during the Sixth IAHS Scientific Assembly at Maastricht, The Netherlands, July 2001, IAHS Publications, no. 270, pp. 317 – 325.

Reproduced with permission of the copyright owner. Further reproduction prohibited without permission.

McGuire, A.D., M. Apps, J. Beringer, J. Clein, H. Epstein, D.W. Kicklighter, C. Wirth, J. Bhatti, F.S. Chapin III, B. de Groot, D. Efremov, W. Eugster, M. Fukuda, T. Gower, L. Hinzman, B. Huntley, G.J. Jia, E. Kasischke, J. Melillo, V. Romanovsky, A. Shvidenko, E. Vaganov, and D. Walker (2002). *Environmental variation, vegetation distribution, carbon dynamics, and water/energy exchange in high latitudes*, Journal of Vegetation Science, Vol. 13: pp. 301-314.

Michaelson, G.J., C.L. Ping, and J.M. Kimble, (1996). *Carbon storage and distribution in tundra soils of Arctic Alaska, U.S.A.*, Arctic and Alpine Research, Vol. 24, No. 4, pp. 414-424.

Miller PC, Ed., (1981) in: *Carbon Balance in Northern Ecosystems and the Potential Effect of Carbon Dioxide Induced Climate Change* (CONF-800033118), Report of a Workshop, San Diego, California, 7-9 March, 1980. Carbon Dioxide Effects Research and Assessment Program, U.S. Department of Energy, Washington, D.C. (NTIS, Springfield, Virginia).

Miller PC, Kendall R, Oechel WC (1983) *Simulating carbon accumulation in northern ecosystems*. Simulation, 40, pp.119-131.

Mitchell J.F.B., Johns T.C., Gregory J.M. and Tett S. (1995) *Climate response to increasing levels of greenhouse gases and sulphate aerosols.* Nature, V. 376, pp.501-504

Nelson, F.E. and S.I.Outcalt (1987) A frost index number for spatial prediction of ground frost zones. *Arctic and Alpine*, 19: 279-288.

Reproduced with permission of the copyright owner. Further reproduction prohibited without permission.

Nelson, F.E., Anisimov, O.A., and Shiklomanov, N. I., (2001). *Subsidence risk from thawing permafrost.* Nature, V.410, pp. 889 – 890.

Nelson, F. E., Lachenbruch, A. H., Woo, M. K., Koster, E. A., Osterkamp, T. E., Gavrilova, M. K. and Chang, G. O., 1993. Permafrost and changing climate. In *Proceedings of the Sixth International Conference on Permafrost*, Beijing, China, vol. 2, pp. 987-1005.

Nicholls, N., Gruza, G. V., Jouzel, J., Karl, T. R., Ogallo, L. A. and D. E. Parker,(1996) *Observed climate variability and change*, in Houghton, J. T., Meira Filho, L. G., Callander, B. A., Harris, N., Kattenberg, A., and Maskell, K. (eds.), Climate Change 1995, The Science of Climate Change, Contribution of Working Group I to the Second Assessment of the Intergovernmental Panel on Climate Change (Ch. 6), Cambridge University Press, Cambridge, U.K., pp. 133-192.

Oechel WC, Billings WD (1992). *Effects of global change on the Carbon Balance of Arctic Plants and Ecosystems.* In: Arctic Physiological Processes in a Changing Climate, (eds. Chapin T, Jeffries R, Reynolds J, Shaver G, Syoboda J), Academic Press.

Oechel, W.C., Vourlitis, G.L., Hastings, S.J., Zulueta, R.C., Hinzman, L. and Kane, D. (2000). *Acclimation of ecosystem CO2 exchange in the Alaskan Arctic in response to decadal climate warming.* Nature 406: pp. 978-981.

Osterkamp, T. E., (1985) *Temperature measurements in permafrost*, Rept. No. FHWA-AK-RD-85-11, Alaska DOTPF, Fairbanks, AK, 87 pp.

Osterkamp, T. E., and W. D. Harrison, (1982). *Temperature measurements in subsea permafrost off the coast of Alaska*, the Roger J. E. Brown Memorial Volume,

Reproduced with permission of the copyright owner. Further reproduction prohibited without permission.

Proceedings of the Fourth Canadian Permafrost Conference, Calgary, Alberta, March 2-6, 1981, H. M. French (ed.), NRC, Ottawa, Canada.

Osterkamp, T. E., and Lachenbruch, A. H., (1990). *Thermal regime of permafrost in Alaska and predicted global warming*, Journal of Cold Regions Engineering., 4(1), pp. 38042.

Osterkamp, T.E. and M.W. Payne, (1981).*Estimates of permafrost thickness from well logs in northern Alaska*, Cold Regions Science and Technology, 5, pp. 13-27.

Osterkamp, T. E., and V. E. Romanovsky,(1999) *Evidence for warming and thawing of discontinuous permafrost in Alaska,* Permafrost and Periglacial Processes, 10(1), pp. 17-37.

Osterkamp, T.E., and V.E. Romanovsky, (1997) *Freezing of the active layer on the Coastal Plain of the Alaskan Arctic*, Permafrost and Periglacial Processes, 8(1), pp. 23-44.

Osterkamp, T. E. and Romanovsky, V. E., (1996). *Characteristics of Changing Permafrost Temperatures in the Alaskan Arctic*, U.S.A. Arctic and Alpine Research, Vol. 28, N3, pp. 267-273

Osterkamp, T. E., D. C. Esch, and V. E. Romanovsky, (1997), *Infrastructure: Effects of climatic warming on planning, construction and maintenance,* in: Implications of Global Change in Alaska and the Bering Sea Region, Proceedings of the BESIS Workshop, June, pp. 115-127.

Reproduced with permission of the copyright owner. Further reproduction prohibited without permission.

Osterkamp, T. E., L. Viereck, Y. Shur, M. T. Jorgenson, C. Racine, A. Doyle, and R. D. Boone, (2000). *Observations of thermokarst and its impact on boreal forests in Alaska*, U.S.A.. Arctic, Antarctic, and Alpine Research, 32(3), pp. 303-315.

Osterkamp, T.E., T. Zhang, and V.E. Romanovsky, (1994). *Evidence for a cyclic variation of permafrost temperatures in northern Alaska*, Permafrost and Periglacial Processes, 5, pp. 137-144.

Pavlov, A. V., (1994). *Current changes of climate and permafrost in the Arctic and Sub-Arctic of Russia.* Permafrost and Periglacial Processes, N5: pp.101-110

Pavlov, A. V., *Heat transfer in landscape complexes of northern Russia* (in Russian with English abstract), Earth Cryosphere, vol. VI, 4, 22-31, 2000.

Pewe T. L., (1983) *Alpine permafrost in contiguous United States: a Review*. Arctic and Alpine research. Vol. 15. N2, pp 145-156.

Pewe T.L., (1982) *Special report 15, Geological hazards of the Fairbanks area, Alaska.* First Edition, Department of Natural Resources. Division of Geological and Geophysical surveys, Fairbanks, Alaska. 200 pp.

Pewe T.L. and Reger R.D. (1983), *Guidebook to permafrost and quaternary geology along the Richardson and Glenn highways between Fairbanks and Anchorage, Alaska.* Fourth International Conference on Permafrost, July l&22, 225 pp.

Polyakov I., Alasofu S., Bhatt U., Colony R., Ikeda M., Makshtas A., Swingley C., Walsh D and Walsh J. (2002) *Trends and variations in Arctic climate system*. EOS (Trans. Amer. Geophys. Union), 83(47), 547-548.

Reproduced with permission of the copyright owner. Further reproduction prohibited without permission.

Post WM (ed. 1990) *Report of a workshop on climate feedbacks and the role of peatlands, tundra, and boreal ecosystems in the global carbon cycle.* ORNL/TM-11457, Oak Ridge National Laboratory, Oak Ridge, TN, pp. 32.

Potter, C., S. Wang, N. T. Nikolov, A. D. McGuire, J. Liu, A. W. King, J. S. Kimball, R. F. Grant, S. E. Frolking, J. S. Clein, J. M. Chen, and J. S. Amthor. (2001). *Comparison of boreal ecosystem model sensitivity to variability in climate and forest site parameters.* Journal of Geophysical Research - Atmospheres 106:33, 671-33, pp. 688.

Przybylak, R., (2000). *Temporal and spatial variation of surface air temperature over the period of instrumental observations in the Arctic*, Int. J. Climatol., 20: pp. 587-614.

Reeburgh, W. S., S. C. Whalen and M. J. Alperin (1993). *The role of methylotrophy in the global methane budget.* In J. C. Murrell and D. P. Kelly (eds.) Microbial Growth on C1 Compounds, Intercept, Andover, UK, pp. 1-14

Roeckner, E., Bengtsson, L., Feichter, J., Lebeveld, J. and Rodhe, H. (1999). *Transient climate change simulations with a coupled atmosphere-ocean GCM including the tropospheric sulfur cycle.* Journal of Climate, 12, pp. 3004-3012.

Romanovsky, V. E. (1987). *Approximate calculation of the insulation effect of the snow cover.* In Geokriologicheskie Issledovania (in Russian), MGU Press, vol. 23, pp. 145-157.

Romanovsky, V. E., and Osterkamp, T. E., (2001) *Permafrost: Changes and Impacts*, in: R. Paepe and V. Melnikov (eds.), "Permafrost Response on Economic Development, Environmental Security and Natural Resources", Kluwer Academic Publishers, pp. 297-315.

Reproduced with permission of the copyright owner. Further reproduction prohibited without permission.

Romanovsky, V. E. and Osterkamp, T. E.,(2003) *Permafrost Monitoring System in Alaska*: *Structure and Results* (in Russian), Earth Cryosphere, in press.

Romanovsky, V. E., and T. E. Osterkamp, (2000), *Effects of unfrozen water on heat and mass transport processes in the active layer and permafrost*, Permafrost and Periglacial Processes, 11, pp.219-239.

Romanovsky, V. E., and T. E. Osterkamp (1997) *Numerical modeling of active layer and discontinuous permafrost temperature dynamics*, Alaska: 1950-1997, EOS, Trans. AGU, 78(46), p. F270.

Romanovsky, V.E., and T.E. Osterkamp. (1997), *Thawing of the active layer on the coastal plain of the Alaskan Arctic*, Permafrost and Periglacial Processes, 8(1), pp. 1-22.

Romanovsky, V.E. and T.E. Osterkamp (1996), *Numerical modeling of active layer thicknesses and permafrost temperature dynamics in Barrow, Alaska*: *1949-1996*, EOS, Trans. AGU, 77(46), p. F188.

Romanovsky, V. E. and Osterkamp, T. E., (1995). *Interannual variations of the thermal regime of the active layer and near-surface permafrost in Northern Alaska.* Permafrost and Periglacial Processes, N6 (4), pp.313-335.

Romanovsky, V.E., T.E. Osterkamp, and N. Duxbury, (1997) *An evaluation of three numerical models used in simulations of the active layer and permafrost temperature regimes*, Cold Regions Science and Technology, Vol. 26, No. 3, pp. 195-203.

V. Romanovsky, M. Burgess, S. Smith, K. Yoshikawa, and J. Brown, (2002) *Permafrost Temperature Records: Indicators of Climate Change,* EOS, AGU Transactions, Vol. 83, No. 50, pp. 589-594.

Reproduced with permission of the copyright owner. Further reproduction prohibited without permission.

Romanovsky, V. E., Sergueev, D. O. and T.E. Osterkamp, (2003). *Spatial and temporal variations in the active layer and near-surface permafrost temperatures in Northern Alaska,* VII International Permafrost Conference, Switzerland, June 2003. In press.

Romanovsky, V., S. Smith, K. Yoshikawa and J. Brown, (2002): *Permafrost temperature records: Indicators of climate change.* EOS, AGU Transactions, 83, pp. 589-594.

Romanovsky, V. E., Osterkamp, T. E., Sazonova, T. S., Shender, N. I. and V. T. Balobaev, (2001) *Permafrost Temperature Dynamics Along the East Siberian Transect and an Alaskan Transect,* Proceedings of the International Workshop on Global Change: Connection to the Arctic, Sendai, Japan, 18-25 August, 2001, in press.

Romanovsky, V. E., Shender, N. I., Sazonova, T. S., Balobaev, V. T., Tipenko, G. S. and Rusakov, V. G., (2001). *Permafrost Temperatures in Alaska and East Siberia: Past, Present and Future,* Proceedings of the Second Russian Conference on Geocryology (Permafrost Science), Moscow, June 6-8, pp.301-314.

Rozenbaum G.E., (1976), *Cryogenic structure of the alluvium of subarctic rivers*, In: Problem of geocryology, v.5, (in Russian), Moscow, Nauka, pp. 61-65

Sazonova T.S. and V.E. Romanovsky. (2003) *A Model for Regional-Scale Estimation of Temporal and Spatial Variability of the Active Layer Thickness and Mean Annual Ground Temperatures.* Permafrsot and Periglacial Processes, *submitted.*

Sazonova T.S., Romanovsky V.E., Walsh J.E., and Segueev D.O., (2003). *Permafrost dynamics in 20th and 21st centuries along the East-Siberian transect,* Arctic and Alpine Research, *in preparation.*

Reproduced with permission of the copyright owner. Further reproduction prohibited without permission.

Santer, B. D., Wiglet, T. M. L., Barnett, T. P. and E. Anyamba, *Detection of climate change and attribution of causes*, , in Houghton, J. T., Meira Filho, L. G., Callander, B. A., Harris, N., Kattenberg, A., and Maskell, K. (eds.), (1996), The Science of Climate Change, Contribution of Working Group I to the Second Assessment of the Intergovernmental Panel on Climate Change (Ch. 6), Cambridge University Press, Cambridge, U.K., pp. 407-443.

Schell DM (1983) *Carbon-13 and Carbon-14 abundances in Alaskan aquatic organisms: Delayed production from peat in arctic food webs.* Science, 219, 1068.

Schell DM, Ziemann PJ (1983) In: *Permafrost, Fourth International Conference*, pp. 1105-1110. National Academy Press, Washington, D.C.

Searby, H.W. and Hunter, M., (1971), *Climate of the North Slope of Alaska*: U.S. Department of Commerce, National Oceanic and Atmospheric Administration Technical Memorandum AR-4.

Serreze, M. C., Walsh, J. E., Chapin, F. S. III, Osterkamp, T. E., Dyurgerov, M., Romanovsky, V. E., Oechel, W. C., Morison, J., Zhang, T., and Barry, R. G., (2000) *Observational evidence of recent change in the northern high-latitude environment*, Climatic Change, 46: 159-207.

Reproduced with permission of the copyright owner. Further reproduction prohibited without permission.

Shender, N. I., Romanovsky, V. E., and Tetelbaum, A. S., (1999). *A forecast of the natural variability of climate in Yakutsk and Fairbanks* (in Russian), Science and Education, 2, pp.24-29

Shiklomanov N.I., and Nelson F.E., (1999). *Analytic representation of the active layer thickness field, Kuparuk River Basin, Alaska,* Ecological Modelling, 123, pp.105-125.

Silvola, U (1986) *Carbon dioxide dynamics in mires reclaimed for forestry in eastern Finland.* Annales Botanici Fennici, 23, pp. 59-67.

Smith S.L., and Burgess M.M., (1999). *Mapping the sensitivity of Canadian permafrost to climate warming,* Proc. IUGG 99 Symp.HS2, IAHS Publications 256, pp.71-80.

Smith, M. W., and Riseborough, D. W. (1996). *Permafrost monitoring and detection of climate change.* Permafrost and Periglacial Processes, 7(4), pp. 301-309.

Soloviev P.A., (1959) *Cryolithozone of the northern part of the Lena-Amga Rivers watershed,* (in Russian), Moscow, Academy of Science USSR, 1959. 144 pp.

Southern Yakutia, (1975), (in Russian), Moscow, Moscow State University Press.

Spravochnik po klimatu SSSR, (1975) vypusk 24, *Yakutskaya ASSR, Meteorologicheskie dannye za otdel'nye gody*, chast' VII, Temperatura pochvy. Yakutsk, (in Russian) .

Stendel M., and Christensen J.H., (2002). *Impact of global warming on permafrost conditionsin a coupled GCM,* Geophysical Research Letters, 29 (13), 10.1029/2002GL014345.

Sturm, M. and Holmgren M., (1994) *Effects of microtopography on texture, temperature and heat flow in Arctic and sub-Arctic snow.* Annals of Glaciology, V.19, pp.63 – 68.

Reproduced with permission of the copyright owner. Further reproduction prohibited without permission.

Sturm, M., Racine, C., and Tape, K., (2001) *Climate change: Increasing shrub abundance in the Arctic,* Nature 411, pp. 546-547

Tikhonov, A. N., and Samarsky, A. A., (1966). *Uravneniya Matematicheskoi Fiziki* (Equations of Mathematical Physics), "Nauka" Moscow, 540 pp.

Tomirdiaro S.V., (1980) *Loess-ice Late Pleistocene-Holocene sediments in Eastern Siberia.* (in Russian), Moscow, Nauka.

Tyrtikov A.P. (1979) *The dynamics of vegetation cover and the development of cryogenic processes.* Moscow, Nauka,. 116 pp.

UCAR. (1988). *Arctic interactions. Recommendations for an Arctic component in the international geosphere-biosphere programme.* UCAR, Office for Interdisciplinary Earth Studies, Boulder, CO.

Varlamov, S. P., Skachkov, Yu. B. and Skryabin, P. N., (1993). *Variability of the ground hydrothermal regime within the slope landscapes in Central Yakutia.* In The Regularities of the Permafrost Landscapes Evolution. (in Russian), Yakutsk, Permafrost Institute Press, pp.12-21

Walker, D.A., Jia, G.J., Epstein, H.E. Raynolds, M.K, Chapin III, F.S., Copass, C. , Hinzman, L.D., Maier, H., Michaelson, G.J., Nelson , F., Ping, C.L,. Romanovsky, V.E. , Shiklomaov, N., Shur ,Y. (2003) *Vegetation-soil-thaw depth relationships along a Low-Arctic bioclimate gradient, Alaska: Synthesis of information from the ATLAS studies.* Permafrost and Periglacial Processes, submitted.

Reproduced with permission of the copyright owner. Further reproduction prohibited without permission.

Weller, R., D. Rudnick, and N. J. Brink, (1995) *Meteorological variability and air-sea fluxes at a closely spaced array of surface moorings*, Journal of Geophysical Research, 100, pp. 4867-4883.

Williams, P. J. (1964). *Unfrozen water content of frozen soils and soil moisture suction.* Geotechnique, 14, 3: pp. 231-246.

Williams, P. J. and Smith, M. W. (1989). *The Frozen Earth: Fundamentals of Geocryology*. Cambridge University Press, 306 pp.

Yakupov V.S., Danilov V.S., Kalinin V.M. (1984). *Permafrost and cryopegs in Western Yakutia based on geophysical data.*-in: XXVII International Geological Congress. V.VIII., Moscow, pp. 184-186.

Yershov E.D. (1998), *General Geocryology*, Cambridge University Press,580 pp.

Yershov E.D. ed. (1998) *Regional and historical world geocryology*. The basics of geocryology. Part.3. (in Russian), Moscow State University Press. 350 pp.

Yershov E.D. ed. (1989), *Eastern Siberia and Far East*, In-Geocryology of USSR, (in Russian), Moscow "Nedra". 515 pp.

Zarling, J.P. (1987). *Approximate solutions to Neumann problem.* ASME invited paper, International Symposium on Cold Regions Heat Transfer, Edmonton, Alberta, pp. 47-54.

Zhang, T. (1998). *Climate and permafrost conditions in northern Alaska, USA*, Earth Geocryosphere 2: 19-27, (in Russian with English abstract).

Zhang, T., et al. (2000), *Further statistics on the distribution of permafrost and ground ice in the Northern Hemisphere.* Polar Geography, 24: pp. 126-131.

Reproduced with permission of the copyright owner. Further reproduction prohibited without permission.

Zhang, T., and T. E. Osterkamp (1993). *Changing climate and permafrost temperatures in the Alaskan Arctic*, Proc. of the 6th Int. Conf. on Permafrost, Beijing, China.

Zhang, T., T.E. Osterkamp, and K. Stamnes. (1997). *Effect of climate on the thermal regime of the active layer and permafrost in Alaska north of the Brooks Range.* Permafrost and Periglacial Processes, 8: 45-67.

Reproduced with permission of the copyright owner. Further reproduction prohibited without permission.